Title
Effects of Oxygen and Salt Transport Across Contact Lenses on Lens-Wear Safety and Comfort

Author
Kim, Young Hyun

Publication Date
2022

Peer reviewed|Thesis/dissertation

Effects of Oxygen and Salt Transport Across Contact Lenses on Lens-Wear Safety and Comfort

By

Young Hyun Kim

A dissertation submitted in partial satisfaction of the

requirements for the degree of

Doctor in Philosophy

in

Vision Science

in the

Graduate Division

of the

University of California, Berkeley

Committee in Charge:

Professor Meng C. Lin, Co-Chair
Professor Clayton J. Radke, Co-Chair
Professor Dorian Liepmann

Spring 2022

Abstract

Effects of Oxygen and Salt Transport Across Contact Lenses
on Lens-Wear Safety and Comfort

by

Young Hyun Kim

Doctor of Philosophy in Vision Science

University of California, Berkeley

Professor Meng C. Lin, Co-Chair
Professor Clayton J. Radke, Co-Chair

There are numerous types of contact-lens materials and designs available for lens wearers today. Regardless of whether the lens is mass produced or customized to an individual patient, oxygen and ion transport across the contact lens is critical to ensure that contact-lens wear is safe and comfortable for the lens wearers. High oxygen-permeable contact lenses allow enough oxygen supply from the environment to the cornea to avoid corneal hypoxia-induced edema. Meanwhile, high ion-permeable contact lenses allow the tear-film between the contact lens and the ocular surface (i.e., post-lens tear film) to be thick enough to avoid lens adherence to the ocular surface. However, high ion-permeable contact lenses could potentially result in post-lens tear-film hyperosmolarity to activate corneal nociceptors and cause discomfort. Effect of contact-lens ion transmissibility (strictly salt transmissibility) on post-lens tear-film hyperosmolarity has not been investigated. Aims of this dissertation is to quantify the effects of contact-lens salt transport properties on post-lens tear-film hyperosmolarity and to quantify central-to-peripheral corneal edema during wear of various types of contact lenses that have yet to be investigated for hypoxic safety.

To quantify central-to-peripheral corneal edema for wear of various contact lenses, one-dimensional metabolic-edema model is initially developed to determine central corneal edema for scleral-lens wear. The model utilizes metabolic kinetics and diffusion to determine accurate concentrations of aerobic and anerobic metabolic species. Change in concentrations of metabolic species due to corneal hypoxia affects the hydraulic pressure and, therefore, the corneal thickness. The severity of corneal hypoxia is dependent on the adjustable lens oxygen transmissibility and the post-lens tear-film thickness. Model results show excellent agreement with the clinical corneal edema measurements made from subjects wearing scleral lenses with various lens oxygen transmissibilities and post-lens tear-film thicknesses. Central corneal edema due to wear of scleral lenses made of silicone-acrylate based materials is clinically insignificant while being awake. However, scleral-lens wear during sleep will cause clinically significant swelling and should be avoided.

The one-dimensional metabolic-edema model is expanded to two dimensions by incorporating central-to-peripheral cornea and contact lens. Alongside, metabolic support from the limbus is incorporated at the peripheral cornea to accurately model non-central corneal edema.

Central-to-peripheral corneal edema is determined for wear of soft contact, scleral, and component embedded contact lenses and is rigorously compared with available clinical data to ensure the accuracy of the metabolic-edema model. Results show that supply of bicarbonate ions and oxygen and removal of lactate ions by the limbal blood supply reduces corneal edema at the midperiphery and the periphery. Due to the limbal metabolic support, central corneal edema measured clinically is a good standard for assessing hypoxic safety for wear of scleral and soft contact lenses despite the variance in lens oxygen transmissibility throughout the lens and higher oxygen demand at the non-central cornea than the central cornea. For component embedded contact lenses, central-to-peripheral corneal edema must be accounted to ensure the hypoxic safety of lens wear. To minimize corneal edema, low oxygen permeable embedments are advised to be embedded in the lens periphery.

Post-lens tear-film osmolarity during contact-lens wear has not been measured clinically because the tear film is microns thick and because the tear film is covered by the contact lens that prevents direct probe interaction. To understand the osmolarity of the post-lens tear film, theoretical osmolarity models are developed to predict spatially-averaged and localized post-lens tear-film osmolarities during wear of soft contact lenses with varying salt diffusivity, lens thickness, and salt partition coefficients. Lenses made of acrylate materials are not studied because those hard lenses are practically ion impermeable compared to those of soft contact lenses. Spatially-averaged osmolarity of post-lens tear film is determined by quantifying the transport of salt and water across the contact lens between the pre-lens and the post-lens tear films. The model also incorporates tear production and evaporation rates, tear mixing, and tear produced from the cornea and the bulbar conjunctiva to accurately model the lens-wear osmotic behavior. Meanwhile, localized post-lens tear-film osmolarity due to tear break-up areas on the pre-lens tear film is determined by developing a 2-dimensional model that allows localized hyperosmotic regions to be formed on the pre-lens tear film. Results show that soft-contact-lens wear can protect the cornea from both localized and spatially-averaged hyperosmolarity when the lens-salt diffusivity is low. Realistic ranges of salt partition coefficient and lens thickness for existing soft contact lenses do not have meaningful impact on the post-lens tear-film osmolarity. Conversion of localized post-lens tear-film hyperosmolarity spike values to pain scores based on a previously conducted clinical study suggests that soft-contact-lens wear can mitigate osmolarity-induced discomfort.

Understanding salt and oxygen transports across contact lenses allow development of safe and comfortable novel contact lenses. Theoretical models in this dissertation allow optimization of future lens designs to minimize hyperosmolarity and hypoxia for safe and comfortable lens wear.

To family, friends, and mentors

This journey would have not been possible without your support

Contents

List of Figures

List of Tables

Acknowledgements

Watching award ceremonies on the TV as a little kid, I often wondered how award recipients had so many people they wanted to acknowledge in their speeches. If time travel was possible, I would go back in time to answer this naïve curiosity in a heartbeat. This PhD journey was only possible because of the support I received from the people around me. It is my lifelong goal to be helpful to those around me as they have been for me.

Foremost, I want to thank my advisors Professor Meng Lin and Professor Clay Radke. I vividly remember the day when Meng pulled me into the CRC office and suggested I pursue a PhD. Freshly graduated with my bachelor's degree, I was there to thank her for her mentorship in my undergraduate research and to say goodbye. That was the first day in my life that I considered doing a PhD and I regularly wonder how different my life would have turned out if I did not see Meng that day. Needless to say, I am glad that I saw her that day. Meng's push to expand my knowledge in clinical study and eye physiology allowed me to conduct multidisciplinary research and become a vision scientist.

When I think about my 10 years at Berkeley, first person that comes to my mind will always be Clay. He was the first to teach me how to conduct research and the first to teach me about the principles of chemical engineering. His demand for high-quality research and countless hours of mentorships prepared me for a career as a scientist and an engineer. Clay even went on to teach me how to write and give presentations. I am not sure what kind of professional I would have become without Clay's teachings. I am going to miss our weekly meetings, his trove of stories, and gatherings at his house. There could have not been a better PhD advisors for me than Clay and Meng. I am fortunate to have them as my mentors and as my friends.

Alongside Clay and Meng's irreplaceable mentorships, I would like to thank other faculties, clinicians, and researchers that helped me throughout my PhD journey. Professor Ken Polse was instrumental in helping me understand the history of ocular-surface research. Professor Dorian Liepmann provided me with information regarding particle velocimetry and Professor Karsten Gronert introduced me to mass spectroscopy. It is unfortunate that I ran out of time to work on the projects I discussed with Dorian and Karsten. I also appreciate Professors Austin Roorda and Marty Banks for always answering my random curiosities throughout my time at Berkeley. Lastly, it was an honor to work with Dr. Byki Huntjens and Dr. Vakishan Nadarajah on our clinical projects. Your clinical insights were invaluable to my growth as a vision scientist.

I would also like to thank the past and the present Clinical Research Center staff and the members of the Radke Group. Bo Tan, Yixiu Zhou, Uyen Do, Wing Li, Kristina Lin, Vivien Tse, Mariel Lerma, Tan Truong, Andrew Graham, Thao Yeh, Nina Tran, Fozia Khan, Erika Mae Reyes, Joy Huynh, Jennifer Ding, Jasmine Ng, Jin Mei, Anoop Sownderraj, Omowumi Oladipo, Lilian Thoi, and Tiana Leung made my transition to the clinical research possible. I also apologize for distracting everyone during their work hours with my conversations. Those conversations kept me going. Current and former members of the Radke Group, Cheng-Chun Peng, Tatyna Svitova, Colin Cerretani, Thomas Dursch, David Liu, Andrew Crothers, Thien Nguyen, and Sho Takatori helped me at various points of my research career to make this dissertation possible. And finally, I can't forget Becca Flitter who helped me appreciate immunology.

This dissertation would have not been possible without the support I received from the Saini (i.e., Eshang, Ashwani, and Jeet) family and the Yi (i.e., Sarah, Mike, and Hyun) families. I am truly thankful for both families for supporting and taking me in like a family. When I was debating between PhD or industry, I was fortunate to have been with the Saini family at India. The

conversation I had with Ashwani in an elephant shed was the moment when I decided to continue school. Without that conversation, I may have never realized the joy of science. I long lost count of how many times I have been invited over to the Yi family for their family events. Being homesick and away from my family for years, Yi family is what got me through the tough times during my PhD education.

Of course, this acknowledgement section would be incomplete without thanking my parents (i.e., Hoseong and So Young) and my relatives. The sacrifice my parents made by immigrating to the United States provided me with the opportunity to pursue invaluable education and see the broader world. My aunts (i.e., Eunsil, Hyesil, Hyekung) and uncles (i.e., Kookjoon, Jongchul, Youngjin) provided me with stability as I moved back and forth between South Korea and the United States. Without them, I would have not been able to focus on my academics.

I am grateful to have met so many amazing people in my life. Although I am finally leaving Berkeley, time spent at Berkeley with these amazing people will always have a special place in my heart.

Chapter 1

Introduction

1.1 Environmental Dependency of Cornea: Oxygen and Osmolarity

The cornea is a unique body tissue in that it is exposed to the environment and relies heavily on that interaction to function. Due to the avascular nature of the cornea, which allows corneal transparency for sight, the cornea receives the majority of its oxygen supply for aerobic metabolism from the environment.[1] When there is a lack of oxygen supply from the environment the cornea must rely only on oxygen from limbal blood vessels.[2,3] Chronic hypoxia of the cornea results in neovascularization to compensate for the loss in oxygen supply, which unfortunately can cause tissue scarring, inflammation, and loss in visual quality.[2,4] Even with the unwanted neovascularization, limbal support to the central cornea is unfortunately limited[3] and the body requires increased anaerobic metabolism to meet the energy demand of the corneal cells.[5] However, anerobic metabolism results in increased lactate concentration and decreased pH and bicarbonate concentration within the cornea.[5–7] Disruption of aerobic homeostasis affects the transport of water between aqueous humor and stroma through the corneal endothelium to result in increased stromal water retention, causing corneal edema.[8]

Maurice discovered experimentally that the corneal endothelium allows water to flow passively into and to be pumped actively out of the stroma, which is coined as the "pump-leak" mechanism.[8] Maurice's experiments further showed that swelling of the cornea is predominantly regulated by the corneal endothelium and not the corneal epithelium.[8] Since the discovery of the pump-leak swelling mechanism, studies found that metabolites affect the amount of corneal edema.[9–11] Eventually the works of Chhabra et al.[12] and Leung et al.[5] linked the effects of hypoxia to anerobic and anaerobic metabolism kinetics and, consequently, to corneal edema.

Similar to oxygen dependence, the osmotic state of the corneal surface also depends on the environment. Tear produced predominately from the lacrimal gland keeps the corneal epithelium hydrated. However, as tear evaporates into the environment during the interblink, the concentration of dissolved ions and other molecules increases in the remaining tear to become hyperosmotic. Hyperosmotic tear then triggers corneal nociceptors causing ocular pain and discomfort.[13,14] In fact, tear-meniscus hyperosmolarity has been shown to correlate with dry eyes.[15–24] Since evaporation rate is negatively correlated with relative humidity and positively correlated with temperature and airflow, individuals are more likely to experience dry eyes in an environment with low relative humidity, high temperature, and high airflow.[25]

It is rather unsurprising that dry-eye patients have higher tear evaporation rates than those without dry eyes considering that tear osmolarity is largely influenced by the tear evaporation rate.[23,26] The difference in tear evaporation rates between normal and dry eyes is attributed to the variance in lipid-layer thickness and composition.[27–29] The 50 – 100 nm lipid layer,[30] secreted from the meibomian glands, is the outermost layer of the tear film that coats the muco-aqueous tear-film layer to retard tear evaporation.[31] Lipid-layer instability due to suboptimal composition and thickness causes localized break-up areas to form, and the time it takes for the break-up areas to form during an interblink varies significantly for normal and dry eyes.[32] Theoretical studies showed that local osmolarity in these break-up areas can reach 600 – 900 milliosmolar (mOsM) in

a 10 s interblink whereas areas without break up have osmolarities less than 400 mOsM.[33,34] Figure 1.1 illustrates the evaporative phenomenon occurring on the ocular surface.

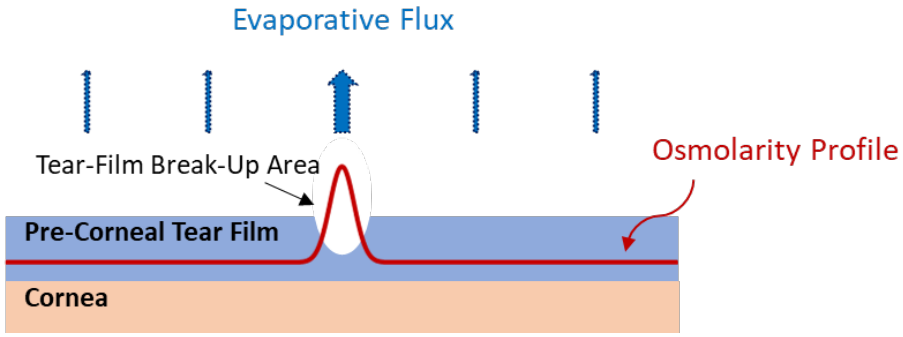

Figure 1.1. Schematic of localized break-up area on the pre-corneal tear film. Localized break-up area has greater evaporation flux and, therefore, higher osmolarity. Multiple break-up areas can occur on the ocular surface during an interblink period and the break-up size typically grows as the interblink period gets longer. Figure is not to scale.

Cerretani and Radke[35] mathematically showed that the spatial osmolarity average including both break-up and non-break-up areas was also significantly different between normal and dry eyes. Equally important, their study revealed that pre-corneal tear-film osmolarity is significantly different from the osmolarity of the tear meniscus, where osmolarity is typically measured in clinical studies.[35] However, possible reason as to why the meniscus osmolarity and the dry-eye discomfort correlates in some studies[15–24] is because the tear menisci and the pre-corneal tear film mix during every blink.[35] It is important to recognize that some studies[36,37] found lack of association between the meniscus osmolarity and the dry-eye discomfort, presumably due to the known limitations of the clinical osmometer.[38] Therefore, association between tear-meniscus osmolarity and dry-eye discomfort remains controversial.

Environmental dependence of the cornea for oxygen and osmolarity regulation is critical for ocular health and comfort. Unfortunately, homeostasis between the cornea and the environment is disrupted with wear of contact lenses. This dissertation reveals how contact-lens types, contact-lens designs, and contact-lens-material properties affect oxygen and ion transport to guide lens development to maximize hypoxic safety and minimize osmolarity-induced discomfort during contact-lens wear.

1.2 Transport of Oxygen and Ion Across Contact Lenses During Lens Wear

Oxygen and ion transport across contact-lens materials is of significant interest to lens designers due to the concern for corneal edema and lens adherence to the ocular surface, which is correlated to ion transport.[39–45] Section 1.2.1 provides information regarding how contact lenses evolved over time due to lens-wear induced hypoxia and why there is renewed interest in investigating corneal hypoxia with contact-lens wear, which is investigated in this dissertation. Section 1.2.2 discusses the relationship between lens adherence to the ocular surface and ion transport across the contact lens. Section 1.2.2 also discusses the motivation for this dissertation, namely to investigate the effects of ion transport across soft contact lenses on tear-film osmolarity during lens wear.

1.2.1 Oxygen Transport

The first widely-used contact lenses were shown to cause corneal edema and edema-induced corneal haze due to hypoxia caused by the oxygen impermeable lens material polymethyl methacrylate (PMMA).[5,46,47] To allow oxygen to reach the cornea, PMMA lenses were designed and fitted on wearers to maximize on-eye lateral movement thus allowing oxygen to reach the cornea.[48] Due to the heavy dependency on lens movement for oxygen, PMMA lens diameters were about 9 – 11 mm,[49] typically smaller than modern soft contact lenses (SCLs). The stiff PMMA material and the small lens size also made wearing these lenses uncomfortable.

To minimize corneal edema and to improve comfort, first-generation soft hydrogel contact lenses were made with hydroxyethyl methacrylate (HEMA) material in the early 1970s.[50] HEMA contact lenses contain water within the lens matrix allowing water-soluble oxygen to diffuse across the lens to reach the cornea. Therefore, oxygen permeabilities (*Dk*) of HEMA lenses depend on the water content. Here, *D* is the oxygen diffusivity of the contact lens and *k* is the partition coefficient of oxygen. *Dk* of HEMA lenses are capped by the *Dk* of water, which is around 90 Barrer.[51] Further, increasing the water content of HEMA lenses increased lens thickness (*L*), meaning that oxygen transmissibility (i.e., *Dk/L*) is reduced.[51] Studies of Holden and Mertz[45] and re-evaluation of the study by Harvitt and Bonanno[41] showed that the HEMA lenses do not eliminate hypoxia altogether. Regardless, HEMA hydrogel lenses were widely used worldwide until the advent of soft silicone hydrogel (SiHy) materials.[52]

In conjunction to hydrogel contact lenses, the 1970s also introduced corneal rigid gas permeable (RGP) acrylate contact lenses.[50] These small hard lenses are made of silicone-based material and allow oxygen to transport across contact lenses unlike the PMMA material. Initially available corneal RGP lenses had lower *Dk* than hydrogel contact lenses but could rely on lens movement for increased oxygen supply to the cornea.[50] Continual improvement of silicone-based acrylate material now allows corneal RGP lenses to be made with *Dk* greater than 100 Barrer and is considered safe from hypoxia.[50] Despite hypoxic safety of RGP lenses, SCLs became the preferred choice for lens wear worldwide due to affordability and, most importantly, easier comfort adaptation.

Similar to corneal RGP lenses, introduction of siloxane into the hydrogel material resulted in soft SiHy contact lenses to attain oxygen permeabilities greater than 100 Barrer.[51] Rather than relying on water to transport oxygen, oxygen transport occurred within the phase-separated silicone domains of these lenses. Therefore, lower-water-content SiHy lenses have higher *Dk* than higher-water-content SiHy lenses.[51] Commercially available SiHy contact lenses still have water content of ~30 to 50 % to allow for comfort, elasticity, and shape of SCLs.[53] Various studies showed that for typical contact-lens thicknesses, SiHy contact lenses eliminate the concern for corneal hypoxia and edema.[5,54]

Although modern soft SiHy and corneal RGP lenses are free of hypoxic concerns during lens wear, advent of modern non-hydrated scleral lenses (SL) and introduction of embedment technologies have revived concern for corneal hypoxia during contact-lens wear. SLs are particularly useful for patients with irregular corneas (e.g., keratoconus) or for patients that suffer intolerable dryness with other types of contact lenses. Superiority of SLs for these patients is due to the thick post-lens tear film (PoLTF) (i.e., the tear film between the contact lens and the ocular surface) keeping the cornea separated from the contact lens, hydrated, and protected from hyperosmolarity induced by tear evaporation. Scleral lenses are large RGP lenses with 15 – 24 mm diameter; lens thicknesses are about 3 to 4 times that of corneal RGP and SiHy contact lenses. Therefore, even with high *Dk* silicone-acrylate materials, *Dk/L* is significantly less than those of

corneal RGP and SiHy contact lenses. Although beneficial for keeping the eye protected and not touching the contact lens, the PoLTF during SL wear is a magnitude thicker than that of PoLTFs during corneal RGP or SiHy lens. This adds additional resistance to oxygen transport with SL wear. Thus, there is a need to understand if modern SLs are hypoxically safe to wear.

Improvements in sensor and drug-releasing technologies are allowing active investigation into multicomponent contact lenses.[55–69] Some of the functions these contact lenses are trying to achieve are controlled drug release, detect biomarkers, display provision, correction for presbyopia, and light regulation. These lenses utilize existing contact-lens base designs but are unique because they have various components embedded within the contact lens. This raises hypoxic concerns because components such as semiconductors have low or zero Dk.[70] Multicomponent lenses, therefore, require understanding of lateral oxygen diffusion, localized corneal hypoxia, and quantitative understanding of limbal metabolic support on corneal edema. All of which are not well understood prior to the work in this dissertation.

Continuous development of contact lenses and their applications demand further understanding of oxygen transport across contact lenses and how that transport impacts the corneal health. By utilizing mass-transport principles and metabolic kinetics, this dissertation answers hypoxic safety of novel contact lenses and provides guidelines to ensure that future designs are safe for human wear.

1.2.2 Ion Transport

Ion transport (strictly salt transport) was historically investigated by the contact-lens community because low ion-permeable hydrogel contact lenses adhered strongly to the ocular surface.[39,40] Therefore, the focus of ion-permeability (D_sk_s) studies of SCLs (e.g., SiHy and HEMA contact lenses) was to understand the relationship between lens adhesion and D_sk_s rather than effect of D_sk_s on PoLTF osmolarity. Here, D_s is the salt diffusivity in the contact lens and k_s is the partition coefficient of that salt for a contact lens. Because RGP and SLs are not hydrated, salt permeability is not an issue. Nevertheless, corneal-RGP contact lenses and SLs are known to adhere to the ocular surface if the lenses do not move for prolonged time periods.[71,72]

During SCL wear, the tear film over-riding the contact lens and exposed to the environment, commonly known as pre-lens tear film (PrLTF), evaporates similar to that of pre-corneal tear film during no lens wear. Because SCLs are ion permeable, increased osmolarity of the PrLTF initiates salt diffusion across the contact lens and into the PoLTF to increase PoLTF osmolarity.

Nicolson et al.[40] recommended D_sk_s of at least 2×10^{-7} cm^2/s to avoid lens adherence of SCLs. Although the recommended guideline seemingly avoids lens adherence to the eye, physical understanding as to why is not concrete. Nicolson et al.[40] argued that D_sk_s indirectly gauges the hydraulic permeability of SCLs, and that water being squeezed in and out of the SCL during blinking allows thick enough PoLTF to avoid lens adherence. However, Monticelli et al.[73] showed that hydraulic permeabilities of SCLs are minuscule and water transport across the lens cannot maintain PoLTF thickness to avoid lens adherence. Cerretani et al.[39] mathematically demonstrated that increased PoLTF osmolarity due to ion transport across SCL can osmotically withdraw water from the cornea to maintain adequate PoLTF to prevent lens adherence. However, further investigation is necessary to ascertain whether the osmotic-withdrawal mechanism actually controls SCL adherence.

Although efforts have been made to understand how SCL D_sk_s affects lens adhesion, PoLTF osmolarity due to increased SCL D_sk_s remained uninvestigated until this dissertation. Understanding PoLTF osmolarity during SCL wear is important because hyperosmolarity of tear

menisci correlates with dry-eye discomfort during no-lens wear.[15–24] However, the PoLTF does not mix well with the tear menisci unlike mixing of the pre-corneal tear film and the tear menisci during no-lens wear. Therefore, it is not surprising that clinical studies measuring tear meniscus osmolarity during SCL wear find no correlation between meniscus osmolarity and lens-wear dryness discomfort.[74–78] Instead, osmolarity of the PoLTF and lens-wear dryness discomfort should be investigated.

Considerable improvement in lens-wear comfort is essential to allow continuous extended wear of SCLs. Analysis of salt transport across SCLs to determine PoLTF osmolarity discussed in this dissertation is crucial in understanding the effect of osmolarity on lens-wear dryness discomfort.

1.3 Dissertation Scope

This dissertation theoretically investigates the effects of oxygen and salt transport across contact lenses and their effects on ocular health and PoLTF osmolarity. Clinical experiments are conducted alongside theory to validate the mathematical predictions and to understand better human physiology of eye behavior. Chapters 2 – 4 establish and validate a metabolic model to predict hypoxia-induced corneal edema during wear of various types of contact lenses. Chapter 5 experimentally quantifies human lacrimal tear production rates to allow accurate modeling of salt transport across SCL during lens wear. Chapters 6 and 7 theoretically investigate whether SCL wear can protect the ocular surface from hyperosmolarity, which has been shown to correlate with dry-eye discomfort without lens wear. Chapters 2 – 4 build up chronologically to develop more sophisticated eye models and to assess more complicated lens systems for corneal edema. Chapters 6 and 7 together quantify both localized and spatial-average hyperosmolarity of the PoLTF to provide comprehensive understanding of lens-wear tear-film hyperosmolarity. Summaries of each chapter are provided below.

Chapter 2 assesses central-corneal edema with SL wear with the developed metabolic-edema model. The metabolic-edema model expands the theoretical work of Leung et al.[5] to include oxygen transport resistance of the PoLTF. The model numerically calculates oxygen transport and metabolic kinetics to determine the metabolic concentrations at the corneal endothelium. Changes in metabolic concentrations due to lens-wear-induced hypoxia are used to calculate corneal edema. PoLTF thickness and *Dk/L* of the SL are varied to assess how these controllable variables affect corneal edema during lens wear. Results indicate that commercially available SL wear results in clinically insignificant amounts of corneal swelling (e.g., 0.5~2% swelling depending on lens *Dk/L* and PoLTF thickness) when worn while awake. However, commercially available SLs result in unhealthy corneal swelling of 6~8% when worn during sleep. Therefore, SLs should not be worn during sleep. Chapter 2 also reports results from our clinical study validating the model results for SL wear while being awake. Due to SLs being deemed unsafe to wear while being asleep, a clinical study measuring corneal edema due to lens-wear sleep was not conducted. The developed metabolic-edema model in Chapter 2 serves as the fundamental basis for Chapters 3 and 4.

To assess noncentral corneal edema during contact-lens wear, the metabolic-edema model of Chapter 2 is expanded in Chapter 3 to include central-to-peripheral geometries of contact lenses and the cornea. Alongside, metabolic support from the blood supply at the limbus is also incorporated into the numerical model to predict accurately noncentral corneal edema during contact-lens wear. Central-to-peripheral corneal edema with both SCL and SL is assessed in Chapter 3. Results show that limbal metabolic support practically eliminates corneal edema at the peripheral cornea. The effect of limbal metabolic support on corneal edema gradually diminishes

when approaching the cornea center and disappears completely ~1 mm away from the corneal center. Results also show that supply of bicarbonate and removal of lactate by the limbus has the predominating effect on reducing corneal edema. Although impactful, oxygen support from the limbus has less effect on reducing corneal edema than does supply of bicarbonate and removal of lactate by the limbus. Chapter 3 reveals that the location of maximum corneal swelling depends on limbal metabolic support and the thickness profiles of the cornea, the PoLTF, and the contact lens. Determined central-to-peripheral corneal edema is verified against published clinical studies as detailed in Chapter 3. The two-dimensional metabolic-edema model developed in Chapter 3 is used in Chapter 4 to assess localized corneal edema induced by multicomponent embedded contact lenses.

Chapter 4 expands the work of Chapter 3 to understand central-to-peripheral corneal edema induced by wear of multicomponent embedded contact lenses. Because embedded components may have low *Dk*, localized regions of the cornea may undergo extreme hypoxia during wear of these novel lenses. Therefore, assessment of localized corneal edema is critical. Various multicomponent embedded contact lenses are designed using both SL and SCL as the encasement. Each lens is designed to have central and peripheral embedments. The placement, the dimensions, and the *Dk* of the embedded components and the encasement are varied to assess their effect on central-to-peripheral corneal edema. Model results show that placement of low-*Dk* materials at the lens periphery minimizes corneal edema due to limbal metabolic support. With oxygen impermeable or low-*Dk* embedments, lateral transport of oxygen is important in lowering localized edema spikes. Expectedly, thinner and higher *Dk* embedments lower corneal edema everywhere. Localized corneal edema results are validated by comparing the model results with the study of Holden et al.,[79] who studied localized corneal edema induced by a donut-shaped contact lens. Results of Chapter 4 allow lens developers to optimize their multicomponent embedded contact-lens designs to minimize corneal edema for safe human wear.

To determine accurately PoLTF osmolarity during SCL wear, salt flux across a SCL between the PrLTF and PoLTF must be accurately quantified. However, PrLTF osmolarity is directly influenced by tear production and evaporation rates. Although there are numerous studies that measured tear evaporation rates, there are no known studies that measured tear production rates directly. Rather, tear production rates are typically calculated from measured tear evaporation and turnover rates. This method is limited because tear evaporation and turnover rates cannot be measured simultaneously. Chapter 5 provides tear-production rates measured directly for the first time using a modified Schirmer Tear Test. A conducted clinical study assures that the tear production rates used to calculate PoLTF osmolarity in Chapters 6 and 7 are accurate.

Chapter 6 builds on the tear dynamics model of Cerretani and Radke[35] to include SCL as well as salt and water transport across a soft contact lens. The proposed model accounts for tear evaporation, tear production, tear drainage, SCL D_s, SCL k_s, SCL thickness, and tear mixing that occurs during SCL wear to determine accurately PrLTF, PoLTF, and menisci osmolarities.[80] Since tear osmolarity is predominantly controlled by tear salt concentration, this dissertation focuses on salt-transport properties to determine various tear-compartment osmolarities. Tear evaporation and production rates are varied to mimic both normal and dry eyes during lens wear. Results reveal that by lowering D_s of the SCL, the cornea can be protected from hyperosmotic PoLTF for both normal and dry eyes. Although a similar effect can be achieved by lowering k_s or by increasing lens thickness, practical limitations of SCL designs make D_s the optimal candidate to regulate PoLTF osmolarity. Results in Chapter 6 indicate that lenses can be designed to minimize PoLTF osmolarity while maintaining enough ion transport to avoid lens adherence to the ocular surface.

Determined osmolarities in Chapter 6 are those of spatially averaged tear osmolarity. Chapter 7 investigates the effect of localized PrLTF hyperosmotic spikes on PoLTF osmolarity. Similar to the pre-corneal tear film during no-lens wear, utilizing mire rings confirm that the PrLTF also undergoes localized break-up during an interblink.[81] Therefore, Chapter 7 makes a reasonable assumption that PrLTF ruptures exhibit similar osmolarity spikes as does the pre-corneal tear film. Chapter 7 focuses on the effect of SCL D_s on PoLTF osmolarity since Chapter 6 reveals that design and material limitations prohibit lens thickness and k_s to have meaningful impact on the PoLTF osmolarity. Although osmolarity of localized PrLTF break-up areas can rise above 500 mOsM during a 10 s interblink,[34] SCL wear can effectively mitigate any rise in the PoLTF osmolarity. This is true for both normal and dry eyes. Surprisingly, even lenses with high D_s can meaningfully reduce the PoLTF osmolarity. Using the clinical results of Liu et al.,[14] PoLTF osmolarity is also converted into ocular discomfort scores to show that SCL wear can protect against osmolarity-induced lens-wear discomfort.

Chapter 2

Central Corneal Edema with Scleral-Lens Wear

Published as: Kim YH, Tan B, Lin MC, Radke CJ. Central corneal edema with scleral-lens wear. Curr Eye Res. 2018;43(11):1305-1315.

2.1 Abstract

Purpose: To evaluate the safety of scleral-lens designs, we model and clinically assess central corneal edema induced by scleral-lens wear for healthy subjects.
Materials and Methods: Central corneal swelling during scleral-lens wear is measured using optical coherence tomography (OCT). Transport resistances are modeled for oxygen diffusion through the scleral lens and post-lens tear-film (PoLTF), and into the cornea. Oxygen deficiency in the cornea activates anaerobic metabolic reactions that induce corneal edema. Oxygen permeability, carbon-dioxide permeability, settled-lens PoLTF thickness, and scleral-lens thickness are varied in the calculations to mimic different lens fits.
Results: Transport modeling predicts that for open eyes, increasing PoLTF thickness from 50 to 400 μm increases central corneal swelling by approximately 1–1.5% when oxygen transmissibility (*Dk/L*) is greater than 10 hBarrer/cm (i.e., hectoBarrer/cm). Although swelling is larger for oxygen *Dk/L* < 10 hBarrer/cm, PoLTF thickness has minimal impact in this range. For open eye, oxygen transmissibility of the lens plays a significant role in corneal edema, but is negligible when oxygen *Dk/L* is > 40 hBarrer/cm. For closed eye, central corneal swelling is greater than 5% for an oxygen *Dk/L* range of 0–100 hBarrer/cm with typical lens-fitting parameters. For carbon-dioxide transmissibilities increasing from 50 to 250 hBarrer/cm and with a fixed oxygen *Dk/L* of 25 hBarrer/cm, calculated swelling diminishes by an additional 0.5%. Comparison of model calculations to clinical-swelling data is within the error range of the clinical measurements.
Conclusions: Oxygen/metabolite transport calculations for open-eye scleral-lens wear show that typical PoLTF thicknesses fitted by clinicians (i.e., PoLTF thicknesses < 400 μm) with modern scleral lenses (i.e., oxygen *Dk/L* > 25 hBarrer/cm) produce corneal swelling of less than 2% in agreement with experiment. Therefore, scleral lenses prescribed today evoke less than physiological hypoxic swelling (i.e., less than 4%) for healthy corneas during open-eye. Closed-eye wear, however, appears clinically unsafe.

2.2 Introduction

Human corneal health relies on avascular oxygen supply through direct exposure to the environment for open eyes or to the palpebral conjunctiva for closed eyes.[5,12,42] Compared to soft-contact lenses, the considerably larger lens and post-lens tear-film (PoLTF) thicknesses of rigid-gas-permeable scleral lenses (SLs) raise concern over sufficient oxygen transport from the atmosphere/palpebral conjunctiva to the cornea.[43] Previous studies with soft-contact lenses establish that oxygen deprivation of the cornea can result in adverse corneal events, such as keratitis, microcysts, acidosis, and corneal edema.[82–84]

Two main approaches are available to assess corneal hypoxia with SL wear. First, corneal edema is measured clinically with imaging instruments, such as Scheimpflug camera, ultrasound

pachymeter, or optical coherence tomography (OCT).[44,85–88] The amount of corneal edema is reported as a gauge of corneal hypoxia. Although Scheimpflug camera, ultrasound pachymetry, and OCT used in previous studies[44,85–87] have similar accuracy limitations of about 3 μm,[89] 5 μm,[90] and 3 μm,[91] respectively, OCT is known to have better repeatability in measuring central corneal thickness than the former methods.[92,93] A major limitation of existing clinical studies[44,85–88] is lack of SL thickness measurements. Despite having known oxygen permeabilities, lens oxygen transmissibilities (*Dk/L)* may differ significantly. We find that oxygen transmissibility of SLs varies as much as ± 10 hBarrer/cm (i.e., hectoBarrer/cm) due to lens-thickness variance.

In a second approach following considerable effort on soft-contact lenses,[5,12,42] mathematical models calculate oxygen-tension profiles through the lens and cornea, and especially at the anterior surface of the cornea.[88,94,95] However, these models only predict oxygen profiles and cannot directly predict corneal swelling associated with hypoxia. Unlike studies done with soft-contact lenses,[5,12,41,42,45] oxygen-tension models and clinical-study results on SL wear yield conflicting conclusions on safe-fitting parameters.[44,85–88,94,95] Based on oxygen-tension calculations, Compañ et al.[44] suggested that the PoLTF thickness should be smaller than 150 μm to avoid hypoxia. Conversely, Giasson et al.[94] performed an *in-viv*o goggle study to estimate oxygen tension at the surface of the cornea and suggested avoidance of settled-PoLTF clearances greater than 200 μm and lens thicknesses greater than 250 μm. Arlt[85] found with OCT, however, that 350 μm thick SLs fit to 200–600 μm PoLTF thickness exhibited less than 4% swelling. Arlt concluded that SLs are safe during open-eye wear.

To overcome these inconsistencies, we extend the edema calculations of Leung et al.[5] to SLs, and we validate our modeling effort with clinical measurements. By considering how oxygen tension controls corneal metabolism, we directly calculate the amounts of corneal edema expected under hypoxic conditions and compare those to measured edema with SL wear. This approach validates prediction of conditions of safe-wear parameters unavailable with only oxygen-tension estimates of previous studies.

2.3 Methods

2.3.1 Model

Ample description of the metabolic-edema model is available.[5,12] We provide only a brief nonmathematical summary here. Pioneering studies of corneal edema suggest that corneal swelling is due to aqueous imbibition from the anterior chamber (AC) caused by the proclivity of stroma (St) to uptake water.[8,10,96–98] Maurice suggested that swelling is regulated by an active ion pump that lowers the osmolality at the basolateral endothelium (En), relative to that of the aqueous humor, and osmotically drives fluid from the St into the AC.[8] Hodson and Miller later determined that the ion pump actively transports bicarbonate.[99]

Leung et al.[5] built upon these prior works and those of Klyce and Russel,[10] and Li and Tighe[11] by utilizing the Kedem-Katchalsky membrane-transport formalism[100] for the ion pump. Despite extensive studies into the pump-leak mechanism and correlation between corneal swelling and anaerobic glycolysis,[101,102] direct mathematical connection to hypoxia-induced corneal swelling was not made until Leung et al.[5] The key was inclusion of aerobic and anaerobic glucose metabolic-consumption reactions.[12]

When local oxygen tension diminishes, glucose metabolism shifts towards the anaerobic pathway producing lactate ions and lowering pH. Buffering reactions then decrease bicarbonate-ion concentrations. Changes in lactate and bicarbonate-ion concentrations at the En alter corneal water uptake through membrane osmotic transport and the active ion pump. Leung et

al.[5] successfully related hypoxia to corneal edema and demonstrated that lactate and bicarbonate-ion concentrations at the En play key roles in corneal swelling.

We extend the 1D hypoxia-edema transport model of Leung et al.[5] to include a SL and a thick PoLTF, as drawn in Figure 2.1. The lens/cornea comprises the AC, En, St, epithelium (Ep), PoLTF, SL, and pre-lens tear film (PrLTF). A SL is significantly thicker (250–500 μm) at the center than a standard soft-contact lens (80 μm).[42] Diffusion resistances in the PoLTF can no longer be ignored, due to the increased thickness (100–400 μm thickness vs. approximately 3-μm thickness under a soft-contact lens).[5] We calculate the steady concentration profiles of oxygen, carbon dioxide, glucose, lactate ion, hydrogen ion, bicarbonate ion, sodium ion, and chloride ion to determine corneal swelling for different SL transmissibilities and fitting parameters, specifically the PoLTF thickness. Electroneutrality and zero current throughout the cornea are imposed, fluxes of the various species obey the Nernst–Planck relation,[103] and oxygen consumption rate of aerobic and anaerobic reactions follow nonlinear Monod-based kinetics.[5,12] All transport equations and metabolic reactions are given in Appendix A of Leung et al.[5] Parameters necessary for the present calculations are listed in Tables 2A.1–2A.4 of Appendix 2A.[1,5,6,9–12,104–110] If not specified, central-lens thickness is 400 μm. Since carbon-dioxide permeability in SLs is not currently available, *Dk* for carbon dioxide was set at 600 Barrer based on Fatt et al.'s[104] analysis of carbon-dioxide permeability in rigid-gas-permeable contact lenses.

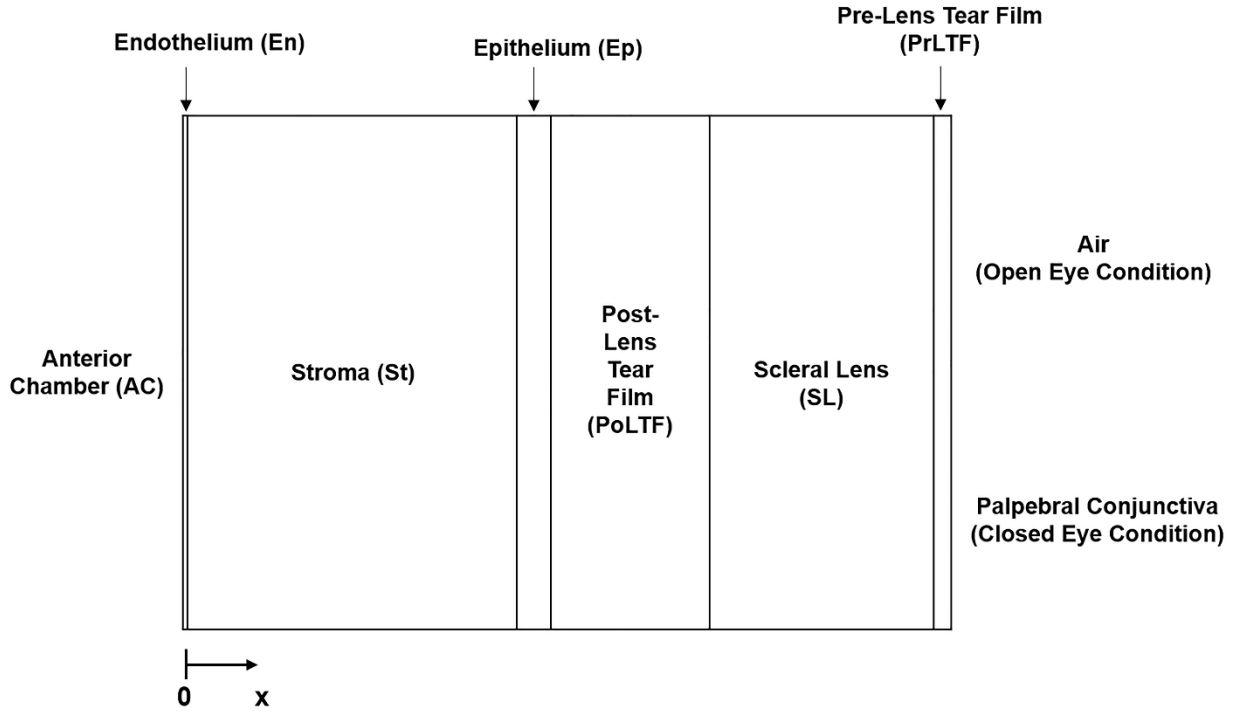

Figure 2.1. Schematic of the cornea-scleral lens geometry including cornea, thick post-lens tear film, thick scleral lens, and pre-lens tear film.

Two variations are made to the analysis of Leung et al.[5] First, water-hydration profiles across the cornea determined by Leung et al.[5] exhibit very small changes. Total water content varies with oxygenation, but is essentially a constant across the cornea. It follows that steady water flow across the cornea is minimal.[5,11] Thus, following Li and Tighe,[11] we invoke zero water flux.

Under this approximation, metabolite fluxes and hydraulic pressure differences across the En and Ep are given by the following Kedem-Katchalsky expressions, respectively.

$$J_i = -\omega_i(RT\Delta C_i + z_i < C_i > F\Delta\psi) + J_{ai} \tag{2.1}$$

$$\Delta P = \sum_i \sigma_i(RT\Delta C_i + z_i < C_i > F\Delta\psi) \tag{2.2}$$

Here, J_i is the molar flux of solute species i, ω_i is the membrane permeability of solute i, J_{ai} is the active flux of solute species i, σ_i is the reflection coefficient of solute i, R is the ideal gas constant, T is the absolute temperature, ΔC_i is the i solute fluid concentration difference across the membrane, z_i is the valence of solute i, $< C_i >$ is the mean of the solute fluid concentration difference across the membrane, F is the Faraday constant, and $\Delta\psi$ is the electrostatic-potential difference across the membrane. Once Equation 2.2 is satisfied, swelling of the cornea follows from the swelling-pressure measurements of Hedbys and Mishima[98]

$$\Delta P = P - IOP = -\gamma e^{-H_w} \tag{2.3}$$

where IOP is the intraocular pressure, P is the pressure in the St, γ is an empirical fitting constant, and H_w is water hydration. Corneal thickness, and hence, swelling follows from mass balance. The first term in the summation on the right of Equation 2.2 and Equation 2.3 are pivotal to predict the role of oxygen in corneal swelling. Because of the metabolic reactions, lactate and bicarbonate-ion concentrations at the endothelium/stroma interface change significantly with local oxygen tension. These changes induce swelling-pressure variations at the endothelium, which, in turn, swell or deswell the cornea.

The second model alteration from that of Leung et al.[5] arises from the larger PoLTF thickness under SLs. Because a temperature difference exists across the relatively thick PoLTF, natural convection is possible there, similar to that occurring in the AC.[111] Appendix 2B presents a quantitative argument establishing that even in a 400-μm thick PoLTF, natural convection is minimal. Hence, we adopt diffusion as the dominant transport mode in the PoLTF.

In addition, aqueous species that transport across the Ep but are not soluble in a rigid SL must accumulate in or deplete from the near-stagnant PoLTF.[86] For these particular species, steady transport is not possible. To overcome this limitation, we investigated the swelling effects of hydrogen, hydroxide, sodium, and chloride ions in the PoLTF. Varying the PoLTF concentrations of these species over a large range resulted in imperceptible swelling changes. Therefore, the PoLTF concentrations of these four species were set to those in standard ophthalmic saline solutions (0.9 wt% NaCl, pH = 7.6). Glucose and lactate concentrations in the PoLTF were taken as zero because of the high resistance to transport of these two species across the epithelial layer and because of their trace amounts found in human tear.[5,12] Finally, using the transport model, we estimated the flux of bicarbonate into the PoLTF caused by transport of carbon dioxide across the corneal Ep.[6] Resulting bicarbonate concentration in the PoLTF rose from 0 to 4 mM over 8 h. Corneal-swelling change induced by a 4-mM PoLTF bicarbonate concentration was negligible. Therefore, bicarbonate concentration in the PoLTF was also set to zero and buffering equilibrium of bicarbonate in the post-lens tear was not considered.

The resulting set of highly nonlinear, algebraic, coupled ordinary differential equations was solved numerically by centered finite differences and Newton iteration to obtain concentration profiles of the chemical species and the hydraulic pressure difference at the AC-En boundary.

Details are available in Appendix A of Leung et al.[5] Calculations were performed in MATLAB R2016b (Mathworks, Natick, MA). To ensure that the model produces accurate estimates, we compared model predictions to the commonly accepted physiological swelling of 4% for no-lens closed eye[5,45] and to previous swelling calculations of Leung et al.[5] for soft-contact lenses. Parameter values in Table 2A.2 reflect this comparison.

Figure 2.2 confirms the importance of lactate and bicarbonate ions in hypoxic edema.[5,8] Figure 2.2A graphs the predicted fall in oxygen tension at the endothelium with declining SL oxygen *Dk/L* for open eye and a PoLTF thickness of 200 μm. Figure 2.2B displays the effect of the oxygen-tension decline on endothelial lactate-ion (solid line) and bicarbonate-ion (dashed line) concentrations. The reason for these changes is that as oxygen tension diminishes, metabolism shifts toward the anaerobic consumption of glucose producing lactate or

$$C_6H_{12}O_6 \rightarrow 2C_3H_5O_3^- + 2H^+ \tag{2.4}$$

The concomitant increase in acidity is buffered by a decline in bicarbonate concentration via the reaction

$$HCO_3^- + H^+ \leftrightarrow CO_2 + H_2O \tag{2.5}$$

Changing lactate and bicarbonate-ion concentrations alter the hydration of the cornea through membrane transport described in Equations 2.1 and 2.2, and through swelling pressure in Equation 2.3. Figure 2.2B highlights that lactate-ion concentration is more sensitive to changes in oxygen partial pressure than is bicarbonate ion.

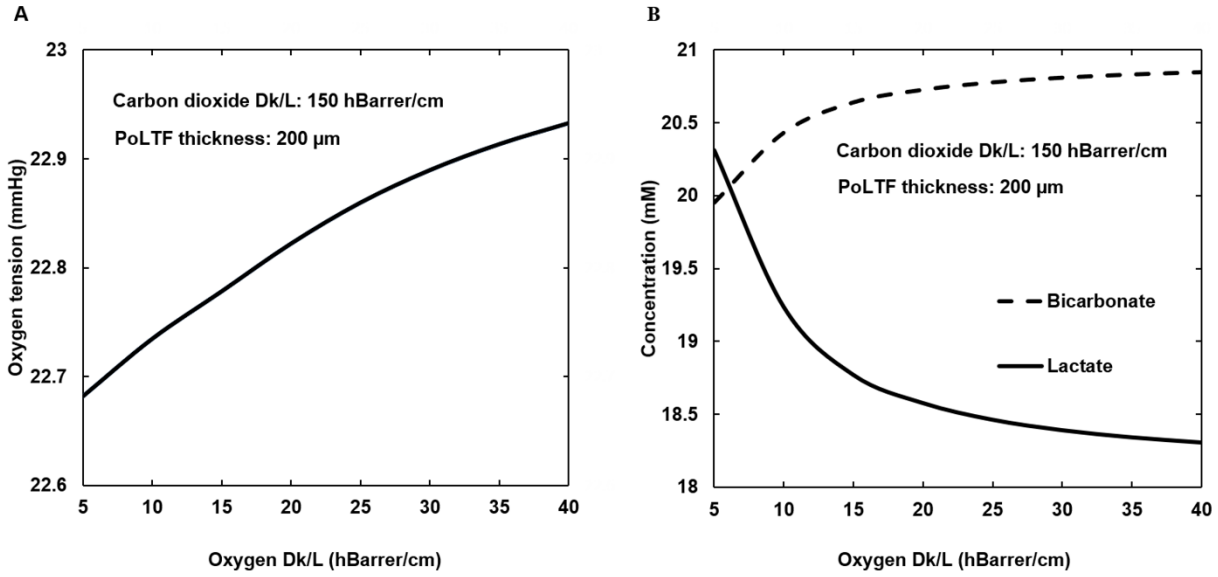

Figure 2.2. Model-calculated endothelial/stromal boundary concentrations as a function of oxygen transmissibility. (A) Oxygen partial pressure; (B) bicarbonate and lactate-ion concentrations.

2.3.2 Clinical Edema

To validate the proposed cornea-edema model, we analyze the recent swelling data of Tan et al.[86] plus new swelling measurements for eight subjects wearing three different commercial lenses of somewhat larger oxygen *Dk/L* values. Five females and three males (Mean ± SD

age = 22.0 ± 2.1 years) with no prior contact-lens wear for at least one year prior to enrollment and were free of ocular disease were recruited from the University of California, Berkeley campus and from the surrounding community. Subject demographics consisted of 50% Asian, 25% Caucasian, 12.5% Indian, and 12.5% Hispanic. Informed consent was obtained from all participants after full description of the goals, potential risks, benefits, and study procedures. This study adhered to the tenants of the Declaration of Helsinki and was approved by the Committee for Protection of Human Subjects, University of California, Berkeley.

Similar to the protocol of Tan et al.,[86] each of the eight subjects participated in four visits with at least 24-h washout between visits. The first visit consisted of ocular-health assessment and lens fitting. Three different commercial SLs with refractive correction were ordered for each subject: Optimum Extra (Dk = 100 Barrer; Contamac, Ltd. Saffron Walden, UK), Boston XO2 (Dk = 141 Barrer; Bausch & Lomb, Rochester, NY), and Menicon Z (Dk = 163 Barrer; Menicon Co., Ltd., Nagoya, Japan). All ordered lenses were 15.6 mm in diameter and had standard spherical curves. The settled-central PoLTF thickness after 5 h of lens wear was measured by OCT (ENVISU 2300, Bioptigen Inc, Durham, NC). Subjects wore the lens on either the right or the left eye; choice of the specific eye, as well as the order of lens type for visits 2–4 were determined randomly.

For visits 2–4, subjects awoke at least 2 h before each visit to ensure that the cornea had deswollen from overnight edema.[45] Subjects discontinued prior usage of topical creams, allergy medications, and eye drops for at least one full day. Immediately after lens insertion, baseline central corneal thickness was measured using OCT. Central lens and PoLTF thicknesses were measured 10 times with OCT throughout the 5-h lens-wear duration. Repeated measurements of the PoLTF thickness throughout the 5-h wear period ensured that the lens had mostly settled within 2 h. Repeated central-lens thicknesses measurements were averaged to determine the central oxygen transmissibility of each lens used in the study. Immediately prior to lens removal, central corneal thickness was measured with OCT. Central corneal swelling for each subject and visit was determined from corneal thickness (after 5 h of wear) minus that at baseline and expressed as a percentage of the baseline value. Lens oxygen transmissibility followed from the manufacture-reported permeability divided by the OCT-measured lens central thickness. Lens thickness varied from about 300–500 μm, resulting in a range of lens oxygen transmissibility from about 20 to 45 hBarrer/cm.

2.4 Results

2.4.1 Model Results

Figure 2.3 reports open-eye swelling of the cornea during SL wear as a function of oxygen Dk/L for five settled PoLTF thicknesses. For the typical settled-PoLTF-thickness range of 100–250 μm, oxygen transmissibility of 25 hBarrer/cm or greater results in corneal edema of less than 1.5%. However, for a settled-PoLTF thickness of 400 μm, oxygen transmissibility must be about 40 hBarrer/cm or greater to maintain corneal edema below 1.5%. Transport modeling predicts that for open eyes, increasing PoLTF thickness from 50 to 400 μm increases central corneal swelling by approximately 1–1.5% when oxygen Dk/L is greater than 10 hBarrer/cm. For settled-PoLTF thickness less than 400 μm, oxygen Dk/L of about 10 hBarrer/cm or less results in swelling greater than that of normal overnight no-lens swelling.

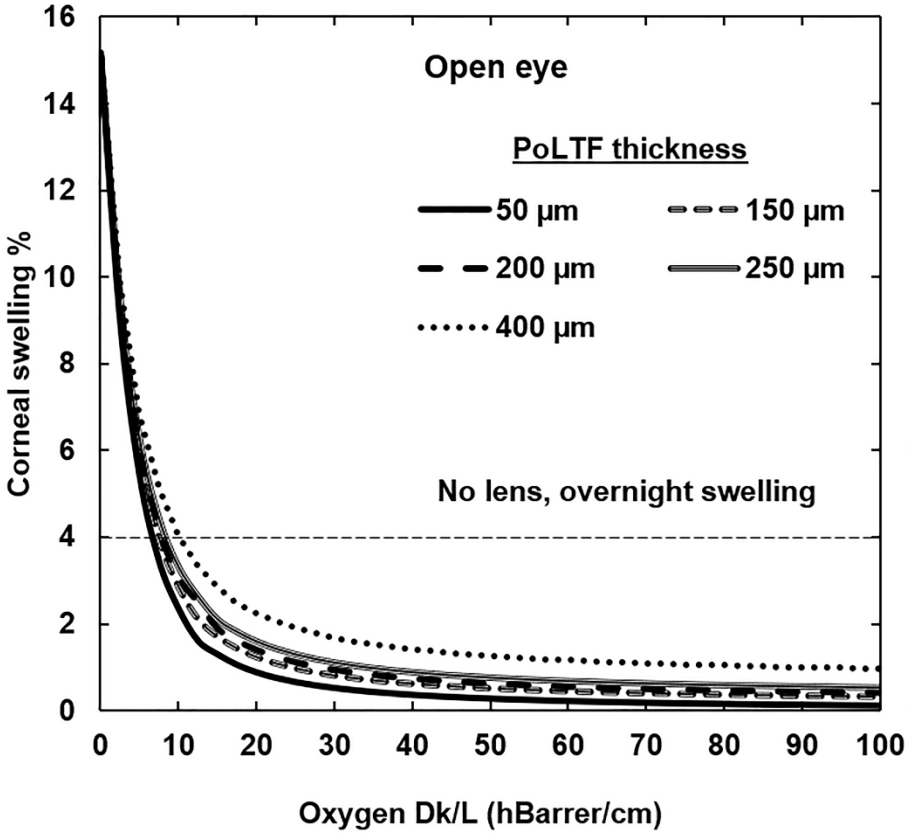

Figure 2.3. Predicted central corneal swelling as a function of lens oxygen transmissibility for open eye. A dashed horizontal line represents the typical amount of swelling for no-lens overnight closed eye. Five curves correspond to settled-PoLTF thicknesses of 50 µm, 150 µm, 200 µm, 250 µm, and 400 µm.

Figure 2.4, however, reveals that closed-eye SL wear results in corneal edema above physiologic. Even at large values of oxygen transmissibility, corneal swelling lies considerably above the overnight 4% value. Also with closed-eye wear, the PoLTF thickness has more significant impact on edema than for open-eye wear. There is up to a 2.5% increase in swelling for PoLTF thickness between 50 µm and 400 µm, whereas open-eye lens wear induces only up to 1.7% corneal swelling.

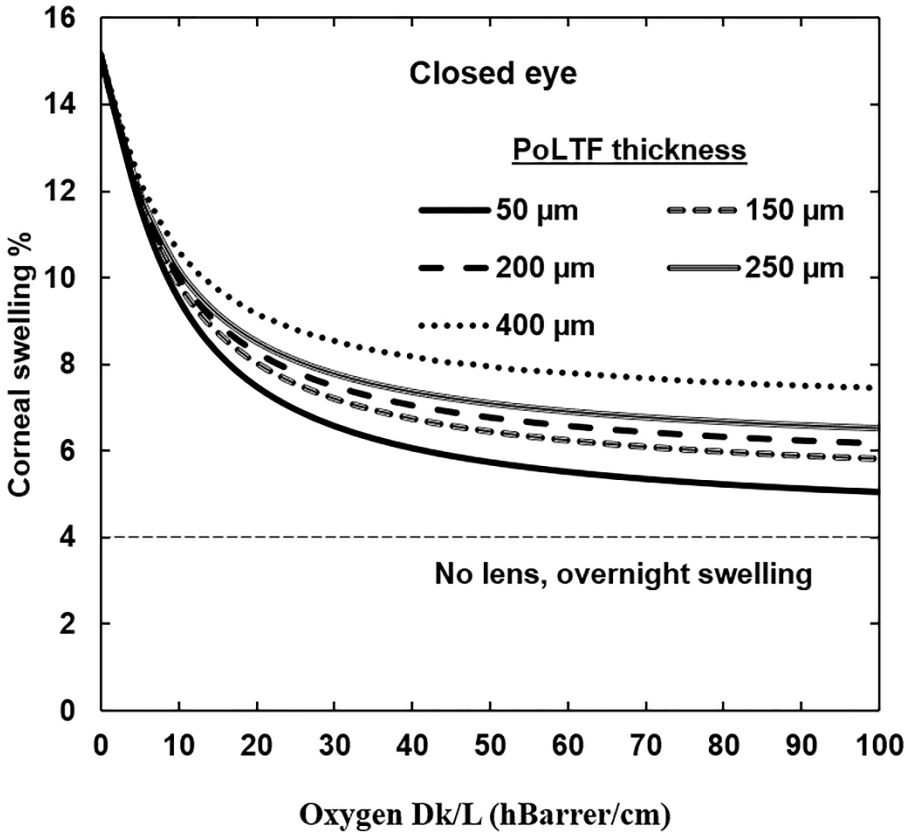

Figure 2.4. Predicted central corneal swelling as a function of lens oxygen transmissibility for closed eye. A dashed horizontal line represents the typical amount of swelling for no-lens overnight closed eye. Five curves correspond to settled-PoLTF thicknesses of 50 µm, 150 µm, 200 µm, 250 µm, and 400 µm.

Figure 2.5 illustrates the role of lens carbon-dioxide transmissibility on corneal swelling during open-eye lens wear for a 400-µm PoLTF thickness and an oxygen *Dk/L* of 25 hBarrer/cm. Percentage swelling in Figure 2.5 includes edema originating from oxygen. Similarly, Figures 2.3 and 2.4 include the effects of carbon dioxide on edema. Rigorous separation of the two effects is not possible due to linked dependence of carbon dioxide and oxygen in corneal metabolism. A closed diamond in Figure 2.5 marks the carbon-dioxide transmissibility utilized in Figures 2.3 and 2.4. Over a large range of carbon-dioxide transmissibilities, there is a 1% change in swelling. Precise estimates of carbon-dioxide *Dk/L* for SLs are not available. However, for the carbon-dioxide permeability range predicted by Fatt et al.[104] for rigid-gas-permeable lenses (i.e., 50–250 hBarrer/cm), there is up to a 0.5% change in corneal swelling.

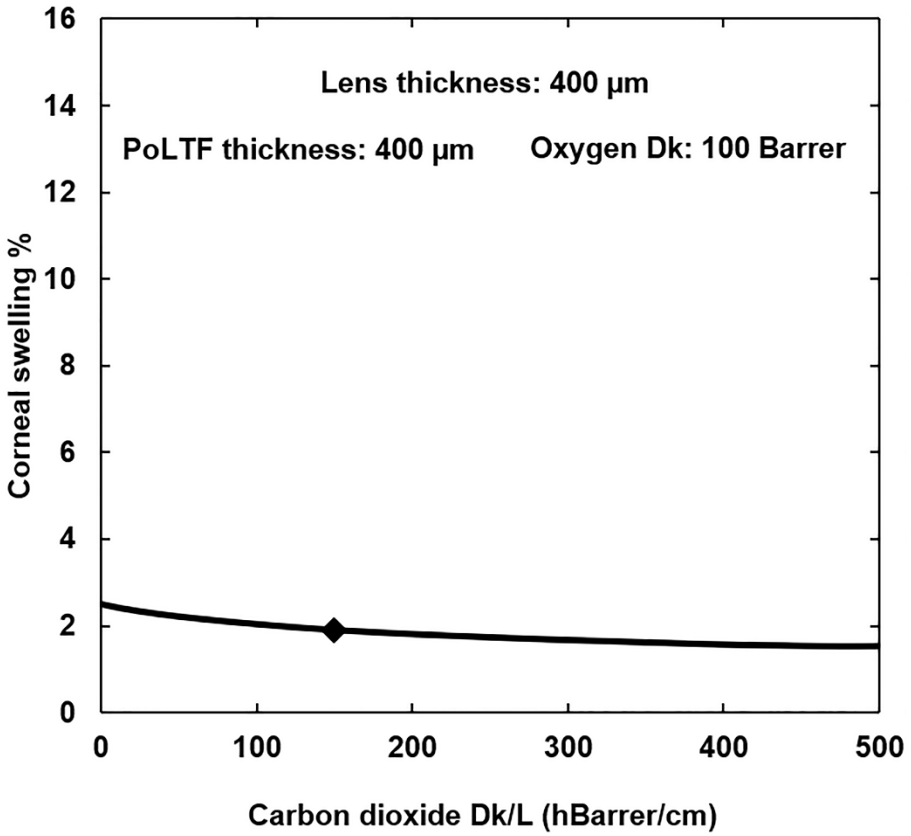

Figure 2.5. Predicted central corneal swelling as a function of carbon-dioxide transmissibility for open eye. Post-lens tear-film and lens thicknesses are both 400 µm; oxygen *Dk* is 100 Barrer. A closed diamond marks the carbon-dioxide transmissibility utilized in Figures 2.3 and 2.4.

2.4.2 Clinical Results

Figure 2.6 shows central swelling for 82 separate OCT measurements as a function of lens oxygen transmissibility. Not all points can be highlighted because they overlap on the scale of the figure. Open circles correspond to the results from Tan et al.[86] while open triangles report current measurements. OCT-thickness precision is about ± 0.5% (i.e., ~3 µm).[91] Settled-PoLTF thickness cannot be controlled clinically. For each lens fit on each subject, final settled-PoLTF thickness varied, sometimes substantially. Thus, it is not possible to investigate preset settled-PoLTF thicknesses. For this reason, data in Figure 2.6 scatter revealing no discernable relationship to PoLTF thickness.

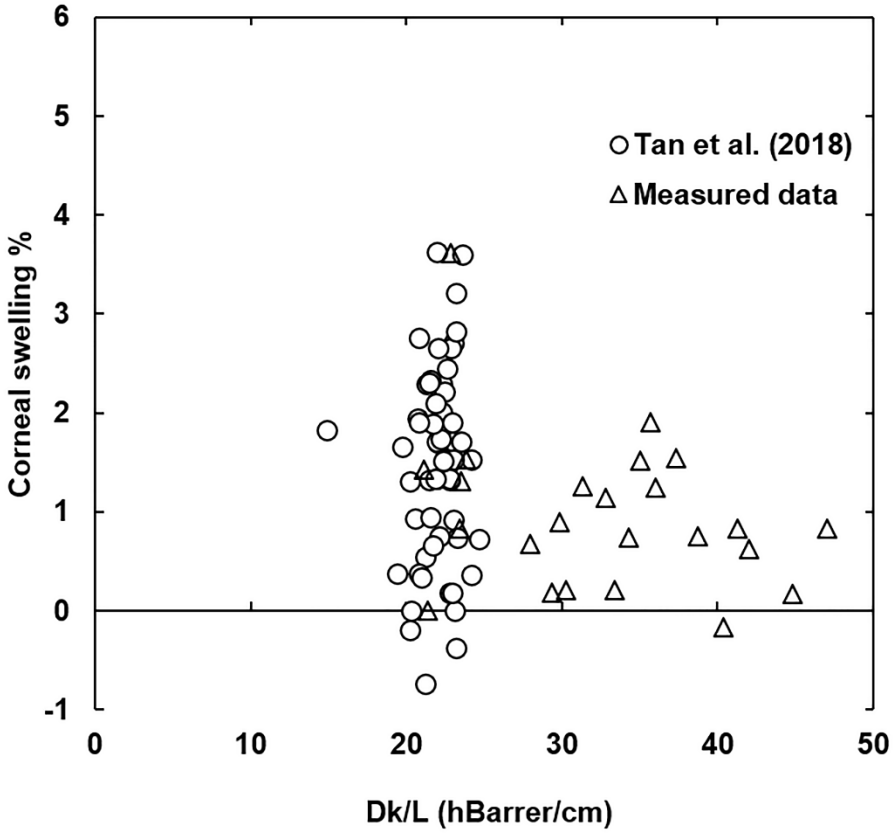

Figure 2.6. OCT-measured central corneal swelling in percent for 82 measurements as a function of scleral-lens oxygen transmissibility in hBarrer/cm. Open circles are from Tan et al.[86]; open triangles are from this study. Four measurements showed deswelling after lens wear. OCT-swelling precision is approximately ± 0.5%.[91] Data scatter is amplified due to differing settled-PoLTF thicknesses.

To overcome this deficiency, we parceled the measured swelling data into eight discrete increments of settled-PoLTF thickness, each with a 50-μm width. Over this increment thickness range, the data of Tan et al.[86] and theory establish that a 50-μm PoLTF thickness range has an insignificant influence on corneal swelling.

Figure 2.7 replots the raw swelling results as function of oxygen *Dk/L* but parceled into PoLTF thickness intervals of 75–125 μm, 175–225 μm, and 375–425 μm, respectively. These ranges were chosen to represent shallow, medium, and steep fits for PoLTF thickness. Results for the remaining PoLTF thickness intervals can be found in Appendix 2C. Solid lines in Figure 2.7 and those in Figure 2C.1 give theory prediction using no adjustable parameters. For each plot, PoLTF thickness in the corneal-edema model was set as the median over that specific range. For those plots with sufficient data, i.e., for Figures 2.7A−C, and Figure 2C.1B, C, and E, theory compares well with experiment. For the PoLTF thickness increments of 25–75 μm and 275–325 μm, data are insufficient in numbers to allow comparison. Nevertheless, even for these cases, agreement with theory is acceptable.

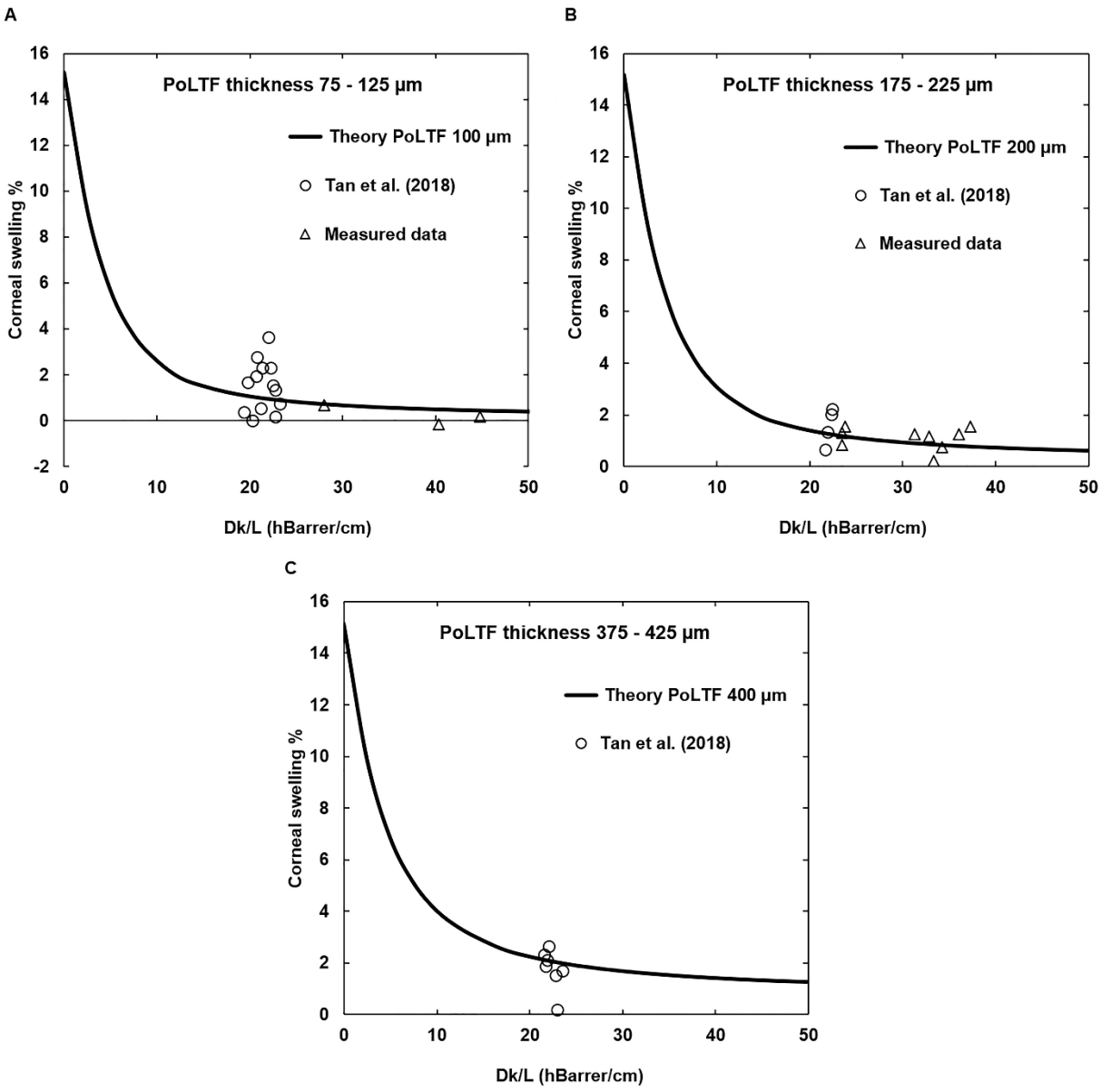

Figure 2.7. Comparison of theory (solid line) to OCT-measured central corneal swelling as a function of scleral-lens oxygen transmissibility for parceled settled-PoLTF thicknesses. (A) 75 −125 µm, (B) 175–225 µm, and (C) 375–425 µm, respectively. Open circles are from Tan et al.[86]; open triangles are from this study. OCT-swelling precision is approximately ± 0.5%. Theory is for median PoLTF thickness of each parcel using no adjustable parameters.

2.5 Discussion

Predicted corneal swelling for open-eye wear of SLs shows that typical settled-PoLTF thicknesses in the range 100–250 µm, and commercially available oxygen transmissibilities provoke less than 2% swelling. Emphasis for preventing hypoxia should focus on oxygen *Dk/L* rather than on the thickness of the PoLTF. This recommendation is especially true for oxygen *Dk/L* less than 10 hBarrer/cm, as Figure 2.3 shows minimal impact of PoLTF thickness

on corneal swelling within that region. When oxygen *Dk/L* is greater than 25 hBarrer/cm, corneal edema is minimal (i.e., less than 2% swelling) during open eye for settled-PoLTF thicknesses up to 400 μm. Figure 2.3 also shows that swelling plateaus above oxygen transmissibilities of about 40 hBarrer/cm. Oxygen transmissibility greater than 40 hBarrer/cm provides little additional benefit in reducing edema for daily-lens wear. In this range of *Dk/L* values, the influence of PoLTF thickness on central corneal edema also is minimal for values below about 250 μm. However, the safety of chronic swelling of the cornea during SL wear (i.e., less than 2% swelling during day lens wear followed by physiological corneal swelling during no-lens-wear overnight sleep) requires further investigation.

Corneal-swelling predictions for closed eye demonstrate that a settled-PoLTF thickness range of 50–400 μm and an oxygen *Dk/L* less than 100 hBarrer/cm cause significant corneal edema. Thus, SL wear during sleep is not recommended, even for healthy corneas. When the cornea is hypoxic, oxygen *Dk/L* and PoLTF thickness both contribute more to corneal edema than when the cornea is not deprived of oxygen.

Because of high water permeability and thin PoLTF and lens thicknesses, the influence of carbon dioxide on corneal edema is minimal for soft-contact-lens wear. However, with SL wear and larger PoLTF and lens thicknesses, the effect of carbon dioxide on corneal edema needs to be revisited. Upon comparing carbon-dioxide transmissibilities of 0 and 500 hBarrer/cm in Figure 2.5, we note a decline of 1% in corneal swelling. The reason for this decrease is that with higher lens carbon-dioxide transmissibility, more carbon dioxide exits the cornea. This exit shifts the chemical equilibrium in Equation 2.5 toward carbon-dioxide production and reduces the concentration of bicarbonate ion in the cornea. Lower bicarbonate-ion concentration at the endothelial layer decreases the swelling pressure in Equation 2.3 and, hence, reduces swelling. In this study, the contributions of lactate and bicarbonate ions to the endothelial pump and, subsequently, to edema are consistent with the *in-vivo* findings of Nguyen and Bonanno.[112]

Within the current precision of OCT-measured corneal swelling, our cornea-edema model for SLs agrees with available swelling data. However, clinical data with controlled settled-PoLTF thickness and lens transmissibility are limited. Further well-controlled studies are warranted. The proposed theory uses no adjustable physical constants. It, therefore, provides a useful tool for evaluating possible hypoxia with SL wear. We find that open-eye wear of SLs by healthy subjects induces clinically acceptable central corneal edema, whereas closed-eye wear for healthy corneas does not. Long term effects of SL wear are not addressed in this study.

2.6 Appendix 2A. Parameters

Tables 2A.1−2A.4 report parameter values used in the calculations.

Table 2A.1. Physical Parameters at the Anterior Chamber and the Tear Films

	Anterior Chamber	PoLTF	PrLTF (open/closed)
P_O (mmHg)	24†	(Solved for)	155†/61.5†
P_C (mmHg)	38‡	(Solved for)	0.5§/38‡
C_{Na} (mM)	146.55‖	150*	150‖
C_{Cl} (mM)	102.85‖	150*	137.9‖
C_B (mM)	36‖	0*	12.1¶
pH	7.6#	7.6*	7.6◊
C_L (mM)	7.7□	0∟	0∟
C_G (mM)	6.9§	0§	0§
P (Pa)	2670⍊	0	0

* Determined by using the model. Explained in Methods.
† Obtained from Brennan.[105]
‡ Obtained from Bonanno et al.[6]
§ Obtained from Fatt et al.[1]
‖ Obtained from Leung et al.[5]
¶ Obtained from Rismondo et al.[106]
# Obtained from Giasson et al.[107]
◊ Obtained from Fischer et al.[108]
□ Obtained from Imre.[109]
∟ Obtained from Klyce.[9]
⍊ Obtained from Klyce et al.[10]

Table 2A.2. Membrane Coefficients for the Endothelium and Epithelium Boundary Layers

Coefficient	Endothelium	Epithelium
σ_{Na}	0.45‡,§	0.79‡,§
σ_{Cl}	0.45‡,§	0.79‡,§
σ_{B}	0.48*	0.79‡,§
σ_{H}	0.45‡,§	0.79‡,§
σ_{L}	0.54*	1‡
σ_{G}	0.45‡,§	1‡
σ_{O}	0.45‡,§	0.79‡,§
σ_{C}	0.45‡,§	0.79‡,§
$\omega_{Na}RT \times 10^{5}$ (cm/s)	8‡,§	0.019‡,§
$\omega_{Cl}RT \times 10^{5}$ (cm/s)	8‡,§	0.019‡,§
$\omega_{B}RT \times 10^{5}$ (cm/s)	8‡,§	0.019‡,§
$\omega_{H}RT \times 10^{5}$ (cm/s)	8‡,§	0.019‡,§
$\omega_{L}RT \times 10^{5}$ (cm/s)	3‡,§	0‡,§
$\omega_{G}RT \times 10^{5}$ (cm/s)	8‡,§	0‡,§
$\omega_{O}k_{O}RT$ (mol O_2 cm/ (s mm Hg cm^3))	15.8×10^{-12}‡	$\frac{D_O k_O}{\Delta x}$†
$\omega_{C}k_{C}RT$ (mol O_2 cm/ (s mm Hg cm^3))	316×10^{-12}‡	$\frac{D_C k_C}{\Delta x}$†
$J_{ai} \times 10^{10}$ (mol/cm^2 s)	-9.4‡ (bicarbonate)	0.16‡ (chloride)

* Adjusted from Leung et al.[5], and Klyce and Russel[10].
† Calculated following Leung et al.[5] ωkRT is set as Dk divided by the mesh size.
‡ Obtained from Leung et al.[5]
§ Obtained from Klyce and Russel.[10]

Table 2A.3: Diffusion and Reaction Parameters of the Corneal-Lens System*

	Endothelium	Dry Stroma	Epithelium	PoLTF	SL	PrLTF
Corneal Thickness (μm)	1.5	78	50	Variable	Variable	3
$D_{Na} \times 10^6$ (cm^2/s)	-	9	9	-	-	-
$D_{Cl} \times 10^6$ (cm^2/s)	-	9	9	-	-	-
$D_B \times 10^6$ (cm^2/s)	-	1.5	0.22	-	-	-
$D_H \times 10^5$ (cm^2/s)	-	1.18	0.19	-	-	-
$D_L \times 10^6$ (cm^2/s)	-	4.4	4.4	-	-	-
$D_G \times 10^6$ (cm^2/s)	-	3	3	-	-	-
$D_O k_O$ (Barrer)	5.3	29.5	18.8	90	Variable	90
$D_C k_C$ (Barrer)	106	590	376	900	Variable†	900
$\mathrm{Q_O^{max}} \times 10^9$ (mol/(cm^3 s))	-	6.28	11.6	-	-	-
$\mathrm{Q_L^{min}} \times 10^9$ (mol/(cm^3 s))	-	24.7	4.83	-	-	-

* Obtained from Leung et al.[5]
† When not varying carbon dioxide *Dk*, 600 Barrer is used.[104]

Table 2A.4. Physical Constants

Parameter	Value
IOP (Pa)	2670*
γ (Pa)	$2.41 * 10^{5}$†
ρ_d (g/cm^3)	1.49‡
ρ_w (g/cm^3)	1.00‡
K_O^O (mm Hg)	2.2§
K_O^L (mm Hg)	2.2§
K_G^O (mM)	0.4§
K_G^L (mM)	0.4§
K_{pH}	0.1§
pK_B	6.04§
s_C (mM/mm Hg)	0.0258§
T (K)	310.5
R (J/(mol K)	8.314
F (C/mol)	9.648×10^4

* Obtained from Leung et al.[5]
† Obtained from Fatt et al.[110]
‡ Obtained from Li et al.[11]
§ Obtained from Chhabra et al.[12]

2.7 Appendix 2B. Diffusion versus Natural Convection in the PoLTF Behind a Scleral Lens

To establish whether species diffusion versus natural convection dominates transport through the PoLTF behind a scleral lens, we estimate Péclet number.[113]

$$Pe \equiv \frac{u\delta}{D} \tag{2B.1}$$

where δ is the characteristic thickness of the PoLTF, u is the characteristic velocity due to natural convection, and D is the diffusivity of the aqueous species. $Pe \leq 1$ indicates that diffusion dominates solute transport and vice versa.[113]

Diffusivities of metabolic species in water are near 2×10^{-5} cm^2/s.[113] The PoLTF thickness (central) was ranged from 100 to 400 μm. To establish the characteristic velocity in the PoLTF, we adopted the simple analysis in Bird et al.[113] of natural convection between two vertical parallel plates with a set temperature difference between them. Thus, we assumed that the cornea and the lens are locally flat with a fixed thickness corresponding to that of the central PoLTF. Bird et al.[113] give the following result for the characteristic (i.e., average) velocity for natural convection between two parallel vertical plates as

$$u = \frac{\rho\beta g\delta^2\Delta T}{192\mu} \tag{2B.2}$$

where ρ is mass density of the tear, β is the coefficient of volume expansion of tear (0.000301/°C), g is gravitational acceleration, μ is the viscosity, and ΔT is the temperature difference between the epithelial-PoLTF interface and the scleral lens-PrLTF interface. To estimate ΔT in Equation 2B.2, we adopt Dursch et al.'s[114] early-time corneal temperature-profile calculations with incorporation of PoLTF and scleral-lens thermal resistances. Specific heat and thermal conductivity of PoLTF were set as 3997 *J/(kg K)* and 0.58 *W/(m K)*, respectively. Lens thickness and density were set as 400 μm and 1185 kg/m^3, respectively.[5,115] Reasonable ranges of the thermal properties of fluorosilicone-acrylate scleral lenses were tested: 1000-3000 *J/(kg K)* for specific heat and 0.1–0.4 *W/(m K)* for thermal conductivity, respectively, as they are not readily available in the literature. We calculate ΔT to be less than 1 °C for PoLTF thicknesses of up to 400 μm. Accordingly, we adopt a 1 °C temperature difference for our estimates of *Pe*. Results for several PoLTF thicknesses are given in Table 2B.1.

Table 2B.1. Calculated Natural-Convection Péclet Numbers

PoLTF Thickness (μm)	Velocity (mm/h)	Péclet Number
100	0.70	0.010
150	1.57	0.033
200	2.79	0.077
250	4.35	0.151
300	6.27	0.261
400	11.14	0.619

Within the typical PoLTF settled-thickness range seen in the clinic, i.e., 100–400 μm, the Péclet number is less than about 0.5. Equation 2B.2 overestimates the characteristic velocity in the

PoLTF because of gap narrowing near the lens periphery. Likewise, our temperature-difference estimate is likely high. Consequently, the assumption appears valid that the PoLTF behind a scleral lens is stagnant.

2.8 Appendix 2C. Comparison Plots for Parceled-PoLTF Clinical Data to the Model

Comparison of theory (solid lines) to OCT-measured central corneal swelling as a function of scleral-lens oxygen transmissibility for parceled settled-PoLTF thicknesses is shown in Figure 2C.1.

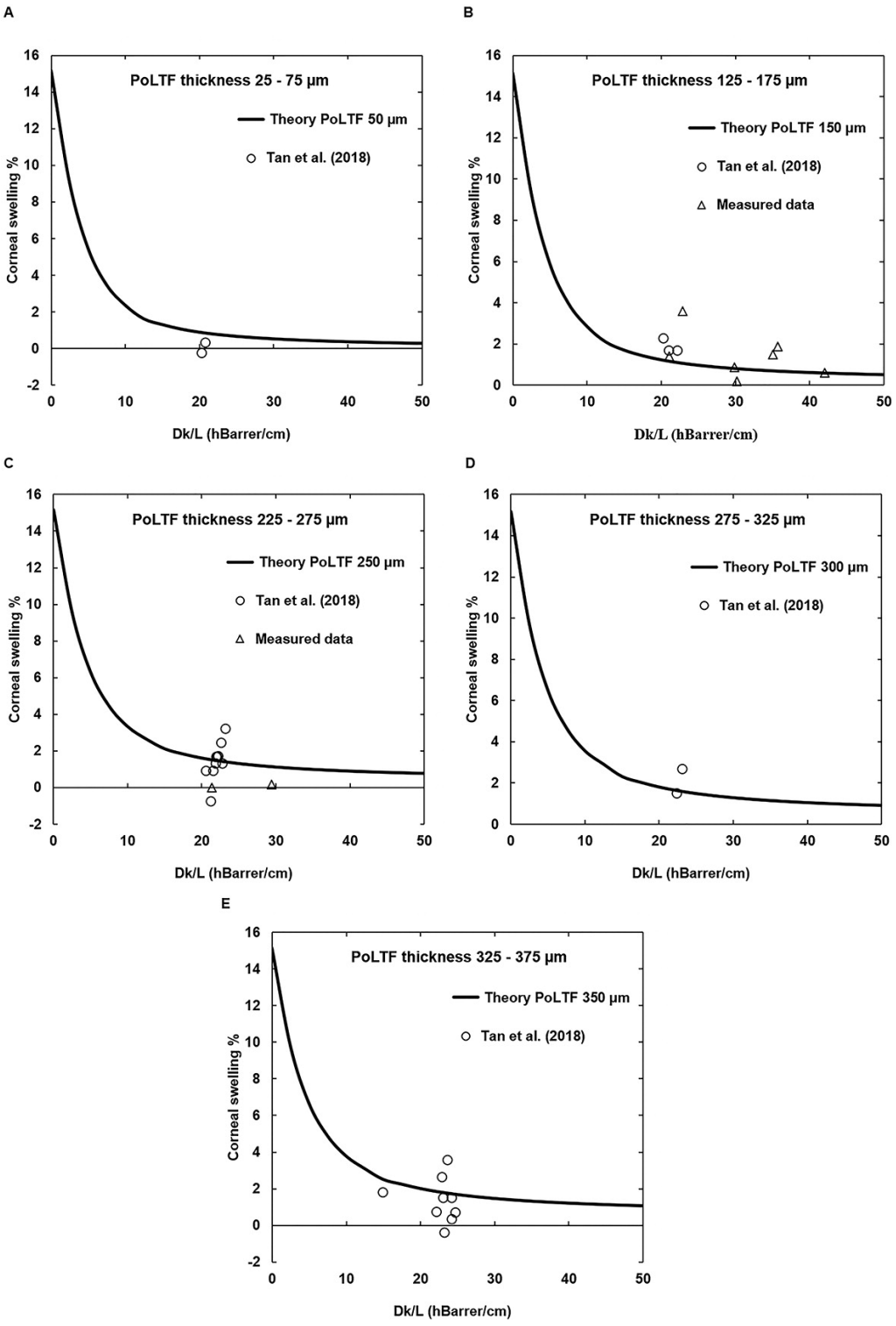

Figure 2C.1. Comparison of theory (solid line) to OCT-measured central corneal swelling as a function of scleral-lens oxygen transmissibility for parceled settled-PoLTF thicknesses. (A) 25–75 µm, (B) 125–175 µm, (C) 225–275 µm, (D) 275–325 µm, and (E) 325–375 µm, respectively. Open circles are from Tan et al.[86]; open triangles are from this study. OCT-swelling precision is approximately ± 0.5%. Theory is for median PoLTF thickness of each parcel using no adjustable parameters.

Chapter 3

Limbal Metabolic Support Reduces Peripheral Corneal Edema with Contact-Lens Wear

Published as: Kim YH, Lin MC, Radke CJ. Limbal metabolic support reduces peripheral corneal edema with contact-lens wear. Transl Vis Sci Technol. 2020;9(7):44.

3.1 Abstract

Purpose: To assess the influence of limbal metabolic support on corneal edema during scleral-lens (SL) and soft-contact-lens (SCL) wear for healthy lens wearers.
Methods: A two-dimensional (2D) model of the cornea and sclera was designed on Comsol Multiphysics 5.4 along with SL and SCL architectures to mimic lens-wear induced hypoxia. The cornea is suffused with oxygen and metabolites from the limbus and aqueous humor. Air oxygen is supplied from and carbon dioxide is expelled to the atmosphere. Lens-oxygen permeability (*Dk*) was adjusted to investigate lens-wear safety against edema in different wear conditions. The 2D concentrations of oxygen, carbon dioxide, bicarbonate, lactate, sodium, chloride, glucose, and pH are quantified. Central-to-peripheral swelling of the cornea is determined by the change in stromal hydration caused by changing metabolite concentrations at the endothelium during hypoxia.
Results: The metabolic model assesses central-to-peripheral corneal swelling with different types of lenses, and oxygen *Dk*s. Limbal metabolic support reduces edema from the periphery to approximately 1 mm away from the central cornea. Despite thicker lens designs, the peripheral cornea exhibits practically zero swelling due to limbal metabolic support.
Conclusions: The metabolic model accurately predicts central-to-peripheral corneal edema with various contact-lens designs, post-lens tear-film thicknesses, and lens oxygen *Dk* values. Despite the thicker periphery of most contact-lens designs, lactate and bicarbonate support from the limbus significantly reduces peripheral and mid-peripheral corneal edema, whereas oxygen has a lesser effect.
Translational Relevance: By utilizing metabolic kinetics, we provide a 2D computational tool to predict oxygenation safety across the entire cornea with various types and designs of contact lenses.

3.2 Introduction

Contact lenses can impede oxygenation of the cornea. Two prominent methods of assessing corneal hypoxia with contact-lens wear are (1) to measure corneal edema caused by hypoxia,[45,116] or (2) to quantify oxygen-tension profiles mathematically by utilizing oxygen-utilization kinetics and diffusion properties of the cornea, tear film, and contact lens.[12,41,117–120] Although mathematical determination of oxygen-tension profiles continues, oxygen-concentration profiles in-and-of themselves do not address contact-lens wear safety. That is, wear safety gauged only by oxygen is inexact because oxygen tension profiles alone do not establish corneal swelling.

Conversely, corneal edema provides a direct gauge of hypoxia.[116] For soft contact lenses (SCLs), Holden and Mertz[45] determined the minimum oxygen transmissibility (*Dk/L*), that is, lens oxygen permeability (*Dk*) divided by lens thickness (*L*), required to avoid central corneal swelling.

Their study was re-evaluated by Harvitt and Bonanno[41] to suggest safe wear for a lens oxygen *Dk/L* of 35 hBarrer/cm (i.e., hectoBarrer/cm) for the open eye and of 125 hBarrer/cm for the closed eye. These recommendations, however, apply only to SCL wear and are not applicable to scleral-lens (SL) wear, which includes additional resistances to oxygen transport due to increased lens and post-lens tear-film (PoLTF) thicknesses.

To connect mathematical oxygen-tension profiles and clinical-edema measurements, Leung et al.[5] devised a metabolic model that directly predicts corneal swelling through reactive-diffusive transport of metabolic products and the hydration pump-leak mechanism of Maurice.[8] Leung et al.[5] focused on SCLs. Kim et al.[121] later extended that work to SL. Both analyses are one-dimensional (1D) and quantify only central corneal edema. They do, however, successfully predict measured central corneal edema.[5,121]

Despite the extensive studies on contact-lens wear and hypoxia, essentially all focus on central corneal edema despite the approximately 35% thicker peripheral cornea that requires higher oxygen demand.[42,122–124] Moreover, oxygen support from limbal vasculature further differentiates oxygen demands of the peripheral and central cornea.[2] Clinically, instrumental limitations result in less reliable measurement of edema at the periphery than at the center.[125–130] Despite the limitations in measuring noncentral corneal edema, several authors conclude that the peripheral cornea exhibits less edema than does the central cornea with similar lens oxygen *Dk/L*.[47,131–133] Mathematically, Alvord et al.[122] and Takatori and Radke[42] calculated the oxygen-tension profiles from central-to-peripheral cornea. However, Alvord et al.[122] did not quantify metabolite transport to determine corneal edema, and Takatori and Radke[42] did not assess the effect of metabolite support from the vascularized limbus.

To understand the effects of metabolic support from the limbus and the higher metabolic demand of the mid-peripheral and peripheral cornea during SCL and SL wear on corneal edema, we extend the 1D works of Leung et al.[5] and Kim et al.[121] to incorporate metabolic support from the limbus. Specifically, we account for metabolic transport from central to/from the peripheral cornea, as well as air oxygen and carbon dioxide to/from the aqueous humor. In so doing, we provide a new tool to predict the oxygenation safety of contact lenses across the entire cornea.

3.3 Methods

3.3.1 Lens and Corneo-Scleral Architecture

Figure 3.1 discloses the geometric parameters of the cornea and sclera along with the designed two-dimensional (2D) corneo-scleral architecture.[122,134,135] Geometric designs, and later metabolic species transport and swelling calculations, are computed using the Comsol Multiphysics 5.4 platform (Comsol, Inc., Burlington, MA). Triangular meshes are utilized in the finite-element analysis. Element size for the mesh is based on the default settings of Comsol. Thicknesses are determined radially.[42,47] Although the human cornea is not precisely symmetric, the small variance in the corneal-thickness profile does not result in significant swelling differences between inferior, superior, nasal, and temporal corneal regions. Therefore, a symmetric 2D model provides precise central-to-peripheral swelling profiles.

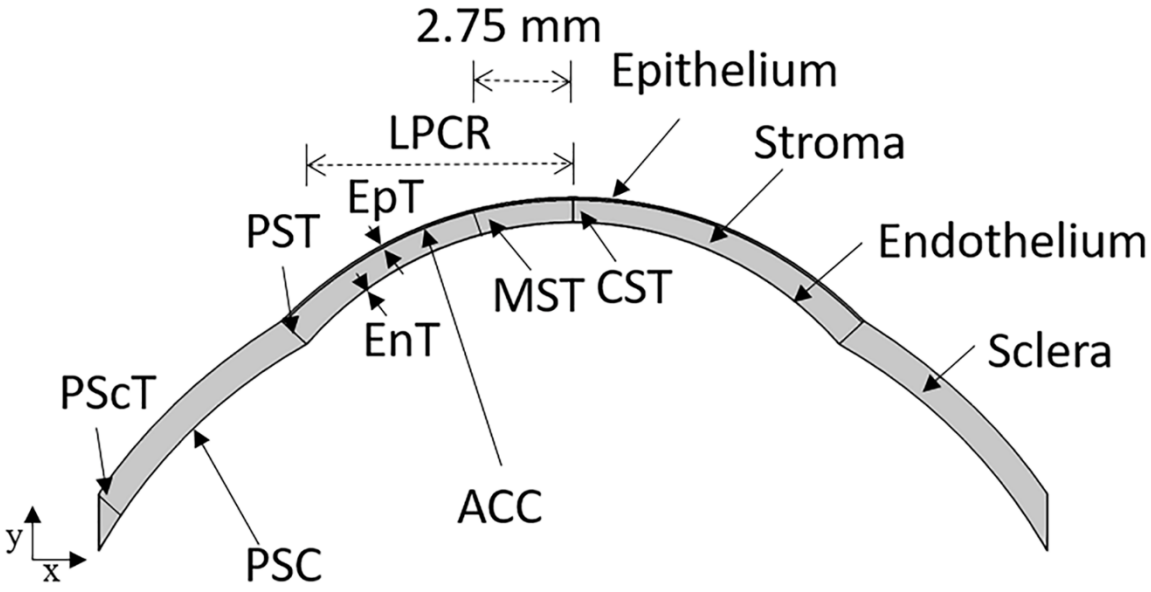

Parameter	Measurement
Anterior Corneal Curvature (ACC)	7.800 mm
Lateral Posterior Corneal Radius (LPCR)	5.617 mm
Epithelium Thickness (EpT)	50 µm
Central Stromal Thickness (CST)	475 µm
Midperipheral Stromal Thickness (MST)	512 µm
Peripheral Stromal Thickness (PST)	677 µm
Endothelium Thickness (EnT)	5 µm
Posterior Sclera Curvature (PSC)	11.500 mm
Peripheral Sclera Thickness (PScT)	602 µm

Figure 3.1. Designed 2D corneo-scleral model. Curvature and thickness parameters of the cornea and the sclera are based on those of Alvord et al.,[122] Grytz et al.,[134] and Sridhar.[135] The peripheral cornea is approximately 35% thicker than that of the central cornea, and the sclera is thinner farther away from the cornea. All corneal thicknesses are reported radially.

Two different types of lenses, SCL and SL, are modeled to assess central-to-peripheral edema with lens wear. Thickness profiles of lens and PoLTF used are shown in Figure 3.2 for the SCL and the SL over the corneal region. With SCLs, central and peripheral lens thicknesses are set as 100 and 180 µm, respectively.[136] As illustrated in Figure 3.2, lens thickness increases from the center to the periphery. The SCL lateral radius is 7.1 mm, and the PoLTF thickness is 3 µm.[12,137,138] Pre-lens tear-film (PrLTF) thickness for both lenses is also set at 3 µm.[12,121,137,138] With SLs, the thickness profile mimics that of a Jupiter Scleral Lens (15.6-mm diameter; 97 Barrer; 1.44 refractive index; –6.00 diopter) measured with a Phasefocus high-precision Lens Profiler (Phasefocus Ltd., Sheffield, UK). Lens thickness was asymmetric, but the difference was minimal. For the chosen SL architecture, central-settled PoLTF thickness is taken as 410 µm. PoLTF thicknesses elsewhere were determined from the geometry of the lens and the cornea. Central-settled PoLTF thickness for the SL was chosen as a steep fit to assess the safety of the worst-case

scenario for SL wear.[86] Because oxygen *Dk/L* of SCL and SL vary with the changing thickness of the lens, the oxygen *Dk* of the lens was varied in our calculations as it is a material property commonly reported by lens manufacturers.

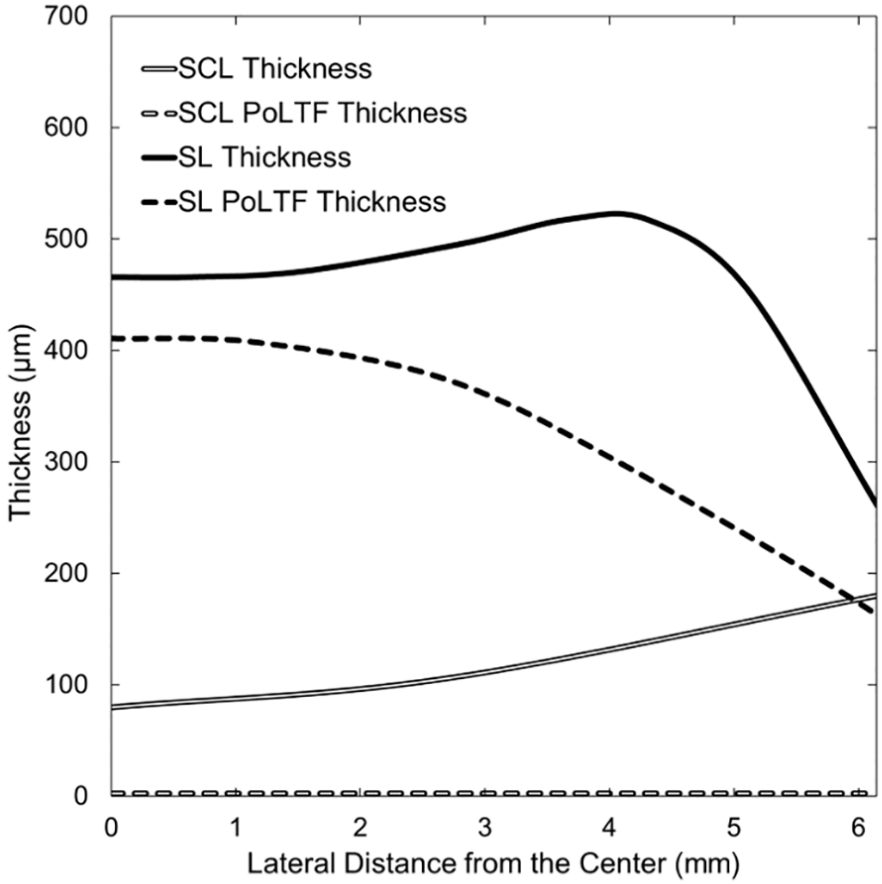

Figure 3.2. Thickness profiles of SL and SCL with respective PoLTF thicknesses. The horizontal axis is the lateral distance from the central cornea (0 mm) to the peripheral cornea (6.15 mm) with the reference point (horizontal axis = 0) being the central cornea at the anterior epithelial surface. The vertical axis represents thickness values determined radially. Thickness profiles were obtained from literature, determined, or measured.[12,121,136–138]

3.3.2 Mathematical Metabolic Model

The metabolic-edema model is explained in detail elsewhere[5,121]; only specifics regarding the 2D model and a brief nonmathematical summary are provided here. Conceptually, hypoxia-induced edema occurs when diminished oxygen concentration shifts glucose metabolism from aerobic to anaerobic. Increased production of lactate and hydrogen ions follows according to the anaerobic reaction

$$C_6H_{12}O_6 \rightarrow 2C_3H_5O_3^- + 2H^+ \quad (3.1)$$

Bicarbonate ions buffer the resulting increase in acidity according to the equilibrium reaction

$$HCO_3^- + H^+ \leftrightarrow CO_2 + H_2O \tag{3.2}$$

The net result is an increase in lactate ions and a decrease in bicarbonate ions because of diminished oxygen supply. Equations 3.1 and 3.2 occur throughout the cornea. The decrease in bicarbonate and increase in lactate ions near the endothelium alter the local osmotic pressure imbibing water through the pump-leak process.[9,139] Accordingly, hypoxia results in higher water retention in the stroma and corneal edema.[121]

The existing 1D metabolic-swelling models of Leung et al.[5] and Kim et al.[121] calculate edema at the center of the cornea only. They do not consider lateral transport of metabolites,[5,121] nor is there metabolic supply/withdrawal from the limbus. In our 2D analysis, lens and PoLTF thicknesses vary from the center to the periphery. Metabolite diffusion occurs in both lateral (*x* axis in Fig. 3.1) and sagittal (*y* axis in Fig. 3.1) directions. Previous Nernst-Planck equations are extended to 2D as follows

$$\boldsymbol{J_i} = -D_i \nabla \mathrm{C_i} - z_i D_i C_i F/(RT) \nabla \psi \tag{3.3}$$

Here, $\boldsymbol{J_i}$ is the vector flux of species *i*, ∇ is the 2D gradient operator in rectangular coordinates (see Appendix 3A), D_i is the diffusion constant for species *i*, C_i is the concentration of species *i*, z_i is the valence of species *i*, *F* is the Faraday's constant, *R* is the ideal gas constant, *T* is the temperature, and ψ is the electric potential relative to the tear film. Equation 3.3 neglects the small water flux across the cornea.[11,121] Subscripts *i* represent the six metabolites directly related to aerobic and anaerobic metabolism, as well as sodium chloride.[5] Metabolites of interest are oxygen, carbon dioxide, bicarbonate, lactate, glucose, and hydrogen ion. Sodium and chloride ions maintain electroneutrality. Temperature is that of the human body: 310.15 K. Diffusion constants are available elsewhere.[5,121] Conservation equations for all aqueous species are expressed in 2D by replacing 1D differentials with the gradient operator. All modified equations are summarized in Appendix 3A.

Information on metabolic supply/withdrawal from the limbus is required in 2D with the introduction of the corneal periphery. Because the limbus is vascularized, metabolic concentrations of the limbus are based on that of blood, as given in Table 3.1.[6,105,107,140,141] The electric potential of the sclera is determined numerically from electroneutrality and the zero-current condition described in Leung et al.[5] In our 2D analysis, reflection coefficients of bicarbonate and lactate ions are 0.53 and 0.65, respectively, compared with those of Leung et al.[5] Remaining parameters, equations, and boundary conditions are unchanged from previous works and can be found in Kim et al.[121]

Table 3.1. Boundary Conditions at the Limbus.

	Limbus
C_{Na}(mM)	130[a]
C_{Cl}(mM)	102.8[a]
C_B(mM)	26[a]
C_L(mM)	1.2[b]
C_G(mM)	6.4[a]
P_O(mmHg)	61.5[c]
P_C(mmHg)	38[d]
pH	7.6[e]|

[a] Obtained from FDA Investigations Operations Manual.[141]
[b] Obtained from Goodwin et al.[140]
[c] Obtained from Brennan.[105]
[d] Obtained from Bonanno and Polse.[6]
[e] Obtained from Giasson and Bonanno.[107]

3.3.3 Comparison to Measured Corneal Edema

The metabolic model compares well to measured central corneal edema in percentage swelling versus oxygen *Dk/L* curves for SCLs[5,45] and for SLs.[121,142] Available periphery or mid-periphery swelling curves are sparse. Instrument imprecision results in less reliable measurement of edema at the periphery than at the center because of the limitations of eye fixation and determination of a repeatable noncentral location before and after lens wear.[125–130] By using ocular coherence tomography, Hitzenberger et al.[143] determined that the error of noncentral corneal thickness is twice that of the central cornea. These limitations also apply to the Schiempflug camera and to ultrasound pachymetry that are also used to measure corneal thickness in vivo. Measurement uncertainty for the earlier mentioned instruments at the noncentral cornea is approximately 6 to 10 μm or 1% to 1.5% of the peripheral corneal thickness.[89–91] Consequently, available instrumentation cannot reliably detect 0% to 2% swelling of open-eye lens wear at the noncentral cornea.

Nevertheless, Wang et al.[47] provide reliable measurement of central-to-peripheral corneal edema. These authors impose extreme hypoxic conditions by employing SCLs with low central oxygen *Dk/L* (i.e., 2.2 hBarrer/cm) worn on patched eyes. These conditions produce more than 4% swelling everywhere on the cornea and, therefore, allow accurate swelling comparison between the central and peripheral cornea. Comparisons of the data of Wang et al.[47] to our metabolic model are given in Figure 3.3 for three lens-thickness profiles: thicker near the periphery (solid line) as illustrated in Figure 3.2, constant thickness (dashed line), and thinner near the periphery (dotted line). Error bars in Figure 3.3 are based on the standard deviations provided by Wang et al.[47] of 3.1% and 2.6% at the center and periphery, respectively. Wang et al.[47] provide only the central oxygen *Dk/L* and no lens thickness profile to assess the noncentral oxygen *Dk/L*. An SCL that thins toward the periphery agrees better with the experimental data, although lenses that either are of constant thickness or that thicken somewhat toward the periphery provide acceptable agreement. Additionally, under extreme hypoxic conditions, swelling is very sensitive to small changes in oxygen tension.[121] Thus, our proposed 2D metabolic model agrees well with clinical central-corneal-edema measurements,[5,45,121,142] and with the swelling-profile data of Wang et al.[47] using consistent parameters.

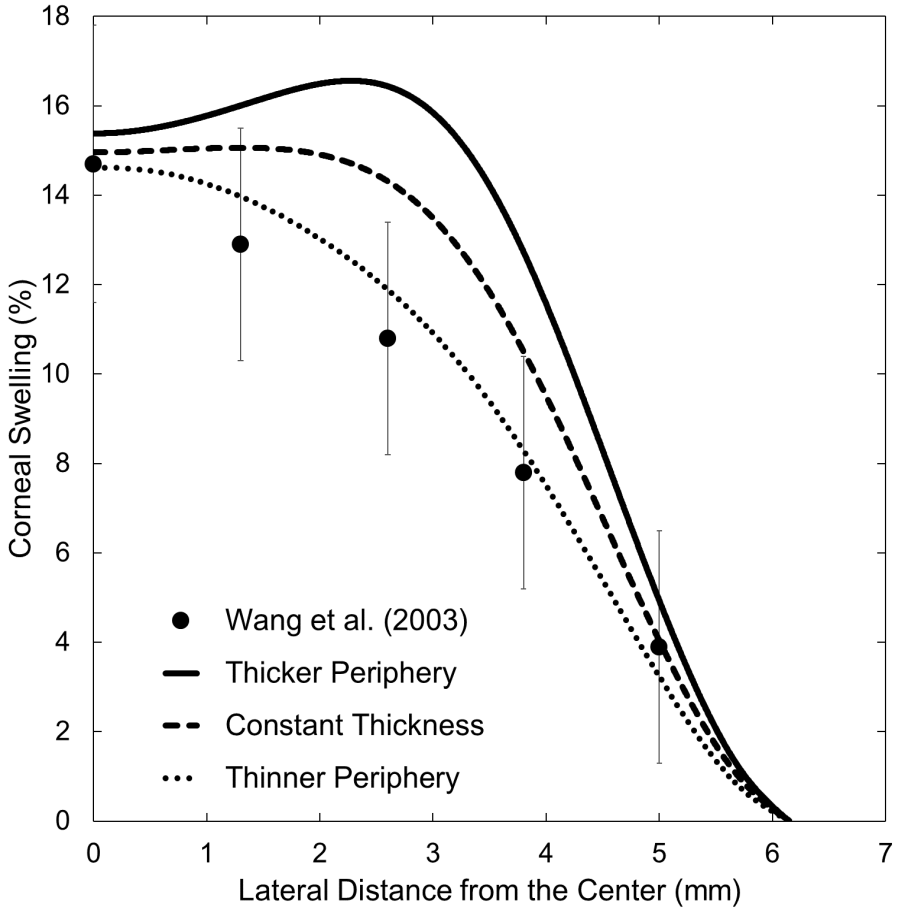

Figure 3.3. Metabolic-model comparison to the experimental corneal-swelling profile of Wang et al.[47] for hydroxyethyl methacrylate SCLs with central oxygen transmissibility of 2.2 hBarrer/cm. Results for three thickness profiles are shown: thickening near the periphery (*solid line*), constant thickness (*dashed line*), and thinning near the periphery (*dotted line*). *Filled circles* and the associated error bars correspond to measurements by Wang et al.[47] Horizontal axis is the lateral distance from the central cornea to the peripheral cornea, with the reference point (horizontal axis = 0) being the central cornea at the anterior epithelial surface. Vertical axis is local percentage corneal swelling due to lens wear.

3.4 Results

Figure 3.4 provides oxygen-tension contours for SL and SCL wear for the parameters described in Methods and with an oxygen *Dk* of 100 Barrer. We define the central-corneal region as up to 1 mm laterally away from the center of the anterior epithelium surface, the mid-peripheral region as 1 to 5 mm laterally away, and the peripheral region as greater than 5 mm laterally away to the limbus. SL wear exhibits more oxygen deprivation in Figure 3.4 because the resistance to oxygen transport from the environment is higher than that for SCL wear. Oxygen supply from the limbus to the cornea is qualitatively apparent with both types of lens wear. Figure 3.5 provides concentration contours of the remaining metabolites directly related to aerobic and anaerobic metabolic reactions for SL and SCL wear with 100 Barrer oxygen *Dk*. Visually, SCL wear exhibits higher levels of bicarbonate, glucose, and pH and lower levels of carbon dioxide and lactate than

does SL wear throughout the cornea. These findings are anticipated because of the larger oxygen transport resistances of SLs versus SCLs.

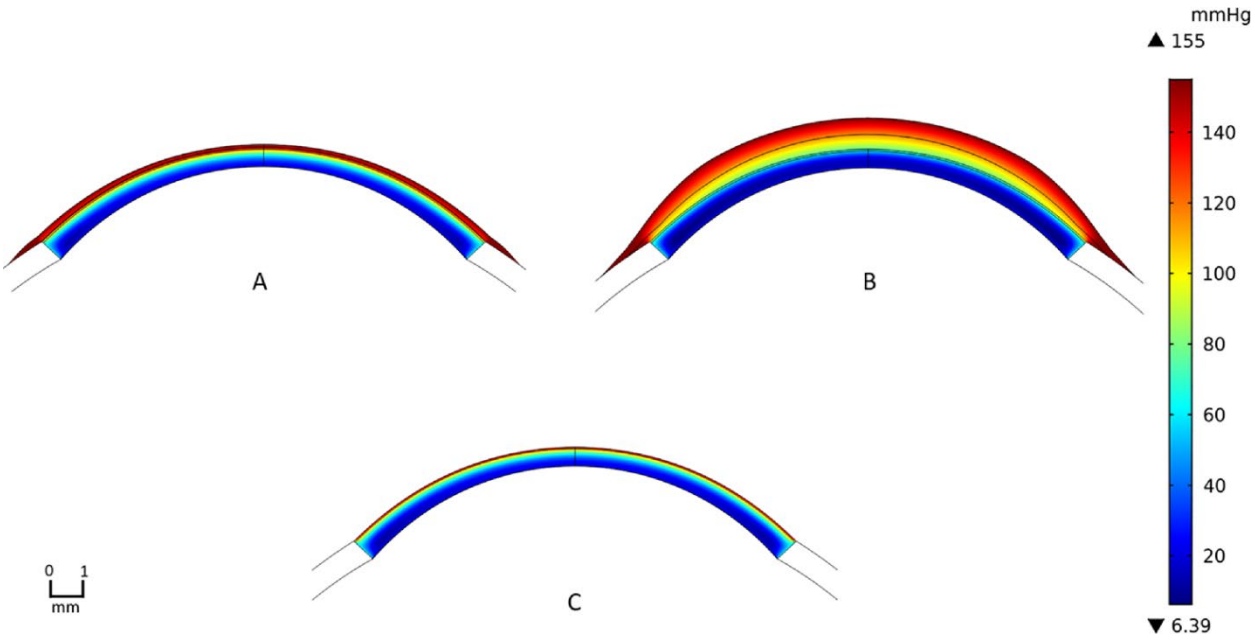

Figure 3.4. 2D oxygen-tension contours for contact lens and corneal system: (A) is SCL wear, (B) is SL wear, and (C) is no lens wear. Contour for the sclera is not displayed as the oxygen tension is set to be that of the blood. Oxygen permeabilities for both lenses are 100 Barrer. Lens and PoLTF thickness profiles are provided in Figure 3.2. Colors are interpreted from the vertical bar on the right. *Red color* indicates high oxygen tension and *navy color* indicates low oxygen tension. The unit of oxygen tension is mm Hg.

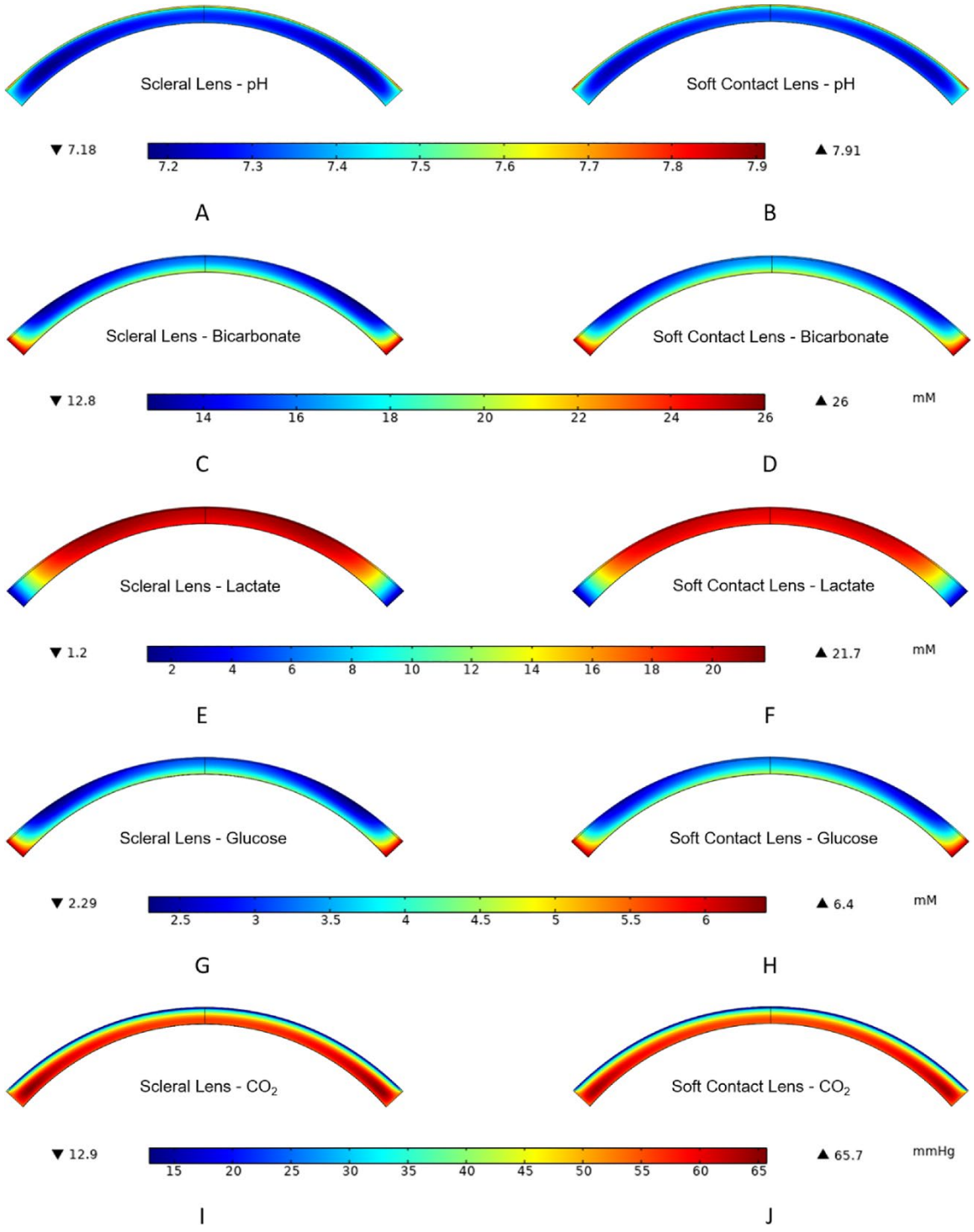

Figure 3.5. Corneal contour graphs for bicarbonate, lactate, glucose, pH, and carbon dioxide for the cornea during SL wear (A, C, E, G, I) and SCL wear (B, D, F, H, J). Oxygen permeability for both lenses is 100 Barrer; thickness profiles are provided in Figure 3.2. Only profiles in the cornea are provided, as the transport of most metabolites across the lens is minimal; the concentrations at the sclera are set to those of blood. The color legend for each row is directly below that respective row. *Red color* indicates high concentration, tension, or pH; and *navy color* indicates low concentration, tension, or pH. The unit of carbon-dioxide tension is mm Hg. Units of glucose, bicarbonate, and lactate are millimolar (mM).

Figure 3.6 displays concentration profiles of lactate and bicarbonate ions from central-to-peripheral cornea at the endothelium for SL and SCL wear. Because SL wear incurs larger hypoxia than does SCL wear, these concentration profiles demonstrate that, in obedience to Equations 3.1 and 3.2, increased hypoxia increases lactate concentration at the endothelium, whereas bicarbonate concentration decreases. In both profiles, the effect of hypoxia decreases in the peripheral region due to limbal support. The limbus provides bicarbonate to the cornea and removes lactate. Similarly, glucose is supplied from the limbus, whereas hydrogen ions are removed from the cornea to the limbus. Meanwhile, oxygen and carbon dioxide concentrations at the endothelium correspond to those of the aqueous humor due to minimal resistance to the transport of these two metabolites between the aqueous humor and the endothelium. The peripheral-region endothelium undergoes very little change in metabolic concentrations during hypoxia, whereas significant change occurs in the central region. The significant metabolic concentrations change across the central corneal region but not in the peripheral region during hypoxia is the reason for reduced peripheral swelling despite the greater peripheral resistance to oxygen transport from the atmosphere with some lenses (e.g. SCL in Fig. 3.2) and the thicker cornea in the periphery.

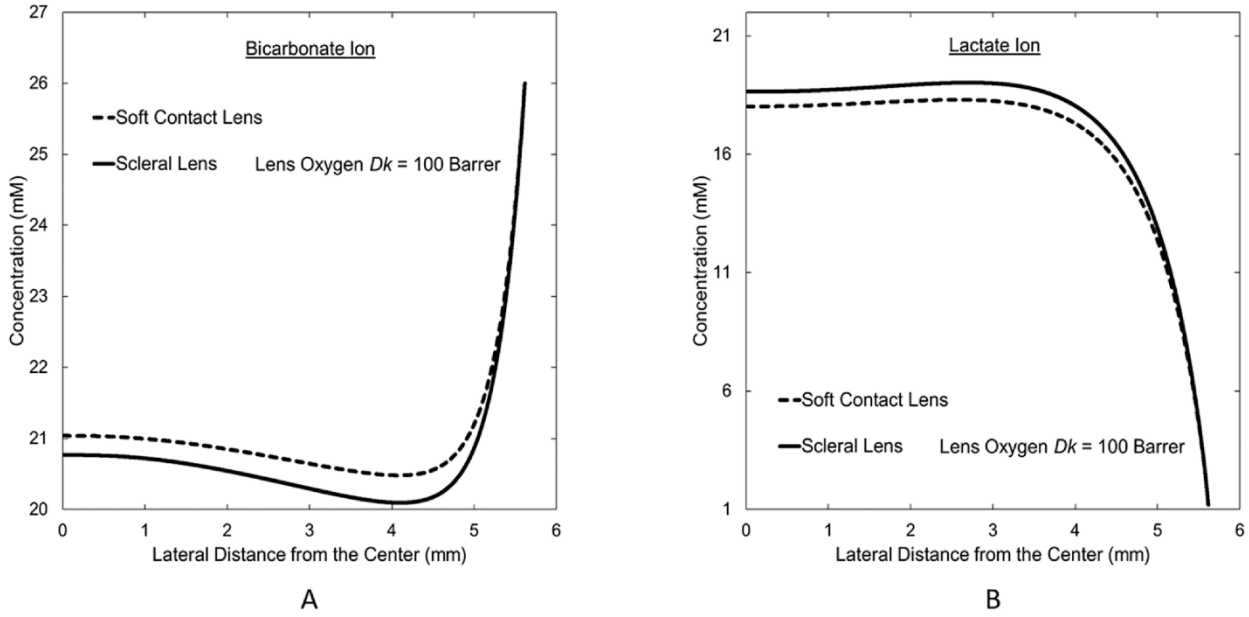

Figure 3.6. Central-to-peripheral concentration profiles at the endothelium for (A) bicarbonate and (B) lactate ions during SCL and SL wear. Vertical axis is the concentration in millimolar (mM). Horizontal axis is the lateral distance from the central cornea with the reference point (horizontal axis = 0) being the central cornea at the endothelial-anterior chamber interface.

Figure 3.7 provides swelling profiles calculated for the SL and SCL of two oxygen *Dk* values with and without limbal metabolic support. Interestingly, limbal metabolic support has a significant effect on mid-peripheral- and peripheral-region swellings, whereas no effect is evident in the central corneal region. Without limbal support, peripheral swelling with SL wear evidences a value greater than physiological overnight swelling of 4%. For both SL and SCL wear, maximum swelling occurs in the mid-peripheral region (i.e., 3–4 mm laterally away from the central cornea at the anterior epithelium surface). The location of the maximum swelling with lens wear depends on lens and PoLTF thicknesses because the localized swelling is determined by

a combination of limbal metabolic support, of difference in localized oxygen demand of the cornea, and of different localized oxygen supply throughout the lens due to different lens oxygen *Dk/L* and PoLTF thickness profile. Maximum swelling, however, is shallow with minimal difference to that of the central cornea.

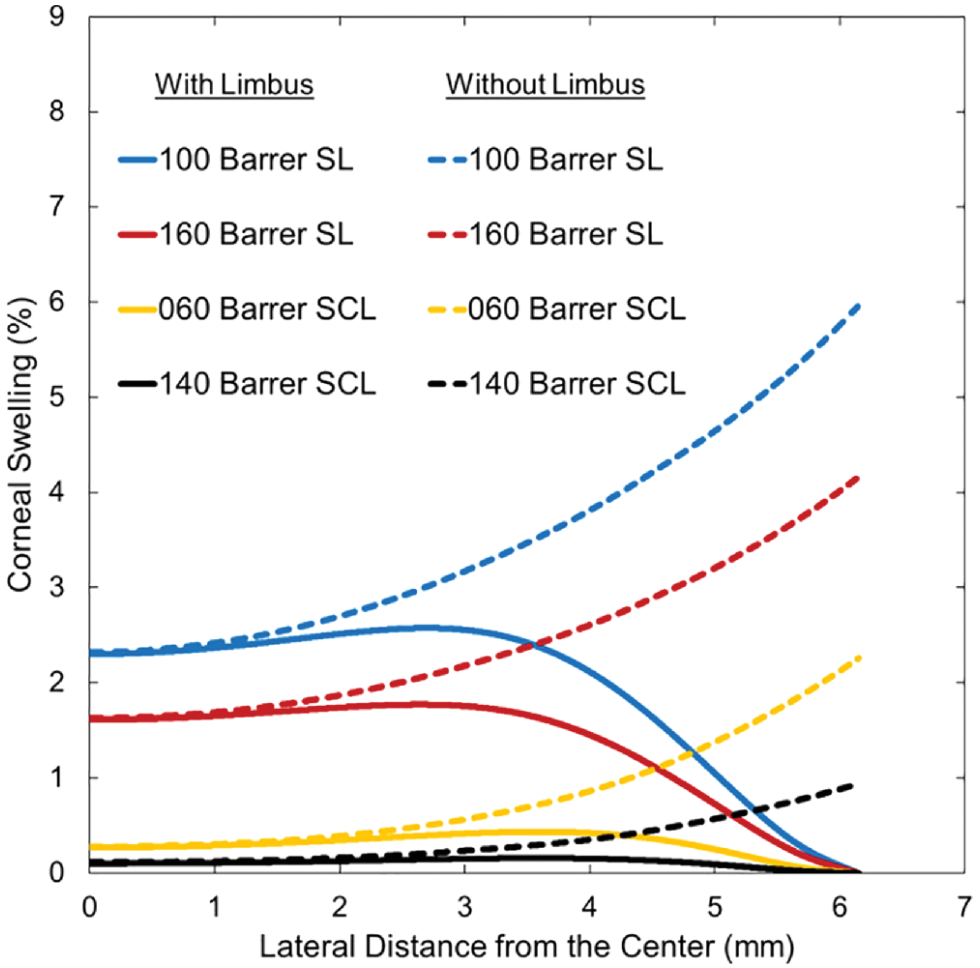

Figure 3.7. Corneal-swelling profiles from the center (horizontal axis = 0) to the peripheral cornea (horizontal axis = 6.15 mm) for SCL and SL wear. *Solid lines* represent predicted swelling with limbal metabolic support, whereas *dashed lines* represent predicted swelling without limbal metabolic support. Horizontal axis is the lateral distance from the central cornea to the peripheral cornea, with the reference point (horizontal axis = 0) being the central cornea at the anterior epithelial surface. Vertical axis is percentage of corneal swelling due to lens wear. Oxygen permeabilities of 100 and 160 Barrer for SLs are *red and blue lines*, respectively. Oxygen permeabilities of 60 and 140 Barrer for SCLs are *yellow and black lines*, respectively.

To assess whether limbal oxygen supply is the primary contributor to minimizing mid-peripheral- and peripheral-region swellings of the cornea during lens wear, comparative calculations were performed between no metabolic support, oxygen only support, and total metabolic support from the limbus. Results for a 100-Barrer oxygen *Dk* for SL wear are shown in Figure 3.8. There is no difference in swelling across the central corneal region because the effect of the limbus reaches only to the mid-peripheral region. Oxygen support from the limbus reduces

peripheral swelling by approximately 1%, whereas the remaining 5% of the peripheral swelling is reduced by remaining metabolites, specifically lactate and bicarbonate ions. In fact, most of the 5% support from nonoxygen metabolites comes from supply of bicarbonate and removal of lactate ions from the limbus. Although the percentage of swelling reduced by limbal support varies with the lens oxygen *Dk/L* and type, the significant effect of limbal bicarbonate and lactate support is consistent for all types of lens designs.

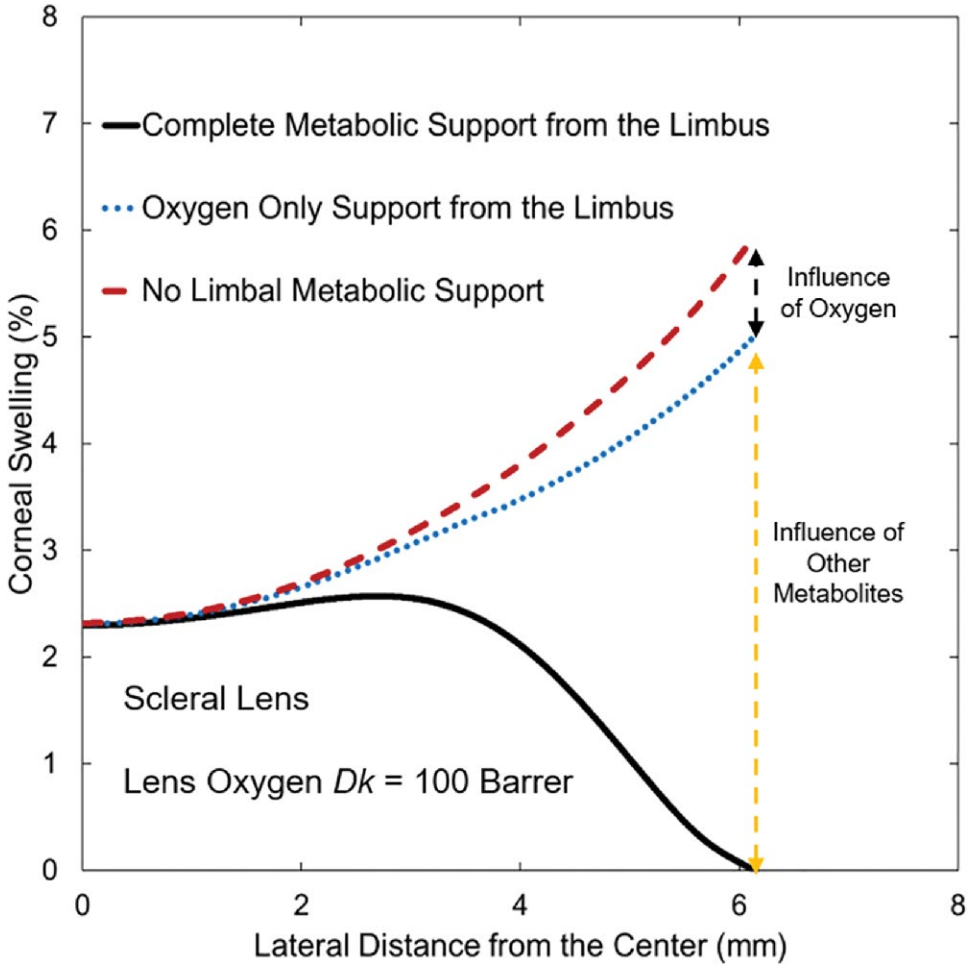

Figure 3.8. Predicted central-to-peripheral corneal-swelling profiles for 100-Barrer oxygen permeability SL wear indicating the contributions from limbal support. Horizontal axis is the lateral distance from the central cornea to the peripheral cornea, with the reference point (horizontal axis = 0) being the central cornea at the anterior epithelial surface. Vertical axis is percentage of corneal swelling. *Red dashed line* is for no metabolic support from the limbus; *blue dashed line* is for only oxygen support from the limbus; *black line* is for total metabolic support from the limbus.

3.5 Discussion

Figures 3.4 and 3.5 show expected metabolic behavior to different hypoxic conditions. Despite the same oxygen *Dk* of both lens types, the thicker lens and PoLTF of SLs result in increased resistance for oxygen delivery to the cornea. Thus SL wear shifts metabolism to more anaerobic reaction per Equation 3.1 than does SCL wear. This is apparent in Figures 3.5 and 3.6

in which there is a higher concentration of lactate and a lower concentration of bicarbonate with SL wear than with SCL wear. The changes in lactate and bicarbonate concentrations during hypoxia regulate the pump-leak mechanism and control swelling of the cornea.[5] Therefore, oxygen supply from the atmosphere has an indirect effect on reducing swelling of the cornea. Lactate and bicarbonate concentrations primarily regulate edema.

Because the cornea thickens from the center to the periphery, the demand for oxygen rises in the peripheral region relative to that in the central region.[42] Without limbal metabolic support, corneal swelling is the least at the center and grows steeply toward the periphery, as shown by the dashed lines in Figure 3.7. Reduction of this rapid rise is accomplished by metabolic support from the limbus. Supply of oxygen from the limbus indirectly reduces edema in the mid-peripheral and peripheral cornea similar to oxygen supply from the atmosphere. Figure 3.8, however, reveals that the effect of increased oxygenation from the limbus on edema is minor compared with the direct supply of bicarbonate and removal of lactate ions from the limbus. Surprisingly, the influence of limbal support in reducing edema is observed from the periphery to approximately 1 mm laterally away from the central cornea. Predicted corneal swelling profiles in Figure 3.7 show that limbal metabolic support has a significant effect in regulating stromal swelling for all types of contact-lens wear.

Papas[2] reported that limbal blood flow increases during hypoxia. His observation is consistent with our findings. Because concentration differences between the limbal vasculature and the peripheral cornea is greater during corneal hypoxia, blood cells in the limbus deplete nutrients and carry away excess lactate at a faster rate than during normoxia. The body increases limbal blood circulation to expose more metabolite-fresh blood cells. Faster blood flow during contact-lens wear, quantified by Chen et al., further supports this explanation.[144] Limbal metabolic support rather far into the cornea is not inconsistent with neovascularization during prolonged hypoxia. Even though the peripheral cornea is adequately suffused by the limbus, the limbal effect on edema is minimal at approximately 1 mm laterally away from the central cornea. Therefore, if the mid-peripheral region and/or the central corneal region is chronically hypoxic where the limbus cannot provide adequate support, new blood vessels will form in the peripheral region to provide sufficient nutrients to the central hypoxic regions.

Figure 3.7 reveals that the maximum swelling of the cornea occurs in the mid-peripheral region of the cornea. However, for current commercial contact lenses, oxygen *Dk/L*s of the lens center and the mid-peripheral region are not different enough to cause a meaningful difference in swelling compared with that at the center during open-eye wear. That is, the maximum in swelling is shallow. Previous clinical[45,86,87,142] and mathematical-modeling efforts[5,121] of central corneal edema, therefore, provide satisfactory gauges of maximum edema during contact-lens wear for open eye. However, as the effect of oxygen tension on edema is significantly greater during extreme hypoxic states (e.g., closed-eye with lens oxygen *Dk/L* <20 hBarrer/cm for SL and <15 hBarrer/cm for SCL wear),[45,121] a small difference in lens oxygen *Dk/L* from the center to mid-periphery may result in a large difference in edema between those regions if the cornea is undergoing significant hypoxia. For example, the model predicts a difference of approximately 1% swelling between dashed and dotted lines at approximately 1 mm away from the central cornea in Figure 3.3 despite a small difference of oxygen *Dk/L* (e.g., <0.5 hBarrer/cm) in that region. Because lens oxygen *Dk/L* can vary by more than 2 hBarrer/cm between the center and the mid-peripheral regions based on our SL thickness profile (Fig. 3.2), his could result in a significant difference in localized swelling. Therefore, detailed analyses of central-to-peripheral corneal

edema may be warranted for closed-eye lens wear, as well as for lenses with significant regional variations in lens oxygen *Dk/L*.

We examined here only two different lens types with two different oxygen *Dk/L*. However, our model is capable of testing any lens type, design, shape, and oxygen *Dk*, as well as any PoLTF thickness profile. Also possible is the calculation of overnight lens-wear swelling. Metabolic support from the limbus with overnight lens wear behaves similarly to open-eye wear: 0% peripheral swelling with the central and mid-peripheral regions exhibiting greater than 4% swelling due to increased hypoxia. Our current model applies to healthy lens wearers with a healthy endothelium and limbus. However, with more information on diseased eye's metabolic transport through the endothelium and limbus, the metabolic model can be extended to determine lens-wear swelling for nonhealthy eyes.

Currently, the metabolic model does not incorporate tear exchange occurring with SCL wear[145] and potential tear circulation[121,146] with SL wear. Both mechanisms potentially provide additional support for oxygen delivery to the cornea. As wear of polymethyl methacrylate lenses, which have significantly more tear exchange than SCLs,[145] results in more frequent cases of corneal hazing than during SCL wear,[147] fresh tear exchange at the periphery with SCL wear cannot be a significant source of oxygen. For SL wear, one-third of the subjects from Tse et al.[146] showed no fresh tear entering the PoLTF at the periphery (i.e., no tear exchange). There was no significant swelling differences between those subjects with and without tear exchange. However, tear circulation within the PoLTF for SL wear (Appendix B in Kim et al.[121]) redistributes oxygen from higher lens-oxygen *Dk/L* regions to lower lens-oxygen *Dk/L* regions. Further understanding is needed on the amount of oxygen delivered through tear exchange with SCL wear and on tear circulation within the PoLTF for SL wear. Because both mechanisms aid transport of oxygen to the cornea, our metabolic model provides a conservative estimate of corneal swelling.

To our knowledge, the proposed metabolic-edema model provides the first quantitative assessment of limbal metabolic support in reducing mid-peripheral and peripheral corneal edema. Corneal edema with contact-lens wear results in different localized swelling. Differences in localized swelling arise from the combined effects of oxygen *Dk/L* of the lens, PoLTF thickness profile, difference in localized oxygen demand of the cornea, and metabolic support from the limbus and anterior chamber. Because of the possibility of considerable lateral variations in swelling due to significant localized differences in lens oxygen *Dk/L* (e.g., with multi-*Dk* component contact lenses) and because of the possibility of small changes in oxygen *Dk/L* causing drastic changes in corneal swelling during sleep,[121] it is prudent to consider localized corneal edema when assessing lens-wear safety for contact lenses with embedded components or during closed-eye wear.

3.6 Appendix 3A. 2D Metabolic Conservation Equations

This appendix extends the 1D metabolic model of Leung et al.[5] to 2D. Only those variables that have changed are introduced. We neglect water flow through the cornea so that use of the dry coordinate, ξ, is not necessary.[5,121] Metabolic conservation of oxygen in the cornea is given in Equation 3.A1; the conservation equation for oxygen in the PoLTF, contact lens, and the PrLTF is given in Equation 3.A2. The difference in conservation equations between the different regions owes to the lack of metabolism in the PoLTF, the contact lens, and the PrLTF. A more detailed explanation can be found in the previously published work.[5]

$$-\nabla \cdot \boldsymbol{J_O} - Q_O^{max}\left[1 + 0.8(7.6 - pH)/(K_{pH} + 7.6 - pH)\right] * [C_G/(K_G^O + C_G)][P_O/(K_O^O + P_O)] = 0 \quad \text{Cornea} \quad (3.A1)$$

$$-\nabla \cdot \boldsymbol{J_O} = 0 \quad \text{Elsewhere} \quad (3.A2)$$

Here, $\boldsymbol{J_O}$ is the 2D vector molar flux of the oxygen and ∇ ($\equiv \frac{\partial}{\partial x}\hat{e}_x + \frac{\partial}{\partial x}\hat{e}_y$) is the 2D vector gradient operator with $\hat{e}_x$ and $\hat{e}_y$ the unit normal vectors in the lateral and sagittal rectangular directions, respectively. The dot following each gradient operator represents the scalar or inner product of two vectors. To ensure both sagittal and lateral transport of oxygen, the differential equations account for both directions, rather than just for the sagittal axis. Maximum baseline oxygen reaction rates for different corneal regions, Q_O^{max}, are given in Chhabra et al.[12] while remaining variables in Equation 3.A1 are defined in Leung et al.[5]

Conservation equations for sodium and chloride ions in the cornea read

$$\nabla \cdot \boldsymbol{J_{Na}} = \nabla \cdot \boldsymbol{J_{Cl}} = 0 \quad (3.A3)$$

where $\boldsymbol{J_{Na}}$ and $\boldsymbol{J_{Cl}}$ are vector molar fluxes for sodium and chloride ions, respectively. Because salt transport is minimal across the lens for SCLs and nonexistent for SLs, we do not need conservation statements for the lens, PoLTF, and PrLTF regions.

Conservation of lactate ion in the cornea is given by

$$-\nabla \cdot \boldsymbol{J_L} - Q_L^{min}[1 + K_O^L/(K_O^L + P_O)][C_G/(K_G^L + C_G)] = 0 \quad (3.A4)$$

where $\boldsymbol{J_L}$ is the vector molar flux for lactate ion. Minimum baseline lactate reaction rates, Q_L^{min}, for different corneal regions are given in Chhabra et al.[12] Remaining variables in Equation 3.A4 are defined in Leung et al.[5] There are no corresponding equations for the lens, PoLTF, and PrLTF as metabolism is absent.

Conservation of glucose in the cornea is expressed by

$$-\nabla \cdot \boldsymbol{J_G} - (Q_L^{min}/2)[1 + K_O^L/(K_O^L + P_O)][C_G/(K_G^L + C_G)] - (Q_O^{max}/6)\left[1 + 0.8(7.6 - pH)/(K_{pH} + 7.6 - pH)\right][C_G/(K_G^O + C_G)][P_O/(K_O^O + P_O)] = 0 \quad (3.A5)$$

where $\boldsymbol{J_G}$ is the vector molar flux of glucose. Glucose concentration is negligible in the remaining regions.

Coupled conservation expression for hydrogen and bicarbonate ions provided in Equation 3.A6 follows the same derivation as those in previous works.[5,121]

$$-\nabla \cdot \boldsymbol{J_H} + \nabla \cdot \boldsymbol{J_B} + Q_L^{min}[1 + K_O^L/(K_O^L + P_O)][C_G/(K_G^L + C_G)] = 0 \quad (3.A6)$$

where $\boldsymbol{J_H}$ and $\boldsymbol{J_B}$ are the vector molar fluxes for hydrogen and bicarbonate ions, respectively. Buffering equilibrium reactions in the cornea remain the same as in Leung et al.[5] We neglect bicarbonate buffering in the remaining regions. The small change in bicarbonate ion within the PoLTF has a small effect on the swelling.[121]

Conservation of carbon dioxide obeys the expressions

$$-\nabla \cdot \boldsymbol{J_C} - \nabla \cdot \boldsymbol{J}_B + Q_O^{max}\left[1 + 0.8(7.6 - pH)/(K_{pH} + 7.6 - pH)\right] * [C_G/(K_G^O + C_G)][P_O/(K_O^O + P_O)] = 0 \qquad \text{Cornea} \tag{3.A7}$$

and

$$\nabla \cdot \boldsymbol{J_C} = 0 \qquad \text{Elsewhere} \tag{3.A8}$$

where $\boldsymbol{J_C}$ is the vector molar flux for carbon dioxide. Similar to bicarbonate transport, we neglect carbon-dioxide buffering outside the cornea.

Chapter 4

Central-to-Peripheral Corneal Edema During Wear of Embedded-Component Contact Lenses

Published as: Kim YH, Lin MC, Radke CJ. Central-to-peripheral corneal edema during wear of embedded-component contact lenses. Cont Lens Anterior Eye. 2022;45(1):101443.

4.1 Abstract

Purpose: With active investigation underway for embedded-circuit contact lenses, safe oxygen supply of these novel lenses remains a question. Central-to-peripheral corneal edema for healthy eyes during wear of soft contact (SCL) and scleral lenses (SL) with embedding components is assessed.
Methods: Various 2-dimensional (2D) designs of SL and SCL with embedded components are constructed on Comsol Multiphysics 5.5. Local corneal swelling associated with the designed lenses is determined by a recently developed 2D metabolic-swelling model. Settled central post-lens tear-film thicknesses (PoLTFs) are set at 400 μm and 3 μm for SL and SCL designs, respectively. Each lens design has an axisymmetric central and an axisymmetric peripheral embedment. Oxygen permeability (*Dk*) of the lens and the embedments ranges from 0 to 200 Barrer. Dimensions and location of the embedments are varied to assess optimal-design configurations to minimize central-to-peripheral corneal edema.
Results: By adjusting oxygen *Dk* of the central embedment, the peripheral embedment, or the lens matrix polymer, corneal swelling is reduced by up to 2.5 %, 1.5 %, or 1.4 % of the baseline corneal thickness, respectively, while keeping all other parameters constant. A decrease in PoLTF thickness from 400 μm to 3 μm decreases corneal edema by up to 1.8 % of the baseline corneal thickness. Shifting the peripheral embedment farther out towards the periphery and towards the anterior lens surface reduces peak edema by up to 1.3 % and 0.6 % of the baseline corneal thickness, respectively.
Conclusions: To minimize central-to-peripheral corneal edema, embedments should be placed anteriorly and far into the periphery to allow maximal limbal metabolic support and oxygen transport in the polar direction (i.e., the θ-direction in spherical coordinates). High-oxygen transmissibility for all components and thinner PoLTF thickness are recommended to minimize corneal edema. Depending on design specifications, less than 1 % swelling over the entire cornea is achievable even with oxygen-impermeable embedments.

4.2 Introduction

With the advance of micro-technology, the feasibility of fabricating embedded-circuit contact lenses is under active study to improve visual acuity, display augmented reality, or monitor health.[56–69] However, introduction of various embedments within a contact lens introduces potential risk to ocular health as semiconductor-based embedments typically have low permeability to oxygen.[62] Because the cornea is oxygenated predominately by the environment, localized oxygen impediment from the embedments may lead to significant localized corneal

hypoxia. Corneal hypoxia, in turn, induces swelling of the stroma due to increased anaerobic metabolism and to changes in metabolic concentrations at the endothelium that regulate water flux into/out of the cornea.[5]

Contact lenses made with oxygen-impermeable materials, such as polymethyl methacrylate (PMMA), cause significant corneal edema that adversely affects cornea health.[148] Corneal striae appear when swelling approaches 6–8 %.[149] Cornea clouding is subjectively visible when the cornea swells by more than 5 % due to increased light scattering within the stroma.[150] Moreover, chronic corneal hypoxia induced by 20 years of continuous PMMA contact-lens wear leads to endothelial polymegathism and potentially results in a decline of the cornea's ability to deswell.[151] These clinical risks motivated the development of oxygen-permeable lens materials such as silicone hydrogels and acrylates to minimize corneal hypoxia during contact-lens wear.[41,44,45,87,121,142]

Two prominent methods are available to assess corneal hypoxia. The first is to measure central corneal edema clinically with, for example, ocular coherence tomography (OCT) or ultrasound pachymetry.[47,92] Unfortunately, due to the uncertainty of noncentral corneal measurements,[143] most clinical measurement of edema is performed centrally. This restriction limits measurement of local differences in corneal edema during the wear of contact lenses with circuit embedments. The second assessment method is to model mathematically the oxygen flux through the lens to interrogate oxygen tension across the cornea with various types of lens wear.[42,44,122] However, knowledge of oxygen tension alone does not allow determination of corneal swelling.

To provide direct comparison between mathematical and clinical analyses, Leung et al.[5] utilized metabolic kinetics[12] and the hydration pump-leak mechanism of Maurice[8] to determine central corneal swelling associated with different hypoxic conditions caused by various types of soft-contact-lens (SCL) wear. Recently Kim et al.[3] expanded this work to 2 dimensions (2D) to determine central-to-peripheral corneal swelling for SCL and scleral-lens (SL) wear. The metabolic-mathematical model revealed that limbal metabolic support significantly reduces mid-peripheral and peripheral corneal swelling. Further, the metabolic model disclosed that corneal efflux of lactate into the limbus and influx of limbus bicarbonate ions into the cornea are the primary contributors to reducing corneal edema at the mid-peripheral and peripheral regions of the cornea.[3] Surprisingly, supply of oxygen from the limbus had a marginal effect on reducing corneal edema everywhere.[3]

The previously developed metabolic model of Kim et al.[3] is expanded here to assess the hypoxic safety of embedded-component contact lenses for various designs and parameters by quantifying central-to-peripheral corneal edema associated with lens wear. Embedded-component contact lenses can utilize various lens-encasement platforms. Here, iterations of one SCL and one SL design are evaluated that are common for commercial contact lenses of today.

4.3 Methods

4.3.1 Lens Design

Details of the corneo-scleral anatomy are provided in Kim et al.[3] SL and SCL with embedments are referred to as ESL and ESCL, respectively. Also, contact-lens matrix that encapsulates the embedments is defined as a lens encasement or simply an "encasement". Geometric design, metabolic species transport, and swelling calculations are computed using the COMSOL Multiphysics 5.5 platform (Comsol Inc, Burlington, MA, USA). Because commercially available SCLs are too thin to allow embedments,[56] ESCL-encasement thickness (radial) is set at

400 µm. For direct comparison, the ESL-encasement thickness (radial) is also 400 µm. Therefore, the only hypoxia-relevant difference between the ESCL and ESL designs is the post-lens tear-film (PoLTF) thickness profile illustrated in Figure 4.1. Lens landing zones, which have no effect on corneal edema,[3] touch 8 mm laterally away from the central cornea. Because the curvature radii of the cornea (anterior curvature of 7.8 mm)[3] and the lenses are constant (see Table 4.1), prescription of the central PoLTF thickness results in a nonuniform central-to-peripheral PoLTF thickness profile. Accordingly, the noncentral PoLTF thickness is larger with the ESCL design in Figure 4.1 than what is typically seen clinically with commercially available SCLs. Overestimation of the PoLTF thickness profile results in overestimation of corneal edema. However, the region with the thickest PoLTF (i.e., at the corneal periphery) experiences significant limbal metabolic support and, consequently, exhibits minimal corneal swelling.[3] Therefore, the PoLTF thickness profile in Figure 4.1 provides accurate swelling predictions for ESCL wear. With ESL wear, the PoLTF thickness is smaller at the periphery than at the center and provides a PoLTF thickness profile representative of commercially available SLs.[142,152]

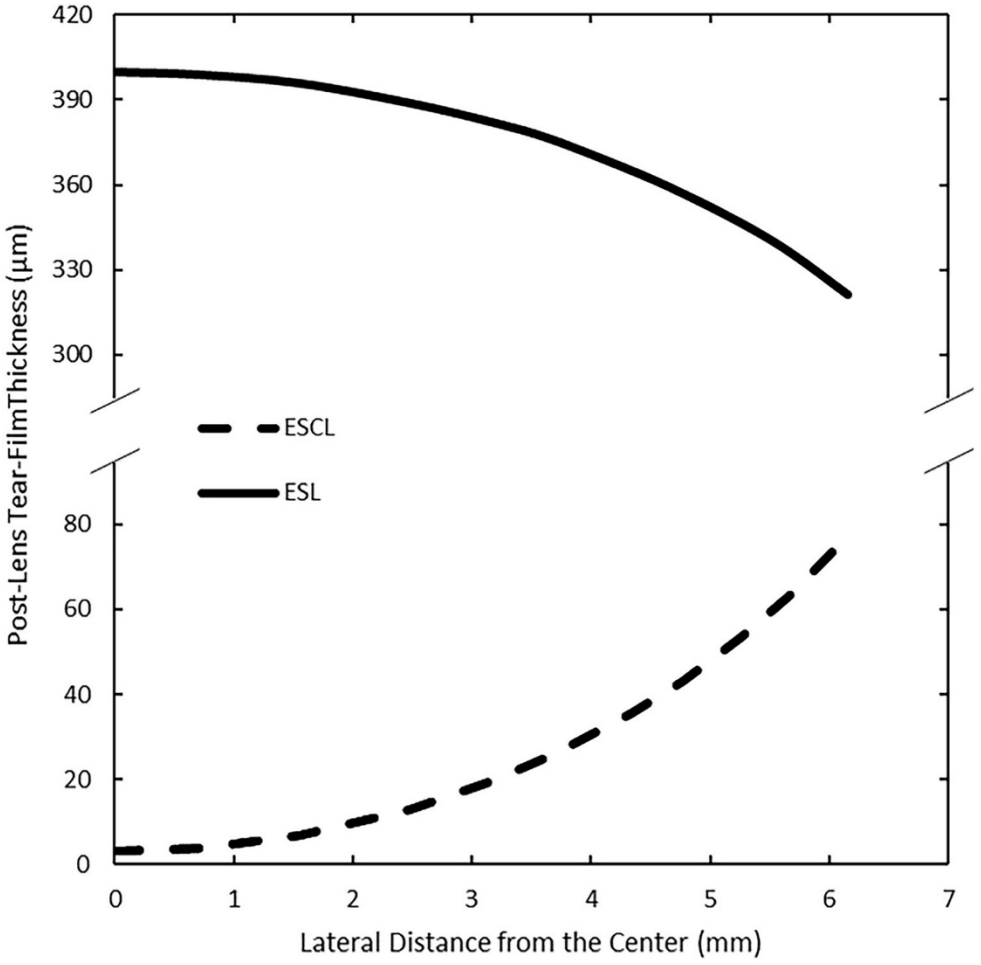

Figure 4.1. Radial post-lens tear-film thickness profiles for the soft-contact-lens (ESCL) and scleral -lens (ESL) designs with embedments. Horizontal axis is the lateral distance from the central cornea to the peripheral cornea with the reference point (horizontal axis = 0) being the central cornea at the anterior epithelial surface. Vertical axis is the post-lens tear-film thickness.

Table 4.1. Lens Design Parameters

Lens-Encasement Anterior Curvature	8.4 μm
Lens-Encasement Posterior Curvature	8.0 μm
Start of the Encasement Landing Zone	6.2 mm
Central-Embedment Anterior Curvature	8.25 mm
Central-Embedment Posterior Curvature	8.15 mm
Central-Embedment Lateral Length from the Central Cornea[a]	3.5 mm
Peripheral-Embedment Anterior Curvature	8.25 mm
Peripheral-Embedment Posterior Curvature	8.15 mm
Peripheral-Embedment Lateral Starting Point from the Central Cornea[a]	4.5 mm
Peripheral-Embedment Lateral Ending Point from the Central Cornea[a]	5.5 mm

[a] Central cornea is located at horizontal axis = 0 in Figure 4.4

Figure 4.2 depicts the corneo-scleral anatomy, two lens designs, and the coordinate axes. One axisymmetric central and one axisymmetric peripheral embedment are inserted in the encasement. Dimensions of the lenses are provided in Table 4.1. Because the designed systems are axisymmetric, swelling profiles are graphed from the center of the cornea to one end of the periphery. The parameters listed in Table 4.1 and Figure 4.1 are utilized for all analyses unless noted otherwise. Oxygen *Dk*s of the encasement, peripheral embedment, and central embedment are varied as is the placement of the embedments. Because radial thicknesses for these three different components are uniform in the corneal region, component oxygen transmissibility (*Dk/L*) is constant for the specified *Dk* value. To gauge the importance of embedment placement on corneal edema, embedment location is adjusted along the curvature radii (θ-polar coordinate in Fig. 4.2) and sagittal (y coordinate in Fig. 4.2) directions.

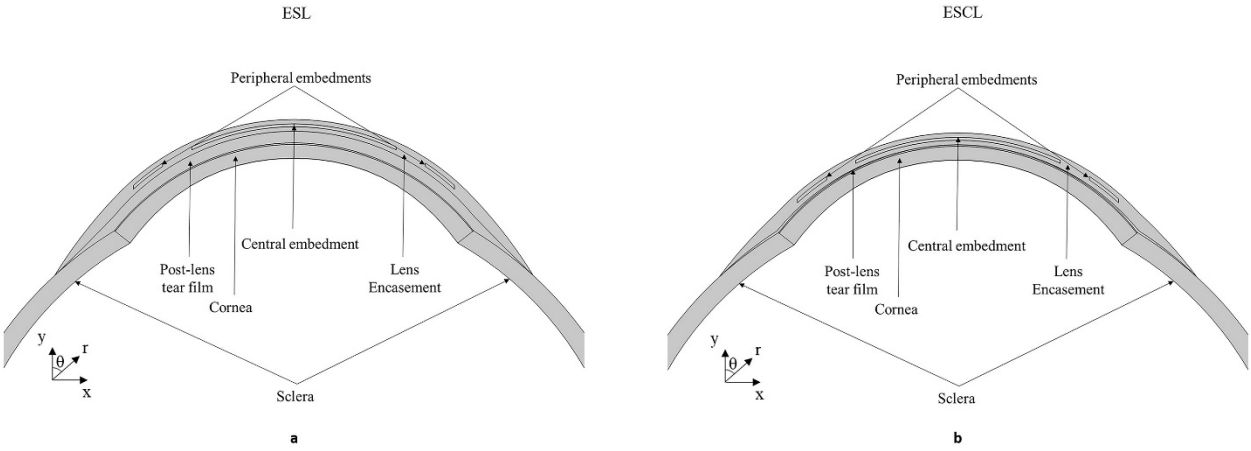

Figure 4.2. Axisymmetric corneo-scleral and contact-lens designs with two embedments: (a) ESL and (b) ESCL. Each major component is labeled. Vertical axis (y axis) is the sagittal direction and horizontal axis (x axis) is the lateral distance. Radial and polar coordinates of the spherical coordinate system are given as r and θ, respectively. A polar coordinate of 0° is equivalent to the sagittal axis (y axis).

Mathematical details of the metabolic-edema model are available in previously published manuscripts.[3,121] A brief non-mathematical summary is provided here. Metabolites of interest are those directly involved in aerobic and anaerobic metabolic reactions: oxygen, carbon dioxide, bicarbonate, lactate, glucose, and hydrogen ion. Sodium and chloride ions maintain local

electroneutrality. Introduction of a contact lens on the ocular surface restricts oxygen delivery from the atmosphere to the cornea and leads to increased anaerobic metabolism to maintain corneal cell function. Increased anaerobic glucose consumption produces excess lactate and hydrogen ions according to the chemical reaction

$$C_6H_{12}O_6 \rightarrow 2C_3H_5O_3^- + 2H^+ \tag{4.1}$$

Hypoxic corneal acidosis from Equation 4.1 is mitigated by the buffering equilibrium reaction

$$HCO_3^- + H^+ \leftrightarrow CO_2 + H_2O \tag{4.2}$$

The net increase in lactate and decrease in bicarbonate ions at the endothelium alters the local osmotic pressure and, consequently, changes the water influx/efflux balance of the pump-leak process at the corneal endothelium.[9,121,139] A decreased osmotic outflow results in higher water retention in the cornea and initiates corneal edema.

Alongside oxygen supply from the atmosphere, the cornea is directly supplied with metabolites from the anterior chamber and from the limbus. In addition, the peripheral cornea is approximately 35 % thicker than is the central cornea and has a higher metabolic demand.[42] Due to the various sources of metabolites and the different metabolic demands within the cornea, transport of metabolites occurs in both polar (center to/from periphery) and radial (corneal epithelium to/from corneal endothelium) directions in spherical coordinates (see Fig. 4.2). Corneal Nernst-Planck equations, epithelium/endothelium Kedem-Katchalsky membrane equations, boundary conditions, stroma-hydration isotherm, and accompanying parameters are available elsewhere.[3,5,12,121] The two-dimensional (2D) steady-state conservation equations used for the various metabolic species are written in rectangular coordinates and solved numerically in Comsol Multiphysics 5.5 using nonlinear finite element analysis.[3] Boundary conditions for the embedments include local species phase equilibria and continuity of species flux. Triangular mesh size and convergence tolerance (relative tolerance = 0.001) were set to ensure accurately converged solutions in reasonable computational times (~10−15 min).

4.3.2 Comparison to Clinical Data

Previously, the metabolic-edema model provided good comparison with clinically measured central and central-to-peripheral corneal edema during contact-lens wear.[3,5,121] Introduction of contact-lens embedments can result in localized regions with both extremely hypoxic and well oxygenated corneal regions. Therefore, the metabolic model is further compared here to the clinical data of Holden et al.[79] These authors studied central-to-peripheral corneal edema during wear of a low-water-content hydroxyethyl methacrylate (HEMA) lens having a central-aperture region of high oxygen delivery to the cornea with the peripheral-lens region having low oxygen delivery from the environment. The lens was a 38 %-water-content HEMA hydrogel that typically has an oxygen *Dk* of 8.9 Barrer.[153] However, the customized lens studied was ~300 μm thick at the non-aperture region and, therefore, had an oxygen transmissibility of ~ 3 hBarrer/cm (i.e., hectoBarrer/cm). Metabolic theory (line) and comparison data (closed circles) are portrayed in Figure 4.3. Swelling at both the lens-center aperture and at the low-oxygen-*Dk* periphery are clearly identified. The decrease in swelling near the lens edge is due to limbal support of metabolites.[3] Model predictions correlate well with the measured data using no

adjustable parameters. Figure 4.3 constitutes a second clinical validation of the 2D metabolic model.[3] Additional clinical validation of the metabolic model comes from studies of overnight central corneal edema with SL wear.[154,155] The metabolic model successfully predicts the observed central corneal swelling of approximately 8 % with overnight wear.[154,155]

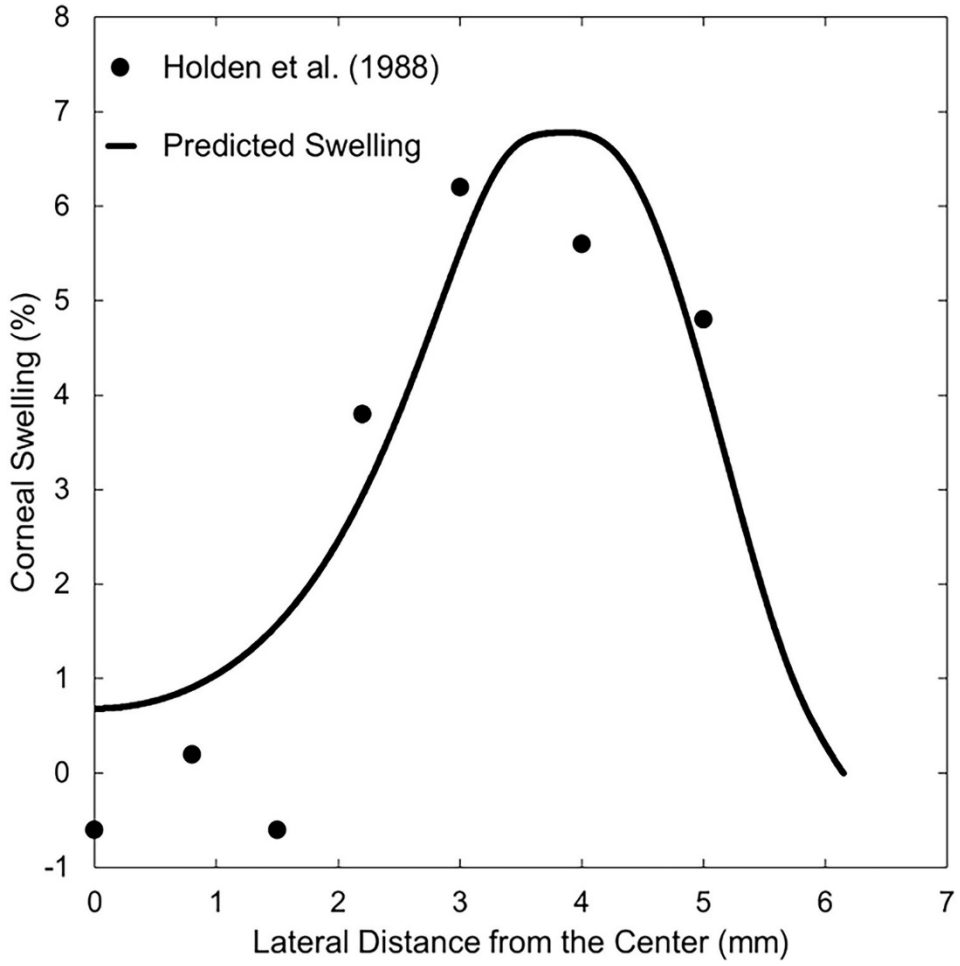

Figure 4.3. Comparison between the clinical data of Holden et al. [37] and the metabolic model with literature parameters.[79] Horizontal axis is the lateral distance from the central cornea to the peripheral cornea with the reference point (horizontal axis = 0) being the central cornea at the anterior epithelial surface. Vertical axis is the percentage of corneal swelling. No data error estimates are available from Holden et al.[79]

4.4 Results

Figure 4.4 illustrates oxygen-tension contours during wear of the SL and the SCL with and without embedments. Peripheral-embedment, central-embedment, and encasement oxygen *Dk*s are 0, 30, and 100 Barrer, respectively. Qualitatively, polar (i.e., θ-direction) oxygen transport provides meaningful oxygen support up to ~0.5 mm laterally away from each side of the central embedment. With a central-embedment oxygen *Dk* of zero Barrer (not shown), which has maximum possible polar oxygen flux, the effect of polar-direction oxygen transport diminishes ~1 mm laterally into each side of the central embedment. For contact lenses with embedments, the cornea underneath the peripheral embedment, which has a *Dk* of zero Barrer, experiences the

greatest deprivation of oxygen, whereas the regions without embedments have the highest oxygen tensions. Polar transport of oxygen is seen from high oxygen-tension regions to low oxygen-tension regions in the lens, the PoLTF, and the cornea. Therefore, corneal regions directly below the peripheral embedment remain oxygenated to some level. Interestingly, although oxygen tension is higher with the ESCL than with the ESL at most corneal surface regions, oxygen tension at the ocular surface immediately below the peripheral embedment for the ESL design is higher than that at the same location of the ESCL. This is due to the thicker PoLTF of the ESL design allowing more room for oxygen transport in the polar direction.

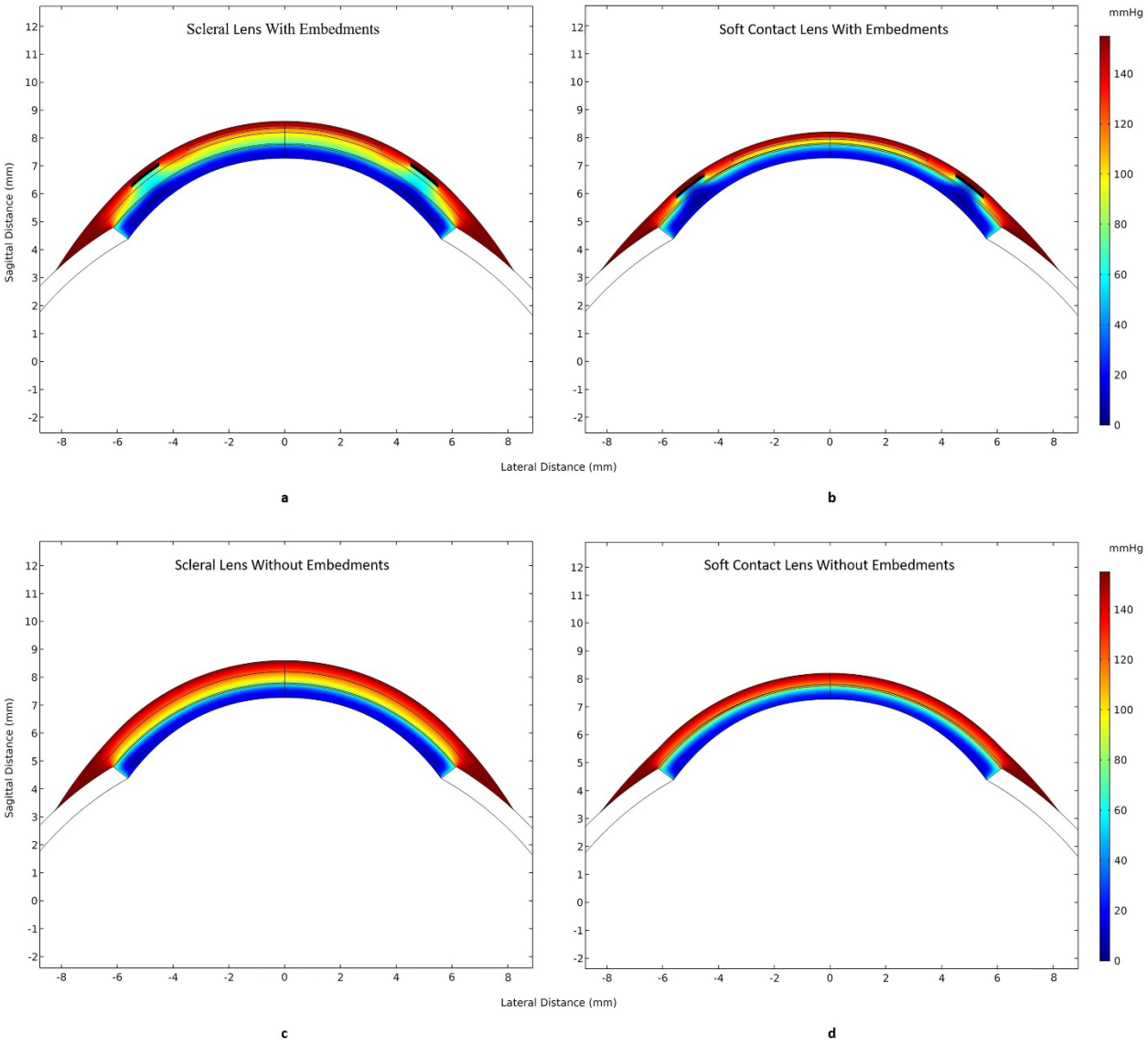

Figure 4.4. Oxygen-tension contours throughout the lens and the cornea for (a) scleral lens with embedments (ESL) and (b) soft contact lens with embedments (ESCL). Oxygen permeability (*Dk*) of the peripheral embedment, central embedment, and lens encasement is 0, 30, and 100 Barrer, respectively. Oxygen-tension contours for (c) scleral lens (SL) and (d) soft contact lens (SCL) without embedments. The only difference between ESL and ESCL designs is the thickness profile of the PoLTF. Oxygen tension within the sclera is that of oxygenated blood (61.5 mmHg) and is not shown. Red, navy, and black colors indicate high, low, and zero oxygen tension, respectively. The unit of oxygen tension is in mmHg. Horizontal axis is the lateral distance with 0 being the central cornea and the vertical axis is the sagittal distance.

Dashed lines in Figures 4.5a and b represent swelling profiles corresponding to Figures 4.4a and b, respectively. Despite the higher oxygen tension beneath the peripheral embedment at the ocular surface for the ESL design than that for the ESCL design, corneal swelling in the corresponding region is larger with the ESL design. The reason behind this seemingly contradictory result is the greater polar fluxes of oxygen and other metabolites within the anterior

cornea for ESCL wear compared to ESL wear at the region below the peripheral embedment. Polar-direction oxygen flux in this region is greater with ESCL wear due to the higher oxygen tension at the regions uncovered by the peripheral embedment than with ESL wear (see Figs. 4.4a and b). This results in a greater oxygen-tension gradient between the regions uncovered by the peripheral embedment and the region covered by the peripheral embedment. Similarly, there is less anaerobic metabolism (i.e., less production of lactate and less consumption of bicarbonate) in those regions uncovered by the peripheral embedment during ESCL wear. This results in a greater θ-directed flux of bicarbonate and lactate ions below the region covered by the peripheral embedment. Therefore, at the endothelium, where the pump-leak mechanism resides,[3,5,10,121] the ESCL design has lower lactate and higher oxygen and bicarbonate concentrations resulting in less swelling than that in the ESL design.

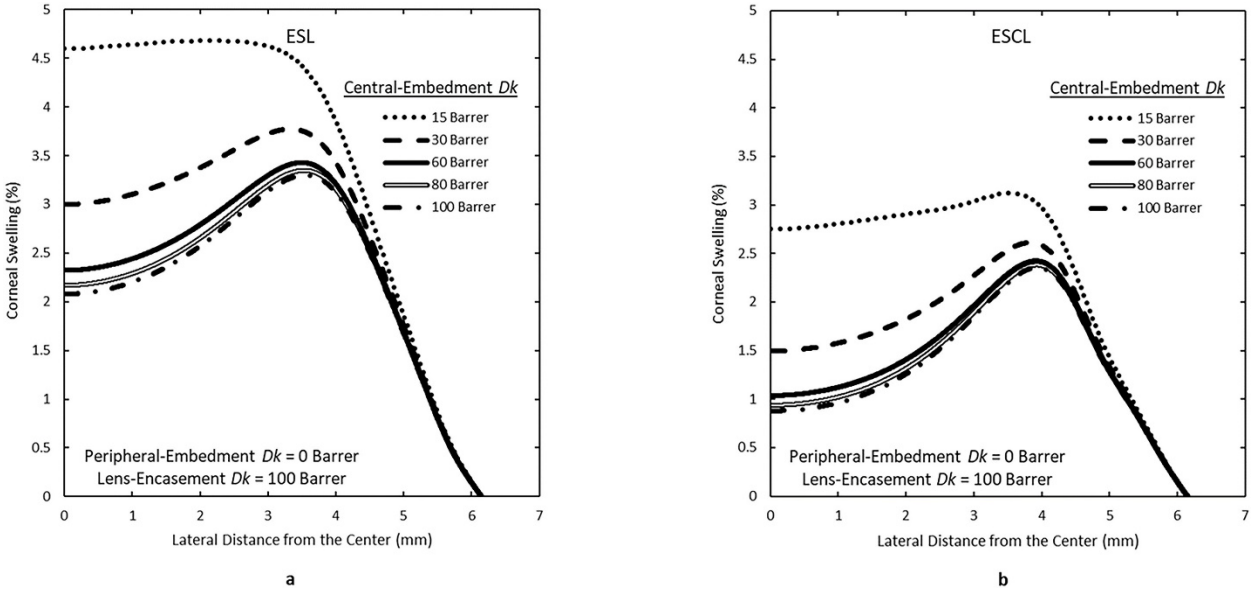

Figure 4.5. Central-to-peripheral corneal edema with (a) ESL and (b) ESCL wear for varying central-embedment oxygen permeabilities (*Dk*). Peripheral-embedment and lens-encasement oxygen *Dk*s are fixed at 0 and 100 Barrer, respectively. Central-embedment oxygen permeabilities are 15, 30, 60, 80, and 100 Barrer for both lens designs. Horizontal axis is the lateral distance from the central cornea to the peripheral cornea with the reference point (horizontal axis = 0) being the central cornea at the anterior epithelial surface. Vertical axis is the percentage of corneal swelling.

Central-to-peripheral corneal swelling is always lower with thinner PoLTFs, as shown by comparison of Figures 4.5a and b. However, for a PoLTF thickness to cause more than 1 % of the baseline corneal thickness change, the PoLTF thickness needs to change by more than 200 μm (during open-eye lens wear). The reason why peak swelling occurs ~3.5 – 4.0 mm laterally away from the center, despite the starting point of the peripheral embedment being 4.5 mm away from the center, is because environmental oxygen transport occurs radially. Also, metabolic demand of the cornea is non-uniform with limbal-metabolic support diminishing towards the central cornea. The small difference in the location of peak swelling between ESCL and ESL designs is the additional polar oxygen transport in the PoLTF of the ESL design and the thickness differences in the PoLTF profiles between the two lens designs.

A large number of lens-design configurations is possible. Examples are given for changing the oxygen *Dk*s of the embedments and the encasement, the sizes of the embedments, and the placement of the embedments. Swellings between about 4 %, corresponding to no-lens-wear sleep,[45] and 5 %, where Maurice noticed corneal hazing,[150] are adopted as qualitative guidelines for safe lens wear.

Figures 4.5a and b also illustrate central-to-peripheral edema for various central embedment oxygen *Dk*s with the ESL and ESCL designs, respectively. Encasement and peripheral-embedment oxygen *Dks* are maintained at 100 and 0 Barrer, respectively. A central-embedment oxygen *Dk* of 100 Barrer (dot-dashed lines) is equivalent to having no central embedment as the oxygen *Dk* of the central embedment is the same as that of the lens encasement. With a central-embedment oxygen *Dk* of 30 Barrer or greater, there is a noticeable peak swelling at ∼3.8 mm and ∼4.0 mm laterally away from the center for ESL and ESCL designs, respectively. For a central-embedment oxygen *Dk* of 15 Barrer, the cornea is significantly deprived of oxygen everywhere but in the peripheral region. Therefore, for this oxygen-*Dk* value, swellings of ∼4.5 % and ∼2.8 % are predicted throughout the central-to-mid-peripheral region for ESL and ESCL designs, respectively. Swelling in the central-to-mid-peripheral region increases whenever the encasement and/or the central-embedment oxygen *Dk* decreases. Even with a high-oxygen-*Dk* encasement (e.g., *Dk* of 160 Barrer), central-to-mid-peripheral swelling can reach physiologically unsafe levels (i.e., greater than 4–5 %)[45,149,150] with a central-embedment oxygen *Dk* of less than 13 Barrer for the ESL design and less than 8 Barrer for the ESCL design. For all central-embedment oxygen *Dk*s, swelling declines in the peripheral regions for both lens designs due to metabolic support from the limbus.[3]

Figures 4.6a and b highlight the effect of changing the peripheral-embedment oxygen *Dk* on central-to-peripheral swelling for the ESL and ESCL designs, respectively. Dotted lines in Figures 4.6a and b correspond to the double-solid lines in Figures 4.5a and b, respectively. A peripheral-embedment oxygen *Dk* of 100 Barrer (dot-dashed lines) corresponds to no peripheral embedment as the encasement-oxygen *Dk* is 100 Barrer. For both lens designs, changing the peripheral-embedment oxygen *Dk* has a negligible effect on central corneal edema. Meanwhile, increasing the oxygen *Dk* of the peripheral embedment lowers the peak swelling of the cornea. A peripheral embedment can raise local swelling of the cornea by up to ∼1.3 % of the baseline corneal thickness for both ESCL and ESL designs.

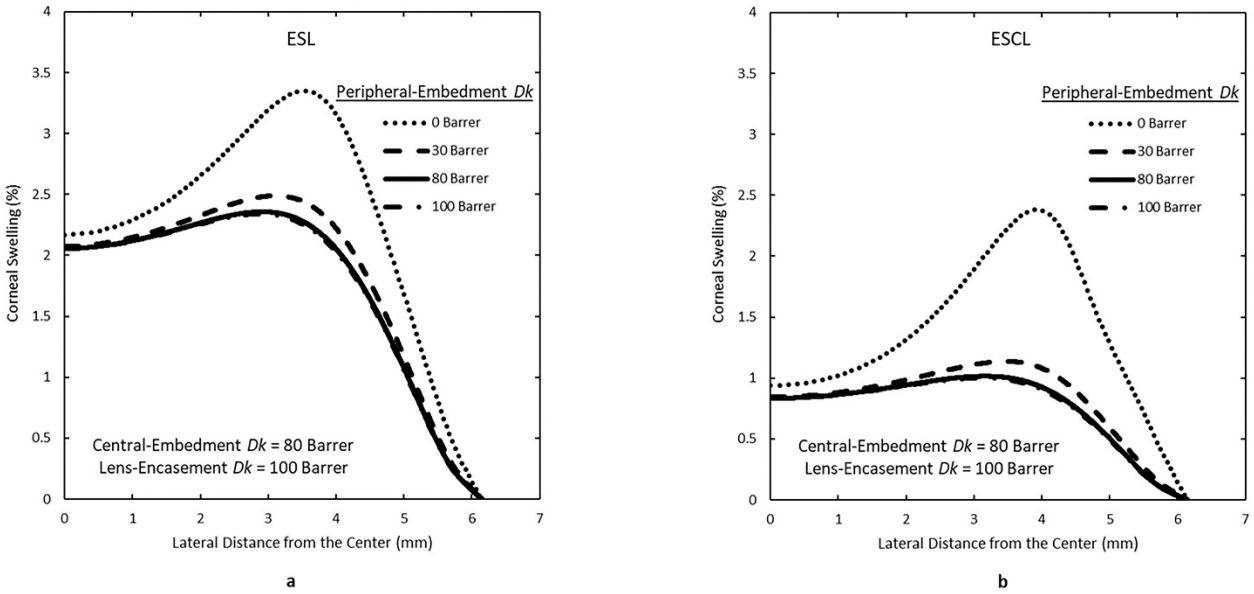

Figure 4.6. Central-to-peripheral corneal edema with (a) ESL and (b) ESCL wear for varying peripheral-embedment oxygen permeabilities (*Dk*). Central-embedment and lens-encasement oxygen permeabilities are fixed at 80 and 100 Barrer, respectively. Peripheral-embedment oxygen permeabilities are 0, 30, 80, and 100 Barrer for both lens designs. Dotted lines in Figures 4.6a and b correspond to the double-solid lines in Figures 4.5a and b, respectively. Horizontal axis is the lateral distance from the central cornea to the peripheral cornea with the reference point (horizontal axis = 0) being the central cornea at the anterior epithelial surface. Vertical axis is the percentage of corneal swelling.

Location of the peripheral embedment is varied to understand the importance of embedment placement on corneal edema. Figures 4.7a and b accentuate predicted swelling profiles associated with various peripheral-embedment placements along their curvature radii. The starting edge of the peripheral embedment is set to 4.0, 4.5, 5.0, and 5.5 mm laterally away from the center, and the lateral length of the peripheral embedment is kept at 1.0 mm. Sagittal shifts corresponding to the various lateral shifts can be determined by the posterior and anterior curvature radii provided in Table 4.1. Shifts described here follow the curvature radii and are equivalent to polar angle changes (in spherical coordinates). Solid lines in Figures 4.7a and b are identical to the double-solid lines in Figures 4.5a and b, respectively. For both lens types, moving the peripheral embedment closer to the central cornea also shifts the location of peak swelling towards the center. Moreover, with a peripheral embedment placed closer to the central cornea, peak swelling increases. Comparison of the swelling of the starting peripheral edge at 4.0 mm and at 5.5 mm in Figure 4.7 reveals that peak swellings differ by ∼0.8 % and ∼1.3 % relative to the unswollen cornea for ESL and ESCL lens types, respectively. Although not shown here, reduction of the lateral length of the peripheral embedment from 1.0 mm to 0.5 mm reduces peak swelling by ∼0.8 % and ∼1.1 % of the baseline corneal thickness for ESL and ESCL wear, respectively.

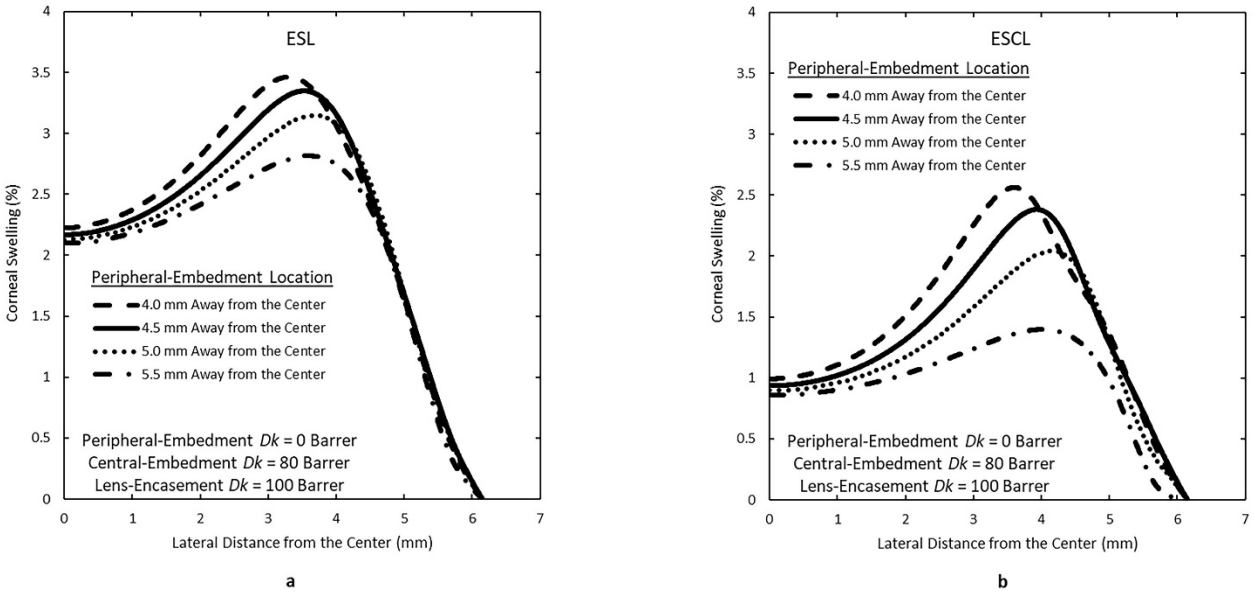

Figure 4.7. Central-to-peripheral corneal edema with (a) ESL and (b) ESCL wear for varying peripheral-embedment locations along curvature radii. Peripheral-embedment, central-embedment, and lens-encasement oxygen permeabilities (*Dk*s) are 0, 80, and 100 Barrer, respectively. Starting edge locations of the peripheral embedment are 4.0, 4.5, 5.0, and 5.5 mm laterally away from the center. Peripheral-embedment lateral length is 1.0 mm. Figures 4.7a and b solid lines are equivalent to Figures 4.5a and b double-solid lines, respectively. Horizontal axis is the lateral distance from the central cornea to the peripheral cornea with the reference point (horizontal axis = 0) being the central cornea at the anterior epithelial surface. Vertical axis is the percentage of corneal swelling.

Figures 4.8a and b accentuate the effect of translating the peripheral embedment in the sagittal direction for ESL and ESCL wear, respectively. Solid lines in Figures 4.8a and b are equivalent to the double-solid lines in Figures 4.5a and b, respectively. Sagittal shifts of the central embedment for ESL and ESCL wear have a negligible effect on central-to-peripheral corneal swelling. Lack of swelling influence by the sagittal shift for the central embedment is also true for extremely low and high central-embedment oxygen *Dk*s. Depending on the sagittal location of the peripheral embedment, peak swelling changes by ~0.3 % and ~0.6 % of the baseline corneal thickness for ESL and ESCL designs, respectively.

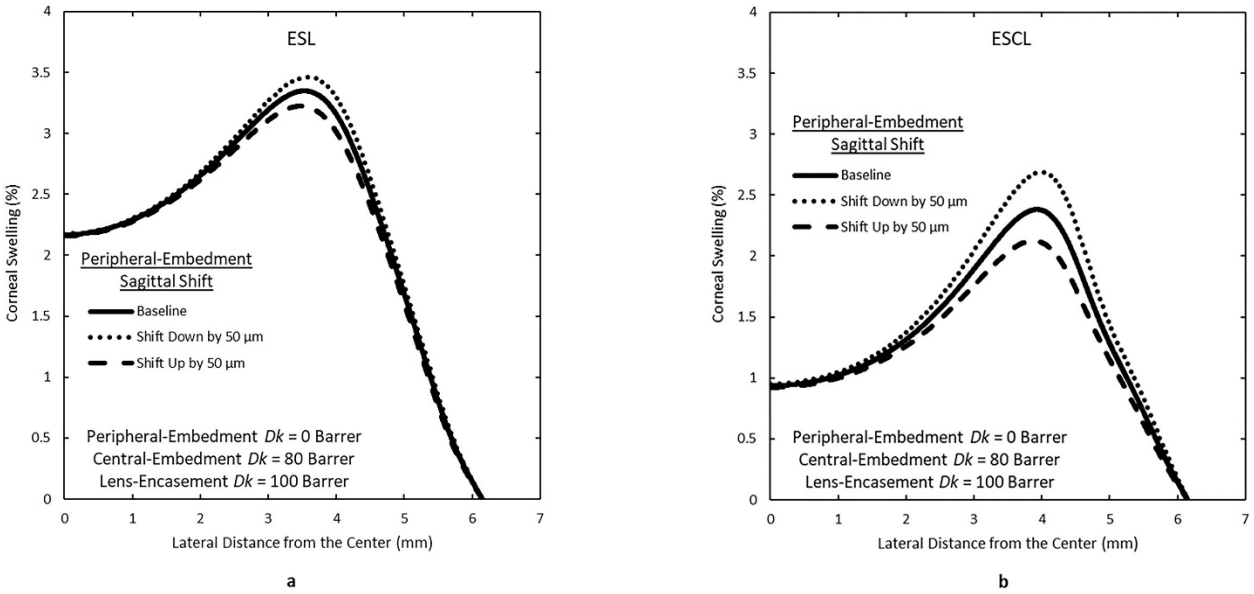

Figure 4.8. Central-to-peripheral corneal edema with (a) ESL and (b) ESCL wear for varying peripheral-embedment sagittal locations. Peripheral-embedment, central-embedment, and lens-encasement oxygen permeabilities (*Dk*s) are 0, 80, and 100 Barrer, respectively. Baseline curves in Figures 4.8a and b are equivalent to the double-solid lines in Figures 4.5a and b, respectively. The peripheral embedment is shifted up and down 50 µm from the baseline to assess the effect of sagittal location on corneal edema. Horizontal axis is the lateral distance from the central cornea to the peripheral cornea with the reference point (horizontal axis = 0) being the central cornea at the anterior epithelial surface. Vertical axis is the percentage of corneal swelling.

Figures 4.9a and b illustrate swelling profiles for various encasement oxygen *Dks* during ESL and ESCL wear, respectively. Dotted lines in Figures 4.9a and b are equivalent to the double-solid lines in Figures 4.5a and b, respectively. Increases in the encasement oxygen *Dk* reduce central-to-peripheral corneal edema for both ESL and ESCL designs. Similar analyses to Figures 4.4 – 4.8 but for encasement oxygen *Dk* of 160 Barrer are provided in Appendix 4A.

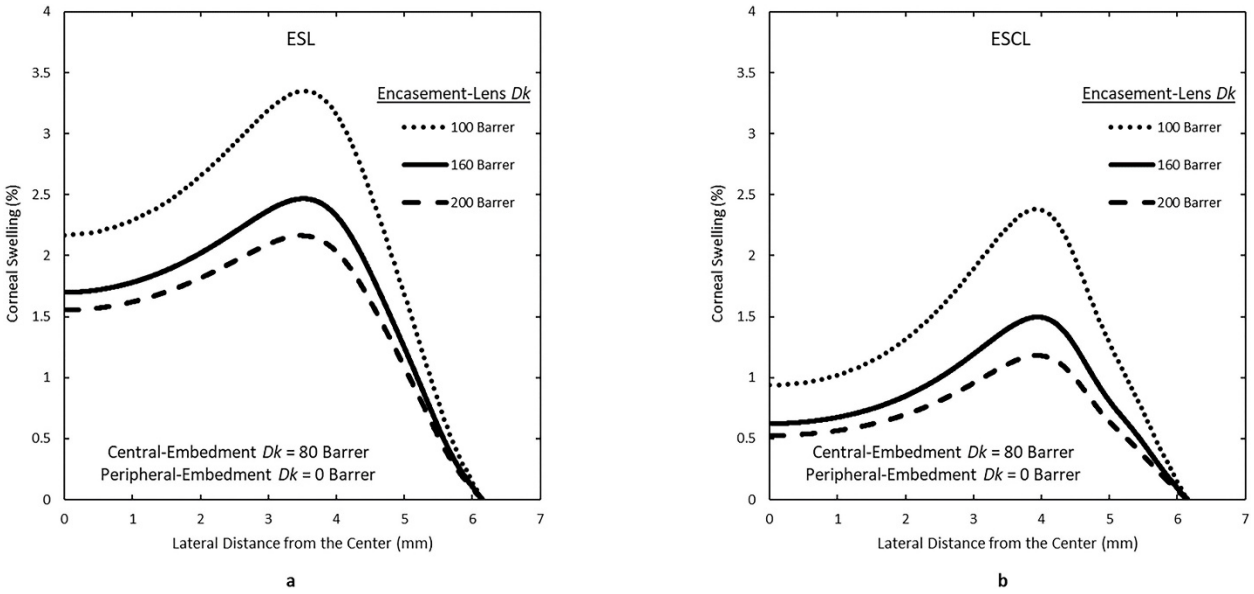

Figure 4.9. Central-to-peripheral corneal edema with (a) ESL and (b) ESCL wear for varying lens-encasement oxygen permeabilities (*Dk*). Peripheral-embedment and central-embedment oxygen *Dk*s are 0 and 80 Barrer, respectively. Lens-encasement oxygen permeabilities are 100, 160, and 200 Barrer for both lens designs. Dotted lines in Figures 4.9a and b are equivalent to the solid-open lines in Figures 4.5a and b, respectively. Horizontal axis is the lateral distance from the central cornea to the peripheral cornea with the reference point (horizontal axis = 0) being the central cornea at the anterior epithelial surface. Vertical axis is the percentage of corneal swelling.

4.5 Discussion

Lens embedments should be constructed with high oxygen-*Dk* materials to minimize central-to-peripheral edema. Unfortunately, applicable elastomer and semiconductor embedment devices typically exhibit lower oxygen *Dk*s[62] than those of silicone-containing materials in use today for commercially available contact lenses.[156] Therefore, incorporation of embedments into a contact lens changes oxygen-transport behavior compared to that of contact lenses without embedments. In addition to the PoLTF thickness and oxygen *Dk/L* of the lens-encasement, corneal edema induced by embedded-component contact-lens wear is sensitive to the location of embedments, to the embedment lengths, and to the embedment-oxygen *Dk/L*s. In the analysis of embedment-oxygen *Dk/L*s, the oxygen *Dk*s are varied rather than the thickness of the embedments. However, the thickness of the embedments can also be altered to change the embedment-oxygen *Dk/L*s.

Limbal metabolic support, notably that from lactate, bicarbonate, and oxygen species, adds to the list of variables influencing corneal edema. The SENSIMED Triggerfish IOP-sensor lens provides a relevant example.[67] This lens has a high *Dk* silicone central region surrounded by a peripheral annular sensor circuit of low but unspecified *Dk*. However, because the sensor is peripheral, limbal metabolic supply protects the cornea from hypoxia. This model prediction is in agreement with the limited 5-subject central-swelling measurements of Pajic et al.[157]

Comparison of swelling profiles of ESL and ESCL designs in Figures 4.5 – 4.9 and Figures 4A.2 – 4A.5 reveal that decreasing PoLTF thickness reduces corneal edema. Increasing a settled, central PoLTF thickness from 3 μm to 400 μm increases localized swelling by up to an additional 1.8 % of the baseline corneal thickness. The effect of PoLTF thickness on swelling increases with

lower central-embedment, peripheral-embedment, and encasement oxygen *Dk*s until the series-resistance combined encasement and embedment oxygen *Dk/L* is less than ~5 hBarrer/cm. At such a low oxygen transmissibilities, oxygen-diffusion resistance of the lens (i.e., $\frac{L_{lens}}{Dk_{lens}} = \frac{L_{encasement}}{Dk_{encasement}} + \frac{L_{embedment}}{Dk_{embedment}}$) dominates PoLTF oxygen-diffusion resistance. This finding is consistent with central-corneal-edema analyses with wear of contact lenses without embedments.[5,121] A thicker PoLTF means more polar oxygen diffusion but less radial oxygen diffusion. Even with a 400-μm PoLTF thickness and a zero *Dk* central embedment, however, polar-directional diffusion supply is marginal ~1.0 mm laterally away from each side of the embedments for encasement oxygen *Dk*s of 100 and 160 Barrer. These observations emphasize the importance of oxygen diffusion through embedment material rather than relying on polar-directed oxygen transport posterior to the embedment.

The significant peak swelling in a high oxygen-*Dk* central embedment with a zero-oxygen-*Dk* peripheral embedment (Fig. 4.5, Fig. 4A.2) also emphasizes that polar oxygen diffusion is not adequate to reduce corneal hypoxia everywhere. Nevertheless, as shown in Figure 4.8 and Figure 4A.5, relocating the peripheral embedment in the sagittal-anterior direction to allow more θ-directed oxygen transport can meaningfully reduce localized corneal edema. This is because the peripheral-embedment lateral length is 1 mm and polar transport of oxygen increases oxygen tension posterior to the peripheral embedment. The effect of polar-directed diffusive-oxygen supply rapidly diminishes ~1 mm laterally from each side of the embedments. Thus, shifting the central embedment in the anterior sagittal direction has minimal effect on corneal edema for both lens types because of the long length (i.e., 7 mm) of the central embedment (not shown). The importance of embedment-lateral length also explains why reducing the length of the peripheral embedment diminishes peak corneal edema significantly (not shown). Therefore, the central-embedment lateral length should not exceed ~ 2 mm when the chosen material is impermeable to oxygen.

Interestingly, sagittal-placement shifts with thicker PoLTFs in Figure 4.8a result in less reduction of edema than those for thinner PoLTFs in Figure 4.8b. There is a diminishing return on corneal edema of θ-directed oxygen supply via thicker PoLTFs and/or via more anterior-located embedments. Another way to increase the polar oxygen flux is to create greater oxygen concentration differences between the high and low oxygen tension regions by increasing the encasement oxygen *Dk*.

In Figure 4.7 and Figure 4A.4, relocation of the peripheral embedment toward the central cornea increases peak corneal edema. This finding is not due to the non-uniform PoLTF as the ESCL design in Figure 4.7b has a thicker PoLTF at the periphery. Rather, the reason for the dependence of corneal swelling on the peripheral-embedment polar location is because limbal-metabolic support diminishes towards the central cornea.[152] Figure 4.7 and Figure 4A.4 also show that θ-direction shifting of the peripheral embedment from 4.5 mm to 5.0 mm decreases peak swelling more than does shifting of the embedment from 4.0 mm to 4.5 mm. Moving the peripheral embedment as far into the periphery as possible, while still remaining within the corneal zone, reduces peak swelling substantially.

Encasement oxygen *Dk* for Figures 4.5 – 4.8 is 100 Barrer as commercial silicone-based lenses are available with this oxygen permeability. Encasement oxygen *Dk* of 160 Barrer, which is also commercially available, is discussed in Appendix 4A. For lower encasement-oxygen *Dk,* the effects of PoLTF thickness, embedment placements, embedment lengths, and embedment oxygen *Dk/L* all increase swelling more than what are presented in Figures 4.5 – 4.8

because the cornea is in a more hypoxic state.[3,5,45,121] Unlike commercially worn contact lenses today, which have oxygen *Dk/L* greater than 20 hBarrer/cm, lenses with embedments can have a combined series-resistance encasement and embedment oxygen *Dk/L* of around ~10 hBarrer/cm. Therefore, the effect of PoLTF on swelling is greater with embedded-component contact lenses than that for conventional SL wear, where a change of 200 μm in settled-PoLTF thickness produces clinically insignificant swelling.[121]

The metabolic-model analysis does not incorporate oxygen supplied from fresh tear at the lens edge. However, SCL and SL exhibit smaller lens movements than those of PMMA lenses that deliver inadequate oxygen to the cornea through tear mixing.[145–147,158] Therefore, the amount of oxygen supplied from fresh tear is minor compared to that supplied by diffusion through the lens. With ESL assessment, settled PoLTF thicknesses greater than 400 μm were not investigated because Kim et al.[121] calculated that thicknesses greater than 400 μm permit buoyancy-driven fluid convection that dominates oxygen mixing compared to molecular diffusion. Therefore, model prediction is accurate up to thicknesses of about 400 μm[121] beyond which a diminishing effect of PoLTF thickness on central corneal edema is expected and in agreement with Fisher et al.[159] Because heat generated by battery-powered embedments may affect buoyancy-driven fluid convection, investigation of PoLTF-temperature profiles is warranted with ESL wear.

The presented metabolic model assesses corneal swelling in the steady state. Time to reach steady state is affected by whether the eyes are open or closed, by the oxygen transmissibility of the tear film and the embedded lens components, by how fast the lens settles on the ocular surface, and by how quickly the stroma swells/deswells upon changes in metabolic species concentrations, among others. Of these effects, swelling/deswelling appears to be rate determining. Li and Tighe[11] mathematically showed that it takes approximately 3–4 h for the cornea to reach steady state after being subjected to a 1-h hyperosmotic shock of 15 mOsM. More recently, Tan et al.[142] showed clinically that the time it takes to reach maximum swelling with SL wear occurs after about 1.5 h of lens wear during open eye. Then, the swelling decreased by 0.2 % of the baseline corneal thickness in a subsequent 3.5 h most likely because of the slow lens settling. Niimi et al.[160] also showed that deswelling after no-lens-wear overnight swelling occurred mostly within 2 h of awake time. The change in concentration of metabolites due to open-eye lens-wear hypoxia is smaller than the hyperosmotic shock considered by Li and Tighe.[11] Therefore, the time to reach steady state with open-eye ESL and ESCL is likely to be closer to the 1.5–2 h observed by Tan et al.[142]

Possible transport resistances of metabolites from scleral-blood vessels into the limbus is not accounted for in the present metabolic model.[3] Therefore, the current model provides an optimistic estimate of limbal-metabolic support. However, comparison of the model to the central-to-peripheral clinical data of Wang et al.[47] provided in Kim et al.[3] and to those of Holden et al.[79] in Figure 4.3 is good using no adjustable parameters. Moreover, the model accurately predicts various contact-lens wear induced central corneal edema for open and overnight closed eyes. [5,45,121,154,155] Therefore, transport resistances of metabolites between the limbus and the cornea are likely to be small.

As previously mentioned, the provided design of ESCL results in mid-peripheral and peripheral PoLTF thicknesses that are thicker than what is typically seen with commercially available SCL wear. However, a change in the PoLTF thickness by 80 μm results in corneal-thickness change of less than 0.35 % of the baseline corneal thickness. Further, the region with the thickest PoLTF, which is the peripheral cornea, has minimal corneal edema due to limbal-metabolic support. Therefore, the 2D metabolic model provides accurate assessment of corneal edema with ESCL wear despite the possibility that the designed ESCL may slightly overestimate

mid-peripheral and peripheral corneal edema compared to that of an actual ESCL. When ESCL and ESL PoLTF thickness profiles are available, those data can readily be incorporated into the present metabolic-edema model to assess corneal edema caused by specific designs of ESCLs and ESLs.

Although this manuscript focuses on circuit-embedded contact lenses, guidance on minimizing corneal edema is also applicable to contact lenses that have other multiple components, such as drug-eluting lenses.[55] For ESCLs, embedments may inhibit ion transport across the lens, potentially adhering the lens to the ocular surface.[39,40] Assessment of ion transport through ESCLs requires further investigation.

Countless lens configurations and corresponding central-to-peripheral corneal-edema profiles can arise. This is especially true since most contact lenses have non-uniform thickness profiles.[136,161] For these multifaceted embedded-lens designs, the metabolic-model calculations provide guidance on how best to minimize corneal edema. Figures 4.5, 4.6, and 4.9 show the importance of having a high oxygen *Dk* for embedments and, most importantly, for the lens encasement regardless of embedment location and PoLTF thickness. Recommended designs to minimize central-to-peripheral edema are those with the highest oxygen *Dk/L* for the lens encasement and embedments as well as the thinnest PoLTF. Embedments do not hinder oxygen delivery to the cornea when they are implanted far into the conjunctival region. When an embedment is placed within the corneal periphery near the limbus, limbal-metabolic support in the peripheral region negates most of the swelling. Therefore, mid-peripheral peak swelling with a zero-oxygen-*Dk* peripheral embedment located near the limbus (i.e., Fig. 4.7 dot-dashed lines) is greater than that with no peripheral embedment (i.e., equivalent to Fig. 4.6 dot-dashed lines) by only ~0.4 % of the baseline corneal thickness. Consequently, embedments should be placed as far into the periphery as possible. Finally, embedment lengths should be minimized; they should be placed as anteriorly as possible to maximize polar-directed oxygen transport. Accordingly, swellings of less than 1 % everywhere should be achievable even with low-oxygen-*Dk* embedments.

4.6 Appendix 4A. Corneal Swelling Profiles with Encasement Oxygen Dk of 160 Barrer

Figure 4A.1 illustrates oxygen-tension contours during wear of the ESL, ESCL, SL, and SCL that compare with Figure 4.4 except that encasement oxygen *Dk* is now 160 Barrer. Peripheral-embedment and central-embedment oxygen *Dk*s for ESL and ESCL are 0 and 30 Barrer, respectively. Dashed lines in Figures 4A.2a and b reflect swelling profiles corresponding to the oxygen-tension contours in Figures 4A.1a and b, respectively.

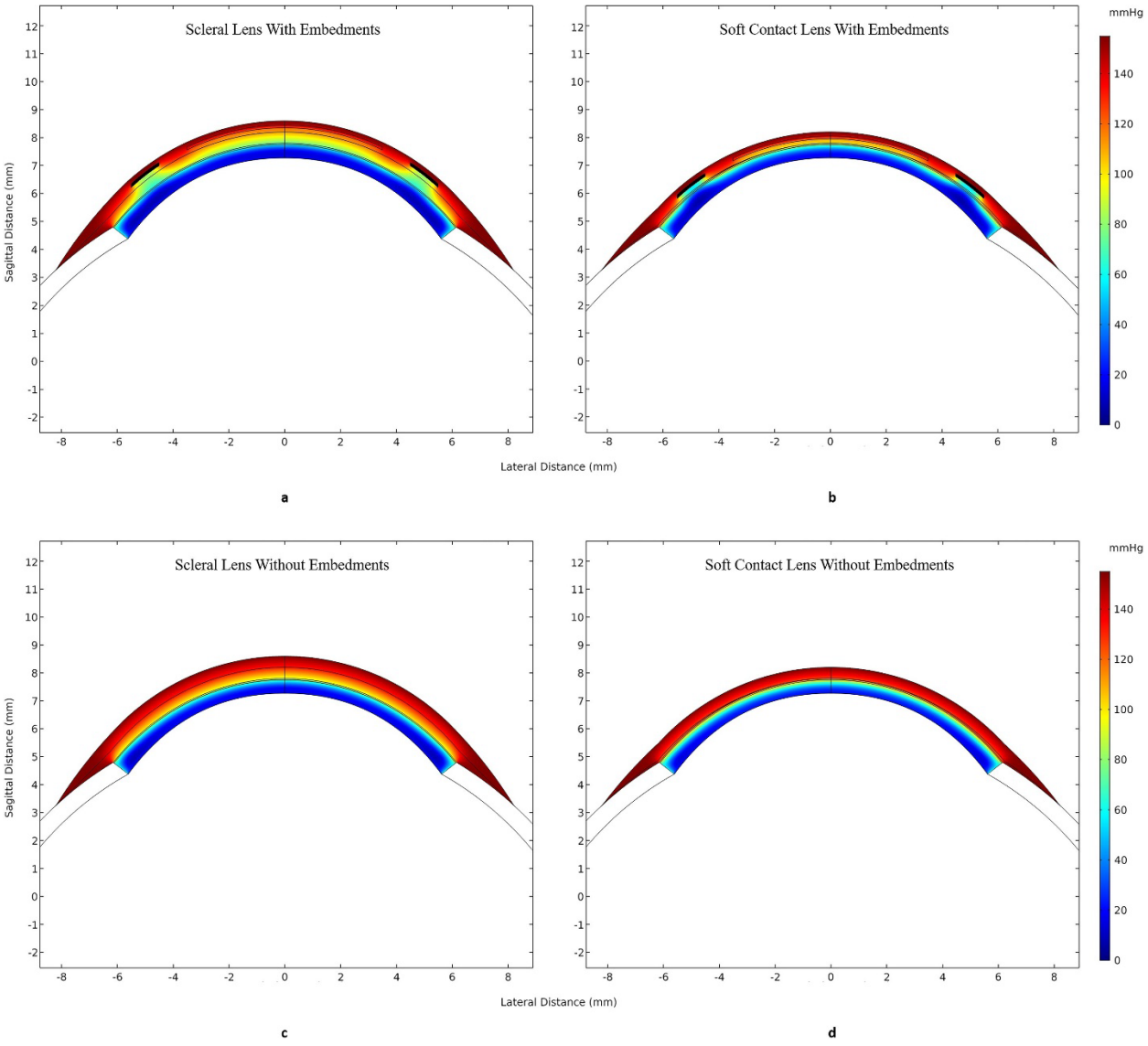

Figure 4A.1. Oxygen-tension contours throughout the lens and the cornea for (a) scleral lens with embedments (ESL) and (b) soft contact lens with embedments (ESCL). Oxygen permeabilities (*Dks*) of the peripheral embedment, central embedment, and lens encasement are 0, 30, and 160 Barrer, respectively. Oxygen-tension contours for (c) scleral lens (SL) and (d) soft contact lens (SCL) without embedments. The only difference between ESL and ESCL designs is the thickness profile of the PoLTF. Oxygen tension within the sclera is that of oxygenated blood (61.5 mmHg) and is not shown. Red, navy, and black colors indicate high, low, and zero oxygen tensions, respectively. The unit of oxygen tension is in mmHg. Horizontal axis is the lateral distance with 0 being the central cornea and the vertical axis is the sagittal distance.

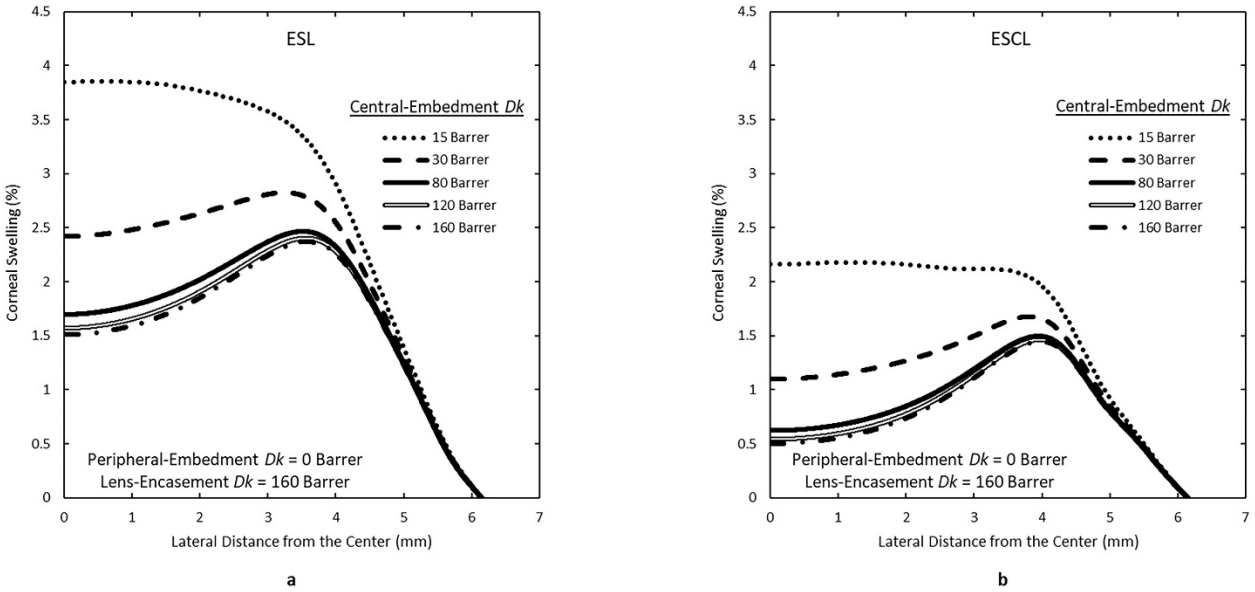

Figure 4A.2. Central-to-peripheral corneal edema with (a) ESL and (b) ESCL wear for varying central embedment oxygen permeabilities (*Dks*). Peripheral-embedment and lens-encasement oxygen *Dk*s are fixed at 0 and 160 Barrer, respectively. Central-embedment oxygen permeabilities are 15, 30, 80, 120, and 160 Barrer for both lens designs. Horizontal axis is the lateral distance from the central cornea to the peripheral cornea with the reference point (horizontal axis = 0) being the central cornea at the anterior epithelial surface. Vertical axis is the percentage of corneal swelling.

Figures 4A.2a and b illustrate the effect of changing central-embedment *Dk* on central-to-peripheral edema for an encasement oxygen *Dk* of 160 Barrer for ESL and ESCL wear, respectively. Results are similar to those of Figures 5a and b, except that swelling is decreased with the higher encasement oxygen *Dk*.

The effect of changing-peripheral embedment *Dk* on central-to-peripheral corneal edema for encasement oxygen *Dk* of 160 Barrer for ESL and ESCL is shown in Figures 4A.3a and b, respectively. The trends seen in Figures 4A.3a and b are comparable to that in Figures 4.6a and b, respectively. Dotted lines in Figures 4A.3a and b correspond to the solid lines in Figures 4A.2a and b, respectively.

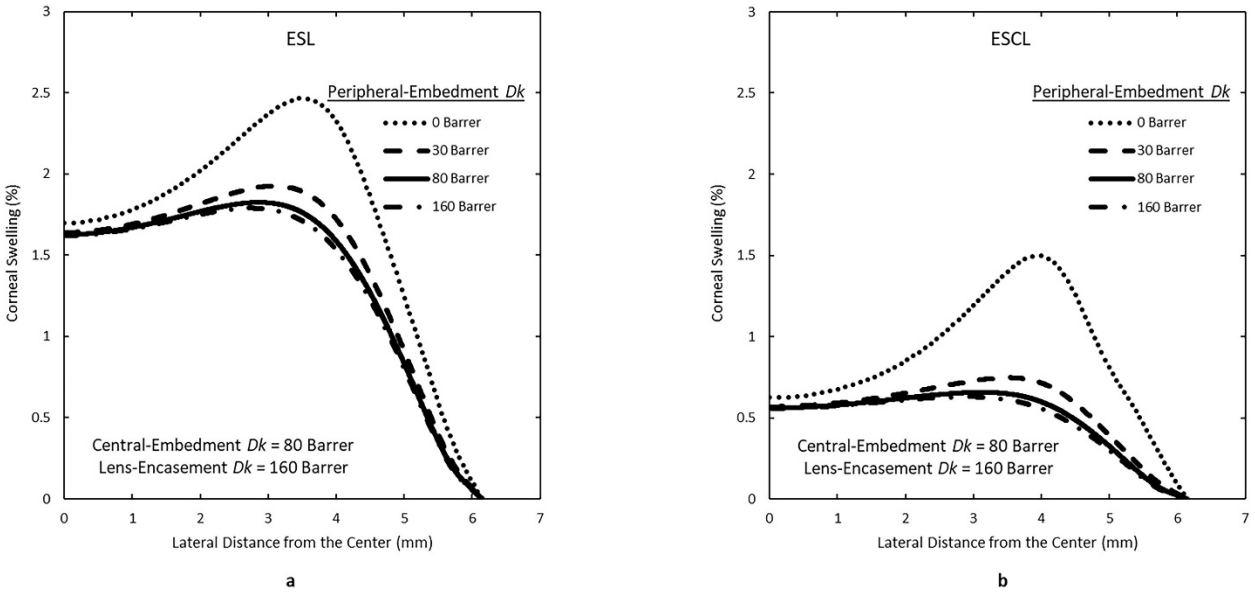

Figure 4A.3. Central-to-peripheral corneal edema with (a) ESL and (b) ESCL wear for varying peripheral-embedment oxygen permeabilities (*Dks*). Central-embedment and lens-encasement oxygen *Dk*s are fixed at 80 and 160 Barrer, respectively. Peripheral-embedment oxygen permeabilities are 0, 30, 80, and 160 Barrer for both lens designs. Dotted lines in Figures 4A.3a and b correspond to the solid lines in Figures 4A.2a and b, respectively. Horizontal axis is the lateral distance from the central cornea to the peripheral cornea with the reference point (horizontal axis = 0) being the central cornea at the anterior epithelial surface. Vertical axis is the percentage of corneal swelling.

Polar-directed shifts of the peripheral embedment are assessed with an encasement oxygen *Dk* of 160 Barrer as illustrated in Figures 4A.4a and b for ESL and ESCL, respectively. Again, the trends seen in Figures 4A.4a and b are comparable to those in Figures 4.7a and b, respectively. Solid lines in Figures 4A.4a and b are identical to the solid lines in Figures 4A.2a and b, respectively. With an encasement oxygen *Dk* of 160 Barrer, reduction of the lateral length of the peripheral embedment from 1.0 mm to 0.5 mm reduces peak swelling by ~0.6 % and ~0.7 % of the baseline corneal thickness for ESL wear and for ESCL wear, respectively.

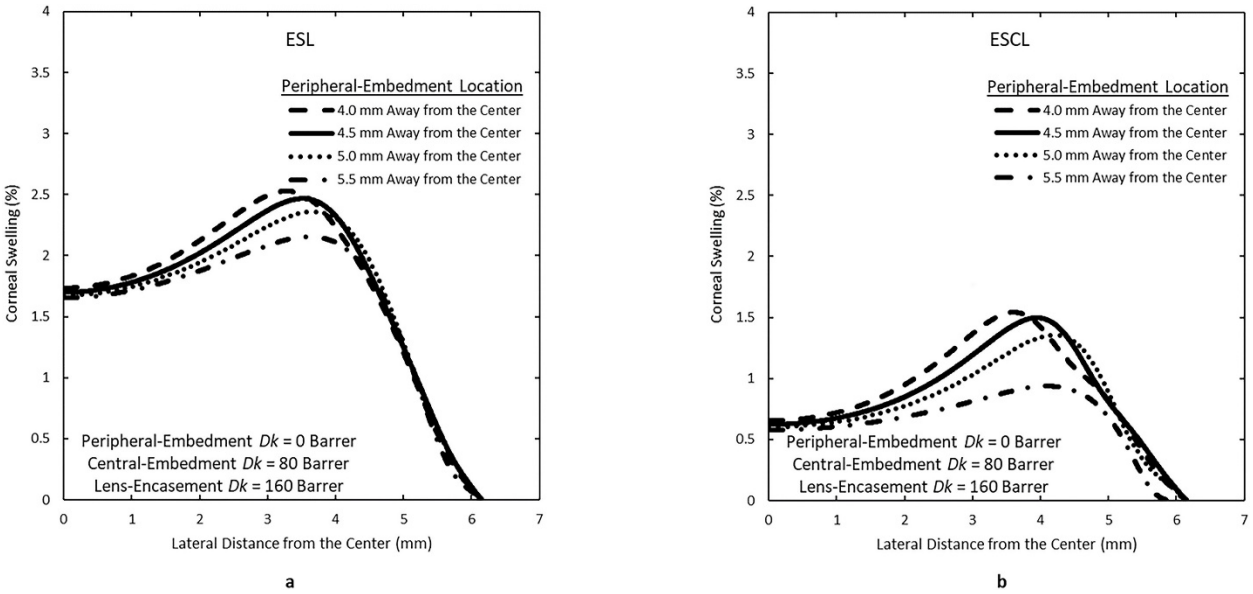

Figure 4A.4. Central-to-peripheral corneal edema with (a) ESL and (b) ESCL wear for varying peripheral-embedment locations along curvature radii. Peripheral-embedment, central-embedment, and lens-encasement oxygen permeabilities (*Dk*s) are 0, 80, and 160 Barrer, respectively. Starting edge locations of the peripheral embedment are 4.0, 4.5, 5.0, and 5.5 mm laterally away from the center. Peripheral-embedment lateral length is 1.0 mm. Figures 4A.4a and b solid lines are equivalent to Figures 4A.2a and b solid lines, respectively. Horizontal axis is the lateral distance from the central cornea to the peripheral cornea with the reference point (horizontal axis = 0) being the central cornea at the anterior epithelial surface. Vertical axis is the percentage of corneal swelling.

The effect of a sagittal shift of the peripheral embedment with an encasement oxygen *Dk* of 160 Barrer are illustrated in Figures 4A.5a and b for ESL and ESCL, respectively. As above, solid lines in Figures 4A.5a and b are equivalent to the solid lines in Figures 4A.2a and b, respectively. Similar to Figures 4.8a and b, shifting the peripheral embedment anteriorly reduces peak edema.

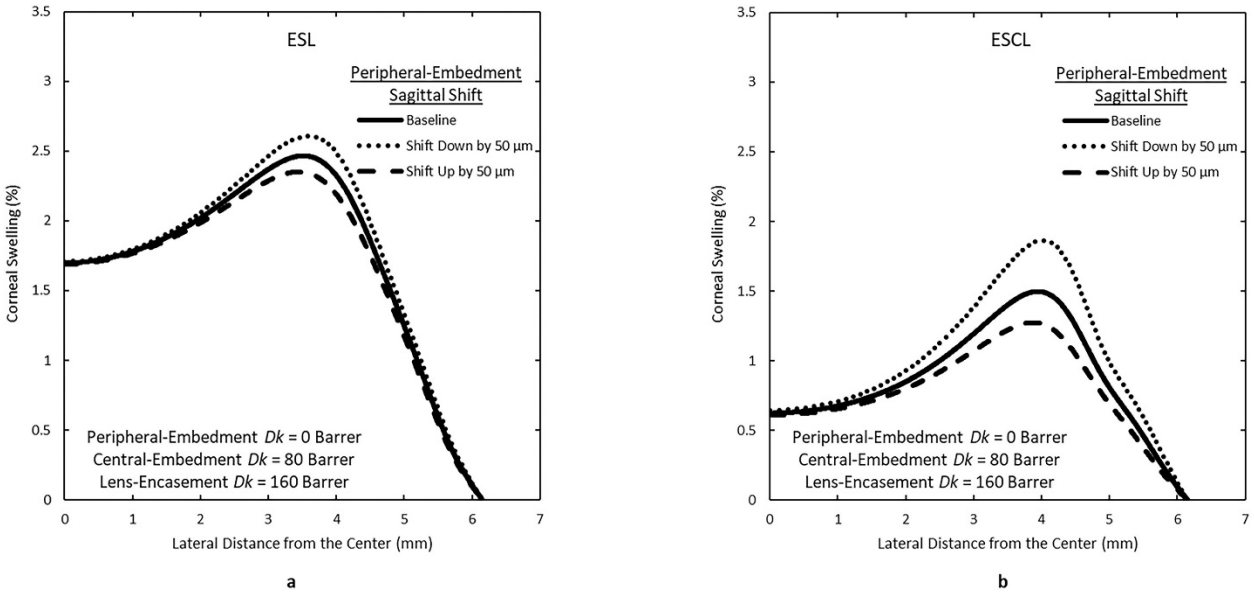

Figure 4A.5. Central-to-peripheral corneal edema with (a) ESL and (b) ESCL wear for varying peripheral-embedment sagittal locations. Peripheral-embedment, central-embedment, and lens-encasement oxygen permeabilities (*Dk*s) are 0, 80, and 160 Barrer, respectively. Baseline curves in Figures 4A.5a and b are equivalent to the solid lines in Figures 4A.2a and b, respectively. The peripheral embedment is shifted up and down 50 µm from the baseline to assess the effect of sagittal location on corneal edema. Horizontal axis is the lateral distance from the central cornea to the peripheral cornea with the reference point (horizontal axis = 0) being the central cornea at the anterior epithelial surface. Vertical axis is the percentage of corneal swelling.

Chapter 5

Human Lacrimal Production Rate and Wetted Length of Modified Schirmer's Tear Test Strips

Published as: Kim YH, Graham AD, Li W, Radke CJ, Lin MC. Human lacrimal production rate and wetted length of modified Schirmer's tear test strips. Transl Vis Sci Technol. 2019;8(3):40.

5.1 Abstract

Purpose: To assess and compare the wetting kinetics of sheathed and unsheathed Schirmer's tear test (STT) strips, and to determine the repeatability of 5-minute wetted length (WL) and basal tear production rate (BTPR).
Methods: Seventeen subjects underwent two sheathed and unsheathed STTs each for both eyes on four visits on separate days. After administration of topical anesthetic, WLs were measured every 30 seconds for 5 minutes, and BTPRs were calculated for sheathed strips. Limits of agreement (LoA), difference-versus-mean plots (DVM), and the coefficient of repeatability (CR) assessed WL and BTPR repeatabilities. Variance estimates were used to calculate sample sizes for future study.
Results: For the unsheathed STT, the mean (SD) difference in WLs between visits was 0.74 (5.05) mm, LoA were [−9.17, 10.64], and CR was 9.17 mm; for the sheathed STT, the mean (SD) intervisit difference was 0.16 (5.94) mm, LoA were [−11.49, 11.8], and CR was 10.53 mm. Eight of 48 sheathed STTs and 20 of 44 unsheathed STTs showed constant WL for the final 90 seconds of the test. The mean (SD) difference between repeated visits for BTPR was approximately 0.0 μL/min, LoA were [−1.82, 1.82], and CR was 1.91 μL/min.
Conclusions: Repeatability of sheathed and unsheathed 5-minute WL and BTPR is inadequate for measuring within-subject changes, but is sufficient for group studies with moderate sample sizes. Constant WL for the final 90 seconds with the eight sheathed STT measurements suggests varying BTPR, whereas constant WL with the unsheathed STT can be explained by balancing evaporation and BTPR.
Translational Relevance: Repeatability of the modified STT is evaluated clinically to establish quantitative BTPRs rather than inference from a strip WL.

5.2 Introduction

Schirmer's tear test (STT) is one of the most commonly employed clinical tests in dry-eye disease evaluation, treatment, and management. It is thought that inserting a strip of filter paper into the inferior fornix and measuring the length of the wetted portion after 5 minutes provides a direct assessment of tear production rate.[162] In clinical practice, use of the STT is hampered by poor repeatability, which has been attributed mainly to a presumed natural variability in tear production rate.[163] This assumption, however, may reflect incomplete understanding of what the test actually assesses. Recent studies highlight two issues that contribute to STT performance.[164,165]

The first issue addresses whether the traditional STT measures only the basal tear production or whether it also measures some degree of residual reflex tearing and/or uptake from

the tear meniscus. There are two reported phases during an STT: rapid wetting upon initial insertion, followed by a slower, typically linear, increase with time.[165] In the traditional STT without anesthetic, this observation is attributed to rapid initial wetting by reflex tearing upon strip insertion, followed by slower wetting due to basal tear production and diminished reflex tearing.[166–169] Li et al.,[165] however, observed significant variability in the initial wetting phase even though the eyes had been anesthetized with two drops of proparacaine, an anesthetic that should nullify most or all reflex tearing.[170] Based on this observation, the authors argued that in addition to reflex tear production, the initial wetting phase is influenced by the preexisting tear reservoir behind the lower lid.[165] Li et al.[165] established that the 5-minute wetted length of a Schirmer strip does not always correlate with the basal tear production rate (BTPR). Due to significant inter- and intrapatient variation in the volume of tears held in the tear reservoir, which is likely influenced by ethnicity,[171] medication use,[172] tasks performed immediately prior to testing (e.g., computer use),[173] and diurnal variation,[174,175] the BTPR can be assessed only in the second phase, during which a slower linear increase in wetting is observed.

The second issue is that environmental conditions impact wetted length. For example, conducting an STT in low room humidity can lead to excessive evaporation from the wetted Schirmer strip that can contribute to an artificially short wetted length. This is in contrast to the wetted length measured in a high-humidity environment.[176] This issue has largely been ignored in clinical practice. In contrast, the mechanistic model of Telles et al.[164] estimates BTPR by accounting for the physical forces acting on the strip during wetting imbibition and quantifies the specific impact that evaporation has on wetted length. Based on the calculations of Telles et al.[164] and the in vitro studies of Li et al.,[165] evaporation can significantly slow wetting dynamics. Li et al.[165] recommend that, in addition to application of anesthetic, Schirmer strips be sheathed with transparent plastic tape to inhibit evaporation. We refer to this procedure as the modified STT.[164,165]

In the current study, after applying anesthetic, we assess whether preventing evaporation from STT strips by sheathing them with plastic tape offers improved repeatability compared with traditional unsheathed strips. We also use the sheathed-strip transient wetted lengths to determine the BTPR, following the work of Li et al.,[165] and assess its repeatability. An STT with improved accuracy, combined with calculation of BTPR, can provide an important tool in the diagnosis and monitoring of dry-eye disease.

5.3 Methods

5.3.1 Study Protocol

Subjects were recruited from the University of California, Berkeley and the surrounding community. Both contact lens wearers and non–contact lens wearers were eligible to participate. Subjects with active ocular infection or inflammation were excluded, as were those who elected not to discontinue contact lens wear, use of makeup, artificial tears, and facial lotion for a minimum of 24 hours prior to all study visits. Written informed consent, with a complete description of the goals, risks, benefits, and procedures of the study, was obtained from all participants. This study observed the tenets of the Declaration of Helsinki and was approved by the University of California, Berkeley Committee for Protection of Human Subjects.

The study consisted of four visits: two visits using standard, unsheathed Schirmer strips bilaterally and two visits using sheathed Schirmer strips bilaterally, alternating visits between the two strip types. The type of strip used at the first visit and the eye to have the first strip inserted at each visit were randomized. Visits were separated by a minimum of 24 hours and were scheduled

at approximately the same time of day (±2 hours) for each subject to minimize the potential for bias due to possible diurnal variation.[174] Subjects were asked to awaken at approximately the same time of day (±1 hour) and to be awake for at least 4 hours prior to every visit.

At the beginning of each visit, room temperature and humidity were measured using a combination digital thermometer and hygrometer (General Tools & Instruments, Secaucus, NJ). For all tests, examination room temperature and relative humidity were held constant at approximately 22°C and 50%, respectively. Anterior ocular health was assessed with slit-lamp biomicroscopy (SL120; Carl Zeiss Meditec, Inc., Jena, Germany) under white light to ensure that there was no active or preexisting ocular pathology (e.g., corneal scars, infiltrates, superficial punctate keratitis). Subjects were acclimated to the ambient room environment for a minimum of 10 minutes prior to insertion of Schirmer strips bilaterally.

To minimize reflex tearing, two drops of 0.5% (wt/vol) proparacaine hydrochloride ophthalmic solution (Akorn Pharmaceuticals, Lake Forest, IL) were administered to each eye sequentially, with a 1-minute interval separating the bilateral applications. The eye previously randomized to have the Schirmer strip inserted also received the first anesthetic drop. If sheathed strips were randomly assigned for that visit, Schirmer strips (Merck Animal Health, Summit, NJ) were sheathed on both sides with water-impermeable transparent tape (One-Arm Bandit Tape Gun; Conros Corporation, North York, Canada) during the period of anesthetic administration. Further details on the sheathing technique can be found in Li et al.[165] After drop instillation, the area around the eye was blotted with tissue paper to ensure that no residual fluid on the skin could come into contact with the Schirmer strip and artificially inflate wetted length. After waiting an additional minute for the second anesthetic drop to take effect, subjects were instructed to fixate on a point on the ceiling while a strip was inserted in each eye, and then to close their eyes. A single investigator was responsible for all strip insertions to eliminate interinvestigator variability in insertion technique. With the eyes still closed, subjects were led to the chinrest of the slit lamp and instructed to direct their eyes along the primary gaze axis. Wetted lengths of the millimeter-ruled Schirmer strip were recorded through the slit lamp to within 0.5 mm every 30 seconds for 5 minutes. Finally, after removal of the Schirmer strips, corneal staining type, depth, and extent were graded on the Brian Holden Vision Institute (formerly CCLRU) grading scales[177] using sodium fluorescein under cobalt blue illumination and viewed through a 530-nm yellow barrier filter.

In addition to monitoring the wetted lengths of the sheathed STT strips, elimination of evaporative tear loss from the strip permitted calculation of the BTPR in microliters per minute. For standard Schirmer strips, Li et al.[165] establish that

$$\mathrm{BTPR} = 0.7S \tag{5.1}$$

where S is the straight-line slope of the measured wetted lengths between 3 and 5 minutes in millimeters per minute. Because of evaporative loss, BTPR is not readily quantified using unsheathed Schirmer strips.

5.3.2 Statistical Analysis

The repeatability of wetted-length measurement with sheathed and unsheathed Schirmer strips was first assessed by limits of agreement (LoA) with a variance estimate corrected for repeated measures, difference-versus-mean (DVM) plots,[178] and the coefficient of repeatability (CR).[179] The sheathed and unsheathed Schirmer-strip methods were then compared using the methods above and additionally by using multivariable linear mixed-effects models to account for

the internal correlations engendered by the repeated-measures study design while statistically adjusting for external factors, including temperature and humidity, both outdoors and inside the examination room; outdoor wind speed (indoor ventilation "wind speed" was assumed to be constant); and time awake before measurement. Variance-component analysis partitioned the total variance of 5-minute wetted lengths into contributions from between-subject variability as well as differences between strips, visits, and eyes, and residual error. To obtain preliminary estimates of the sample variance and to estimate sample sizes necessary for statistical validity, 20 subjects were recruited for this investigation of sheathed Schirmer strips in modified STTs. Sample-size estimates for future larger group comparisons were made for differing wetted lengths and BPTRs, under the assumptions of 95% confidence and 80% power, using a range of between-subject variances from the current study as well as from the literature.[180,181]

Strip-wetting lengths were discerned only for subjects that exhibited wetted lengths greater than 5 mm after 5 minutes of strip insertion due to length-visibility limitations caused by eyelid concealment.[165] For visits that resulted in unobservable wetted lengths at 5 minutes, wetted lengths were imputed to the median of the unobservable region (2.5 mm).

To avoid the initial nonlinear phase contribution from the tear meniscus, BTPR was calculated from the linear slope of the 3-, 4-, and 5-minute wetting lengths from Equation 1.[165] Repeatability of the BTPR and the relationships of the BTPR to external factors were assessed using an approach similar to that described above for 5-minute wetted lengths. Wetted-strip lengths <5 mm were unobservable, so BTPR calculation was not possible whenever a subject did not exhibit at least three wetting lengths ≥5 mm recorded from 3 to 5 minutes.[165] Readings of completely saturated strips (i.e., wetted lengths of 35 mm) 3 minutes after strip insertion were also excluded from the BTPR determination because no wetting-length dynamics could be assessed.

5.4 Results

Of the 20 subjects initially recruited, 17 subjects (5 males and 12 females, mean [SD] age = 34.4 [9.2] years) completed the study. Three subjects completed only the first visit and discontinued participation due to scheduling conflicts. Subject demographics consisted of 12 East Asians, 3 Caucasians, 1 African American, and 1 South Asian. Out of 17 subjects, eight were contact lens wearers and nine were non–contact lens wearers. Of the 136 total readings taken, nine subjects contributed 41 readings that were less than 5 mm in wetted length after 5 minutes of strip insertion. For those subjects, wetting lengths could not be evaluated. Twenty-one of the 41 readings were from unsheathed strips, and 20 were from sheathed strips. Descriptive statistics for all visits are shown in Table 5.1 for the sheathed and unsheathed Schirmer-strip 5-minute wetted lengths, along with examination room temperature and relative humidity.

Table 5.1. Descriptive Statistics for 5-Minute Wetted Lengths (mm) of Unsheathed and Sheathed Schirmer Strips

Unsheathed Strips	**Min**	**Max**	**Median**	**Mean**	**SD**
Wetted Length (mm), Visit 1	2.5[a]	26	7.5	8.88	6.81
Exam Room Temperature (°C), Visit 1	22.2	23.4	22.8	22.8	0.34
Exam Room Relative Humidity (%), Visit 1	44	53	49.5	48.9	2.86
Wetted Length (mm), Visit 2	2.5[a]	18	7.0	8.15	5.36
Exam Room Temperature (°C), Visit 2	21.3	23.3	22.6	22.6	0.46
Exam Room Relative Humidity (%), Visit 2	35	57	49	48.6	5.58
Sheathed Strips					
Wetted Length (mm), Visit 1	2.5[a]	35	12.0	12.04	8.81
Exam Room Temperature (°C), Visit 1	21.9	23.4	22.7	22.7	0.38
Exam Room Relative Humidity (%), Visit 1	44	54	50	49.5	2.83
Wetted Length (mm), Visit 2	2.5[a]	35	10.5	11.88	8.18
Exam Room Temperature (°C), Visit 2	21.4	23.4	22.8	22.7	0.51
Exam Room Relative Humidity (%), Visit 2	39	55	50	49.1	4.57

[a] Minimum wetted length was interpolated to the median of unobservable region of the Schirmer strip (2.5 mm).

The mean difference between repeat visits in 5-minute wetted length was less than 1 mm for both sheathed and unsheathed Schirmer strips; the two strip types showed comparable repeatabilities. For unsheathed Schirmer strips, the mean (SD) difference was 0.74 (5.05) mm, and for sheathed strips the mean (SD) difference was 0.16 (5.94) mm (Table 5.2). LoA for unsheathed Schirmer strips were [−9.17, 10.64 mm], and for sheathed strips the LoA were [−11.49, 11.8 mm]. Figure 5.1 accentuates no dependence of the intervisit difference on the magnitude of the 5-minute wetted length. The CR between visits for unsheathed strips was 9.17 mm, meaning that the difference between two repeated tests lies within 9.17 mm with 95% probability. The CR for sheathed strips was 10.53 mm.

Table 5.2. LoA Between Visits in 5-Minute Wetted Lengths (mm) of Unsheathed and Sheathed Schirmer Strips

	Mean	**SD**	**LoA**		
Unsheathed Strips	**Diff**	**Diff**	**Lower**	**Upper**	**Width**
Wetted Length Δ (V1-V2)	0.74	5.05	-9.17	10.64	19.81
Sheathed Strips					
Wetted Length Δ (V1-V2)	0.16	5.94	-11.49	11.81	23.30

V indicates visit

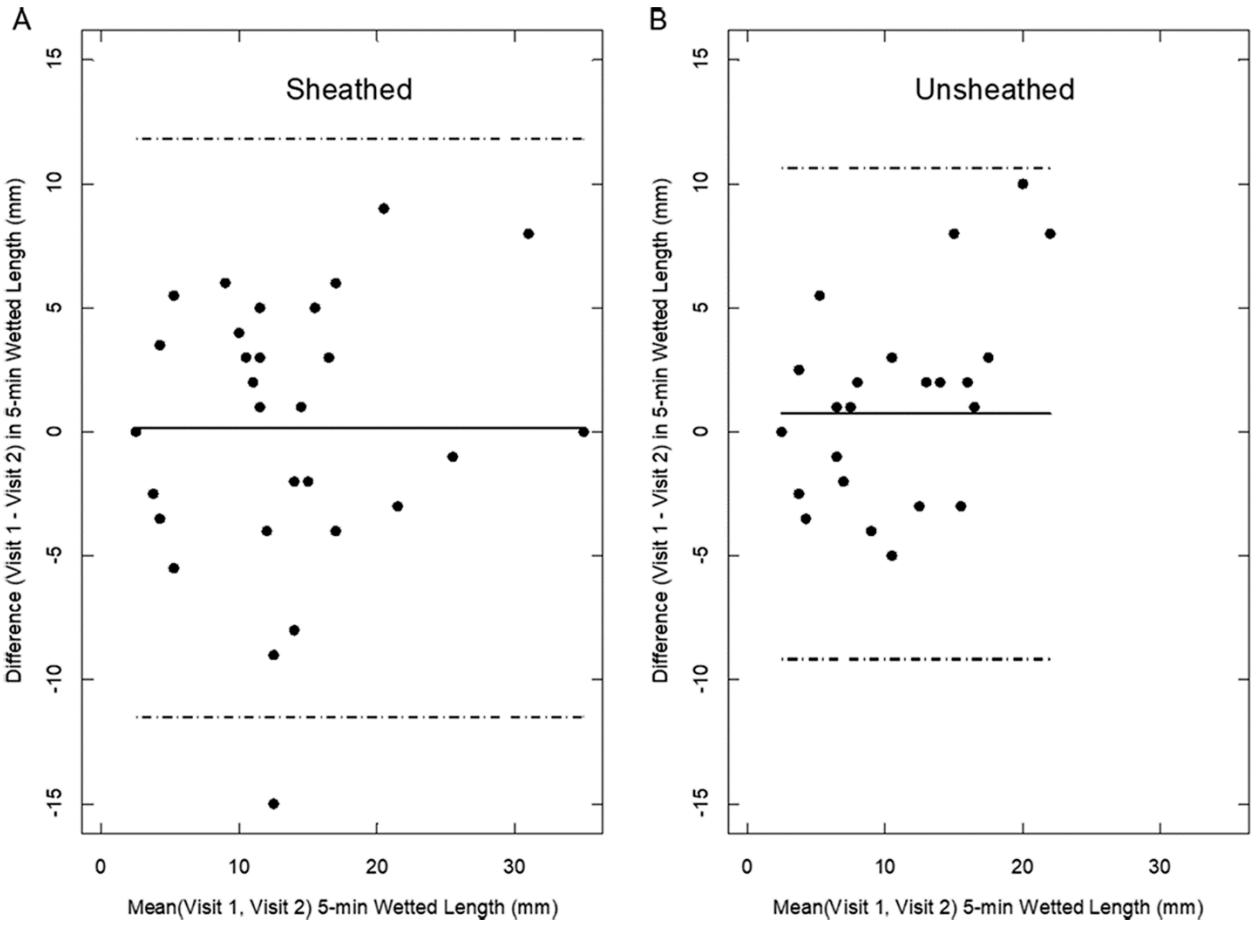

Figure 5.1. Subject visit difference-versus-mean wetting lengths at 5 minutes for (A) sheathed and (B) unsheathed Schirmer strips. A *solid line* designates the mean intervisit difference. *Dashed lines* mark the LoA.

Comparison in Table 5.3 reveals a mean (SD) difference (sheathed − unsheathed) in wetted length of 3.16 (6.04) mm for the first set of visits (i.e., first sheathed visit compared to first unsheathed visit) and 3.74 (6.54) mm for the second set of visits. LoA between the two types of strips were [−8.67, 14.99 mm] for the first visit and [−9.08, 16.55 mm] for the second visit. DVM plots revealed no dependence of the difference between methods (sheathed versus unsheathed) on the magnitude of the 5-minute wetted length. As seen in Figure 5.2, sheathing the strips to inhibit evaporation generally increased wetted lengths compared to the unsheathed strips. Large differences between sheathed and unsheathed wetting lengths are evident for the longest 5-minute lengths because longer unsheathed wetted lengths expose more surface area for evaporation. Mixed-effects models of wetted length revealed sheathed strips to average 3.45-mm longer lengths than unsheathed strips ($P < 0.001$) after accounting for the repeated-measures structure. There was no significant difference between visits ($P = 0.539$) and no significant effects of indoor or outdoor temperature or indoor or outdoor humidity, outdoor wind speed, or time awake before measurement.

Table 5.3. LoA Between Sheathed and Unsheathed Strip 5-Minute Wetted Lengths (mm)

Unsheathed Strips	Mean Diff	SD Diff	LoA Lower	LoA Upper	LoA Width
Wetted Length Δ (S-U)	3.16	6.04	-8.67	14.99	23.66
Sheathed Strips					
Wetted Length Δ (S-U)	3.74	6.54	-9.08	16.55	25.62

S indicates sheathed, U, unsheathed

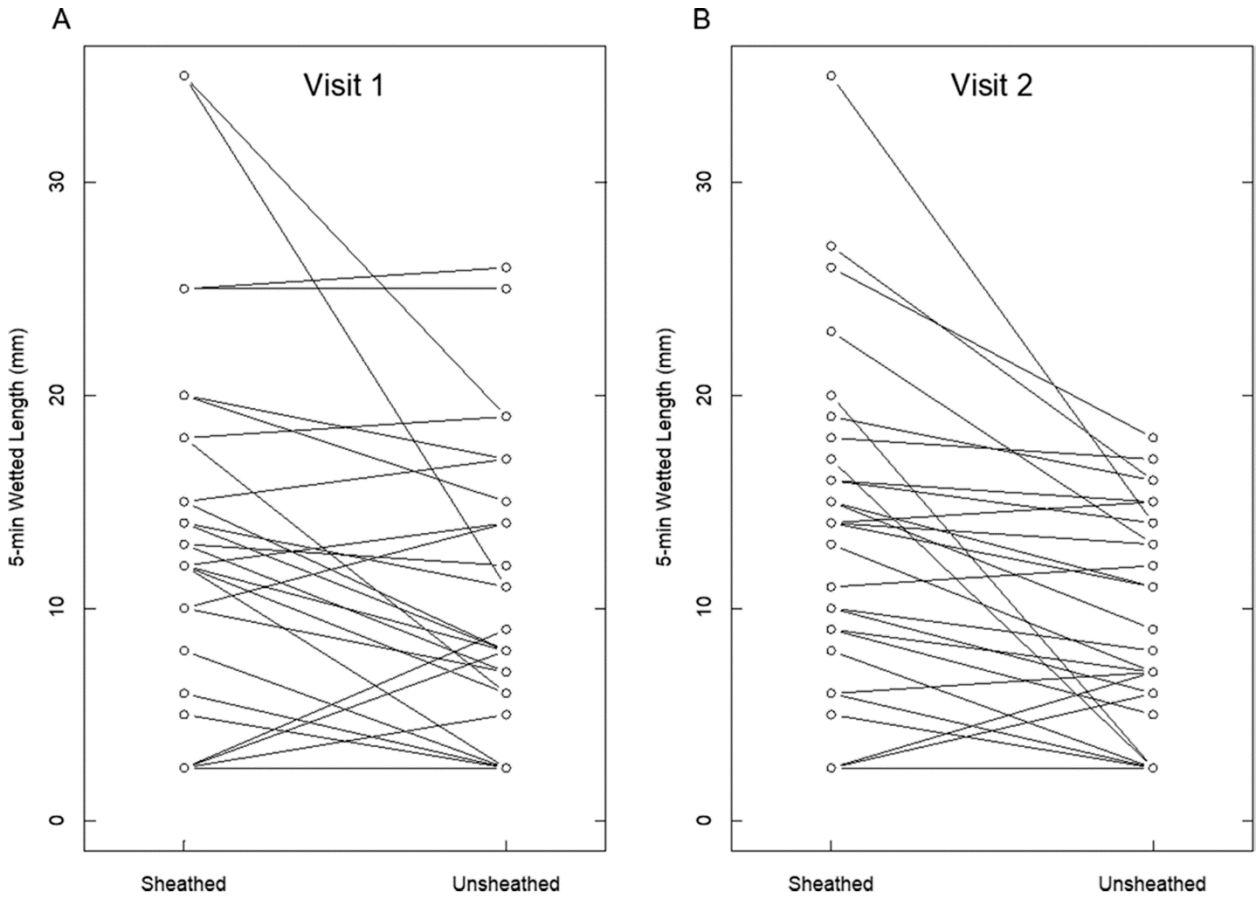

Figure 5.2. Five-minute wetting lengths for each subject with sheathed and unsheathed strips on (A) visit 1 and (B) visit 2. Sheathing inhibits evaporation during testing and allows for greater 5-minute wetted lengths on average.

Sample-size estimates for a hypothetical two-group comparison of Schirmer-strip 5-minute wetted lengths are shown in Table 5.4. As with all such estimates, the larger the variance or the smaller the difference one wishes to detect, the larger is the sample size required. For example, with a sample size of 100 subjects (most efficiently, assuming homoscedasticity, with 50 subjects in each of the groups to be compared[182,183]), group mean differences as small as 2 mm can be detected with at least 95% confidence and 80% power if the smaller of the variance estimates prevails in the population. If the larger variance estimates prove more accurate, 100 subjects suffice if group mean differences of at least 5 mm are of interest.

Table 5.4. Sample-Size Estimates for Comparing 5-Minute Wetted Lengths Between Two Group

SOURCE	Variance (σ^2)	Minimum Difference of Interest (mm)				
		1	2	3	5	10
Smallest σ^2 from Literature (Lee, 1988)	19.536	308	78	36	14	4
Smallest σ^2, Current Study (2018)	22.279	350	88	40	14	4
Largest σ^2 Current Study (2018)	94.743	1488	372	166	60	16
Largest σ^2 from Literature (Lira, 2011)	112.36	1764	442	196	72	18

Figure 5.3 graphs transient wetting lengths as a function of time for one subject with sheathed (closed symbols) and unsheathed (open symbols) strips. Here again, sheathed data evidence longer wetting lengths because evaporation is precluded. Sheathed Schirmer-strip wetted lengths continued to increase linearly for both eyes, allowing calculation of BTPRs; that is, slopes of the solid straight lines drawn for the last 2 minutes of the sheathed STTs give BTPRs from Equation 5.1.[165] Conversely, the unsheathed wetted lengths flattened in time and did not sensibly increase for the last 90 seconds for either eye. BTPRs cannot be directly assessed when Schirmer strips are exposed to the environment. Wetted lengths also could not be assessed below the dashed horizontal line due to visibility limitations.

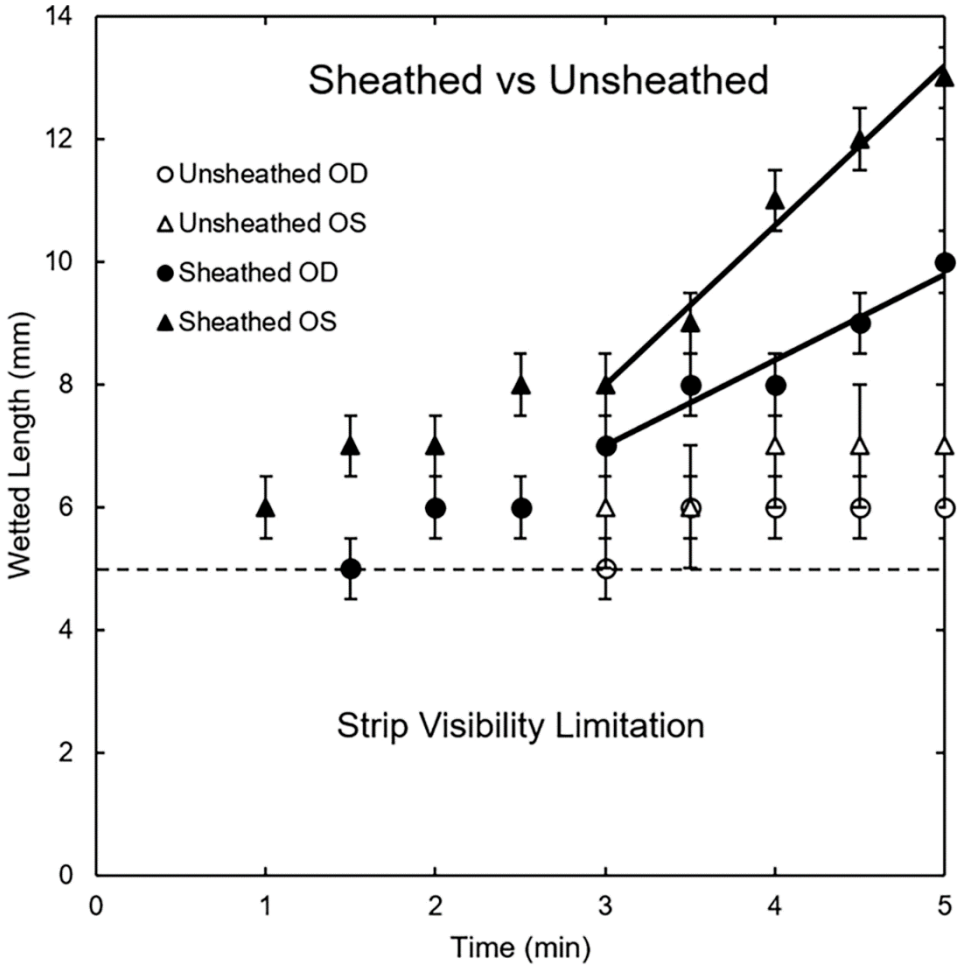

Figure 5.3. Wetting-length dynamics for right and left eyes of subject 15. *Closed symbols* reflect sheathing. *Open symbols* correspond to unsheathed strips. Slopes of the *straight lines* drawn after 3 minutes give the BTPR. Wetted lengths cannot be assessed below the *dashed horizontal line* due to visibility limitation. BTPRs are not available for unsheathed strips because of evaporation. Error bars represent the precision of the Schirmer-strip markings.

Due to evaporation loss, flattening of the wetted lengths occurred in 45% of unsheathed strips. Upon excluding data for completely wetted Schirmer strips (one subject, three readings), 20 out of 44 (45%) of unsheathed Schirmer strip readings had no change in wetted length for the final 90 seconds. Interestingly, 8 out of 48 (17%) of sheathed Schirmer-strip readings also showed similar behavior. This result cannot be explained by evaporation as for unsheathed STTs. Moreover, all eight of these sheathed readings had wetted lengths of ≤10 mm at 5 minutes, while only 11 out of 20 unsheathed Schirmer strip readings with no change in wetted length had wetted lengths of ≤10 mm at 5 minutes.

For 22 sheathed readings, wetting lengths did not exceed 5 mm for at least three of the last observed times. Accordingly, BTPRs could not be quantified for these readings, giving a total of 46 quantifiable BTPRs. Of the 32 eyes with measureable BTPRs, 14 eyes had BTPRs available for repeatability analyses. These are graphed in Figure 5.4. Sheathed BTPRs ranged from 0 to 2.16 μL/min, with a grand mean (SD) of 1.19 (0.61) μL/min. Results stratified on visits were nearly identical (Table 5.5). The CR for BTPR was 1.91 μL/min, meaning that repeated BTPR measurements on the same subject, under the same conditions, and by the same observer, fall

within 1.91 µL/min with 95% probability. Employing the variance estimate corrected for repeated measures,[178] the LoA for BTPR were [−1.82, 1.82] µL/min, with a mean difference of <0.001 ≈ 0 µL/min. There was no dependence of the intervisit difference on the magnitude of the tear production rate (Fig.5.4). Furthermore, there were no significant relationships between BTPR and external factors, including indoor or outdoor temperature or outdoor humidity, outdoor wind speed, or time awake before measurement. Indoor humidity was around 50% and did not influence BTPR. BTPRs are not available for unsheathed strips because of evaporation loss.

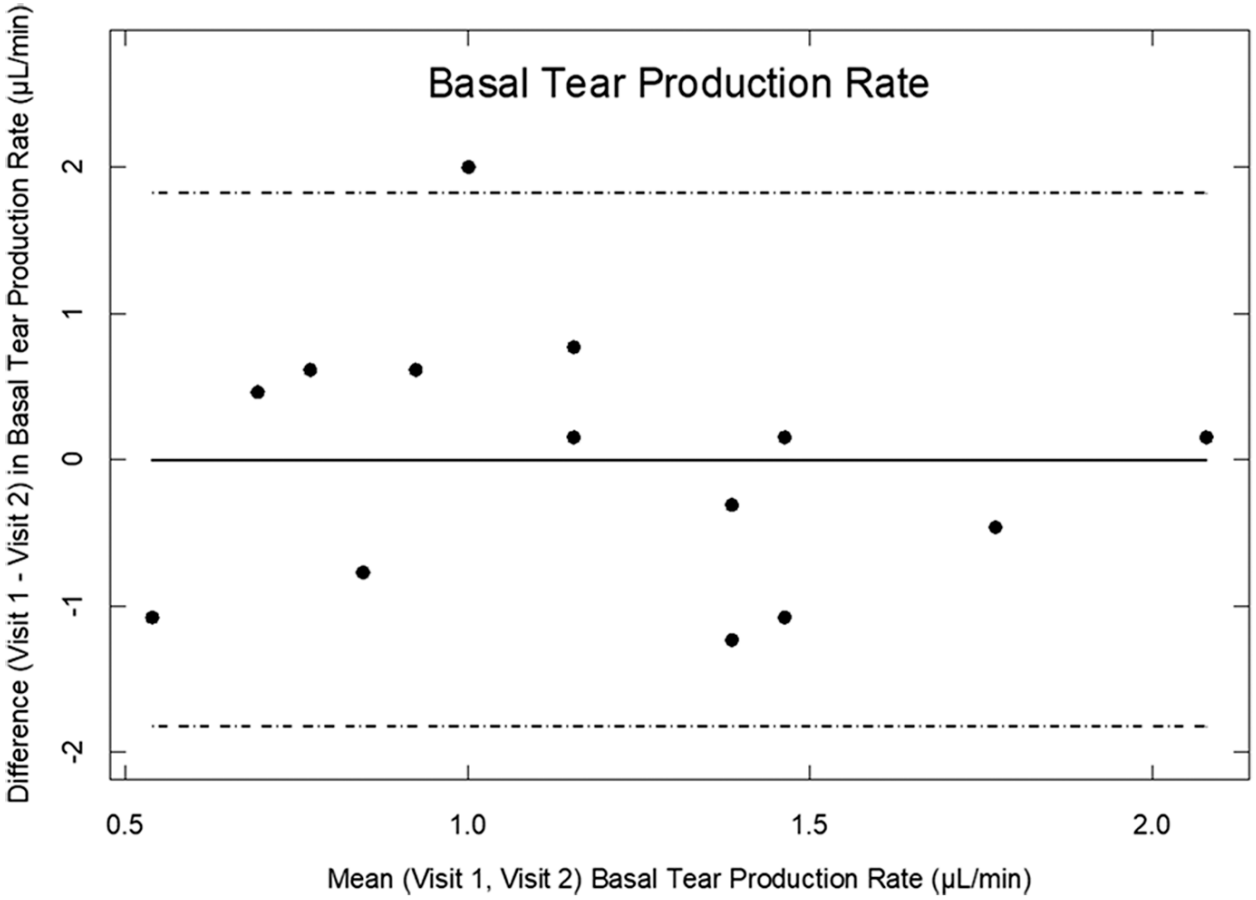

Figure 5.4. Subject visit DVM BTPRs for sheathed Schirmer strips. A *solid line* indicates the mean intervisit difference in BTPR. *Dashed lines* mark the LoA.

Table 5.5. Descriptive Statistics for BTPR (µL/min) From Dynamic Wetted Lengths of Sheathed Schirmer Strips

	Min	Max	Median	Mean	SD
BTPR, Visit 1	0.00	2.16	1.23	1.19	0.57
BTPR, Visit 2	0.00	2.00	1.16	1.19	0.67

Sample-size estimates for a hypothetical two-group comparison of BTPR are shown in Table 5.6. As with all such estimates, the larger the variance or the smaller the difference one wishes to detect, the larger is the sample size required. In this case, because there is currently no understanding as to what a clinically meaningful difference in BTPR might be, we estimated

sample sizes required to detect differences of 5%, 10%, 15%, 20%, and 25% of the maximum BTPR observed (2.156 μL/min, which to our knowledge, is very close to the only published estimate of the maximum BTPR of 2.2 μL/min[184,185]). Confidence and power were set at 95% and 80%, respectively, and variance estimates from current study data were used. In a hypothetical two-group comparison of BTPR, 100 total subjects sufficed to detect a difference in mean BTPR as small as 10% (i.e., 0.2156 μL/min, see Table 5.6). Should the variance in the hypothetical two-group study prove to be closer to our largest, unpartitioned total-variance estimate, 100 subjects are sufficient to detect a difference in mean BTPR as small as 15% (i.e., 0.3234 μL/min, see Table 5.6). The actual BTPR in microliters per minute, or percent change in BTPR, for clinical concern remains to be determined.

Table 5.6. Sample-Size Estimates for Comparing BTPR Between Two Groups

		Minimum Difference of Interest (μL/min)				
SOURCE	**Variance (σ^2)**	**0.1078**	**0.2156**	**0.3234**	**0.4312**	**0.5390**
Smaller (V2) Between-Subject σ^2	0.0928	126	32	14	8	6
Larger (V1) Between-Subject σ^2	0.1250	170	44	20	12	8
Total Unpartitioned σ^2	0.3722	504	126	56	32	22

5.5 Discussion

For anesthetized eyes, sheathed and unsheathed Schirmer-strip wetted-length methodologies yield similar repeatabilities based on DVM plots, LoA, and the CR. Subject awake time prior to measurement, room temperature, outdoor temperature, outdoor relative humidity, and outdoor wind speed had no significant effect on wetted-length dynamics of the strips. Similar repeatability performance of sheathed and unsheathed strip wetted length suggests little reason to sheath Schirmer strips. However, wetted-length dynamics (Fig. 5.3) and the method-comparison analysis clearly demonstrate reduction of wetting lengths with unsheathed Schirmer strips due to evaporation. Out of 11 eyes (eight subjects) that had average unsheathed wetted lengths between 5 and 10 mm at 5 minutes, seven eyes (five subjects) had sheathed wetted lengths greater than 10 mm at 5 minutes. In traditional STT, a wetted length between 5 and 10 mm at 5 minutes post insertion is considered equivocal for aqueous-deficient dry eye.[186] Therefore, evaporation is a significant factor in traditional STTs for patients with <10-mm wetted length at 5 minutes. Most importantly, sheathing the Schirmer strip allows quantification of tear production rates; BTPR is not necessarily correlated with 5-minute wetted lengths.

The most likely reason for the comparable repeatability of the sheathed-versus-unsheathed methodologies is that the single testing site had nearly constant room temperature and humidity for all subjects and all visits. Unsheathed STT strips, therefore, did not have sufficient variability in evaporative flux to display wider LoA. Buckmaster and Pearce[176] found that a relative humidity difference of 60% resulted in a significant difference in 5-minute wetted length but that a difference of 30% did not. Within a constant environment such as a single, climate-controlled examination room, sheathing STT strips, although representative of BTPR, does not improve repeatability. However, for unbiased comparison between different testing sites or between different regions of the world, environmental differences can play an important role. We

recommend sheathing Schirmer strips foremost to maintain consistent repeatability by minimizing or eliminating the effects of external factors and to obtain quantitative BTPRs, for example, in microliters per minute.

Eight of 48 sheathed Schirmer-strip readings showed no change in wetted length for the final 90 seconds, indicating a change in the BTPR to 0 μL/min. This observation has not been reported previously and was not observed in the majority of the current study data that shows constant BTPR for each STT.[164,165] Li et al.[165] showed in vitro that sheathing effectively eliminates the impact of environmental factors, making the abovementioned anomaly difficult to explain unless BTPR diminishes in time during STT for some subjects. It is interesting that seven subjects involved in these eight readings exhibited Schirmer-strip wetted lengths between 5 and 10 mm at 5 minutes post insertion, which is within the range of debate for aqueous-deficient dry eye.[186] In the case of unsheathed STTs, approximately half of the measurements showing no change in wetted length for the final 90 seconds produced wetted lengths >10 mm, resulting in a larger wetted surface area and enhanced evaporative loss. For unsheathed STT strips, wetting length that slows to a constant value is attributed to a balance between evaporation and BTPR. Therefore, wetted lengths >10 mm using unsheathed strips do not necessarily indicate normal BTPRs. This provides an explanation for why traditional STT results correlate poorly with other clinical signs and symptoms.[187] Further studies are necessary to examine the relationships between aqueous-deficient dry eye and BTPR and with changes in that rate over time, especially for subjects whose STT strips wet within the range of 5 to 10 mm.

There are limitations to our study. Due to the visibility limitation for wetted lengths <5 mm, subjects who had less than 5 mm of wetting at 5 minutes post strip insertion were assigned the median wetted length of the nonobservable region, or 2.5 mm. This approximation led to nearly identical 5-minute wetted lengths, as did assigning 5 or 0 mm for nonobserved wetted lengths (i.e., the largest or smallest they could be, respectively, without being observed). This approximation, however, had no bearing on production rate analysis since BTPR could not be determined for these test outcomes. Additionally, without at least three measurable wetted lengths at 3-, 4-, and 5-minute time points for each trial, the BTPR was not assessable. Although the BTPR is not calculable in these situations, patients exhibiting the abovementioned wetting behavior would be classified as aqueous-deficient dry eye by existing STTs.[186] Due to the limitations outlined above, only 14 repeated intrasubject BTPRs were obtained. Additional data are warranted for better population estimates of BTPR and for a fuller assessment of repeatability, taking into account a wider range of testing conditions.

Even after sheathing to minimize or eliminate external environmental effects, sheathed Schirmer-strip 5-minute wetted lengths and BTPRs exhibited relatively poor repeatability. Because the same operator performed the tests in an identical environment, and because theory and in vitro studies validate Schirmer-strip wetting kinetics,[164,165] this observation strongly supports the hypothesis that individuals exhibit substantial day-to-day variability in tear production.[163] Although the unsheathed STTs from our single testing site under controlled conditions exhibited repeatability similar to the modified STTs, sheathing the strips carries the distinct advantage that BTPR can be directly estimated (from Equation 1 following the procedure of Li et al.[165] to eliminate the effects of evaporation and variability in the preexisting lower-lid tear reservoir volume). It is important that modified STT results can be compared without bias across different testing environments.

Chapter 6

Protection Against Corneal Hyperosmolarity with Soft-Contact-Lens Wear

Published as: Kim YH, Nguyen T, Lin MC, Peng C-C, Radke CJ. Protection against corneal hyperosmolarity with soft-contact-lens wear. Prog Retin Eye Res. 2022;87:101012.

6.1 Abstract

Hyperosmotic tear stimulates human corneal nerve endings, activates ocular immune response, and elicits dry-eye symptoms. A soft contact lens (SCL) covers the cornea preventing it from experiencing direct tear evaporation and the resulting blink-periodic salinity increases. For the cornea to experience hyperosmolarity due to tear evaporation, salt must transport across the SCL to the post-lens tear film (PoLTF) bathing the cornea. Consequently, limited salt transport across a SCL potentially protects the ocular surface from hyperosmotic tear. In addition, despite lens-wear discomfort sharing common sensations to dry eye, no correlation is available between measured tear hyperosmolarity and SCL-wear discomfort. Lack of documentation is likely because clinical measurements of tear osmolarity during lens wear do not interrogate the tear osmolarity of the PoLTF that actually overlays the cornea. Rather, tear osmolarity is clinically measured in the tear meniscus. For the first time, we mathematically quantify tear osmolarity in the PoLTF and show that it differs significantly from the clinically measured tear-meniscus osmolarity. We show further that aqueous-deficient dry eye and evaporative dry eye both exacerbate the hyperosmolarity of the PoLTF. Nevertheless, depending on lens salt-transport properties (i.e., diffusivity, partition coefficient, and thickness), a SCL can indeed protect against corneal hyperosmolarity by reducing PoLTF salinity to below that of the ocular surface during no-lens wear. Importantly, PoLTF osmolarity for dry-eye patients can be reduced to that of normal eyes with no-lens wear provided that the lens exhibits a low lens-salt diffusivity. Infrequent blinking increases PoLTF osmolarity consistent with lens-wear discomfort. Judicious design of SCL material salt-transport properties can ameliorate corneal hyperosmolarity. Our results confirm the importance of PoLTF osmolarity during SCL wear and indicate a possible relation between PoLTF osmolarity and contact-lens discomfort.

6.2 Introduction

Numerous clinical studies of tear-meniscus osmolarity demonstrate that dry-eye patients exhibit higher tear osmolarity than those with normal healthy eyes[15–19,21,22,24]. Tomlinson et al.[23] compiled tear-meniscus osmolarities from studies conducted between 1978 and 2004 and determined that the mean values for normal and dry eyes are 302.2 and 326.9 milliosmolar (mOsM), respectively. Since then, a prospective, multicenter study by Lemp et al.[20] showed that tear-meniscus osmolarity has the highest sensitivity and specificity to detect dry eye compared to tear-film break-up time (TBUT), corneal staining, conjunctival staining, Schirmer tear test, and meibomian-gland grading. In contrast, some studies found no significant correlation between osmolarity and dry-eye symptoms.[36,37]

Tear osmolarity is determined by the dissolved solute concentrations which, in turn, depend on tear production, evaporation, and drainage.[26,188] Clinically measured tear osmolarity[15–19,21–24,36,37] usually corresponds to that in the lower tear meniscus, which is significantly lower than that of the pre-corneal tear film (PrCTF).[35,189,190] The no-lens modeling analysis of Cerretani and Radke[35] in Figure 6.1 contrasts the periodic excursions of osmolarity in the PrCTF relative to the menisci for both normal and dry eyes. This figure demonstrates that dry-eye menisci and PrCTF osmolarities can differ by more than 10 mOsM. Higher osmolarity of the PrCTF than that in the menisci is due to the larger surface area for evaporation and the smaller tear volume of the PrCTF, both of which lead to larger increases of solute concentration in the PrCTF than those in the menisci during an interblink. Osmolarities for dry eyes are higher than those of normal eyes due to higher tear evaporation and lower tear production rates.[33,35,190] Menisci hyperosmolarity correlates with dry eye[15–24] because the salinity of the PrCTF in contact with the cornea influences that in the tear menisci through tear mixing upon blinking.[35] Conversely, lack of significant correlation between osmolarity and dry eye seen by some studies[36,37] might be confounded by incomplete blinking, instrument limitation,[38] and/or lack of severe dry-eye patients recruited for the study.[36]

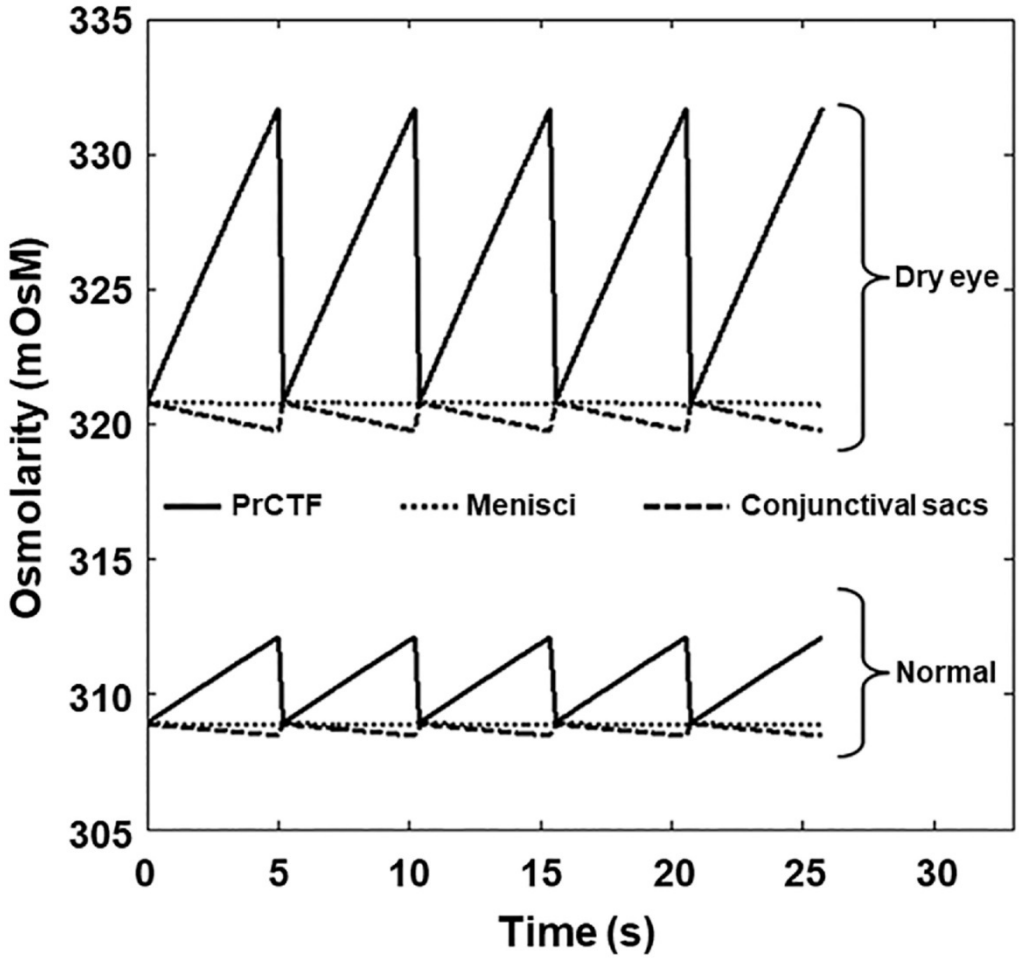

Figure 6.1. Osmolarity of various tear compartments including pre-corneal tear film (PrCTF), menisci, and conjunctival sacs for normal and dry eyes with no-lens wear. Reprinted with permission from Cerretani and Radke.[35] Copyright (2014) Taylor & Francis.

Gilbard et al.[191] first documented the deleterious effects of hyperosmolarity on corneal epithelia using rabbit-eye cells both in vivo and in vitro. When cultured under hyperosmotic conditions, epithelial cells showed adverse responses including decreased intercellular connections, cell-membrane disruptions, and cellular swelling with decreased cytoplasmic density.[191] In-vivo measurements displayed increased cell desquamation.[191] Later, Gilbard et al.[192,193] showed that tear hyperosmolarity also reduces corneal epithelial glycogen and increases conjunctival goblet-cell apoptosis. Studies on the ocular surface of mice[194] and on human limbal epithelial cells[195] demonstrate that hyperosmolar stress activates mitogen-activated protein kinase pathways to produce proinflammatory cytokines, interleukin (IL) - 1β, tumor necrosis factor (TNF) α, and C-X-C chemokine IL-8. The effect of tear hyperosmolarity on ocular-surface immunology was accentuated by Guzmán et al.[196] who established that tear hyperosmolarity initiates nuclear factor-κB signaling in conjunctival epithelial cells and increases dendritic cell recruitment and maturation. These authors also found that tear hyperosmolarity reduces the density of corneal intraepithelial nerves and terminals.[196] Similarly, Hirata and co-authors[13,197,198] revealed adverse effects of tear hyperosmolarity on corneal nerves of rats. Throughout their studies, Hirata et al.[197,198] found that hyperosmolarity leads to corneal sub-basal nerve damage and disappearance of corneal-nerve responses that stimulate tear production. Moreover, those authors documented heightened sensitivity of nociceptive neurons to temperature after a hyperosmolar stress of only 15 min.[13] Liu et al.[14] further showed that exposure of 700-mOsM aqueous salt to bovine corneal epithelial cells for 10–30 s activates mitogen-activated protein kinase (MAPK) pathways, demonstrating that the cornea reacts to a short-term hyperosmolar stress by exacerbating epithelial nerve firing. This observation provides strong evidence for corneal hyperosmolarity initiating dry-eye discomfort.

With soft-contact-lens (SCL) wear, the cornea is over laid by the post-lens tear film (PoLTF) and no longer is exposed to the environment where aqueous evaporation of the pre-lens tear film (PrLTF) increases interblink salinity. Because soft contact lenses experience minor displacements during blinking,[145,199–203] little mixing is expected between pre- and post-lens tear films.[201–203] Thus, at first glance, the PoLTF is isolated from the tear system and should protect corneal nerve endings from hyperosmolar stress. However, increased salt concentration in the PrLTF due to environment evaporation creates a concentration difference that drives salt across the lens and into the PoLTF. Thurs, protection against PoLTF hyperosmolarity may not be complete.

Measurement of on-eye salinity in the approximately 2-μm thick PoLTF has not been achieved, although a number of groups have measured osmolarity associated with SCL wear.[74–78,204,205] Unfortunately, reported lens-wear tear osmolarities are those of the tear meniscus,[74–78] combined tear of all tear compartments,[205] or total tear after lens removal.[204] In view of these major limitations, it is not surprising that no association has been established between measured tear osmolarity and ocular comfort during SCL wear.[74,75,78,204,205] To date, the osmolarity of the PoLTF during SCL wear remains unknown despite the commonality of discomfort symptoms, including dryness, irritation, stinging, and burning, typically attributed to hyperosmolarity.[206]

To determine whether a SCL can act as a barrier against osmolarity increases in the PoLTF, we quantify PoLTF tear osmolarity for differing physiological and lens properties with a tear-dynamics continuum mathematical model. Our proposed model extends the anterior tear-dynamics treatment of Cerretani and Radke[35] to include a SCL and concomitant additional tear films. We incorporate deposition, interblink, and eye-closure phases of blinking as well as tear drainage, evaporation, and production that occur during these phases. The SCL tear-dynamics model also embodies tear exchange occurring between the PoLTF and pre-conjunctival tear films (PrCjTF) observed clinically with fluorophotometry.[203]

6.3 Tear Dynamics

Figure 6.2 illustrates the anterior ocular surface with SCL wear. The drawing is not to scale. The tear film interfacing the environment, either with lens wear (i.e., the PrLTF and PrCjTF) or without lens wear (i.e., the PrCTF and PrCjTF), evaporates during the interblink period. The thickness and cohesive quality of the meibomian-gland exuded tear lipid layer determine the volumetric tear evaporation rate (q_e).[31] Due to black-line formation,[207,208] the tear film is "perched" during the interblink period (t_{ib}) and is effectively isolated from the two surrounding tear menisci.[208] Consequently, evaporation of the tear film into the environment increases salt concentration and, subsequently, tear osmolarity.[209] Meanwhile, menisci osmolarity changes minimally due to the relatively large tear volume and smaller exposed surface area relative to the tear film. During contact-lens wear, the PrLTF evaporates but the lens prevents evaporation of the PoLTF. With zero PoLTF evaporation, the lens theoretically protects the ocular surface from increased salt concentration and, consequently, hyperosmolarity. However, increased salt concentration of the PrLTF due to evaporation creates a concentration gradient of salt, which leads to salt diffusion across the lens into PoLTF. The amount of salt that diffuses under this gradient depends on the lens-salt diffusivity (D_s), the lens-salt partition coefficient (k_s), and the lens thickness (h_{lens})[210] among other variables, such as blink frequency, tear production rate, and evaporation rate. Conversely, diffusive supply of salt from the PrLTF into the PoLTF is opposed by an osmotic-pressure gradient that drives water across the lens from low to high salt concentration.

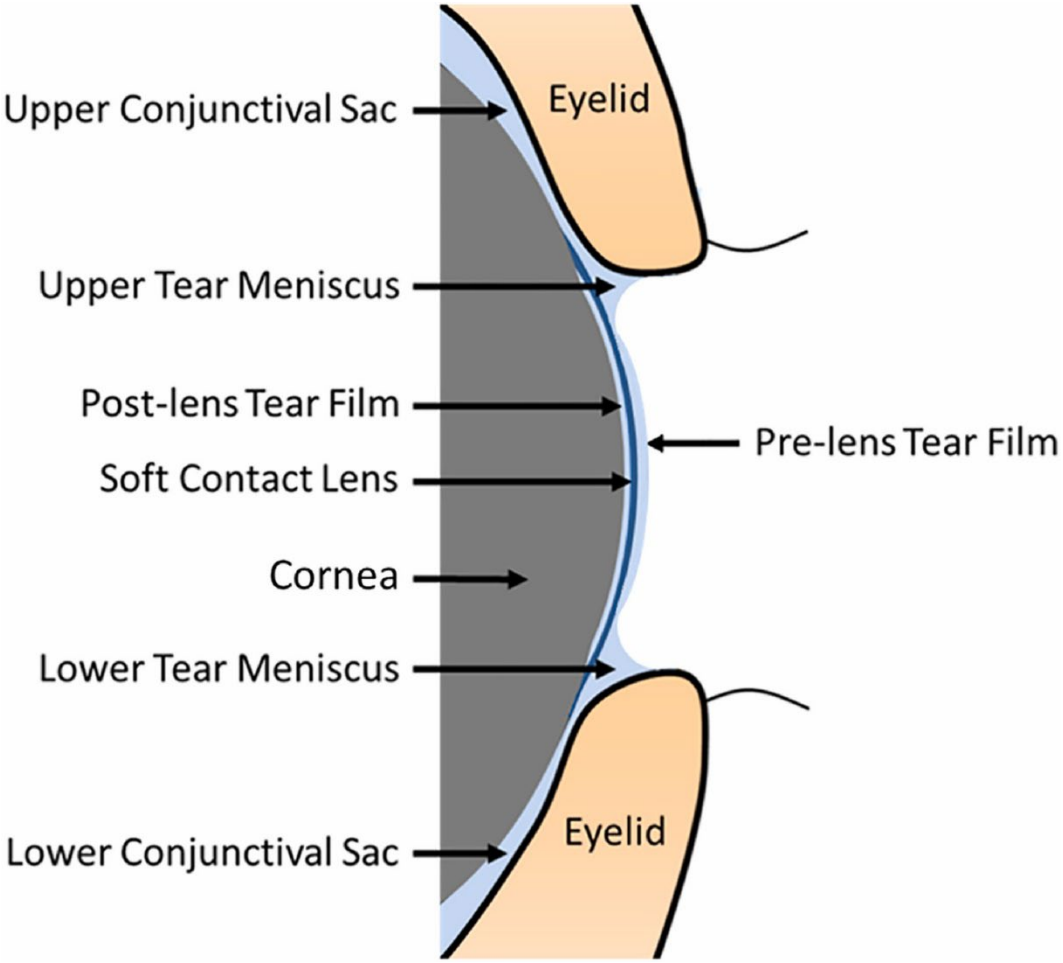

Figure 6.2. Schematic of the ocular surface, tear-film compartments, and soft contact lens. Pre-conjunctival tear film is not visible in this cross-sectional view. The cornea is enveloped by the soft contact lens. The tear film interfacing the cornea is the post-lens tear film (PoLTF). Figure is not to scale.

To quantify PoLTF tear osmolarity, anterior tear dynamics of the PrLTF, PrCjTF, PoLTF, tear menisci, and conjunctival-sac tear compartments all have to be accurately described. Alongside the tear compartments shown in Figure 6.2, the tear-dynamics model must account for the three phases of the blink cycle: eyelid closure, interblink period, and deposition phase. These three major phases of the blink cycle are illustrated in Figure 6.3. Behavior of each compartment during the blink cycle is summarized in the following subsections. Mathematical details are provided in Section 6.5, appendices, and augmented in Cerretani and Radke.[35]

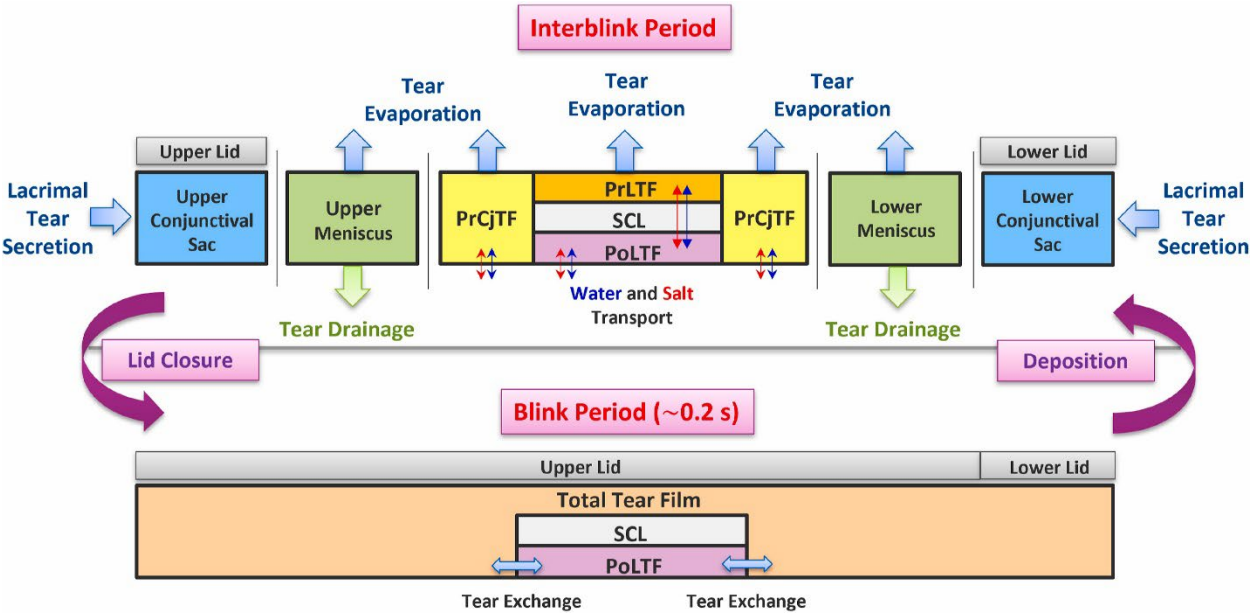

Figure 6.3. Calculation flow diagram of anterior tear system behavior with soft contact lens (SCL) wear. Eyelid closure, interblink, and deposition phases are evident. Upper diagram illustrates open-eye period (5–30 s) while bottom diagram illustrates closed eye (~0.2 s). Salt flux from the bulbar conjunctiva to the PrCjTF is negligible and, therefore, is not included in the calculations. Figure is not to scale.

6.3.1 Eyelid Closure and Opening

During eyelid closure, PrLTF, PrCjTF, tear menisci, and tear in conjunctival sacs mix. Due to the force of the eyelid, the PrLTF, PrCjTF, and tear menisci mix completely to reach a uniform tear osmolarity. However, the extent of fluid mixing in the conjunctival sacs with the PrLTF, PrCjTF, and tear menisci is unclear. With no-lens wear, a scintigraphic study showed that tracer inserted into the menisci rarely travels to the conjunctival sacs.[211] Conversely, several fluorescence studies show that fluorescent dye in the upper and lower conjunctival sacs dilute to the rest of the tear after forceful blinking.[26,184,212,213] Cerretani and Radke[35] argued that the differences in mixing behaviors from the abovementioned studies are likely due to differences in blink strength and eye movement. Even if the tear compartments are not well mixed within a single blink, they will effectively mix with multiple blinks.[35] Therefore, following the detailed discussion of Cerretani and Radke,[35] we argue that PrLTF, PrCjTF, tear menisci, and tear in conjunctival sacs are at a uniform salt concentration upon eyelid closure until the beginning of the subsequent blink during periodic steady state.

Although PrLTF, PrCjTF, tear menisci, and tear in the conjunctival sacs mix during an eye blink, the PoLTF does not mix well with the other tear compartments due to the SCL barrier. Two mechanisms that allow small amounts of tear exchange between PoLTF and the remaining tear compartments are triggered by the force applied from the upper eyelid during a blink.[145] The first type of tear exchange is induced by the lateral (up-down) motion of the lens due to the drag force during eyelid opening and closure. Through mathematical modeling, Chauhan and Radke[199] predicted that lateral movement of the SCL during the blink phase varies depending on the lens elastic modulus and that the lens can move up to 3 mm vertically during a blink cycle.

The second type of tear exchange is caused by transverse (in-out) motion of the lens due to the normal force applied by the upper eyelid during a blink.[145] This results in a lens pumping

motion that squeezes out PoLTF fluid during eyelid closure and suctions in fresh fluid during eyelid opening, respectively. By using aqueous fluorescein isothiocyanate–dextran, McNamara et al.[203] established that the net tear exchange between the PoLTF and rest of the tear compartments is 1–2% of the PoLTF volume per blink cycle. More exchange occurred with small diameter SCLs (i.e., 12.0 mm) than with larger diameter SCLs (i.e., 13.5 mm). McNamara et al.[203] also determined that their tear-exchange values translated to 14.8–19.5 min to deplete 95% of the fluorescein from the PoLTF (T_{95}). For our tear-osmolarity analysis, 1% and 2% PoLTF volume tear exchanges per blink were addressed. Tear osmolarity differences using the two exchange percentage volumes proved negligible for all tear compartments. We set the PoLTF thickness upon eye opening at 2 μm following tear mixing where 1% of the eye-opening PoLTF volume is tear introduced from tear exchange. We chose the 1% PoLTF volume for tear exchange because currently available SCLs have somewhat larger diameters (e.g., 13.8–14.5 mm) than the largest diameter SCL (i.e., 13.5 mm) examined by McNamara et al.[203]

6.3.2 Tear Deposition

During eye opening, the rising upper-lid meniscus deposits a thin tear film on the surface of the contact lens and surrounding basal conjunctiva to form the PrLTF and PrCjTF, respectively.[214] Similar to the PrCTF, the PrCjTF consists of a mucin-rich region, an aqueous interlayer, and a thing lipid layer.[215] Because of the interposed contact lens, the PrLTF is no longer exposed to corneal glycocalyx and corneal mucin-producing goblet cells.[216] The lipid layer covering both the PrLTF and PrCjTF is secreted by the lid meibomian glands[217] while the majority of the aqueous layer is produced from the lacrimal glands.[218] Tear production is discussed more in depth in Section 6.3.3.

The thicknesses of the tear films deposited on the conjunctiva and the lens surface depend on the upper tear-meniscus radius (R_{um}) and the relative upper-eye-lid velocity.[35,214] Mathematically, the relationship of PrCjTF or PrLTF thicknesses to upper-tear meniscus radius and relative velocity is obtained from Bretherton[219] and extended from that of Cerretani and Radke[35] to include the effect of a SCL.

$$h_{tf,j} = 1.34 R_{um} [\mu_w (u_{lid} - u_{s,j}) / \gamma]^{2/3} \tag{6.1}$$

where $h_{tf,j}$ is the thickness of PrCjTF or PrLTF at the beginning of the interblink period, subscript j indicates whether the film is PrCjTF (j =PrCj) or PrLTF (j = PrL), μ_w is tear viscosity, u_{lid} is the velocity of the upper lid, $u_{s,j}$ is the velocity of the bulbar conjunctiva (j = PrCj) or the contact lens (j = PrL) during eye opening, and γ is tear surface tension. Since the bulbar conjunctiva does not move during a blink, $u_{s,PrCj}$ is zero when determining the thickness of PrCjTF. Conversely, the upward velocity of the contact lens in nonzero due to the drag force exerted by the eyelid on the lens as determined from the lens-displacement analysis of Chauhan and Radke.[199] Parameter values used to determine the tear-film thicknesses at the start of the interblink period are provided in Table 6.1. Tear surface tension has been measured by multiple groups with significantly different results.[220–222] Variability is understandable because of the complex procedure to collect human tear and lipid for ex-vivo study and because of the dynamic nature of lipid spreading. We employ the higher tension value of Tiffany and co-authors[220,221] in Table 6.1 since surface tension is expected to be higher near the upper meniscus during lid opening.

Table 6.1. Tear, Lid, and Palpebral Aperture Parameters

Parameter	Symbol	Value (unit)
Tear viscosity	μ_w	1.5[a] $(mPa \cdot s)$
Tear surface tension	γ	45[b] (mN/m)
Upper Eyelid Velocity	u_{lid}	0.05[c] (m/s)
Contact Lens/Conjunctiva Velocity	$u_{s,j}$	0.02[c]/0 (m/s)

[a] Obtained from Ehlers[223] and Tiffany.[224]

[b] Obtained from Nagyová and Tiffany[220] and Tiffany et al.[221]

[c] Derived from Chauhan and Radke.[199]

Because of the upward motion of the lens during a blink, the PrLTF is thinner than the PrCjTF or the PrCTF. This result is supported by the measurements of Wang et al.,[137] who found PrLTF thicknesses after lens fitting to be 3.6 ± 2.1 μm and PrCTF thicknesses to be 4.7 ± 2.3 μm, and King-Smith and his co-authors, who found PrLTF thicknesses of 2.3 ± 0.8 μm[138] and PrCTF thicknesses of 2.7 ± 0.4 μm.[225] A thinner PrLTF compared to the PrCTF suggests earlier tear-film breakup over a SCL compared to breakup over the cornea.[226,227]

6.3.3 Tear Production

Volumetric aqueous production rate (q_{lac}), tear drainage rate (q_d), and tear evaporation rate (q_e) strongly regulate tear osmolarity. The lacrimal glands produce the vast majority of the aqueous fluid of the tear.[218] In comparison, the cornea and conjunctiva provide relatively small amounts of aqueous fluid.[218] Without lens wear, lack of sufficient aqueous production from lacrimal glands results in aqueous-deficient dry eye.[228,229] A decreased aqueous-tear-layer volume leads to a more rapid increase in osmolarity upon tear evaporation. Glasson et al.[230] determined that wetted lengths of phenol-red threads were not statistically different with and without lens wear. In the same study, Glasson et al.[230] showed that intolerant SCL wearers produced shorter wetted lengths than those for tolerant SCL wearers. Unfortunately, measured wetted lengths are not an accurate representation of q_{lac} because the tear volume within the tear lake and the aqueous evaporation from the thread are not accounted for in the phenol-red thread test.[165] We assume the same tear production rate with lens and no-lens wear because to date there are no substantiated differences in aqueous production rates.

Until recently, direct clinical measurement of q_{lac} was not available. Accordingly, Cerretani and Radke[35] used available literature data[26,231,232] for q_e, tear turnover rate, tear volume, and lower meniscus osmolarity (c_{lm}) to back calculate q_{lac}. Since then, significant effort was directed towards modifying the Schirmer tear test to quantify q_{lac} directly.[164,165,233] In a limited clinical study, Kim et al.[233] established a mean q_{lac} of 1.19 μL/min for 17 subjects. The inter- and intra-subject variability of q_{lac} was significant and q_{lac} did not exceed 2.2 μL/min. This observation is consistent with the calculated values of Mishima et al.[184] from tear-turnover rates. However, Kim et al.[233] could not determine q_{lac} from dry-eye subjects that did not wet the Schirmer strip past 5 mm within the 5-min testing time. Therefore, the determined mean qlac excludes the data of those dry-eye subjects and is likely closer to that of normal eyes. Since the measured mean q_{lac} of Kim et al.[233] is very similar to that calculated for normal eye by Cerretani and Radke,[35] we simply used the q_{lac} values of normal and dry eyes determined by those authors as listed in Table 6.2. Details of how q_{lac} was determined are provided in Appendix D of Cerretani and Radke.[35] We also incorporate the small rates of corneal and conjunctival tear production following the work of Cerretani and Radke.[35]

Table 6.2. Tear Production and Evaporation Rates

Case	Lacrimal Production Rate (q_{lac})	Tear Evaporation Rate (q_e)
Normal (μL/min)	1.10	0.15
Dry Eye (μL/min)	0.55	0.30
Normal Lens-Wear[a] (μL/min)	1.10	0.23

[a] Determined based on measurements of Guillon and Maissa[234] with 30–40% relative humidity.

6.3.4 Tear Drainage

By using high-speed photography, Doane[235] visualized and explained tear drainage during blink cycles. Upon eyelid closure, the upper eyelid sweeps downward to consolidate tear film into the lower meniscus, while the lower eyelid moves laterally in the nasal direction to deliver tear in the lower meniscus into the medial canthus for eventual tear drainage.[235] During the first ~1/3 of lid closure, upper and lower puncta are occluded by the lid margins. The remaining 2/3 of eyelid closure squeezes tear in the canaliculi and lacrimal sac into the nasal cavity through the nasolacrimal canal. When the eyelid retracts, relaxation of canaliculi and lacrimal sac lowers the liquid pressure below that of the environment. Consequently, once the eye opens and the puncta are no longer occluded, tear in the medial canthus is sucked into the puncta by capillary action filling the canaliculi and lacrimal sac and restoring liquid pressure. Thus, tear drainage from the ocular surface occurs during the interblink and depends on the tear-meniscus radii and blink strength.

Tomlinson and Khanal[26] estimated tear-drainage rate by clinically measuring the tear-turnover rate upon instilling aqueous fluorescein dye into the eye and following the reduction in fluorescein intensity. With known initial fluorescein concentration, volume of the fluorescein drop, and transient decline in fluorescein intensity, tear-drainage rate can be calculated. This method, however, is indirect, assumes that the tear volume remains constant, and requires a correction factor for the fluorophotometer.[26] Tear-turnover rates from various authors tabulated by Tomlinson and Khanal[26] ranged from 0.12 to 1.47 μL/min.

Based on Doane's observations,[235] Zhu and Chauhan[236] developed a sophisticated mathematical tear-drainage model recognizing that the drainage rate through the puncta arises primarily from capillary suction. They established that the range of drainage rates for normal eyes is rather large from 0.10 to 4.00 μL/min depending on the canaliculus thickness and Young's modulus. Subsequently, Cerretani and Radke[35] simplified the Zhu and Chauhan[236] analysis by relating the capillary-pressure-driven drainage rate to the upper and lower menisci radii. We utilize the formulation of Cerretani and Radke[35] here for our q_d estimates. Although q_d ranged from 0.10 to 4.00 μL/min for the model of Zhu and Chauhan,[236] the semi-empirical model of Cerretani and Radke[35] ranged q_d from 0 to 2.00 μL/min since tabulated tear-turnover rates of Tomlinson and Khanal[26] suggest that tear-drainage rates do not exceed 2.00 μL/min. Further information can be found in Section 6.5.2.1.

6.3.5 Tear Evaporation

Upon completion of eye opening, PrCjTF, PrLTF, and tear menisci are exposed to the environment and undergo evaporation, thereby increasing compartment tear osmolarities. Similar to no-lens wear, lens-wear q_e is affected by the quantity and quality of the tear-lipid layer[217] in addition to environmental factors, such as surrounding temperature, airflow, and humidity.[237] McCulley and Shine[238] suggested a lamellar-stack structure for the lipid layer that is approximately

10 nm in thickness. Observed colors in the spreading lipid layer[239] and the in-situ interferometry measurements of King-Smith et al.,[240] however, indicate a much thicker layer, greater than about 50 nm. Rosenfeld et al.[30] found that fully organized lamellar structure is not consistent with the discrete melting behavior found in their rheologic, x-ray scattering, and differential scanning calorimetry studies. Instead, a duplex-film waxy-suspension structure of 50–100 nm in lipid-layer thickness was proposed. Although retardation of q_e by the lipid layer has been well documented,[31,217] the molecular architecture of the lipid layer and how much it reduces tear evaporation are not settled.

As reviewed by Tomlinson et al.,[26,212] most studies of in-situ tear evaporation use closed-chamber evaporimeters that are misinterpreted as well mixed in both temperature and relative humidity. Interferometry measurement of tear film thinning under open air and under a goggle by Kimball et al.[241] further suggest that closed-chamber evaporimeters do not provide accurate measurement of tear-film evaporation. To overcome the well-mixed deficiency and to quantify the role of room air circulation, Peng et al.[242] developed an in-vivo flow evaporimeter that quantifies the effects of airflow velocity and relative humidity while measuring environmental temperature. Figure 6.4 illustrates the device. Inlet air of known relative humidity, R_H, temperature, and volumetric air flow, Q, gently impinges on the eye where tear evaporation humidifies the outlet flow stream. The rate of tear evaporation is calculated from the measured humidity increase of the return air. In a limited three-subject analysis, they showed that increasing the inlet relative humidity from 20 to 40% resulted in up to a 40% decline in q_e and varying the airflow velocity from 5 to 16 cm/s resulted in up to 50% increase in q_e. The preliminary clinical results of Peng et al.[242] at the lowest flow velocities fall within the rather wide range of q_e values tabulated by Tomlinson et al.[26,212] This finding accentuates the need for q_e measurements with well-defined airflow and relative humidity. For our tear-system calculations, q_e values without lens wear for both normal and dry eyes were averaged from the groups tabulated by Tomlinson et al.[26,212] along with the data from Peng et al.[242] at a relative humidity of 40% following the procedure of Cerretani and Radke.[35] Table 6.2 gives the resulting values.

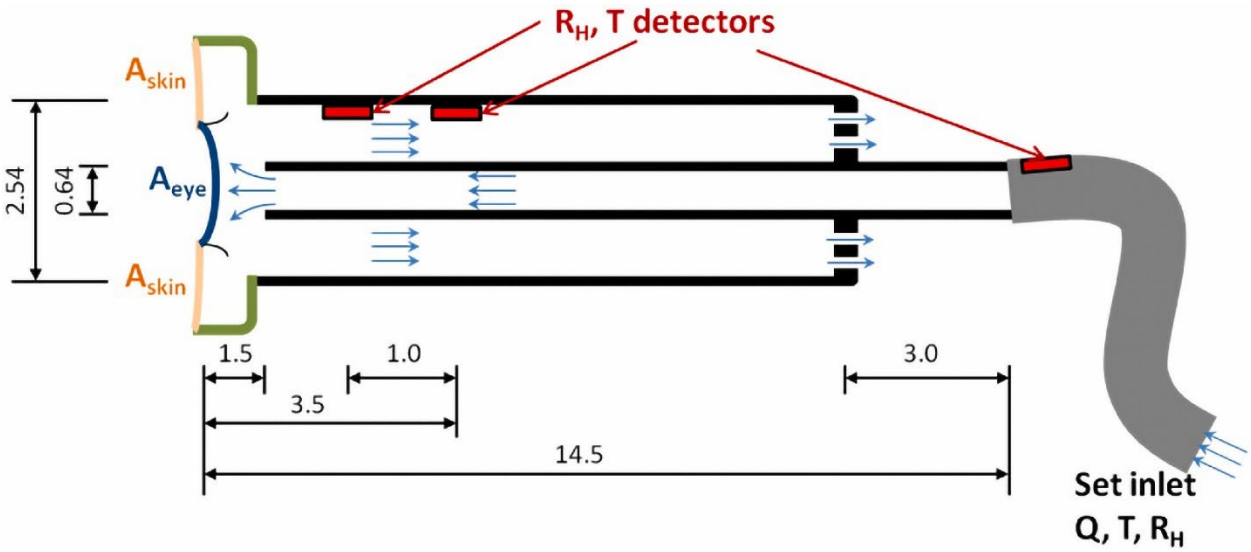

Figure 6.4. Schematic of flow evaporimeter. At a set air flow volumetric rate, Q, inlet and exit relative humidities, R_H, and temperatures are measured permitting calculation of evaporation rate. Dimensions are in cm. Drawing is not to scale. Reprinted with permission from Peng et al.[242] Copyright (2014) American Chemical Society.

6.3.6 Soft Contact Lens

Simultaneous water and salt transport occur between the PrLTF and the PoLTF because SCL materials are both water[243] and salt permeable.[210] Salt concentration differences, which occur across the SCL due to PrLTF evaporation, and lens properties (i.e., D_s, k_s, and h_{lens}) determine the rate of salt transport across the lens. Salt transport occurs from high to low concentration whereas simultaneous water transports in the opposite direction due to the osmotic-pressure difference.

The rate of water transport through the lens depends on h_{lens}, on water viscosity, and on the hydraulic permeability of water (K).[73] Because of the difference in deposited tear-film thickness between the PrLTF and the PrCjTF during lens wear, there also exists a lateral salt-concentration difference between these two regions to cause water and salt transport at the lens landing zone where the PrLTF interfaces with the PrCjTF. Potential impacts of salt and water transport between different tear compartments and across the SCL are further discussed in Section 6.6.

For salt transport, D_s describes how fast salt travels within a SCL material, whereas k_s describes the ability for salt to partition into the lens material at the SCL/tear-film interfaces when in equilibrium with a given aqueous salinity. In steady state, D_s and k_s appear as the product of the two as the salt permeability, $D_s k_s$. Because our tear system is dynamic, values for both D_s and k_s are required separately in this study.[244] Yasuda et al.[245] established that an increase in water content of a cross-linked hydrogel increases both D_s and k_s. Therefore, in Section 6.4 to follow, we determine individual lens properties (D_s, k_s, and K) necessary to quantify lens salt and water transport rates.

6.3.7 Perched Tear Film

From both a clinical in-vivo study using aqueous fluorescein and an in-vitro study, McDonald and Brubaker[207] showed that the tear film near the tear menisci thins due to a Young-Laplace[246] pressure difference between the concave menisci and the less curved tear film during an interblink period. Thus, a lower liquid pressure exists in the curved menisci compared to that in the less curved convex tear film because of surface tension and the curvature difference of the air/liquid interface.[208,247] The resulting capillary pressure difference drives flow from the tear film into the menisci. The flow resistance in the thin tear film is strong enough for the capillary-pressure suction to create a thin dimple in the tear film directly adjacent to menisci immediately upon stoppage of the upper eyelid opening.[208] When viewed under fluorescein instillation, the thin dimples appear as "black lines"[207,208] due to quenching of the fluorescein.[248] Black lines effectively isolate the tear film from mixing with the menisci leading to so-called "perched" tear films.[208,249] Thus, evaporative salinity increases in the tear film are not diluted by mixing with the connecting menisci.

However, based on clinical observations of one of our co-authors (MCL), not all subjects display visible black lines after fluorescein insertion. This may be caused by conjunctival folds preventing formation of meniscus concavity and a smaller pressure difference between the menisci and the adjacent convex tear films. In such cases, there is a possibility that the tear film is not strongly isolated during the interblink period. We deal with this situation in Appendix 6E and establish that salt exchange between the PrLTF and the menisci has negligible effect on the determined compartment osmolarities.

With SCL wear, black lines are not observable due to dye solubility in the lens obscuring black-line visualization.[250] Numerous studies have reported and quantified concave tear menisci with SCL wear.[251–254] This observation plus the very low hydraulic permeability of SCLs indicate that the PrLTF can also be considered as perched during an interblink.

Proceeding Sections 6.4 and 6.5 provide detail on the lens transport-property measurements and on the tear-system modeling mathematics. Readers interested in results may proceed to Section 6.6.

6.4 Lens Transport Properties

With the advent of silicone-hydrogel SCLs to minimize corneal hypoxia during lens wear, considerable effort has been made to determine water and salt transport coefficients across SCLs.[40,73,210,243,244,255] We now outline the experimental measurements that set the transport parameters of the SCL pertinent to assess PoLTF salinity during contact-lens wear. Salt and water transport are discussed separately.

6.4.1 Salt Transport

Lens-salt permeability, $D_s k_s$, is directly measured in a modified Stokes cell: a two-chamber system separated by the SCL.[40,210,244,256] A schematic of the apparatus developed by Guan et al.[210] is highlighted in Figure 6.5. The bottom chamber of the apparatus is initially filled with a salt-water solution of known concentration while the top chamber is initially filed with deionized water. Both chambers are well stirred to eliminate mass transfer resistances at each side of the lens. By detecting the electrical conductivity in the top cell over time and by invoking pseudo-steady salt diffusion across the lens, the value of $D_s k_s$ is obtained directly.[210,244] To garner individual values of D_s and k_s, both Guan et al.[210] and Peng and Chauhan[244] measure the equilibrium partition coefficient in a separate back-extraction experiment. A lens of known dry mass is first soaked in an aqueous solution of known high salt concentration until equilibrium is reached. The salt-equilibrated lens is then placed in well-mixed deionized water where salt leaches out until a new equilibrium is attained. k_s is calculated from the difference in initial and final equilibrium leached-salt concentrations by mass conservation. Once k_s is known, lens-salt diffusivity follows from the Stokes-cell measured salt permeability.

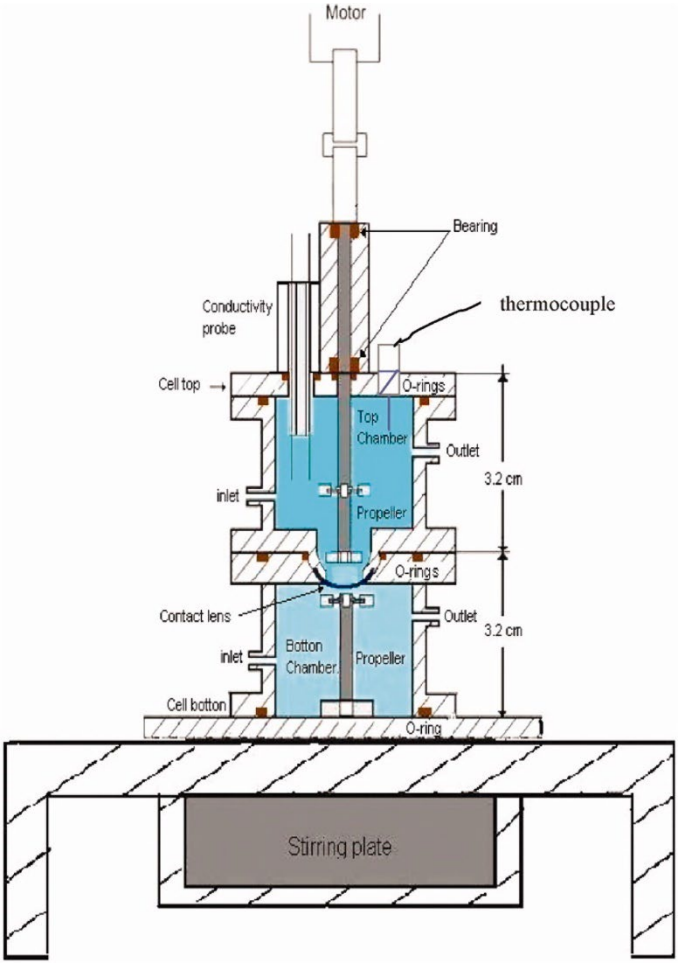

Figure 6.5. Schematic of the Stokes cell developed by Guan et al.[210] to measure the salt permeability (D_sk_s) of SCLs. Bottom chamber has a known initial salt concentration while the top chamber is initially filled with deionized water. Electrical conductivity determines the rise in salt concentration of the top chamber. Reprinted with permission from Guan et al.[210] Copyright (2011) John Wiley and Sons.

Alternatively, Peng and Chauhan[244] extend the back-extraction procedure by monitoring the leached salt concentration in time until equilibrium emerges. The time course of the leached salt concentration is fit to Fick's second law to establish D_s. The salt partition coefficient, k_s, is ascertained by the back-extracted equilibrium concentration as above; salt permeability is then given by the product of D_s and k_s. These authors found that the pseudo-steady Stokes-cell and the transient back-extraction methods give comparable results.

Figure 6.6 shows measured equilibrium salt partition coefficients of 1 M NaCl in silicone-hydrogel (open symbols) and HEMA-based (filled symbols) SCLs as a function of lens fractional water content reproduced with permission from Guan et al.[210] The solid line corresponds to a partition coefficient equaling the water content of the lens. Except at high water contents, salt partitioning into SCLs falls below this simple relationship.

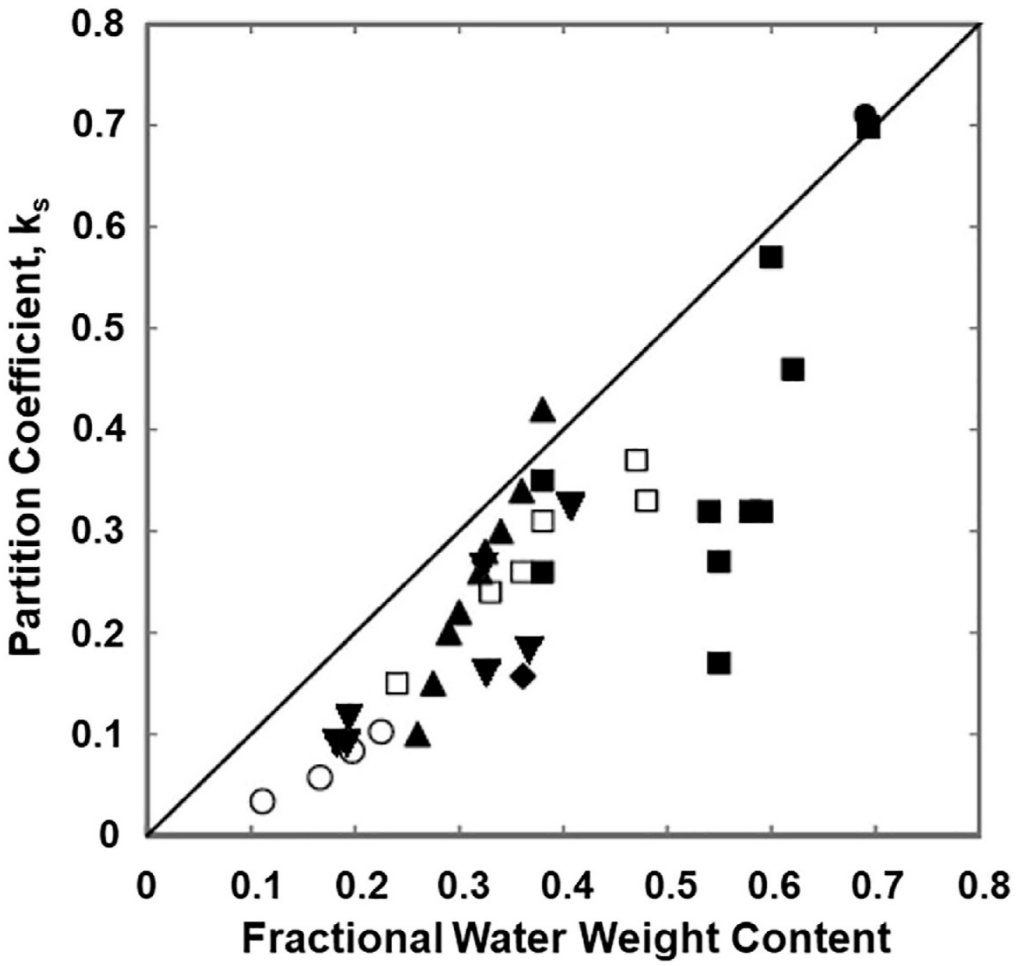

Figure 6.6. Partition coefficient, k_s, versus fractional water weight content at 35° C. Open symbols correspond to silicone-based material lenses (SiHy) and filled symbols represent hydroxyethyl-methacrylate-based material lenses (HEMA). Rectangles represent commercial lenses while other symbols represent hydrogel membranes studied from various authors. The solid line corresponds to when the partition coefficient equals the lens water content. Reprinted with permission from Guan et al.[210] Copyright (2011) John Wiley and Sons.

Guan et al.[210] and later Dursch et al.[257] note that ideal salt partitioning into hydrogels corresponds to $k_s = \varphi_w$ where φ_w is the water volume fraction in the lens. Deviations from ideal partitioning are accounted for by introducing a salt-enhancement factor: $E_s (\equiv k_s / \varphi_w)$. Dursch et al.[257] suggest that the enhancement factor is the product of at least three contributions $E_s = E_s^{ex} E_s^{el} E_s^{ad}$ where E_s^{ex} designates hard-sphere exclusion from the gel, E_s^{el} reflects nonspecific electrostatic repulsion or Donnan exclusion, and E_s^{ad} corresponds to specific adsorption of salt to the polymer chains of the gel. The small deviations from ideality in Figure 6.6 and the high ionic strength of the aqueous salt solution dictate that the electrostatic-repulsion factor is close to unity. We do not expect strong specific adsorption of salt to the lens polymeric strands so the adsorption enhancement factor is also unity. Thus, partial rejection of salt from the SCLs in Figure 6.6 suggests hard sphere repulsion exclusion so that E_s^{ex} is slightly less than unity. Calculations in

Guan et al.[210] and Dursch et al.[257] reveal that this suggestion is reasonable and that $k_s = \varphi_w$ at large water contents consistent with Figure 6.6.

Figure 6.7 reports measured aqueous salt diffusion coefficients in SCLs as a function of inverse water content from the work of Guan et al.[210] As in Figure 6.6, open symbols correspond to silicone-hydrogel lenses and filled symbols correspond to HEMA-based lenses. As water content decreases, salt diffusivity in the lenses decreases by orders of magnitude from its value in water. Solute diffusivities in hydrogels relative to that in bulk water can be expressed as the product of a hydrodynamic resistance factor, F, and an obstruction factor, S: $D_s/D_\infty = FS$.[257,258] Here, D_∞ represents bulk molecular diffusion coefficient of aqueous sodium chloride. The myriad of small cross-linked polymer strands in swollen hydrogels causes both hydrodynamic and obstruction factors to be considerably smaller than unity. Several theories for diffusion in hydrogels suggest that $D_s/D_\infty = \exp[-a(1-\varphi_w)^b]$ where a and b are adjustable constants.[259] For b = 1, Yasuda et al.[245] demonstrate that for large water contents this expression can be rewritten as $\ln(D_s/D_\infty) = -a[\varphi_w^{-1} - 1]$. If we approximate water volume fractions in the lenses by lens water content, the eye-fit straight line in Figure 6.7 confirms this relationship. Another way of understanding the strong reductions in salt diffusion coefficients by SCLs is from the expression $D_s = D_\infty/\tau_s^2$ where τ_s is the lens-salt tortuosity or the ratio of path length taken by the salt ions as they traverse through the gel to the gel thickness.[210] According to Table III of Guan et al.,[210] τ_s in SCLs varies from 2 to close to 10 or reductions in aqueous salt diffusivities by up to 100, consistent with Figure 6.7. D_s values adopted in this manuscript were chosen based on the values of Guan et al.[210] and of Mann et al.[256] for more modern SCLs.

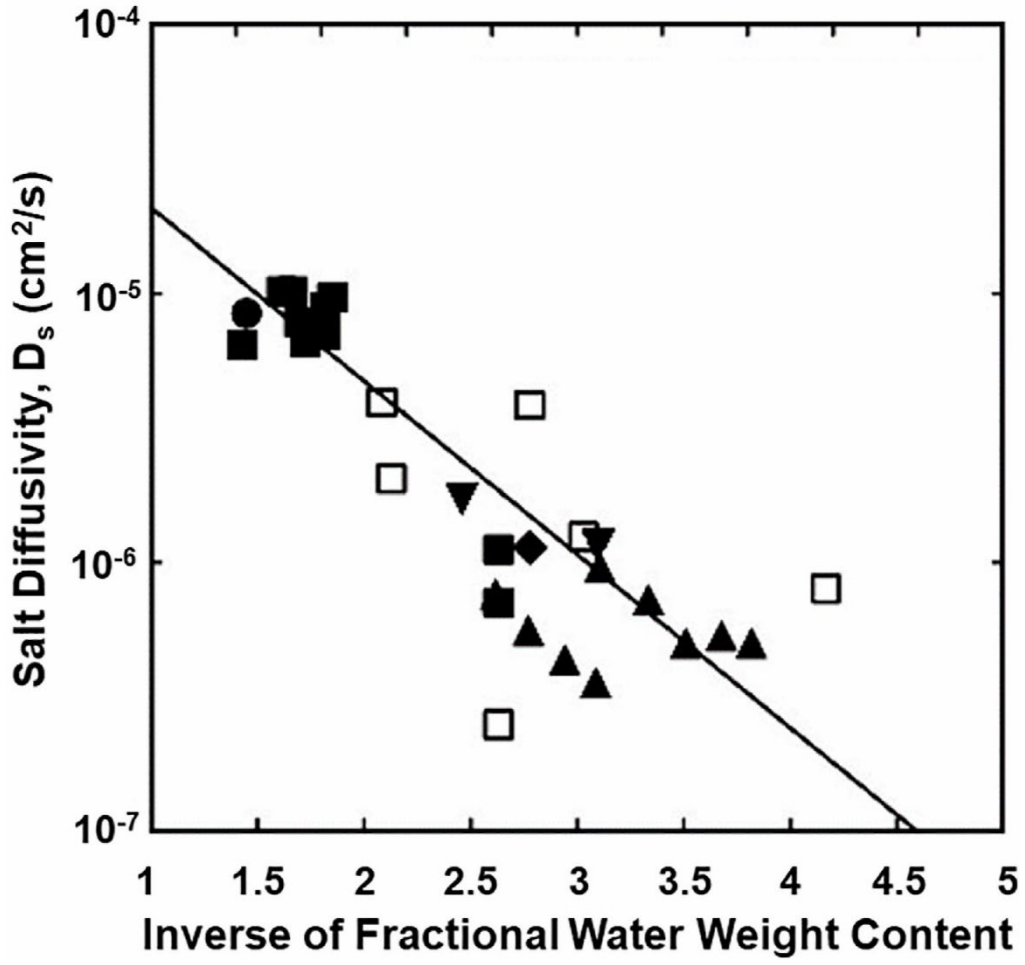

Figure 6.7. Semilogarithmic graph of salt diffusivity, Ds , versus the inverse frac tional water weight content at 35° C. Horizontal axis of unity corresponds to the diffusivity of salt in pure water at 35° C. Open symbols correspond to silicone-based material lenses (SiHy) and filled symbols represent hydroxyethyl-methacrylate-based material lenses (HEMA). Squares represent commercial lenses while other symbols represent hydrogel membranes studied from various authors. The solid line guides the eye. Reprinted with permission from Guan et al.[210] Copyright (2011) John Wiley and Sons.

6.4.2 Water Transport

Hydrodynamic permeability, K, of a SCL for pressure-driven aqueous flow is necessary to predict osmotic-pressure back flow through a lens exposed to a salt concentration difference. We rely on the values measured by Monticelli et al.[73] Figure 6.8a is a schematic of the apparatus. Water is forced through the membrane by an air-pressure-driven constant-head tank. Volumetric flow rate is measured by the water-height change rate in the small-diameter vertical capillary tube. Flow rates through the SCL membrane sheets are very small requiring data collection over many hours. With such small flows, care must be taken to prevent leakage around the membrane. Figure 6.8b displays the membrane-holder design and the requisite O-ring seals. With the pressure drop and volumetric flow rates measured for varying applied pressure drops, and with the known water viscosity, thickness of the membrane, and membrane cross-sectional area, K follows from Darcy law[260]: $v_w = (K/\mu_w)[-\Delta P/L]$ where v_w is superficial velocity, μ_w is tear viscosity, L is membrane

thickness, and ΔP is pressure drop. Defined in this manner, the units of hydraulic permeability are length squared: K equal to 1 Darcy, characteristic of beach sand, corresponds to 1 μm^2.

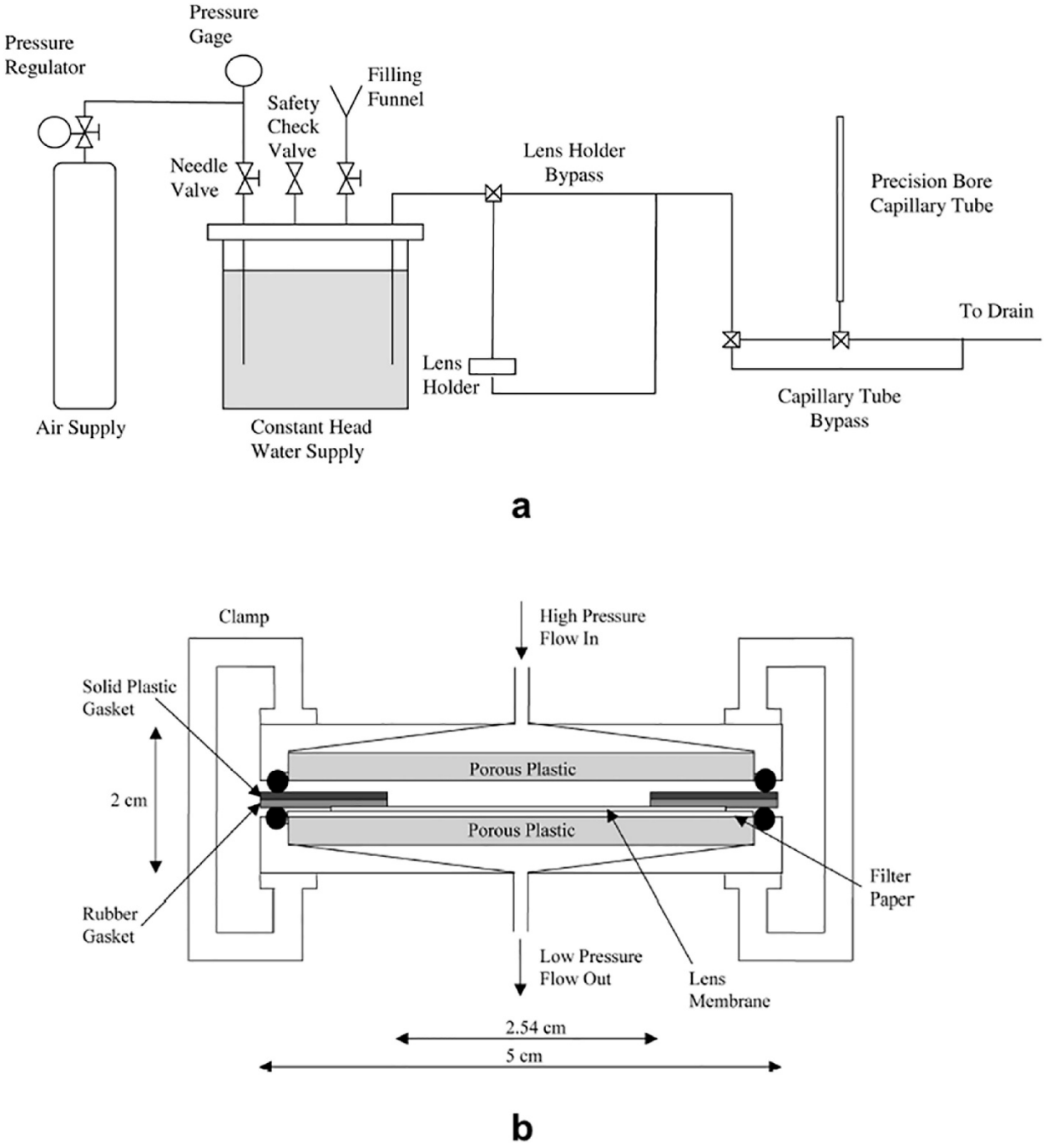

Figure 6.8. Schematic of the flow apparatus to measure Darcy hydraulic permeability, K, of a SCL membrane. (a) Overall design and (b) detailed design of the lens-membrane holder are provided. Water is forced through the lens membrane that is placed in the lens-membrane holder by a known pressure difference. Water rise in vertical capillary tube allows determination of the volumetric flow rate to measure K. Reprinted with permission from Monticelli et al.[73] Copyright (2005) Taylor & Francis.

Figure 6.9 from Liu et al.[261] reports K values as a function of $(1-\varphi)^3/\varphi^2$ from Monticelli et al.[73] and Refojo[262] at typical water contents of SCLs and Quinn and Grodzinsky[263] for hydrogels of much higher water contents where φ is the polymer volume fraction in the lens. Liu et al.[261] write the functionality of K with polymer content as

$$K = \frac{(1-\varphi)^3}{8\varphi^2\tau_H^2} a_f^2 \tag{6.2}$$

where a_f is the polymer-strand characteristic radius and τ_H is the hydrodynamic tortuosity. Equation 6.2 motivates the $(1-\varphi)^3/\varphi^2$ choice for the abscissa in Figure 6.9. On log-log axes, Equation 6.2 demands a straight line and allows calculation of a_f/τ_H. Liu et al.[261] identify a strand radius of around 2 nm and a hydrodynamic tortuosity of about 5, in general agreement with those above for salt-diffusion tortuosities determined by Guan et al.[210] An important finding from Figure 6.9 is the extremely small SCL hydrodynamic permeabilities in the pico-Darcy range. The reason for these small valves is the very small molecular polymer fiber size.

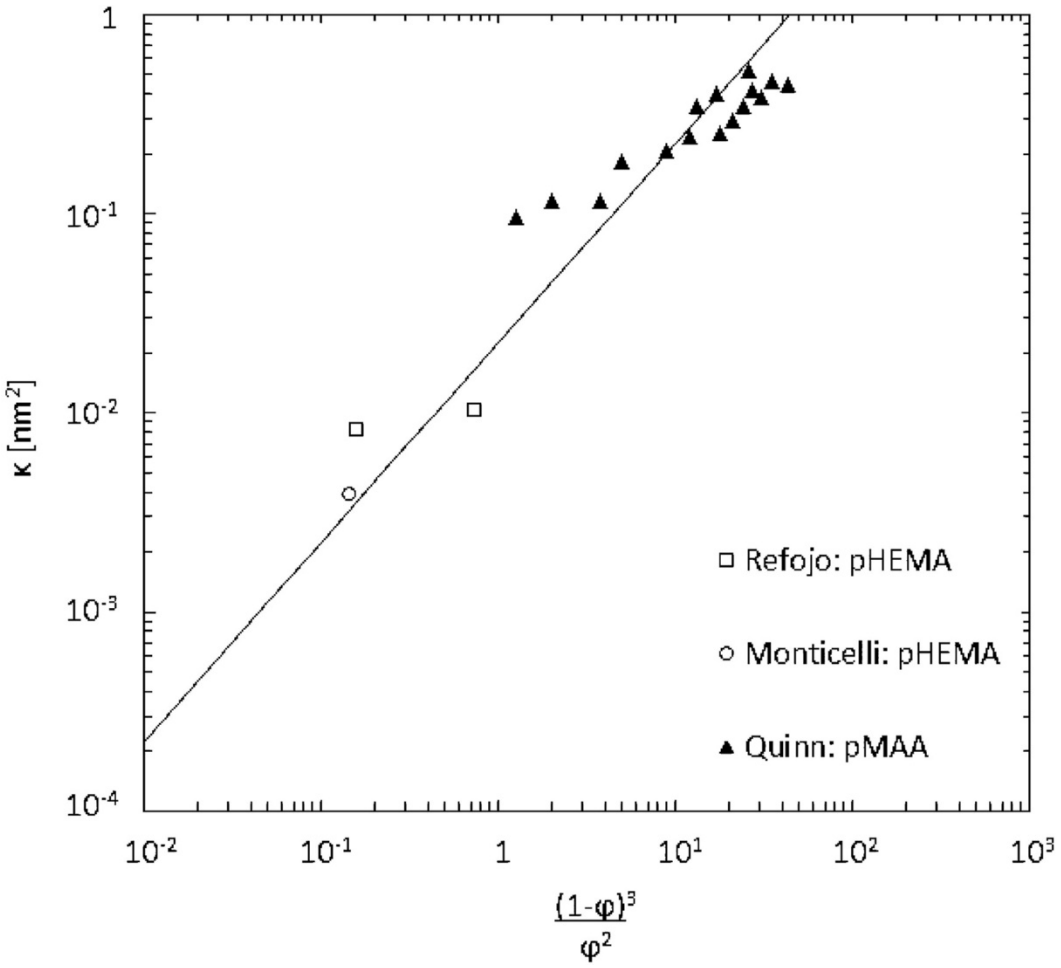

Figure 6.9. Hydrodynamic permeability, K, as a function of polymer content expressed as $(1-\varphi)^3/\varphi^2$ for hydrogels similar to 70-wt% hydroxyethyl methacrylate (HEMA)/30-wt% methacrylic acid (MAA): Refojo[262] (□); Quinn and Grodzinsky[263] (▲); Monticelli[73] (○). With a_f = 2 nm, the best-fit unity-slope straight line on log-log scales gives a hydrodynamic tortuosity of τ_H = 4.7. Reprinted with permission from Liu et al.[261] Copyright (2013) American Chemical Society.

6.5 Mathematical Formulation

In this section, we outline the isothermal tear-dynamics model with SCL wear for time-periodic blinking. To predict tear osmolarity in the PoLTF, PrLTF, PrCjTF, and tear menisci with SCL wear, water and salt mass must be conserved in all tear compartments during blink and interblink periods. We assume that the properties of salt are those of aqueous sodium chloride, which is the dominant solute in tear. The proposed model accounts for PrLTF evaporation, tear exchange at the lens periphery, tear-film deposition, lacrimal-gland tear production, tear drainage, water and salt fluxes through the SCL, and tear production from the cornea and conjunctiva. All calculations are performed in Matlab R2019b (Mathworks, Natick, MA). Computation of the three phases of the blink cycles (i.e. deposition period, interblink period, and eyelid closure) are repeated until periodic-steady state is attained. We assess the importance of lens parameters (i.e., D_s, k_s, K, and h_{lens}), duration of interblink period (i.e., t_{ib}), and tear evaporation and production (i.e., q_e and q_{lac}) on tear-film compartment osmolarities. Fundamental equations are summarized in the

following subsections while detailed equations are available in the appendices or in the work of Cerretani and Radke.[35]

6.5.1 Deposition Phase

The tear-deposition period involves formation of upper and lower menisci, PrLTF, and PrCjTF during upper-lid rise. Due to the short time ~0.2 s interval of the deposition phase, we assume that evaporation is negligible. At the beginning of deposition, the initial tear volume and salt concentration of the menisci are determined iteratively so that the mass of salt and water are conserved in all tear compartments. This calculation is unchanged from that of Cerretani and Radke[35] (see Appendices B and D of that reference).

Due to upward lens motion during eye opening,[199] deposited film thicknesses are different in the PrLTF (lens region) and PrCjTF (no-lens region) as determined from Equation 6.1. Consequently, upon completion of PrLTF and PrCjTF deposition, upper meniscus volume and curvature radius differ between the PrLTF and PrCjTF regions. As the meniscus-volume difference between the two regions is small and has minimal effect on the meniscus osmolarity during the interblink period, the two upper-meniscus volumes are averaged to determine an average upper-meniscus radius.

6.5.2 Interblink Period

During the interblink period, the transient partial differential equation for transport across the lens is solved numerically with forward finite difference.[103] Meanwhile, the time-dependent ordinary differential equations for the compartment mass balances are solved with a Runge-Kutta marching algorithm (ode45 command in Matlab) following the work of Cerretani and Radke.[35] Ordinary differential equations are converged every time step of 0.01 s until periodic steady state is reached. Except for the SCL, we assume that each tear compartment is well mixed during the interblink period. Mathematical representation of salt and water transport for each compartment is provided below. Required physical constants are provided in Table 6.3. Values for physical constants not specifically listed and details regarding the numerical methodology are available elsewhere.[35,103]

Table 6.3. Physical Constants

Parameter	Symbol (Unit)	Value
Lid margin perimeter	S_{lid} (mm)	30[a]
Maximum drainage rate	q_m (μL/min)	1.0[b]
Minimum drainage radius	R_0 (μm)	120[b]
Bulbar conjunctival area uncovered by eyelid	A_{cj} (cm^2)	1.05[a]
Lens area uncovered by eyelid	A_{lens} (cm^2)	1.54[c]
Corneal area uncovered by eyelid	A_{cn} (cm^2)	1.05[a]
Lens water concentration	$c_{w,lens}$ (mol/cm^3)	0.02[c]
Lens hydraulic water permeability	K (μm^2)	9.7×10^{-9}[d]
Lens thickness	h_{lens} (μm)	60 ~ 200
Interblink period	t_{ib} (s)	5 ~ 30
Lens salt diffusivity	D_s (cm^2/s)	$0 \sim 6 \times 10^{-6}$
Salt partition coefficient	k_s	0 ~ 1
Secreted tear salt concentration	c_{blink} $(mOsmol/L)$	150[a]
Salt diffusivity in water	D_∞ (cm^2/s)	2.25×10^{-5}[e]
Gas constant	R $(J/(mol * K))$	8.3145
Temperature	T (K)	310
Reflection coefficient of salt	σ_{cn}	0.79[f]
Corneal epithelium membrane salt permeability	ω_{cn} (cm/s)	7.37×10^{-11}[f]
Water volume fraction	ϕ_w	0.38[g]
Length from lens center to meniscus	λ (mm/s)	5.5

[a] Obtained from Cerretani and Radke.[35]
[b] Obtained from Zhu and Chauhan.[236]
[c] See Main Text
[d] Obtained from Monticelli et al.[73]
[e] Pratt and Wakeham.[264]
[f] Leung et al.[5]
[g] Determined from Hoch et al.[255] and Guan et al.[210]

6.5.2.1 Tear Menisci

In the interblink period, tear flows into the upper and lower menisci from the upper and lower conjunctival sacs, respectively. Following Cerretani and Radke,[35] 80% of q_{lac} flows into the upper conjunctival sac from the lacrimal gland while the remaining 20% of q_{lac} flows into the lower conjunctival sac. Meanwhile, tear also drains from the menisci via capillary suction through the puncta.[35,235,236] Water conservation for each tear meniscus is written as

$$\frac{dV_{im}}{dt} = q_{laci} - q_{di} - q_{e,im} \qquad i = u, l \qquad (6.3)$$

where i = u or l to denote upper or lower meniscus, respectively, t is time, $V_{im} = 2(1-\pi/4)R_{im}^2 S_{lid}$ is the meniscus volume, S_{lid} is the lid perimeter, R_{im} is the tear-meniscus radius, q_{laci} is the volumetric lacrimal flow rate entering the meniscus from the conjunctival sac where $q_{lacu} = 0.8q_{lac}$ and $q_{lacl} = 0.2q_{lac}$, $q_{di} = q_m(1-R_0/R_m)$ is the volumetric tear drainage rate based on Cerretani and Radke[35] of upper (i = u) or lower (i = l) puncta, q_m is the maximum drainage rate, and R_0 is the meniscus radius when drainage ceases. q_{di} changes transiently due to dependence on the shrinking

menisci radii and ranges between 0 and 1.00 μL/min based on q_m and R_0 determined by Cerretani and Radke[35] to match the results of Zhu and Chauhan.[236] As previously stated, the maximum tear-drainage rate (i.e., $q_d = q_{du} + q_{dl}$) is 2.00 μL/min. Calculated q_d values fall within the range of tear-turnover rates tabulated (i.e., 0.12–1.47 μL/min) by Tomlinson and Khanal.[26] $q_{e,im}$ is the set volumetric evaporation rate of upper or lower menisci and is determined by multiplying the volumetric evaporation flux, $\tilde{J}_{w,e}$, with the cross-sectional area of upper or lower meniscus ($A_{im} = \pi R_{im} S_{lid}/2$). Additional detail regarding this mass balance is provided in Appendix B of Cerretani and Radke.[35]

Salt conservation for each tear meniscus reads

$$\frac{d(c_{im}V_{im})}{dt} = c_{si}q_{laci} - c_{im}q_{di} \qquad i = u, l \tag{6.4}$$

where c_{si} is the salt concentration of the conjunctival sac and c_{im} is the salt concentration of the meniscus. c_{im} depends on the tear-film salt concentration from the well-mixed blink period and the lacrimal gland salt concentrations. Although the upper and lower menisci osmolarities are calculated separately, the two menisci osmolarities are approximately the same due to their large tear volumes.

6.5.2.2 Pre-Conjunctival Tear-Film Balances

Aqueous conservation in the palpebral aperture not covered by the contact lens (i.e., the PrCjTF) is similar to that of the pre-corneal tear film.[35,265] However, water is gained only from osmotic-driven flow through the bulbar conjunctiva instead of from both the bulbar conjunctiva and the cornea. Water conservation for this region is written as

$$\frac{dV_{PrCj}}{dt} = -q_{e,PrCj} + \alpha q_{cj} \tag{6.5}$$

where V_{PrCj} is the volume of water in the PrCjTF, $q_{e,PrC} = A_{cj}\tilde{J}_{w,e}$ is the volumetric evaporation rate of tear for the PrCjTF, $q_{cj} = A_{cj}\tilde{J}_{w,cj}$ is the volumetric flow rate of water from the bulbar conjunctiva into the PrCjTF, A_{cj} is the cross-sectional area of the bulbar conjunctiva that is uncovered by the eyelids, $\tilde{J}_{w,cj}$ is the volumetric water flux from the bulbar conjunctiva, and α is the fraction of bulbar conjunctiva not covered by the contact lens and the eyelids. Detailed information to determine α is provided in Appendix 6A. Calculation of $\tilde{J}_{w,cj}$ is outlined in Appendix B of Cerretani and Radke.[35]

The bulbar conjunctiva secretes ions into the PrCjTF[266] but the rate is not expected to be large.[35,267] Thus, salt conservation for the PrCjTF is written as

$$\frac{d(c_{PrCj}V_{PrCj})}{dt} = 0 \tag{6.6}$$

where c_{PrCj} is the transient salt concentration in the PrCjTF.

6.5.2.3 Pre-Lens Tear-Film Balances

New PrLTF and PoLTF compartments unique to SCL wear are added to the previous Cerretani-Radke model[35] to determine the osmolarities of the two tear films. Because SCLs are

permeable to both salt and water, PrLTF osmolarity depends on both tear evaporation and transport of salt and water across the contact lens. Water conservation for the PrLTF is described by

$$\frac{dV_{PrL}}{dt} = -q_{e,PrL} + q_{lens} \tag{6.7}$$

where V_{PrL} is the volume of water in the PrLTF, $q_{e,PrL} = A_{lens}\tilde{J}_{w,e}$ is the volumetric evaporation rate of tear for the PrLTF, $q_{lens} = A_{lens}\tilde{J}_{w,lens}$ is the volumetric water transport rate across the lens, A_{lens} is the cross-sectional area of the lens exposed to the environment, and $\tilde{J}_{w,lens}$ is the volumetric water flux across the lens. Details regarding $\tilde{J}_{w,lens}$ are provided in Section 6.5.2.4.

Salt conservation in the PrLTF is mathematically represented as

$$\frac{d(c_{PrL}V_{PrL})}{dt} = A_{lens}J_{s,lens} \tag{6.8}$$

where $J_{s,lens}$ is the molar salt flux at the anterior surface of the lens directed from the PoLTF to the PrLTF. Because the difference in salt concentration between the PrLTF and PoLTF can be either positive or negative, $J_{s,lens}$ similarly may be positive or negative. Details regarding $J_{s,lens}$ are provided in Section 6.5.2.4.

6.5.2.4 Soft-Contact-Lens Balances

Volumetric water flux across the lens follows a modified Darcy law and is given by

$$\tilde{J}_{w,lens} = v_w = \frac{2KRT}{\mu_w}\frac{(c_{PrL} - c_{PoL})}{h_{lens}} \tag{6.9}$$

where R is the ideal gas constant, T is the temperature of the lens, c_{PrL} is the PrLTF salt concentration, and c_{PoL} is the PoLTF salt concentration. Detailed derivation is provided in Appendix 6B. $\tilde{J}_{w,lens}$ is determined from the osmotic salt-concentration difference between PoLTF and PrLTF and can be positive or negative depending on that difference.

Water-flow-driven salt convection and salt diffusion determine the salt flux at the PrLTF and PoLTF lens interfaces. The transient salt concentration profile across the lens is determined from the following partial differential equation

$$\frac{\partial c_{lens}}{\partial t} + \tilde{J}_{w,lens}\frac{\partial c_{lens}}{\partial z} = D_s\frac{\partial^2 c_{lens}}{\partial z^2} \tag{6.10}$$

where c_{lens} is the salt concentration within the lens per unit lens volume and z is the spatial location within the lens from the posterior ($z = 0$) to the anterior ($z = h_{lens}$). Equation 6.10 is solved numerically with finite differences and boundary conditions: $c_{lens}(0) = k_s c_{PoL}$ and $c_{lens}(h_{lens}) = k_s c_{PrL}$. Transient solution to Equation 6.10 is nested within each time step of the numerical solution of the ordinary differential equation tear-compartment balances. Therefore, the iteration time step used for the lens salt balance is 0.001 s and is an order of magnitude smaller than the time step used to solve the compartment mass balances. Convergence for the nested numerical evaluation of Equation 6.10 is achieved for each of the time steps used for the compartment mass balances.

Once the lens-salt transient concentration profile is established at each compartmental time step, molar salt fluxes at the PrLTF and PoLTF lens interfaces are calculated by the expression

$$J_{s,lens} = \tilde{J}_{w,lens} c_{lens} - D_s \frac{\partial c_{lens}}{\partial z} \qquad z = 0, h_{lens} \tag{6.11}$$

Lens salt flux is evaluated at the lens anterior surface, z = h_{lens}, and at the lens posterior surface, z = 0, and is used in the PrLTF and PoLTF compartment balances of Equations 6.8 and 6.13 (to follow), respectively. Further details regarding lens-salt transport are outlined in Appendix 6C.

6.5.2.5 Post-Lens Tear-Film Balances

In addition to water flow from/to the lens, water also flows from the cornea and the bulbar conjunctiva into the PoLTF. Therefore, water conservation in the PoLTF is given by the relation

$$\frac{dV_{PoL}}{dt} = (1-\alpha) q_{cj} + q_{cn} - q_{lens} \tag{6.12}$$

where V_{PoL} is the volume of water in PoLTF, $q_{cn} = A_{cn}\tilde{J}_{w,cn}$ is the volumetric flow rate of water from the cornea into the PoLTF, A_{cn} is the cross-sectional area of the cornea not covered by the eyelids, and $\tilde{J}_{w,cn}$ is the volumetric water-flux supply from the cornea. Details regarding $\tilde{J}_{w,cn}$ are presented in Appendix B of Cerretani and Radke.[35] Again, q_{lens} is the volumetric water-transport rate across the lens obtained from Equation 6.9.

Similar to lens water flow, there is a salt flux into/out of the PoLTF across the lens during the interblink period. In addition, salt transports from the cornea into the PoLTF.[5] Salt transport across the bulbar conjunctiva is ignored, as previously discussed. Salt conservation in the PoLTF is, therefore, represented as

$$\frac{d(c_{PoL}V_{PoL})}{dt} = -A_{lens}J_{s,lens} + \left[(1-\sigma_{cn})\,\tilde{J}_{w,cn} < c_{cn} > -\omega_{cn} RT \Delta c_{cn}\right] A_{cn} \tag{6.13}$$

where the bracketed terms represent the Kedem-Katchalsky membrane equation for salt transport across the cornea[100] and $J_{s,lens}$ is the molar salt flux through the SCL from Equation 6.11. σ_{cn} is the corneal-epithelium reflection coefficient of salt, $< c_{cn} >$ is the arithmetic average salt concentration in the corneal epithelial layer, ω_{cn} is the corneal epithelium membrane permeability to salt, and Δc_{cn} is the salt-concentration difference between the PoLTF and the corneal epithelium. Details and constants of the Kedem-Katchalsky equation can be found in Leung et al.[5] σ_{cn} and ω_{cn} are those of sodium or chloride; the corneal epithelial salt concentration is set as 150 mOsM.

6.5.3 Eyelid Closure

At the end of the interblink period, the eyelid takes approximately 0.2 s to close.[1,35] During this phase, salt and water in the menisci, conjunctival sacs, PrLTF, PrCjTF, and a fraction of the PoLTF all mix together. The mixed concentration, c_{bulk}, is the same for all compartments, except the PoLTF, for the next interblink period. Salt and water balances during the mixing process are given by

$$c_{bulk}V_{total} = c_{PrL}V_{PrL} + c_{PrCj}V_{PrCj} + c_{um}V_{um} + c_{lm}V_{lm} + c_{su}V_{su} + c_{sl}V_{sl} + c_{blink}V_{blink} + \beta c_{PoL}V_{PoL} \tag{6.14}$$

and

$$V_{total} = V_{PrL} + V_{PrCj} + V_{um} + V_{lm} + V_{su} + V_{sl} + V_{blink} + \beta V_{PoL} \quad (6.15)$$

respectively. V_{blink} and c_{blink} are tear volume and salt concentration produced by the lacrimal glands during the blink phase, respectively. Lacrimal-production details are provided in Appendix 6D. V_{total} is the total volume of the mixed-tear compartments during the blink phase, c_{bulk} is the concentration of the mixed-tear compartments during the blink phase, V_{um} is the upper-meniscus tear volume, cum is the upper-meniscus salt concentration, V_{lm} is the lower-meniscus tear volume, V_{su} is the upper conjunctival-sac tear volume, c_{su} is the upper conjunctival-sac salt concentration, V_{sl} is the lower conjunctival-sac tear volume, and c_{sl} is the lower conjunctival-sac salt concentration. Since the upper and lower conjunctival-sac salt concentrations correspond to profiles from the end of the fornix to the upper and lower menisci, respectively, the concentration profile in each fornix is averaged for evaluating Equation 6.14. Mixing of the conjunctival sacs and other tear compartments is due to the motion of the lids and the eye. Cerretani and Radke[35] found only small differences in compartment osmolarities for no mixing and well mixing of the conjunctival sacs. Due to the very short blink time, bulbar and conjunctival tear production during the blink phase are negligible and, thus, are ignored. β is the fraction of PoLTF that mixes with the total tear film during each blink cycle. V_{PoL} at the beginning of deposition phase is set so that the PoLTF thickness is 2 μm at the start of the deposition phase. Accordingly, β is determined so that tear entering the PoLTF from mixing is 1% of the set PoLTF deposition volume.[203]

6.6 Results and Discussion

For the small values of hydraulic permeabilities, K, for commercial SCLs in Figure 6.9, water flow through the lens has minimal effect on all tear-compartment osmolarities. As discussed in Appendix 6E, comparison between perched and non-perched tear films also reveals no difference in tear osmolarity for all tear compartments. Further, salt diffusion between PrLTF and PrCjTF is also negligible since the salt-concentration difference between the PrLTF and PrCjTF is smaller than that between the PrLTF and the tear menisci. Therefore, we assume that the PrLTF and the PrCjTF are perched and isolated from the menisci, and that there is no transport between the PrLTF and the PrCjTF. The following subsections present results of tear-compartment osmolarities for various lens salt-transport properties and tear-production and tear-evaporation rates. In Sections 6.6.1 and 6.6.2, we analyze the impact of SCL wear on PoLTF salinity in normal and dry eyes, respectively. In Section 6.6.3, we assess the individual effect of tear evaporation rate and tear production rate on PoLTF osmolarity. Effect of lens properties on PoLTF osmolarity is explored in Section 6.6.4 and the effect of interblink duration on PoLTF osmolarity is investigated in Section 6.6.5. In all subsections, we focus on what circumstances SCLs might protect the cornea against hyperosmolarity.

6.6.1 Effects of Lens-Salt Diffusivity for Normal Eyes

Figure 6.10 portrays the effect of the lens-salt diffusion coefficient, D_s, on tear-compartment osmolarities as a function of time for normal eyes while keeping other variables constant. Evaporation and lacrimal production rates used for this analysis are provided in the first row of Table 6.2. The selected D_s values in Figure 6.10 fall within the range of commercially available SCLs today (see also Fig. 6.7).[210,256] Repeated "shark-fin" patterns represent separate blink cycles in periodic-steady state (i.e., osmolarity patterns repeat every blink). All compartments experience periodic increases in osmolarity but menisci and PoLTF cycle changes are small and thus not apparent on the ordinate scale chosen of Figure 6.10. As expected, the largest

fluctuations in osmolarity are seen in the PrLTF and PrCjTF because of tear evaporation (Fig. 6.10, red and black lines, respectively).

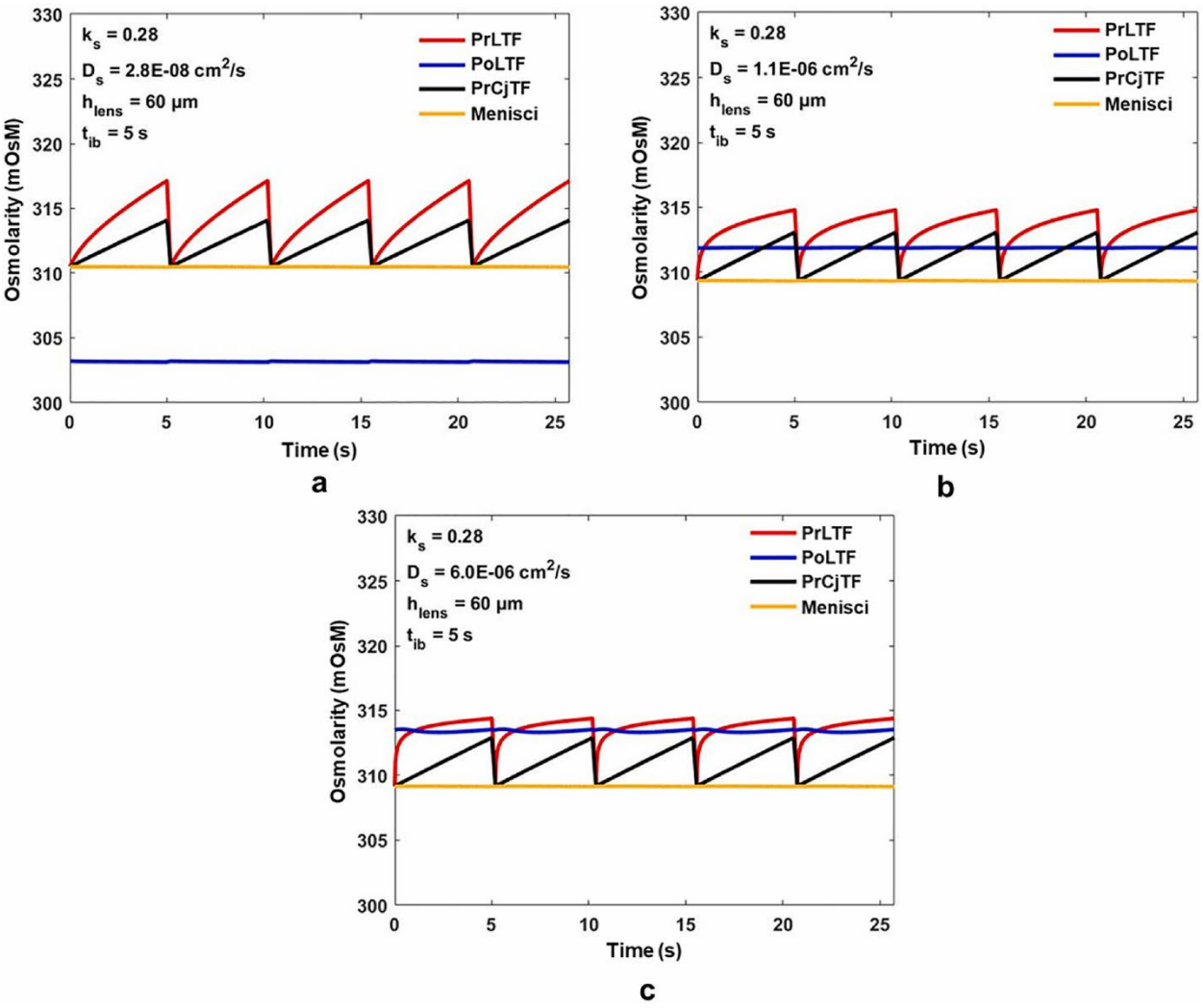

Figure 6.10. Periodic-steady tear osmolarity of PrLTF, PoLTF, PrCjTF, and tear menisci for normal eyes. (a) low D_s (= 2.8 × 10^{-8} cm^2/s), (b) medium D_s (= 1.1 × 10^{-6} cm^2/s), and (c) high D_s (= 6.0 × 10^{-6} cm^2/s). Interblink period is 5 s. Tear evaporation rate is that of normal no-lens wear from Table 6.2. All parameters are constant except salt diffusivity, D_s.

The most important finding in Figure 6.10 is that by decreasing D_s, the PoLTF is immunized against hyperosmolarity as shown by the blue line in Figure 6.10a. In fact, with low enough D_s, PoLTF osmolarity is even lower than that in the tear meniscus. Conversely, large D_s values result in PoLTF osmolarities similar to those of the PrLTF and PrCjTF as shown in Figure 6.10c. Moreover, the lower is the D_s value, the more drastic is the increase in PrLTF salt concentration because less salt transfers across the lens. PrLTF osmolarity is higher than that of PrCjTF during the interblink period because of the thinner deposited tear film over the SCL (see Section 6.3.2) than over the bulbar conjunctiva, which makes PrLTF more susceptible to evaporation-driven salt concentration increase compared to the PrCjTF. Due to the relative large volume and small exposed surface area to environmental evaporation, both upper and lower

meniscus osmolarity change is insignificant during the interblink period. During every blink period, all tear-compartment osmolarities converge to the same well-mixed value except for the PoLTF, as illustrated in Figure 6.3. This is reflected at the beginning of each interblink cycle of Figure 6.10. Different osmolarity of the PoLTF than the tear compartments at the beginning of each interblink cycle also indicates that the relatively small (1–2%) of PoLTF tear exchange upon every blink is not a significant mechanism to prevent hyperosmolarity in the PoLTF during SCL wear.

At the beginning of each interblink period for SCLs with higher Ds (i.e., 6.10b–c), the PrLTF osmolarity is lower than that of the PoLTF. In these cases, salt travels from the PoLTF to the PrLTF until, at some later time point in the blink cycle, the increased PrLTF osmolarity, due mainly to evaporation, becomes higher than that of the PoLTF. During this initial phase of the interblink period, water transport, albeit small, occurs from the PrLTF to the PoLTF. Thus, PoLTF osmolarity also decreases during this initial time interval. This finding is qualitatively visible in Figure 6.10c but is not as apparent in Figure 6.10b because the PoLTF and PrLTF osmolarity difference at the beginning of the interblink period is smaller than that in Figure 6.10c. Once the PrLTF osmolarity becomes higher than that of the PoLTF, salt transports from the PrLTF to PoLTF and water flows from the PoLTF to PrLTF. For Figure 6.10a, where the PoLTF osmolarity is always lower than the PrLTF, salt always travels from the PrLTF to PoLTF while the water transports in the opposite direction from the PoLTF to the PrLTF within every blink cycle.

6.6.2 Effects of Lens-Salt Diffusivity for Dry Eyes

To represent dry-eye conditions, an increased evaporation rate, q_e, and a reduced production rate, q_{lac}, compared to those in normal eyes are selected for analysis (see second row, Table 6.2). Figure 6.11 displays the influence of D_s on tear-compartment osmolarities for dry-eye conditions. All remaining variables are constant and identical to those in the normal-eye analysis of Figure 6.10. Due to the higher evaporation and lower lacrimal production rates, osmolarities are elevated in Figure 6.11 for all compartments compared to those of normal eyes. Although similar patterns are observed compared to those for normal eyes (i.e., PrCjTF osmolarity is lower than that of the PrLTF, and menisci osmolarity is lower than those for both PrCjTF and PrLTF) osmolarity fluctuations are more sensitive to D_s with dry eye than they are with normal eyes. With the low-diffusivity SCL in Figure 6.11a, the osmolarity in the PoLTF is lower than that of the menisci of a dry eye without lens wear reported by Tomlinson et al.[23] and displayed in Figure 6.1. PoLTF osmolarity in Figure 6.11a is approximately the same as that of the menisci of normal eye with lens wear (Fig. 6.10, yellow line). This observation reinforces the potential for a SCL to protect the corneal surface from hyperosmolarity, especially for dry eyes. However, such protection gradually deteriorates with higher D_s, as shown in Figure 6.11b and c.

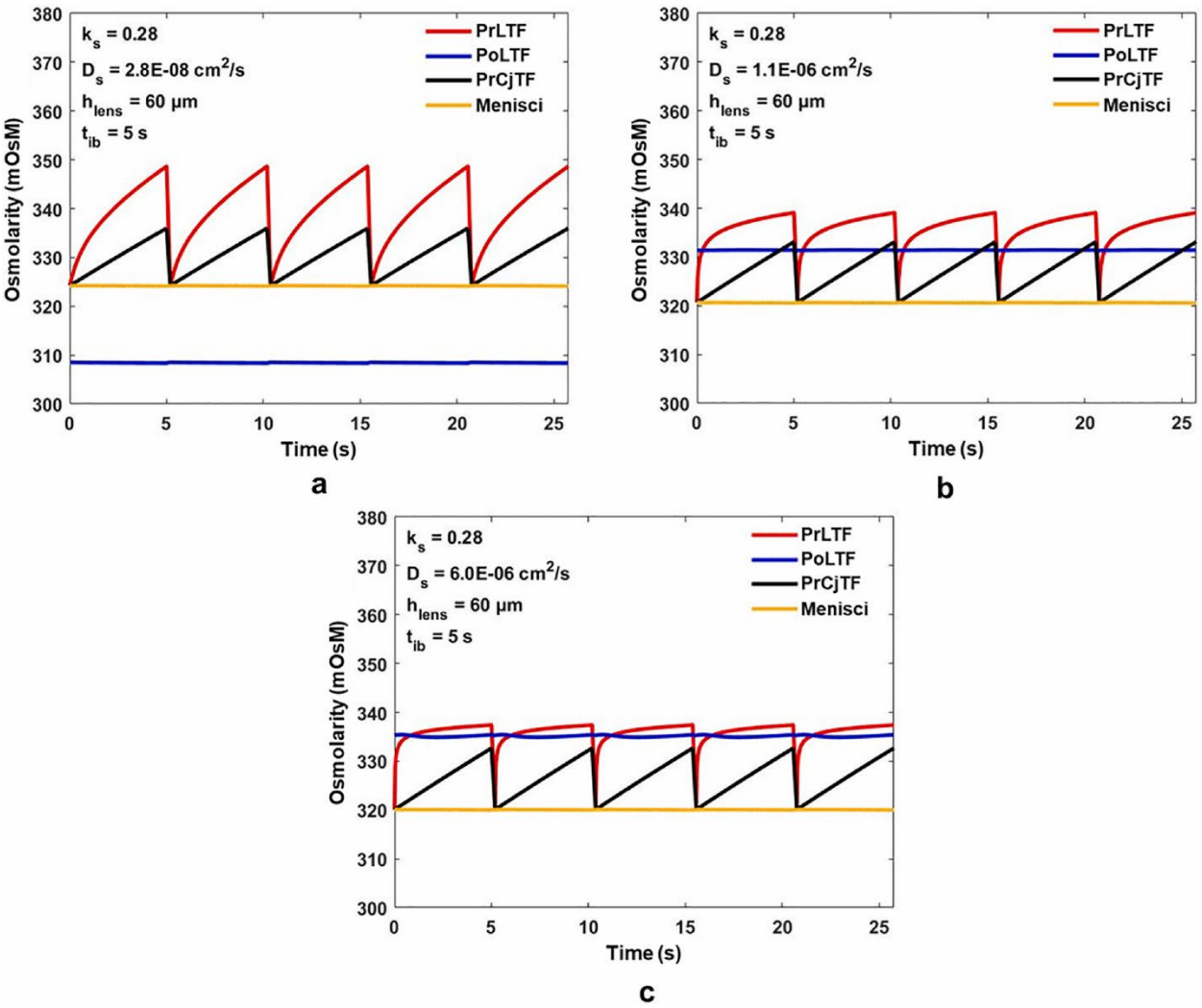

Figure 6.11. Periodic-steady tear osmolarity of PrLTF, PoLTF, PrCjTF, and tear menisci for dry eye. (a) low D_s (= 2.8 × 10^{-8} cm^2/s), (b) medium D_s (= 1.1 × 10^{-6} cm^2/s), and (c) high D_s (= 6.0 × 10^{-6} cm^2/s). Tear evaporation and production rates are those of dry eye from Table 6.2. Other than tear evaporation and production rates, all parameters in Figure 6.11 are identical to those in Figure 6.10. Interblink period is 5 s.

Although decreasing D_s decreases the PoLTF osmolarity, the dry-eye analysis discloses that decreasing D_s increases the menisci, PrLTF, and PrCjTF osmolarities, which is similar to the observation from the normal-eye analysis in Section 6.6.1. Again, the inverse effect of D_s on menisci, PrLTF, and PrCjTF osmolarities due to less salt transported to the PoLTF during the interblink period is more sensitive with smaller D_s in dry eye compared to that in normal eye.

6.6.3 Effects of Tear-Evaporation and Lacrimal-Production Rates

Guillon and Maissa[234] documented a 40–50% increase in ocular-surface evaporation rate during SCL wear. Since their study did not separate normal and dry-eye subjects, Figure 6.12 assesses how an increase in evaporation rate by 50% on a normal eye affects the osmolarities of the tear compartments during SCL wear. Tear-evaporation and lacrimal-production rates used are documented in the third row of Table 6.2. Remaining parameters are the same as those for Figure 6.10b.

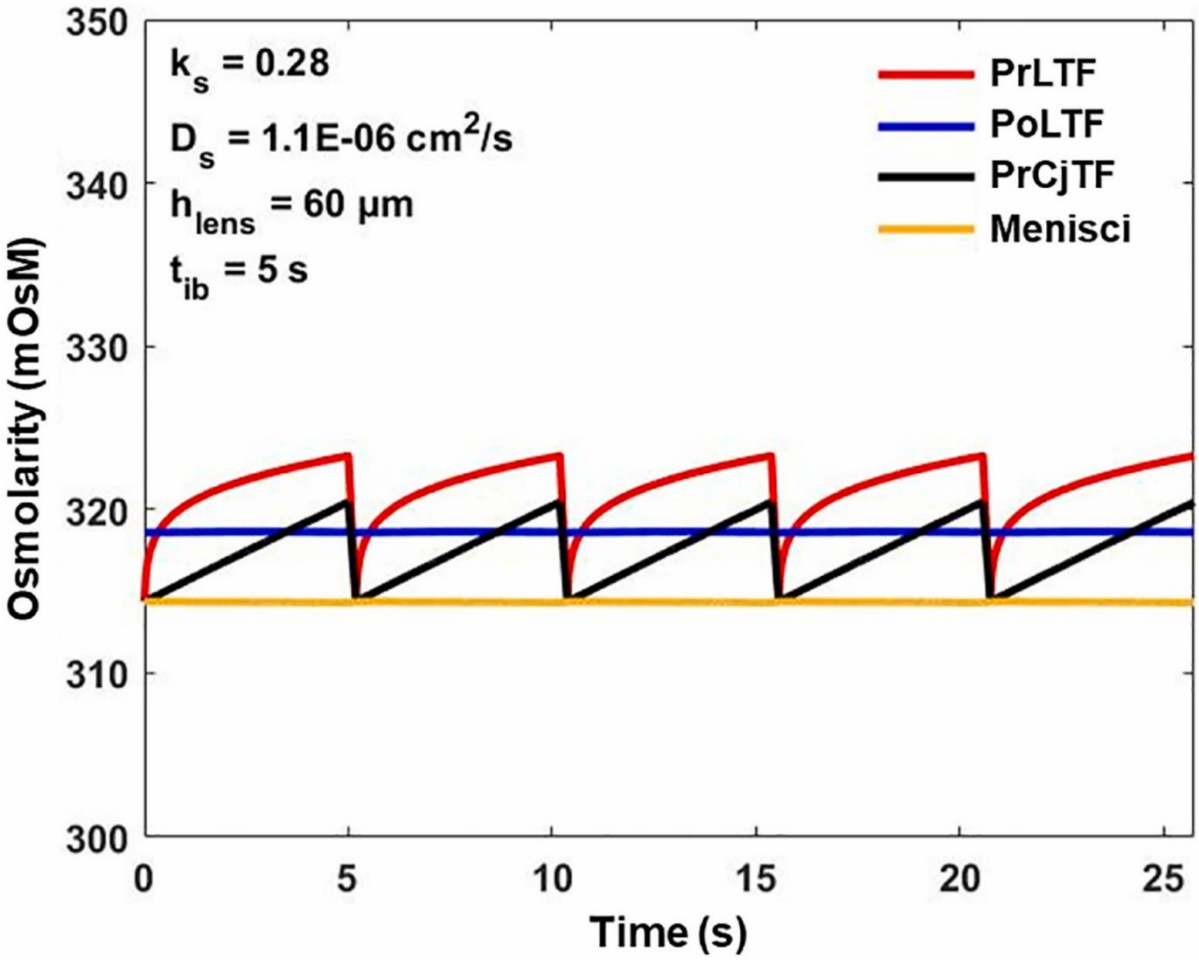

Figure 6.12. Periodic-steady tear osmolarity of PrLTF, PoLTF, PrCjTF, and tear menisci for normal eye with lens wear with higher evaporation rate. Tear evaporation rate is that of normal lens-wear based on measurements of Guillon and Maissa[234] listed in Table 6.2. Interblink period is 5 s.

In Figure 6.12, the increase in evaporation rate by 50% of the normal eye for SCL wear while keeping lacrimal-production rate constant increases osmolarity in all tear compartments by ~5 mOsM. Thus, ineffective evaporation retardation by the tear lipid layer of the PrLTF during SCL wear[217] is important to tear-compartment osmolarities. Since the effect of SCL wear on tear-production rate is unknown, we also investigated the effect of increased lacrimal-production rate while maintaining a constant evaporation rate. Evaporation rate of a normal eye (first row, second column of Table 6.2) and lacrimal-production rate of a dry eye (second row, first column of Table 6.2) with medium lens D_s result in a PoLTF osmolarity that is ~3 mOsM greater than that of a normal eye with medium lens D_s wear previously shown in Figure 6.10b. These results accentuate the importance of tear production and evaporation on tear osmolarity during SCL wear.

6.6.4 Effect of Lens Properties on PoLTF Salinity

To clarify further the effect of lens properties (i.e., D_s, k_s, and h_{lens}) on PoLTF salinity, a series of calculations varying individual properties was conducted and findings are summarized in Figures 6.13-6.15. Figure 6.13 highlights the relationship between the time-averaged PoLTF osmolarity and D_s for normal eyes with a blink interval of t_{ib} = 5 s. As before, the D_s range chosen

in Figure 6.13 lies within the range of what is available with commercially available SCLs today.[210,256] At low D_s, PoLTF osmolarity declines sharply because lens resistance to salt transport increases drastically. The shaded region in Figure 6.13 accentuates the corresponding osmolarities in the tear menisci where in-vivo salt concentrations are measured. When the lens-salt diffusivity, D_s, falls below about 5×10^{-7} cm^2/s for normal (Fig. 6.13) and dry-eye (not shown) SCL wear, the PoLTF osmolarity falls below that in the tear menisci. Lenses with D_s below this value can provide protection against corneal hyperosmolarity.

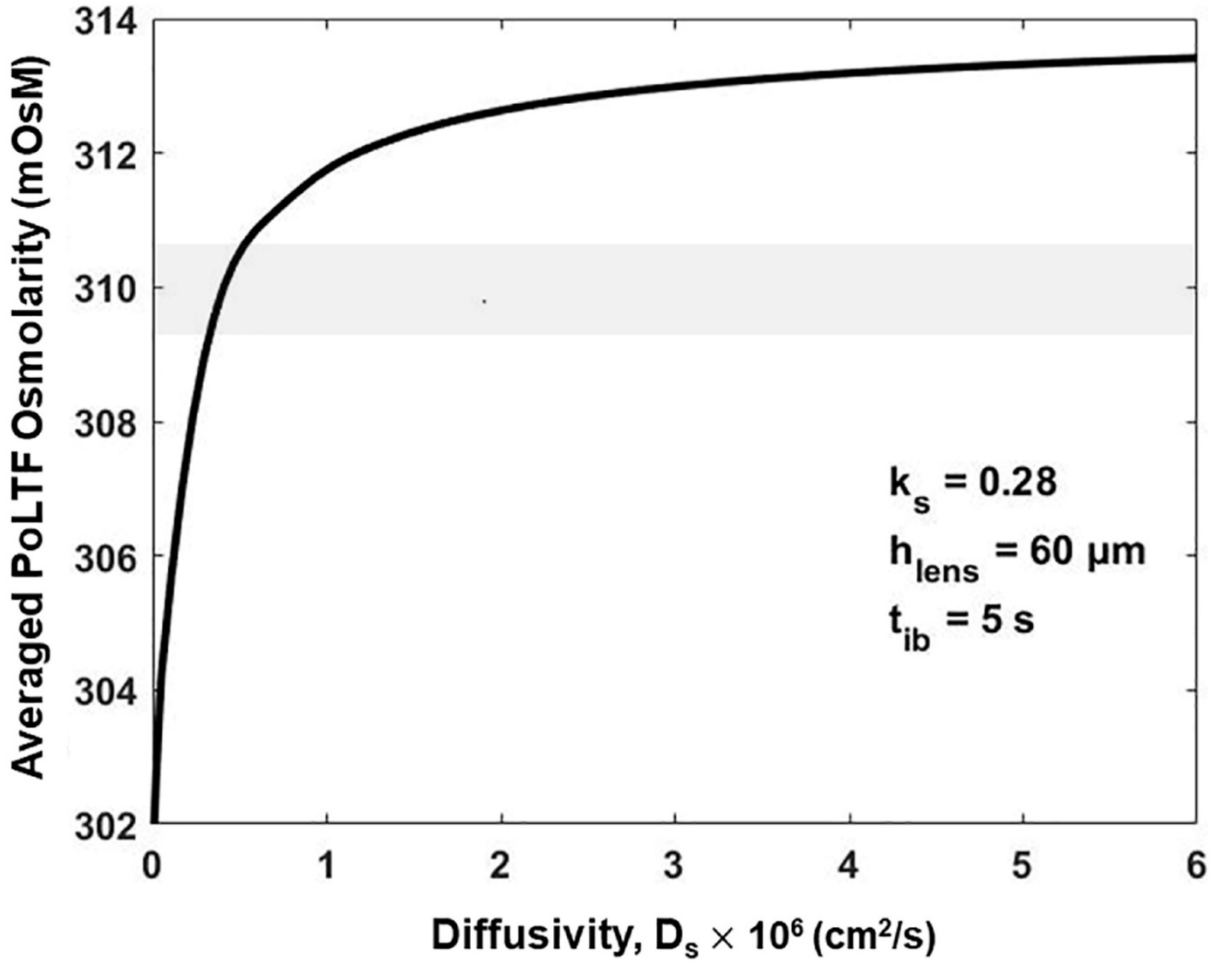

Figure 6.13. Time-averaged PoLTF tear osmolarity as a function of lens-salt diffusivity for normal eyes. Shaded region corresponds to menisci salt concentration for normal eyes.

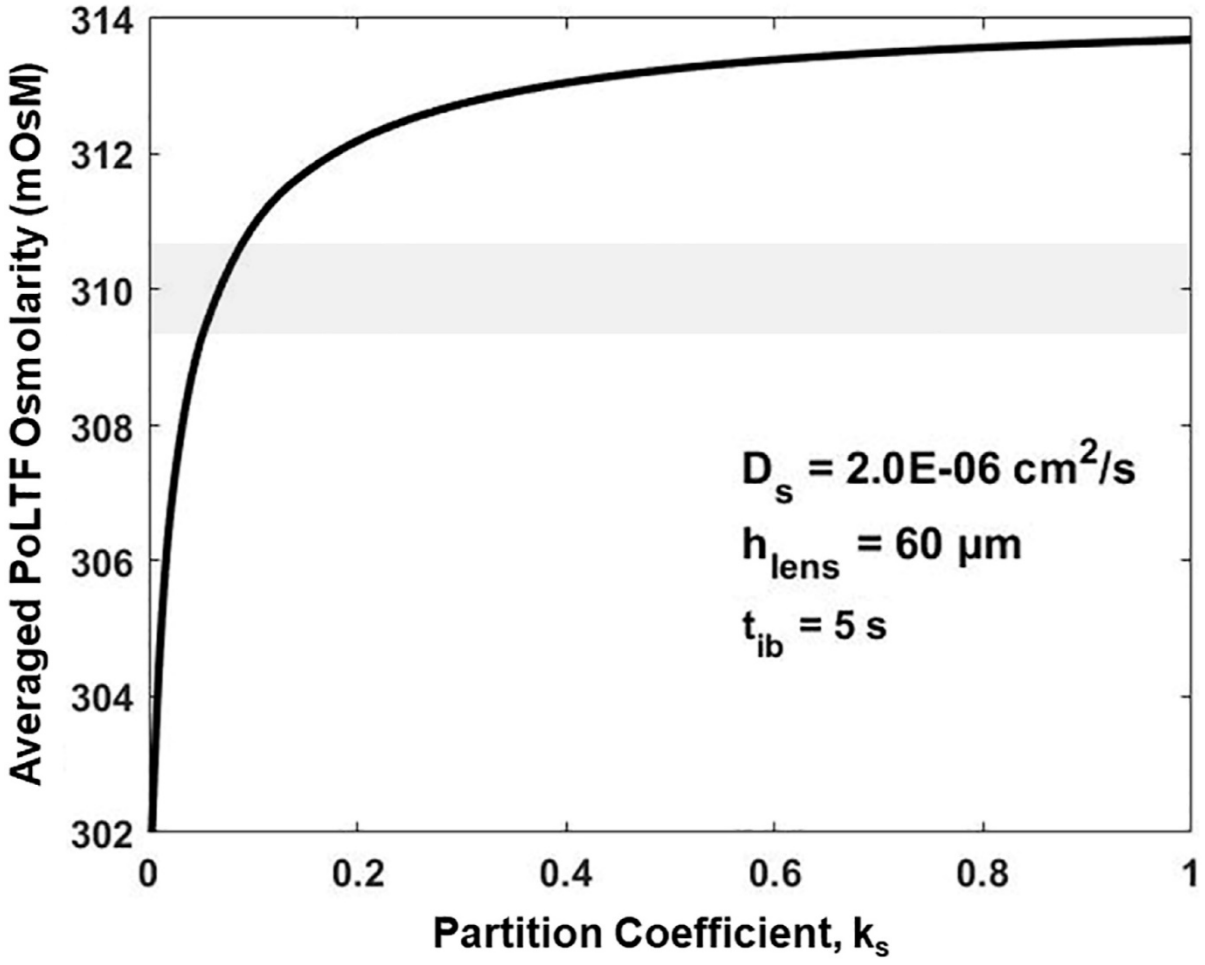

Figure 6.14. Time-averaged PoLTF tear osmolarity as a function of lens-salt partition coefficient for normal eyes. Shaded region corresponds to menisci salt concentration for normal eyes.

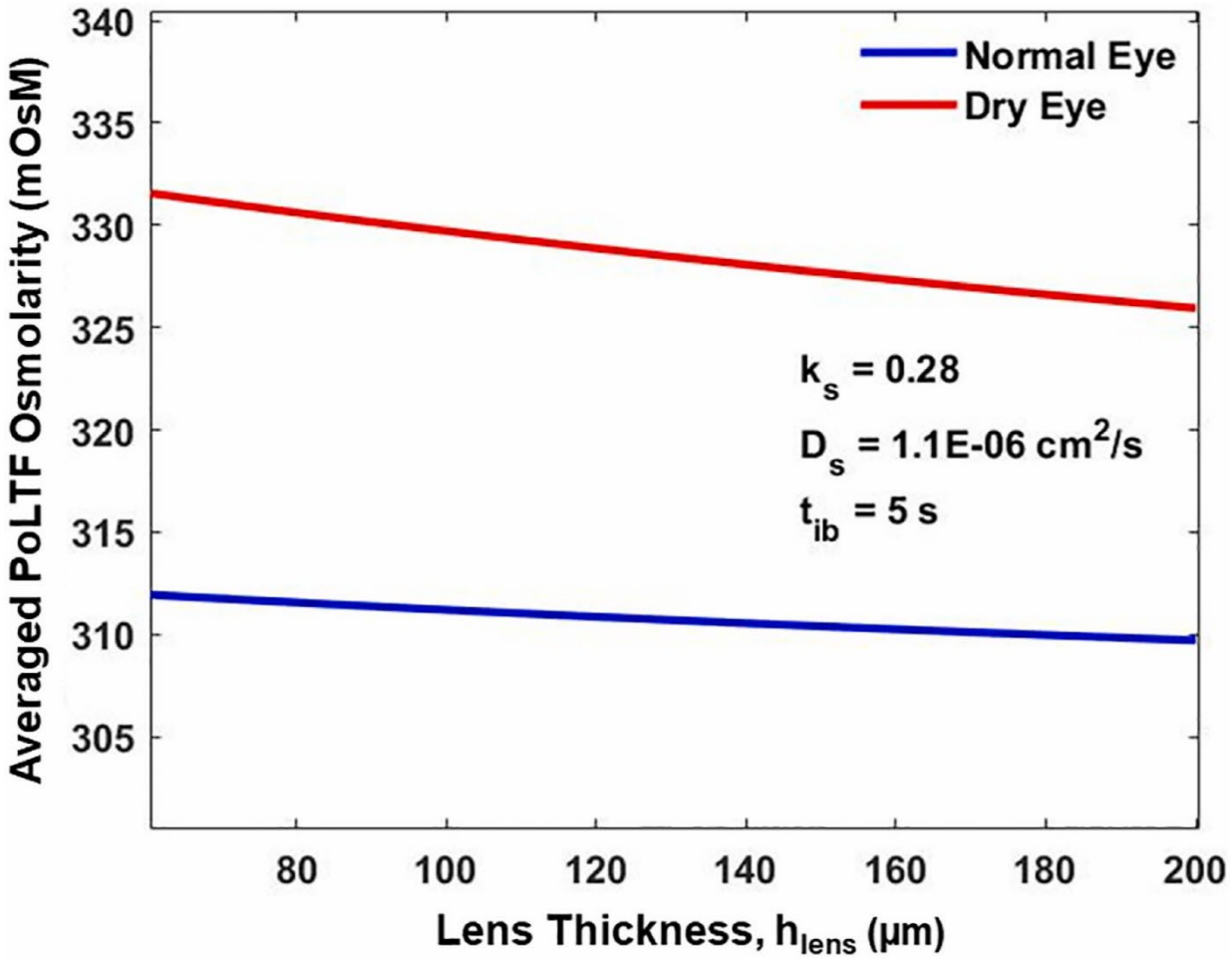

Figure 6.15. Time-averaged PoLTF tear osmolarity as a function of lens thickness for normal and dry eyes.

Figure 6.14 portrays the effect of salt partition coefficient, k_s, on time- average PoLTF osmolarity keeping all other parameters constant and t_{ib} = 5 s. Again, the shaded region encompasses osmolarities in the tear menisci. Both D_s and k_s have significant effects on lowering PoLTF osmolarity when their values are low. When their values are high, sensitivity to their values diminishes. Although low k_s values reduce PoLTF osmolarity, the range of k_s currently available for SCLs is 0.15–0.70.[210] Within this range, k_s affects PoLTF osmolarity by ~2 mOsM. Since D_s and k_s act independently in transient lens-salt diffusion rather than as the product of the two (i.e., D_sk_s or salt permeability) focus should be more on reducing D_s to lower PoLTF osmolarity for SCL wear.

Figure 6.15 graphs the effect of lens thickness, h_{lens}, on time-averaged PoLTF osmolarity for normal and dry eyes. Thicker lenses result in lower PoLTF osmolarity as expected since the lens thickness affects the salt transport resistance. Similar to the effect of D_s, PoLTF osmolarity is more sensitive to h_{lens} in dry eye than it is in normal eye. Overall, however, the influence of h_{lens} on PoLTF osmolarity is not strong within the limited range of SCL thickness for comfortable wear, partly because during each periodic interblink, salt diffusion through the lens does not reach pseudo steady state. Accordingly, salinity fluctuations in the PrLTF do not significantly penetrate

through the lens. To minimize PoLTF hyper osmolarity, ideal lens designs should primarily minimize D_s.

6.6.5 Effect of Interblink Period of PoLTF Salinity

All above analyses were conducted assuming a normal blink pattern of a 5-s interblink. Because a longer interblink period, t_{ib}, allows more time for tear to evaporate, PoLTF osmolarity clearly depends on how frequent SCL wearers blink their eyes. Figure 6.16 shows the effect of t_{ib} on the time-averaged PoLTF osmolarity. As expected, PoLTF osmolarity increases with longer t_{ib}. This result may help explain why lens wearers feel discomfort when they blink infrequently and feel the urge to blink when they do not blink frequently enough. Similar to lens properties, PoLTF osmolarity is more sensitive to t_{ib} for dry eye than for normal eye.

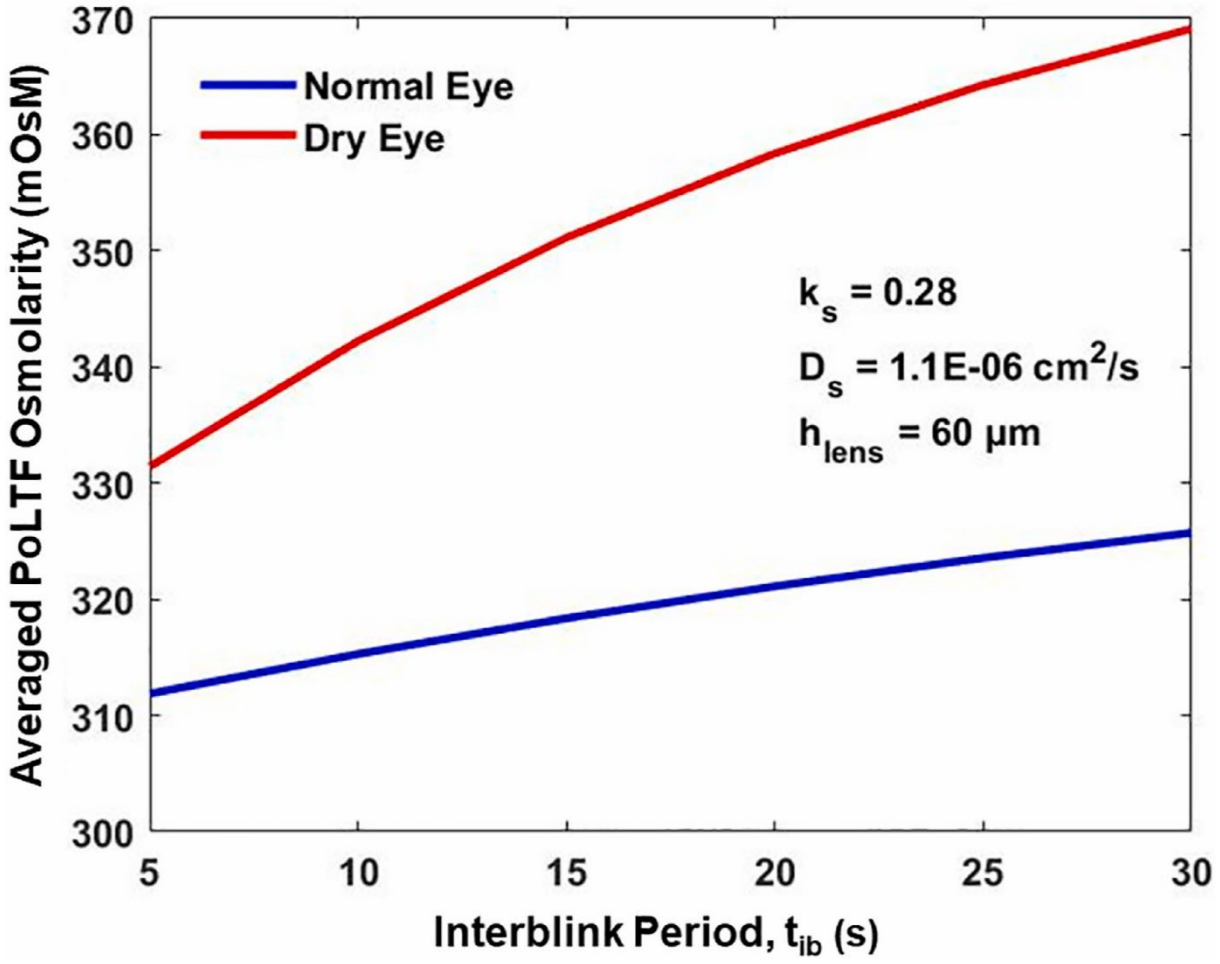

Figure 6.16. Time-averaged PoLTF tear osmolarity as a function of interblink period for normal and dry eyes.

6.6.6 Comparison Between SCL Wear and No-Lens Wear

To evaluate how lens-wear osmolarities for various tear compartments compare to those for no-lens wear, results from normal-eye lens-wear (Fig. 6.10a) and normal-eye no-lens-wear (Fig. 6.1) are plotted together in Figure 6.17 for ease of comparison. All tear-evaporation and tear-production parameters are kept the same. Menisci osmolarities of no-lens wear are slightly lower

than those of the menisci osmolarities during SCL wear (by ~ 2 mOsM). This observation is consistent with clinical studies that measured meniscus osmolarity with and without lens wear[75–78,204,205] and is explainable by the fact that the menisci volumes with lens wear are slightly larger than those for no-lens wear because of the thinner tear film deposited with lens wear than without lens wear. However, normal-eye lens-wear menisci osmolarities do not reach the elevated menisci osmolarities of those with dry-eye no-lens wear. This observation potentially explains why elevated meniscus osmolarity during lens wear does not correlate with lens-wear discomfort.[205] Figure 6.17 also demonstrates that the PrLTF osmolarity rises significantly higher than that of the PrCTF during no-lens wear. This too is due to the thinner deposited PrLTF than that of the PrCTF.

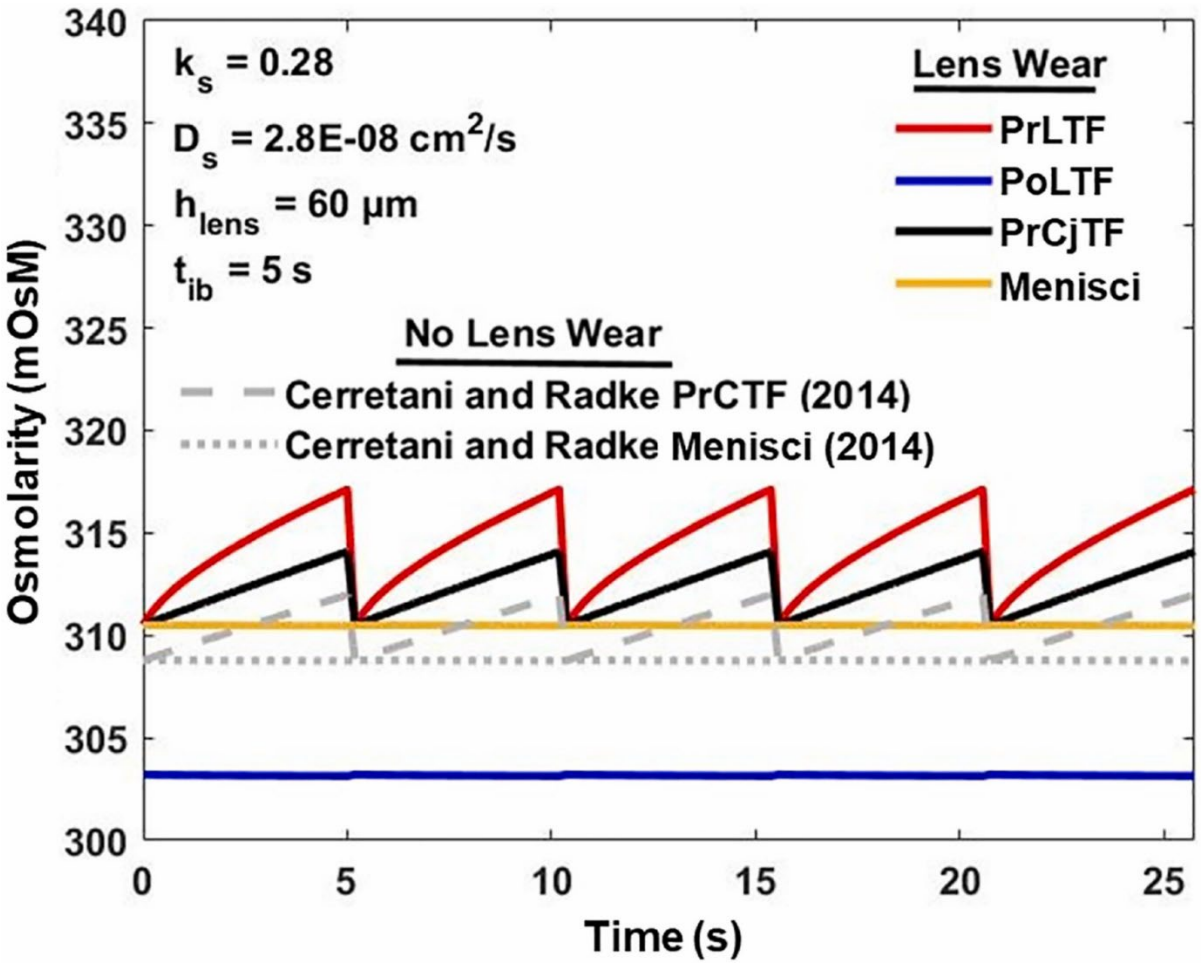

Figure 6.17. Periodic-steady tear osmolarity during lens wear compared to no-lens wear. Tear evaporation and production rates are those of normal no-lens wear from Table 6.2. All lens properties are identical to those of Figure 6.10a. No-lens wear data are those of normal eyes from Figure 6.1. Interblink period is 5 s.

Comparison between PrCTF osmolarity for normal and dry eyes with no-lens wear (Fig. 6.1) to that of PoLTF osmolarity for lens-wear normal (Fig. 6.10) and dry eyes (Fig. 6.11) shows that lens wear can increase or decrease significantly the osmolarity of the tear interfacing the cornea. Although a direct correlation of PoLTF osmolarity to ocular safety and comfort is not available to date due to the limited understanding of PoLTF osmolarity, positive correlation between no-lens-wear dry-eye symptoms and osmolarity[15–19,21–24] suggests that PoLTF hyperosmolarity could positively correlate with lens-wear discomfort. Although osmolarity for

PrCTF during an interblink period is significantly higher than that of PoLTF in Figure 6.17, higher D_s can result in peak osmolarities in the PrCTF higher than those for the PoLTF while the time-averaged osmolarities in the PoLTF are higher than those of PrCTF (not shown). The significance of higher time-averaged osmolarity versus the peak osmolarity observed at the end of each interblink on lens-wear discomfort remains unknown. In either case, tear-meniscus osmolarity is not a good representation of PrCTF and PoLTF osmolarities, which are those in direct contact with the corneal epithelium during no-lens wear and lens wear, respectively.

6.7 Conclusions and Future Directions

For the first time, our proposed physiological-based mathematical model interrogates the PoLTF osmolarity during SCL wear and demonstrates the importance of lens-material properties, PrLTF thickness, and lipid-layer quality on PoLTF osmolarity. Our time-periodic tear-compartment continuum model predicts that SCL wear can protect the cornea from hyperosmolarity even when the PrLTF is hyperosmolar. To produce a low PoLTF osmolarity with SCL wear, both D_s and k_s should be reduced while increasing h_{lens}. However, practical material limitations constrain h_{lens} and k_s. Further, maximizing oxygen delivery to the ocular surface to avoid corneal hypoxia relies on minimizing the h_{lens}.[3,5,42] Thus, SCLs designed to avoid corneal hyperosmolarity should focus on lowering lens D_s. Too low a salt diffusivity, however, can adhere the lens to the ocular surface.[35,40] To prevent lens adherence, Nicolson et al.[40] suggest a minimum D_sk_s threshold of 2 x10^{-7} cm^2/s. The actual minimum threshold value may be lower based on more recent D_sk_s measurements of commercial SCLs.[210,256] Nevertheless, the threshold of Nicolson et al.[40] is a helpful guideline.

The significant difference between the PoLTF osmolarity and the tear menisci during lens wear emphasizes the need to investigate the correlation between lens-wear discomfort and PoLTF osmolarity. As osmolarity has been shown to correlate with dry-eye symptoms (e.g., irritation, stinging, burning, prickling, and cooling) during no-lens wear,[14] it is likely that the PoLTF osmolarity correlates with lens-wear discomfort that has the same etiology as dry eyes but not other forms of discomfort induced by lid-wiper epitheliopathy, blurry vision, lens edge, SCL surface dehydration, or other forms of lens awareness. To answer this important clinical question, a method to measure PoLTF osmolarity in vivo is requisite. Recent developments in sensor technology with contact lenses hold promise.[268,269] Chiou[270] developed a prototype contact lens with electronics to measure tear osmolarity continuously. However, no peer-reviewed manuscript is available to date for detailed information. Also, multiple groups are actively investigating contact lenses with fluorescent dyes embedded to measure ion concentrations.[59,271] For ion-specific fluorophores to determine the PoLTF concentration accurately, additional investigation is needed on how well fluorophores bind only to the targeted ions clinically. Finally, sensor-embedded contact lenses must ensure that the tagged lens material and/or sensor embedments are designed compatible with conventional SCLs. Otherwise, the prototype lenses may not mimic those of commercially available SCLs today.

PoLTF osmolarity is near constant throughout the interblink period. Conversely, PrCTF osmolarity without lens wear increases rapidly during the interblink period. Depending on the lens material, PoLTF time-averaged osmolarity can be higher than that of the PrCTF with no-lens wear but not higher than the peak osmolarity. In such a situation, the question arises whether lens wear or no-lens wear results in more osmolarity-driven discomfort. It is possible that protection against high peak osmolarity of the PrCTF with lens wear is the reason why lens wearers, compared with no-lens wear, have longer maximum interblink intervals during a stress test.[272] The effect of time-

averaged osmolarity and interblink peak osmolarity on ocular discomfort requires investigation. Importantly, SCL wearers should put conscious effort into blinking more frequently because longer interblink times increase PoLTF osmolarity significantly.

Our tear-dynamics osmolarity analyses on normal and dry eyes reveal that tear-production and tear-evaporation rates have a significant effect on the tear osmolarity during SCL wear. Therefore, robust meibomian-gland lipid expression and lacrimal-tear production, common metrics for assessing evaporative and aqueous-deficient dry eyes, should be considered in optimal SCL fitting. Our proposed tear-dynamics SCL model also shows that lens properties have greater effect on tear osmolarity for dry eyes than for normal eyes. With lower D_s values, SCLs can protect against hyperosmolarity for normal and especially for individuals suffering from dry eyes. Further studies are needed to determine the optimal lens D_s, k_s, and h_{lens} for different q_e and q_{lac} to maximize osmotic comfort with lens wear without compromising hypoxic safety[3] and lens adhesion.[39]

Although the best available data were used to determine osmolarity of the various tear compartments, more information on tear-evaporation flux during lens wear for normal and dry eyes and a better understanding of the evaporation-flux difference between PrLTF and PrCjTF is needed. As discussed in Section 6.3.5, tear-evaporation rates depend strongly on the environmental humidity, airflow velocity, and temperature. Therefore, future measurements should be made with flow evaporimeters (e.g., Peng et al.[242]) rather than with closed-chamber evaporimeters widely used in the past.

We determined that the upper- and lower-meniscus osmolarities exhibit negligible salinity differences for complete blinks. Gad et al.[273] found no difference in upper and lower meniscus osmolarities for normal-eye lens wear but, however, found a significant difference between the upper and lower menisci osmolarities in symptomatic lens-wearing group during lens wear. It is difficult to justify this latter result. Measurement difficulties arise in the detection of upper meniscus osmolarities and/or in the known low sensitivity of the TearLab (TearLab Corp., San Diego, CA, USA) instrument.[38] Another possibility is that symptomatic contact-lens wearers experience more frequent incomplete blinks leading to imperfect mixing of the tear. In such a case, the majority of the hyperosmotic tear film mixes with the upper meniscus resulting in higher osmolarity than that of the lower meniscus. Further investigation on upper and lower menisci osmolarity is warranted.

Similar to tear-evaporation rates, the effect of SCL wear on tear-production and tear-drainage rates also requires further research. For instance, cold receptors are thought to influence basal tear production.[274] SCLs can potentially act as a thermal insulator to the ocular surface thereby affecting basal tear production. The recently devised modified-Schirmer tear test[164,165,233] allows direct measurement of tear-production rates for the first time. Further clinical studies are necessary to understand the difference in tear-production rates between normal and dry eyes and between no lens and lens wear. To date, tear-drainage rate has only been determined with physical models[236] or calculated from clinically measured tear-turnover rates.[26] However, tear-drainage rates calculated from tear-turnover rates assume that the volume of PrCTF remains constant and does not influence the fluorescein-dye concentration. With accurate tear-production and tear-evaporation rates in hand, tear-drainage rates can theoretically be determined without measuring the tear-turnover rate. Additional research is needed to establish whether tear-production and tear-drainage rates are altered by SCL wear. With more information on tear dynamics for normal and dry eyes including as well as no-lens and lens wear, precise calculation of tear-compartment osmolarities is possible.

Spatially localized variance in salt osmolarity (e.g., due to random local lipid-layer breakup on the PrLTF) within each tear-film compartment is not included in the current tear-dynamics model. With no-lens wear, mathematical studies showed that local PrCTF osmolarity can reach 600–900 mOsM in areas with lipid-layer breakup during a 10-s interblink period.[33,34] The effect of localized PrLTF osmolarity spikes on the PoLTF and the importance of localized spikes on ocular-surface discomfort remains unknown.

Our tear-dynamics model analysis of tear-compartment osmolarities reveals the major differences in osmolarities of the tear compartments during SCL wear. These differences potentially explain why no correlation has been found between clinically measured meniscus osmolarity and SCL wear discomfort.[74,75,78,204,205] Here, we demonstrate that careful design of SCLs, specifically lowering lens-salt diffusivity, can lower PoLTF osmolarity and can protect the cornea from hyperosmotic stress.

6.8 Appendix 6A. Determination of the Exposed Surface-Area Fraction (α) of Bulbar Conjunctiva

To determine α, the surface-area fraction of bulbar conjunctiva not covered by the contact lens or the eyelids, we used a SCL radius of 7.0 mm as our lens geometry.[199] Using Comsol Multiphysics 5.5 platform (Comsol Inc, Burlington, MA, USA), a 2-dimensional computer-aided design of the ocular surface and lids was performed based on the measurements of Malbouisson et al.[275] Geometries of the cornea and eyelids were modified to ensure that the area of bulbar conjunctiva exposed to the environment (A_{cj}) and cornea (A_{cn}) matched those of Cerretani and Radke.[35] Then, in the design, the contact lens was placed on top of the ocular surface to determine the area of the exposed bulbar conjunctiva that was underneath the lens. The area of bulbar conjunctiva covered by the contact lens and not by the eyelid ($A_{cj,lens}$) was 24.1 mm^2. Meanwhile, the total bulbar conjunctiva that was uncovered by the eyelid was 105.1 mm^2. Since α is the surface-area fraction of bulbar conjunctiva exposed to air, (1- α) represents for the fraction of bulbar conjunctiva that is underneath the contact lens and not covered by the eyelid. This gives the following expression

$$\alpha = 1 - \frac{A_{cj,lens}}{A_{cj}} \tag{6A.1}$$

Evaluation of Equation 6A.1 gives α = 0.77.

6.9 Appendix 6B. Lens Water Flux

We assume that salt diffusion through the lens does not materially influence opposing osmotic-driven water hydrodynamic flow. Water flux is governed by a modified Darcy law[260]

$$J_{w,lens} = \tilde{J}_{w,lens} c_{w,lens} = -\frac{K}{\mu_w} \frac{(\Delta P - \Delta \Pi)}{h_{lens}} c_{w,lens} \tag{6B.1}$$

where, $J_{w,lens}$ is the molar flux of water through the lens, $\tilde{J}_{w,lens}$ is the volumetric water flux (or the superficial velocity), $c_{w,lens}$ is the water concentration per unit lens volume, K is the Darcy hydraulic permeability of the lens, μ_w is tear viscosity, P is applied pressure, Π = 2RTc is the osmotic pressure, R is the gas constant, c is the aqueous salt concentration, and h_{lens} is the lens thickness. Here, $c_{w,lens} = \varphi_w 55.85M$ is the water concentration within the lens, and φ_w is the water

volume fraction of the lens.[257] We used a φ_w of 0.38 based on the works of Hoch et al.[255] Guan et al.[210] Since water flow within the lens is osmotic driven and not due to an applied pressure difference and because we assume constant water concentration within the lens, Equation 6B.1 reduces to

$$J_{w,lens} = \frac{2KRT}{\mu_w} \frac{(c_{PrL} - c_{PoL})}{h_{lens}} c_{w,lens} \tag{6B.2}$$

where, c_{PrL} and c_{PoL} are tear salt concentrations at the PrLTF and PoLTF interfaces, respectively. The factor of two is required because water flux depends on the salt osmotic concentration and not molar salt concentration. Division of Equation 6B.2 by $c_{w,lens}$ gives the volumetric water flux as

$$\tilde{J}_{w,lens} = v_w = \frac{2KRT}{\mu_w} \frac{(c_{PrL} - c_{PoL})}{h_{lens}} \tag{6B.3}$$

where, v_w is the superficial velocity. Determined $\tilde{J}_{w,lens}$ values for the three chosen lens-salt diffusivities are provided in Table 6B.1 for normal (Fig. 6.10) and dry (Fig. 6.11) analyses.

Table 6B.1. Averaged Volumetric Water Flux for Various Salt-Diffusivity Contact Lenses

Normal/Dry Eye	Salt Diffusivity D_s (cm^2/s)	Volumetric Water Flux $\tilde{J}_{w,lens}$ (m/s)
Normal	2.8×10^{-8}	2.9×10^{-9}
Normal	1.1×10^{-6}	4.4×10^{-10}
Normal	6.0×10^{-6}	9.2×10^{-11}
Dry	2.8×10^{-8}	8.2×10^{-9}
Dry	1.1×10^{-6}	1.3×10^{-9}
Dry	6.0×10^{-6}	2.6×10^{-10}

6.10 Appendix 6C. Lens-Molar Salt Flux

The counter flux of water in Equation 6B.3 induces a convective term in addition to diffusion for the salt flux across a lens. Transient salt mass conservation demands the following expression, where the lens-salt flux, $J_{s,lens}$, is given in Equation 6.11 of main text,

$$\frac{\partial c_{lens}}{\partial t} + \nabla \cdot J_{s,lens} = 0 \tag{6C.1}$$

where ∇ is the divergence operator. Therefore, Equation 6C.1 reads

$$\frac{\partial c_{lens}}{\partial t} + \tilde{J}_{w,lens} \frac{\partial c_{lens}}{\partial z} = D_s \frac{\partial^2 c_{lens}}{\partial z^2} \tag{6C.2}$$

where c_{lens} is the local salt concentration per unit lens volume within the lens, z is the spatial location within the lens directed from the posterior to anterior surface, $\tilde{J}_{w,lens}$ is the superficial water velocity defined in Equation 6B.3, D_s is the lens-salt diffusivity, and t is time. Equation 6C.2 is given in the main text as Equation 6.10.

To assess whether the salt flux due to $\tilde{J}_{w,lens}$ is important compared to that of salt diffusion, we determined the Péclet number (Pe) for the three salt diffusivities used for both normal (Fig. 6.10) and dry-eye (Fig. 6.11) conditions. The Péclet number is a dimensionless ratio of convective transport and diffusive transport rates and is expressed by the following definition

$$Pe \equiv \frac{\tilde{J}_{w,lens} h_{lens}}{D_s} \tag{6C.3}$$

where h_{lens} is the lens thickness. Averaged $\tilde{J}_{w,lens}$ for the periodic steady state from Appendix 6B is used to calculate the Péclet number as enumerated in Table 6C.1. Following Figures 6.10 and 11, h_{lens} for the Péclet number is set as 60 μm. Since the Péclet number is very small for all relevant conditions, salt transport across the lens due to counter-water transport $\tilde{J}_{w,lens}$ is negligible. Thus, Equation 6C.2 simplifies to Fick's second law

$$\frac{\partial c_{lens}}{\partial t} = D_s \frac{\partial^2 c_{lens}}{\partial z^2} \tag{6C.4}$$

Likewise, $\tilde{J}_{w,lens}$ in Equation 6.11 is negligible for assessing the lens salt flux at the anterior and posterior surfaces of the lens.

Table 6C.1. Péclet Number for Various Salt-Diffusivity Contact Lenses

Normal/Dry Eye	Salt Diffusivity (cm^2/s)	Péclet Number
Normal	2.8×10^{-8}	6.6×10^{-2}
Normal	1.1×10^{-6}	2.6×10^{-4}
Normal	6.0×10^{-6}	9.6×10^{-6}
Dry	2.8×10^{-8}	1.8×10^{-1}
Dry	1.1×10^{-6}	7.2×10^{-4}
Dry	6.0×10^{-6}	2.7×10^{-5}

6.11 Appendix 6D. Tear Supply from the Lacrimal Gland During the Blink Phase

The blink phase includes both deposition and eyelid-closure phases. The elapsed time for this process is ~0.2 s.[35] We lump the lacrimal-production rate during the blink phase as

$$V_{blink} = 0.2 q_{lac} \tag{6D.1}$$

where q_{lac} varies and can be found in Table 6.2.

6.12 Appendix 6E. Salt Diffusion from Non-Perched PrLTF to Menisci and PrCjTF

Although formation of tear-menisci black lines upon lid opening perches or isolates the PrLTF and PrCjTFs, lack of visualization of black lines in some subjects makes a non-isolated tear possible. Therefore, salt flux from the tear film to the adjacent tear menisci during the interblink period was investigated. We picture a thin but non-perched tear film directly connected to a meniscus. Salt diffusion from the PrLTF to a meniscus follows Fick's second law or

$$\frac{\partial c}{\partial t} = D_\infty \frac{\partial^2 c}{\partial x^2} \tag{6E.1}$$

where c is aqueous salt concentration, D_∞ is the bulk diffusion constant of salt in water, and x is the spatial coordinate to the center of the PrLTF directed from the menisci. Thus, x = 0 is the interface between PrLTF and the meniscus while x = λ is located at the center of the PrLTF. The requisite boundary conditions are

$$c(0,x) = c_{im} \tag{6E.2}$$

$$c(t,0) = c_{im} \tag{6E.3}$$

$$c(t,\lambda) = c_{PrL} \tag{6E.4}$$

Equations 6E.2–6E.4 are nondimensionalized as $\theta = (c - c_{im})/(c_{PrL} - c_{im})$, $X = x/\lambda$, and $\tau = D_\infty t/\lambda^2$. The nondimensionalized partial differential equation is solved using Laplace transformations to obtain

$$\bar{\theta}(s,X) = \frac{1}{s}\frac{\sinh(\sqrt{s}X)}{\sinh(\sqrt{s})} \tag{6E.5}$$

where $\bar{\theta}$ is the Laplace dimensionless concentration and s is the Laplace variable. At early time, Equation 6E.5 inverts to

$$\theta(\tau,X) = erfc[\frac{(1-X)}{2\sqrt{\tau}}] \tag{6E.6}$$

Since salt flux $J_{s,Bl} = -D_\infty\frac{\partial c}{\partial t} = -[\frac{D_\infty}{\lambda}(c_{PrL} - c_{im})]\frac{\partial\theta}{\partial X}$, the flux at X = 0 can be solved to yield the magnitude of salt flux from the tear film to the meniscus as

$$J_{s,Bl} = \frac{D_\infty}{\sqrt{\pi\tau}\lambda}[c_{PrL} - c_{im}]e^{-1/(4\tau)} \tag{6E.7}$$

Since upper and lower menisci have approximately the same concentration, cim is the concentration of either meniscus. To assess the influence of a non-perched tear film, $J_{s,Bl}h_{um}L_{um,PrL} + J_{s,Bl}h_{lm}L_{lm,PrL}$ is subtracted from the right side of Equation 6.8, $J_{s,Bl}h_{um}L_{um,PrCj} + J_{s,Bl}h_{lm}L_{lm,PrCj}$ is subtracted from the right side of Equation 6.6, and the subtracted upper and lower meniscus terms are added to Equation 6.4 for upper and lower meniscus balances, respectively. h_{um} and h_{im} are upper and lower meniscus heights, respectively, $L_{um,PrL}$ and $L_{lm,PrL}$ are arc lengths of upper and lower eyelids at the PrLTF region, respectively, and $L_{um,PrCj}$ and $L_{lm,PrCj}$ arc lengths of upper and lower eyelids at the PrCjTF region, respectively. Arc lengths and meniscus heights are determined from Appendix A of Cerretani and Radke.[35] We find that lack of a perched tear film results in a negligible difference in our tear-compartment osmolarities. Since the tear-compartment osmolarities do not change due to diffusion from PrLTF to tear menisci during the interblink, diffusion from the PrLTF to the PrCjTF is also neglected.

6.13 Glossary

Name	Common Units	SI Units	Symbol
Adjustable constant in lens salt diffusivity			a
Polymer strand characteristic radius	nm	m	a_f
Cross-sectional area of the bulbar conjunctiva that is not covered by the eyelids	cm^2	m^2	A_{cj}
Cross-sectional area of the bulbar conjunctiva covered by the contact lens and not by the eyelids	cm^2	m^2	$A_{cj,lens}$
Cross-sectional area of the cornea that is not covered by the eyelids	cm^2	m^2	A_{cn}
Area of the eye that undergoes tear evaporation	cm^2	m^2	A_{eye}
Cross-sectional area of the meniscus. i = u and l indicate upper and lower menisci, respectively	cm^2	m^2	A_{im}
Cross-sectional area of the lens exposed to the environment	cm^2	m^2	A_{lens}
Area of skin that is within the evaporimeter chamber	cm^2	m^2	A_{skin}
Adjustable constant in lens salt diffusivity			b
Salt concentration	mol/m^3	mol/m^3	c
Salt concentration of the tear film mixed during a blink phase	mol/m^3	mol/m^3	c_{bulk}
Salt concentration of the tear produced by the lacrimal glands during the blink phase	mol/m^3	mol/m^3	c_{blink}
Salt concentration of the meniscus. i = u and l indicate upper and lower menisci, respectively	mol/m^3	mol/m^3	c_{im}
Salt concentration within the lens	mol/m^3	mol/m^3	c_{lens}
Salt concentration in the post-lens tear film	mol/m^3	mol/m^3	c_{PoL}
Salt concentration in the pre-conjunctival tear film	mol/m^3	mol/m^3	c_{PrCj}
Salt concentration in the pre-lens tear film	mol/m^3	mol/m^3	c_{PrL}
Salt concentration of the conjunctival sac. i = u and l indicate upper and lower conjunctival sacs, respectively	mol/m^3	mol/m^3	c_{si}
Water concentration within the lens	mol/m^3	mol/m^3	$c_{w,lens}$
Diffusivity of salt in soft contact lens	cm^2/s	m^2/s	D_s
Diffusivity of salt in water	cm^2/s	m^2/s	D_∞
Salt enhancement factor			E_s
Enhancement factor for nonspecific electrostatic repulsion			E_s^{el}
Enhancement factor for hard-sphere exclusion			E_s^{ex}
Enhancement factor for specific adsorption of salt to the polymer chains			E_s^{ad}
Gel hydrodynamic resistance factor			F
Meniscus height. i = u and l indicate upper and lower menisci, respectively	μm	m	h_{im}
Thickness of the soft contact lens	μm	m	h_{lens}

Thickness of tear film. j = PrCj and PrL indicate PrCjTF and PrLTF, respectively.	μm	m	$h_{tf,j}$
Subscript indicating upper (u) or lower (l)			i
Subscript indicating either pre-conjunctival tear film (PrCj) or pre-lens tear film (PrL)			j
Salt molar flux from the tear film to the menisci	$mol/(m^2 s)$	$mol/(m^2 s)$	$J_{s,Bl}$
Salt molar flux across soft contact lens	$mol/(m^2 s)$	$mol/(m^2 s)$	$J_{s,lens}$
Volumetric water flux from the bulbar conjunctiva	m/s	m/s	$\tilde{J}_{w,cj}$
Volumetric water flux from the cornea	m/s	m/s	$\tilde{J}_{w,cn}$
Volumetric water evaporation flux	m/s	m/s	$\tilde{J}_{w,e}$
Volumetric water flux across the soft contact lens	m/s	m/s	$\tilde{J}_{w,lens}$
Molar water flux across the soft contact lens	$mol/(m^2 s)$	$mol/(m^2 s)$	$J_{w,lens}$
Salt partition coefficient for soft contact lens			k_s
Darcy hydraulic permeability of water	m^2	m^2	K
Membrane thickness in Darcy's law	μm	m	L
Arc length of eyelid at pre-lens tear-film region. i = u and l indicate upper and lower eyelids, respectively	μm	m	$L_{im,PrL}$
Arc length of eyelid at pre-conjunctival tear-film region. i = u and l indicate upper and lower eyelids, respectively	μm	m	$L_{im,PrCj}$
Applied pressure	Pa	Pa	P
Péclet number (Equation 6C.3)			Pe
Volumetric flow rate of water from the cornea	$\mu L/min$	m^3/s	q_{cn}
Volumetric flow rate of water from the bulbar conjunctiva into the pre-conjunctival tear film	$\mu L/min$	m^3/s	q_{cj}
Volumetric tear drainage rate. Sum of q_{du} and q_{dl}	$\mu L/min$	m^3/s	q_d
Volumetric tear drainage rate. Drainage through puncta. i = u and l indicate upper and lower puncta, respectively	$\mu L/min$	m^3/s	q_{di}
Volumetric tear evaporation rate	$\mu L/min$	m^3/s	q_e
Volumetric evaporation rate of the upper and lower menisci. i = u and l indicate upper and lower menisci, respectively	$\mu L/min$	m^3/s	$q_{e,im}$
Volumetric tear evaporation rate for pre-conjunctival tear film	$\mu L/min$	m^3/s	$q_{e,PrCj}$
Volumetric tear evaporation rate for the pre-lens tear film	$\mu L/min$	m^3/s	$q_{e,PrL}$
Volumetric aqueous production rate ($q_{lacu} + q_{lacl}$)	$\mu L/min$	m^3/s	q_{lac}
Volumetric flow rate of water entering the lower meniscus from the conjunctival sac ($q_{lacl} = 0.2q_{lac}$).	$\mu L/min$	m^3/s	q_{lacl}
Volumetric flow rate of water entering the upper meniscus from the conjunctival sac ($q_{lacu} = 0.8q_{lac}$).	$\mu L/min$	m^3/s	q_{lacu}
Volumetric water transport rate across the lens	$\mu L/min$	m^3/s	q_{lens}
Maximum volumetric tear drainage rate	$\mu L/min$	m^3/s	q_m
Volumetric air flow rate	cm^3/s	m^3/s	Q
Ideal gas constant	$J/(mol * K)$	$J/(mol * K)$	R

Meniscus radius where drainage ceases	μm	m	R_0
Relative humidity			R_H
Tear meniscus radius. i = u and l indicate upper and lower menisci, respectively	μm	m	R_{im}
Laplace variable			s
Obstruction factor			S
Lid-margin perimeter	cm	m	S_{lid}
Time	s	s	t
Interblink period	s	s	t_{ib}
Temperature	K	K	T
Time to deplete 95% of the fluorescein from the PoLTF	s	s	T_{95}
Velocity of upper eyelid	m/s	m/s	u_{lid}
Velocity of j where j = PrCj and PrL indicate bulbar conjunctiva and soft contact lens, respectively	m/s	m/s	$u_{s,j}$
Water superficial velocity and is equivalent to $\tilde{J}_{w,lens}$	m/s	m/s	v_w
Tear volume produced by the lacrimal glands during the blink phase	μL	m^3	V_{blink}
Meniscus volume. i = u and l indicate upper and lower menisci, respectively	μL	m^3	V_{im}
Volume of water in the post-lens tear film	μL	m^3	V_{PoL}
Volume of water in the pre-conjunctival tear film	μL	m^3	V_{PrCj}
Volume of water in the pre-lens tear film	μL	m^3	V_{PrL}
Conjunctival sac tear volume. i = u and l indicate upper and lower conjunctival sacs, respectively	μL	m^3	V_{si}
Volume of the tear mixed during a blink phase	μL	m^3	V_{total}
Spatial location from the center of the pre-lens tear film to the periphery	cm	m	x
Spatial location within the lens from the posterior (z = 0) to the anterior of the soft contact lens	μm	m	z
Fraction of bulbar conjunctiva that is not covered by the soft contact lens and the eyelids			α
Fraction of post-lens tear film that mixes with the rest of the tear during each blink cycle			β
Tear surface tension	mN/m	N/m	γ
Salt concentration difference between the post-lens tear film and the corneal epithelium	mol/m^3	mol/m^3	Δc_{cn}
Dimensionless salt concentration			θ
Dimensionless Laplace salt concentration (Equation 6E.5)			$\bar{\theta}$
Distance from the meniscus or the pre-conjunctival tear film to the soft-contact-lens center	cm	m^3	λ
Tear viscosity	mPa	Pa	μ_w
Osmotic pressure	Pa	Pa	Π
Corneal epithelium reflection coefficient of salt			σ_{cn}
Lens hydrodynamic tortuosity			τ_H

Lens salt tortuosity			τ_s
Dimensionless time			τ
Polymer volume fraction of soft contact lens			ϕ
Water volume fraction of soft contact lens			ϕ_w
Dimensionless x			X
Corneal epithelium membrane permeability of salt	m/s	m/s	ω_{cn}
Arithmetic average salt concentration in the corneal epithelium interface	mol/m^3	mol/m^3	$< c_{cn} >$

Chapter 7

Prevention of Localized Corneal Hyperosmolarity Spikes by Soft-Contact-Lens Wear

7.1 Abstract

Purpose: To determine whether localized hyperosmotic spikes on the pre-lens tear film (PrLTF) due to tear break up results in hyperosmotic spikes on the ocular surface during soft-contact-lens (SCL) wear and whether wear of SCLs can protect the cornea against PrLTF osmotic spikes.
Methods: Two-dimensional transient diffusion of salt was incorporated into a computationally designed SCL, post-lens tear film (PoLTF), and ocular surface and solved numerically. Time-dependent localized hyperosmolarity spikes were introduced at the anterior surface of the SCL corresponding to those generated in the PrLTF. Salt spikes were followed in time until they penetrate through the lens into the PoLTF. Lens-salt diffusivities (D_s) were varied to assess their importance on salt migration from the PrLTF to the ocular surface. SCL and PoLTF initial conditions and the lens anterior-surface boundary condition were varied depending on the value of D_s and on dry-eye symptomatology. Determined corneal surface osmolarities were translated into clinical pain scores.
Results: For D_s above about 10^{-7} cm^2/s, it takes around 5 - 10 s for the PrLTF hyperosmotic breakup spikes to diffuse across the SCL and reach the corneal surface. Even if localized hyperosmotic spikes penetrate to the ocular surface, salt concentrations there are much lower than those in the progenitor PrLTF spikes. For D_s less than 10^{-7} cm^2/s, the SCL protects the cornea from hyperosmotic spikes for both normal and dry eyes. When localized corneal hyperosmolarity is converted into transient pain scores, pain thresholds are significantly lower than those for no-lens wear.
Conclusions: A cornea can be protected from localized PrLTF hyperosmolarity spikes with SCL wear. With regular blinking (e.g., < 10 s), SCL wear shields the cornea from significant hyperosmotic pain. Decreasing D_s increases that protection. Low-D_s soft contact lenses can protect against hyperosmotic spikes and discomfort even during infrequent blinking (e.g., > 10 s).

7.2 Introduction

The human ocular surface is coated by a thin tear film that keeps the ocular surface lubricated, hydrated, and protected against infection.[215,276] The outermost layer of the tear film is comprised of a thin lipid layer, which retards the evaporation of the muco-aqueous layer that contains electrolytes, metabolites, and various antimicrobial compounds.[215,242] Between the muco-aqueous layer and the ocular surface is the glycocalyx adlayer that engenders corneal wetting and promotes the epithelial barrier function of the ocular-surface.[277]

During an interblink, evaporation of the muco-aqueous layer results in periodic increased tear-film osmolarity.[26,35] Tear evaporation rate depends on the lipid-layer thickness and composition.[278–280] When a suboptimal lipid layer allows excess tear evaporation, tear becomes hyperosmotic causing deleterious effects on the corneal epithelia[13,191–193,196–198] and triggering dry-eye symptoms.[14] Tear osmolarity is significantly higher in the ocular-surface tear film than in the tear meniscus[35,189,190], where osmolarity is typically measured.[15,16,18,19,21–24,36,37,281]

Recently, Kim et al.[80] showed that soft-contact-lens (SCL) wear can effectively mitigate hyperosmolarity in the post-lens tear film (PoLTF), which directly interfaces the ocular surface, and that PoLTF osmolarity is different from those of the meniscus and pre-lens tear film (PrLTF). The ability of a SCL to attenuate PoLTF osmolarity depends on lens-salt diffusivity (D_s), lens-salt partition coefficient (k_s), and lens thickness (h_{lens}). These three parameters regulate how much salt diffuses across the SCL from the PrLTF to the PoLTF. However, Kim et al.[80] found that physically acceptable ranges for k_s and h_{lens} had a limited effect on PoLTF osmolarity. These authors stated that to minimize PoLTF hyperosmolarity, SCL should be designed with low D_s values while not allowing lens adherence.[39,40,80]

In addition to intrinsic SCL properties, lacrimal tear-production rate, evaporation rate, tear-drainage rate, and interblink period strongly affect PoLTF osmolarity as well. Interestingly, PoLTF osmolarity for dry-eye subjects (e.g., low tear production and/or high evaporation rates) with SCL wear can be reduced to osmolarity lower than that of the pre-corneal tear film of normal-eye subjects during no-lens wear by lowering D_s.[80] However, the analysis of Kim et al.[80] only considered a uniform tear evaporation rate across the whole PrLTF. In other words, they specified spatial average tear-compartment osmolarities and did not account for regional variance in tear evaporation rate within the PrLTF. Understanding both the spatial average osmolarity and the localized osmolarity is essential to understanding tear hyperosmolarity during SCL wear and how osmolarity affect corneal epithelial cells and lens-wear comfort.

Localized break-up regions are widely believed to be caused by localized lipid-layer thickness and/or composition variations resulting in different localized evaporation rates.[34,279] This hypothesis is supported by faster cooling of localized break-up areas in the pre-corneal tear film (PrCTF) that correlates directly with fluorescein break-up areas.[282] Osmolarity of localized break-up areas in the PrCTF can reach 600-800 miliOsmolar (mOsM) during a 10-s interblink period,[33,34] which is approximately 2 to 2.5 times the osmolarity of the spatial average PrCTF.[35] Localized PrLTF salt spikes therefore expose epithelial cells to much higher salinities and hence to higher pain thresholds.[14] Similar to the PrCTF during no-lens wear,[283] localized tear break-up areas exhibiting high evaporation rates also occur on the PrLTF during SCL wear.[81] However, because of minimal mixing of the PrLTF with the PoLTF,[203] salt concentration spikes at the anterior lens surface must first diffuse through the SCL to reach the cornea.[80]

This work addresses the question of whether SCL can effectively attenuate PrLTF salinity spikes and protect the cornea from irritating salinity exposure. The proposed physical model assesses whether SCL wear can protect the PoLTF/cornea from localized PrLTF hyperosmotic break-up areas for normal and dry eyes. Calculated PoLTF osmolarities are then converted to dry-eye pain scores from Liu et al.[14] to predict if SCLs with low D_s can protect wearers from salinity-induced dryness discomfort.

7.3 Methods

Although break-up areas cannot be visualized with fluorescein dye during SCL wear, non-invasive tear break-up analysis using concentric ring patterns confirms that PrLTF exhibits tear break up.[81,284] Therefore, localized evaporation-driven osmolarity spikes in the PrLTF are anticipated to be similar to those on the pre-corneal tear film during no-lens wear. Figure 7.1 provides a schematic of what is expected for PoLTF osmolarity when the SCL is permeable to aqueous salt and there is a localized break-up area in the PrLTF. Because the PoLTF is so thin compared to the SCL, once salt enters the PoLTF, contact with the cornea is essentially immediate.

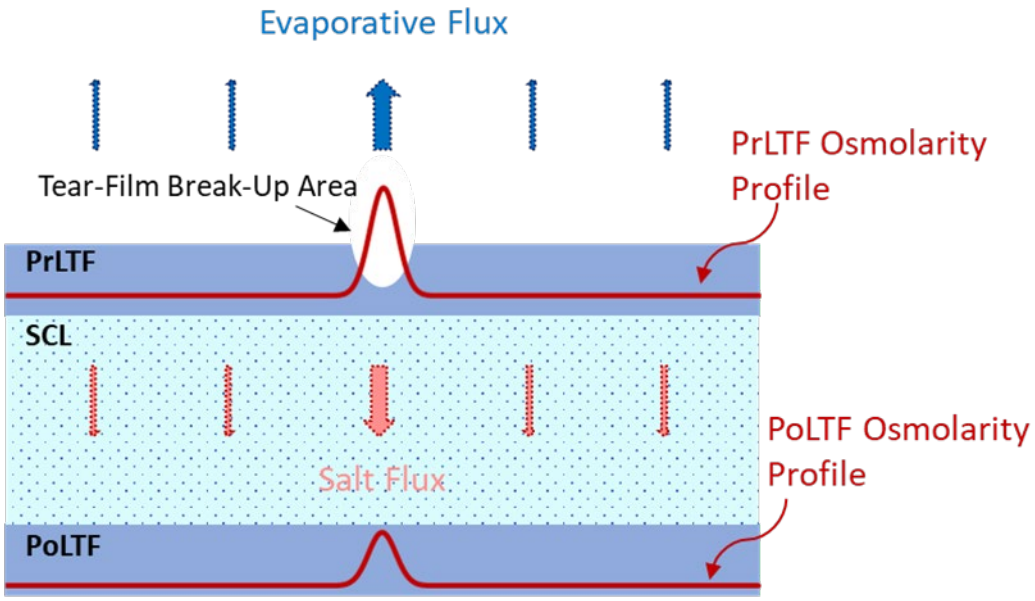

Figure 7.1. Schematic salinity spikes in the PrLTF and PoLTF due to localized pre-lens tear-film break up. Figure is not to scale.

To address whether localized salinity spikes on the cornea with SCL wear can be mitigated with low SCL D_s materials, the original effort of Peng et al.[34] is extended to include a PrLTF, a lens, and a PoLTF. Localized salinity spikes are imposed at the PrLTF/lens interface (i.e., at the lens anterior surface) and traced numerically during interblinks of various duration. A series of D_s values is tested for both normal and dry eyes. Both lateral and sagittal diffusion of salt through the lens and PoLTF are accounted. First, the contact lens overlying the cornea is a translationally invariant rectangle of length 12 mm and height 130 μm. A similar rectangle represents the 3-μm thick PoLTF (h_{PoLTF}) between the lens and the cornea. The 2D coordinate system and boundary conditions are summarized in Figure 7.2.

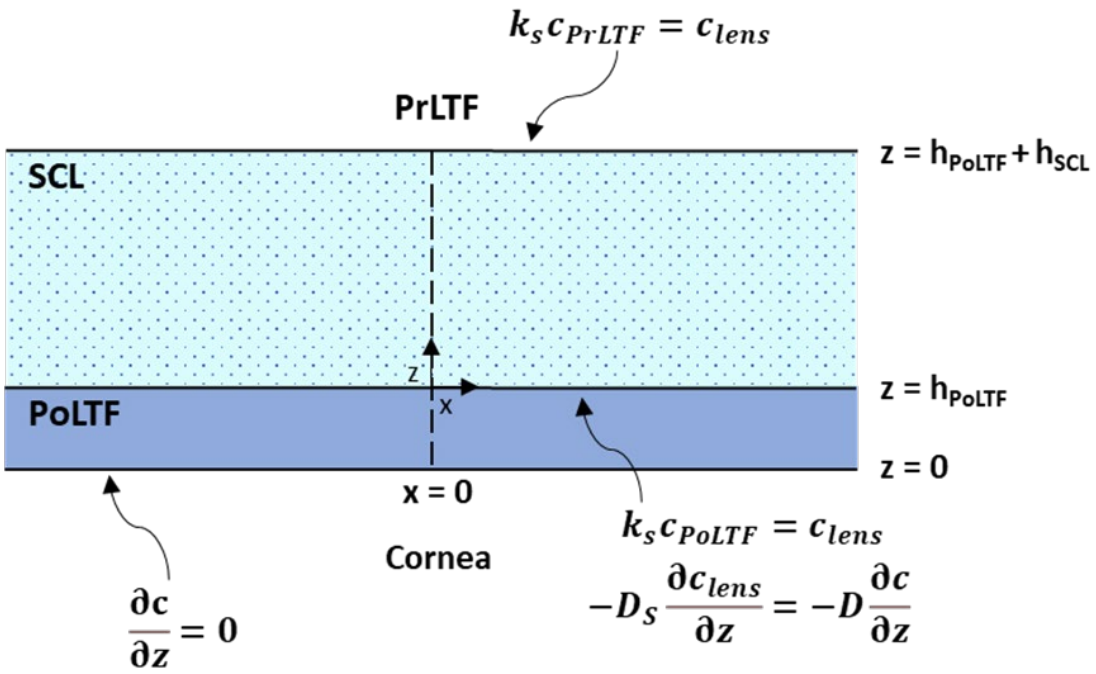

Figure 7.2. Schematic of the translationally invariant calculation domain and the requisite boundary conditions in the z direction. For convenience, the no-flux boundary conditions are not shown at the domain ends (in the x direction). Figure is not to scale.

Salt transports across the lens and through the PoLTF according to Fick's second law written as

$$\frac{\partial c_{lens}}{\partial t} - D_s\left(\frac{\partial^2 c_{lens}}{\partial x^2} + \frac{\partial^2 c_{lens}}{\partial z^2}\right) = 0 \qquad SCL\ (h_{PoLTF} \le z \le h_{PoLTF} + h_{SCL}) \qquad (7.1)$$

and

$$\frac{\partial c}{\partial t} - D\left(\frac{\partial^2 c}{\partial x^2} + \frac{\partial^2 c}{\partial z^2}\right) = 0 \qquad PoLTF\ (0 \le z \le h_{PoLTF}) \qquad (7.2)$$

respectively. Here, $c_{lens}(t,x,z)$ is the molar salt concentration in the lens per lens volume as a function of time, t, and spatial coordinates x and z. x is the lateral coordinate with x = 0 locating the center of the lens, z is the sagittal coordinate with z = 0 demarking the PoLTF/cornea interface. c(t,x,z) is the PoLTF transient aqueous salt concentration, D (= 1.5×10^{-5} cm^2/s) is the bulk water salt diffusivity,[103] and D_s is the salt diffusivity in the contact lens. Consistent with Kim et al.,[80] low D_s (= 2.8×10^{-8} cm^2/s), medium D_s (= 1.1×10^{-6} cm^2/s), and high D_s (= 6.0×10^{-6} cm^2/s) are chosen to investigate the role of lens-salt diffusion rates in attenuating corneal salinity spikes. D_s values chosen are within the range of those available for current commercial SCLs.[80] Equations 7.1 and 7.2 each require four boundary conditions and an initial condition.

The boundary condition at the lens/PrLTF interface (i.e., at $z = h_{PoLTF} + h_{lens}$) is local equilibrium given by Nernst's law

$$k_s c_{PrLTF} = c_{lens} \qquad z = h_{PoLTF} + h_{lens} \qquad (7.3)$$

where c_{PrLTF} and c_{lens} are the salt concentrations at the lens side and the PrLTF side of the lens/PrLTF interface, respectively. k_s is the partition coefficient of the lens and is set constant at 0.28 for all calculations.[80,210]

The imposed transient PrLTF/lens interface salt-spike concentration, c_{PrLTF}, is that in Figure 7.3 obtained from Peng et al.,[34] assuming that tear break up over a SCL is of similar origin to that over the cornea (i.e., due to lipid layer break up and tear evaporation). To quantify the concentration distribution in Figure 7.3 as a function of time and location, we modified a Gaussian function to match the results of Peng et al.[34] for the PrCTF

$$c_{PrLTF} = c(t, x, z = h_{PoLTF} + h_{lens}) = \frac{c_A(t) - c_B(t)}{2} \exp\left(-\frac{x^2}{2\sigma^2}\right) + \frac{c_B(t) + \alpha}{2} \tag{7.4}$$

where $c_A(t)$ is the transient osmolarity peak height in Figure 7.3 and illustrated in Figure 7.4, $c_B(t)$ quantifies the salt osmolarity rise at the lens anterior surface outside the salt spike and depicted in Figure 7.5, and σ is the Gaussian standard deviation set as 0.2 mm to match the pre-corneal tear-film osmolarity plot of Peng et al.[34] α is a constant that shifts Figure 7.3 in sagittal direction so that $c(t = 0, x, z = h_{PoLTF} + h_{lens})$ matches that of PrLTF osmolarity at the beginning of the periodic steady-state interblink for various lens D_s and normal/dry eye results from Kim et al.[80] Since the periodic steady-state osmolarity of the PrLTF upon eye opening varies depending on the D_s value and on dry-eye symptomatology,[80] α is different for each D_s and for normal and dry eyes. Both terms on the right of Equation 7.4 are divided by 2 because Equations 7.1 and 7.2 solve for the salt molar concentration and not for osmolarity. For multi-spike analyses, two peaks are introduced at the PrLTF/SCL interface. The second Gaussian function is shifted laterally to the desired location. σ and α values for the multi-spike analyses remain unchanged from those of the single-spike analyses.

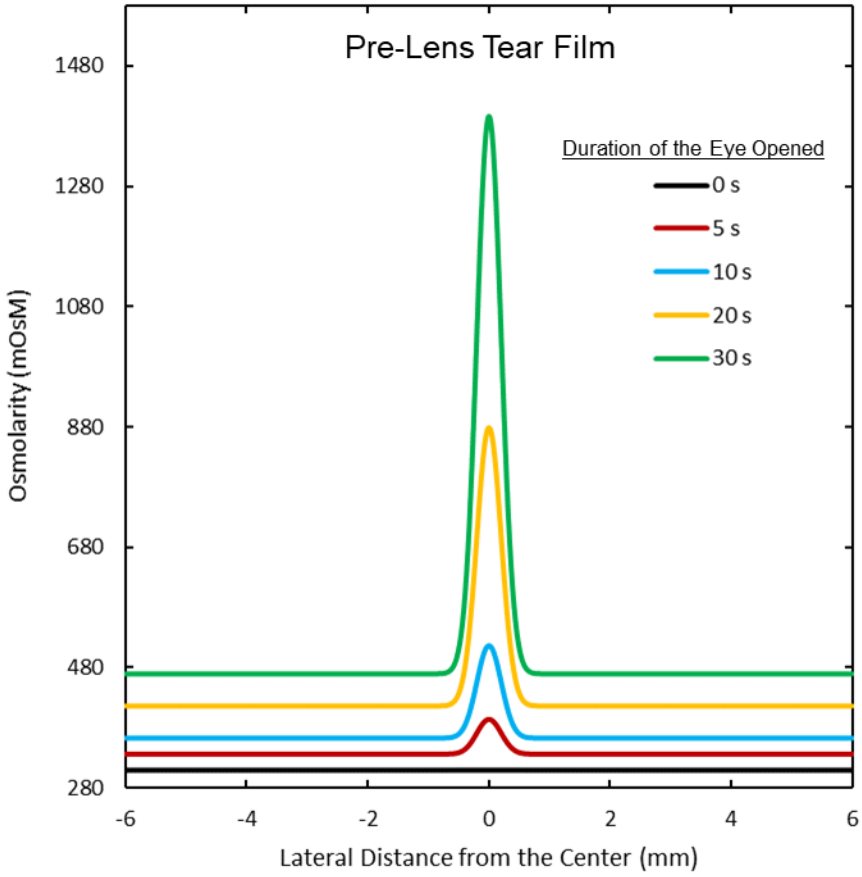

Figure 7.3. Pre-corneal tear-film osmolarity spike arising from pre-corneal tear-film break up. Adopted as pre-lens tear-film osmolarity for our analysis. Reprinted with permission from Peng et al.[34] Copyright (2014) Elsevier B.V.

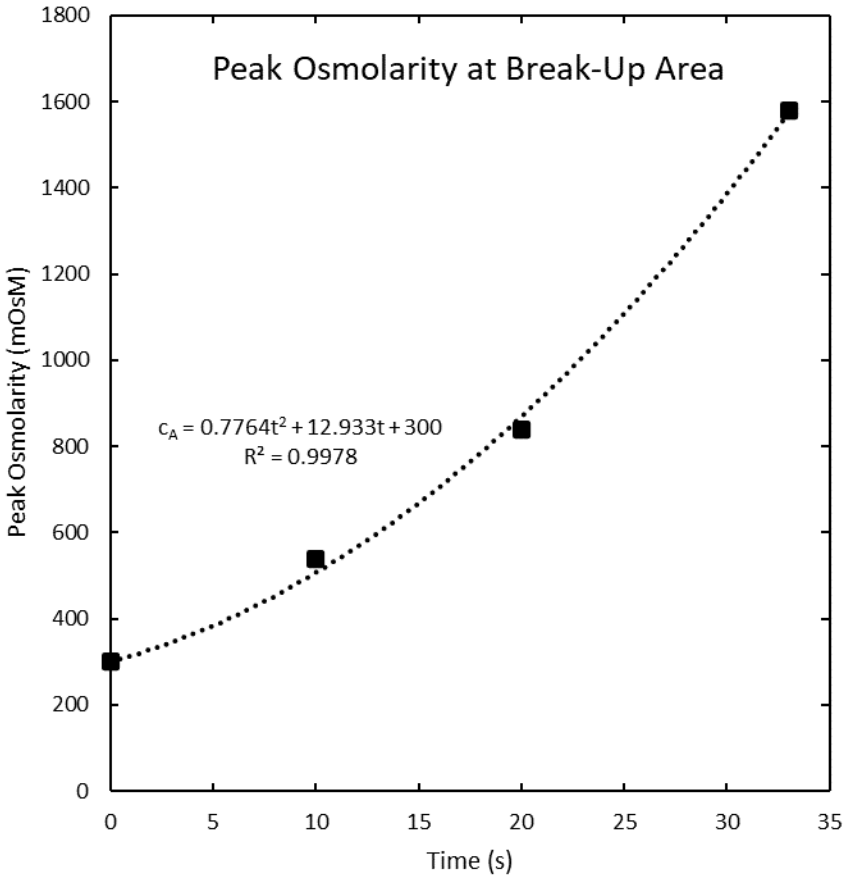

Figure 7.4. Fitting of peak osmolarity in the break-up area, $c_A(t)$ in Equation 7.4 from Figure 7.3. Peak osmolarity data of Peng et al.[34] are given as solid squares. The dashed line is a best fit of the data to the quadratic equation listed in the figure.

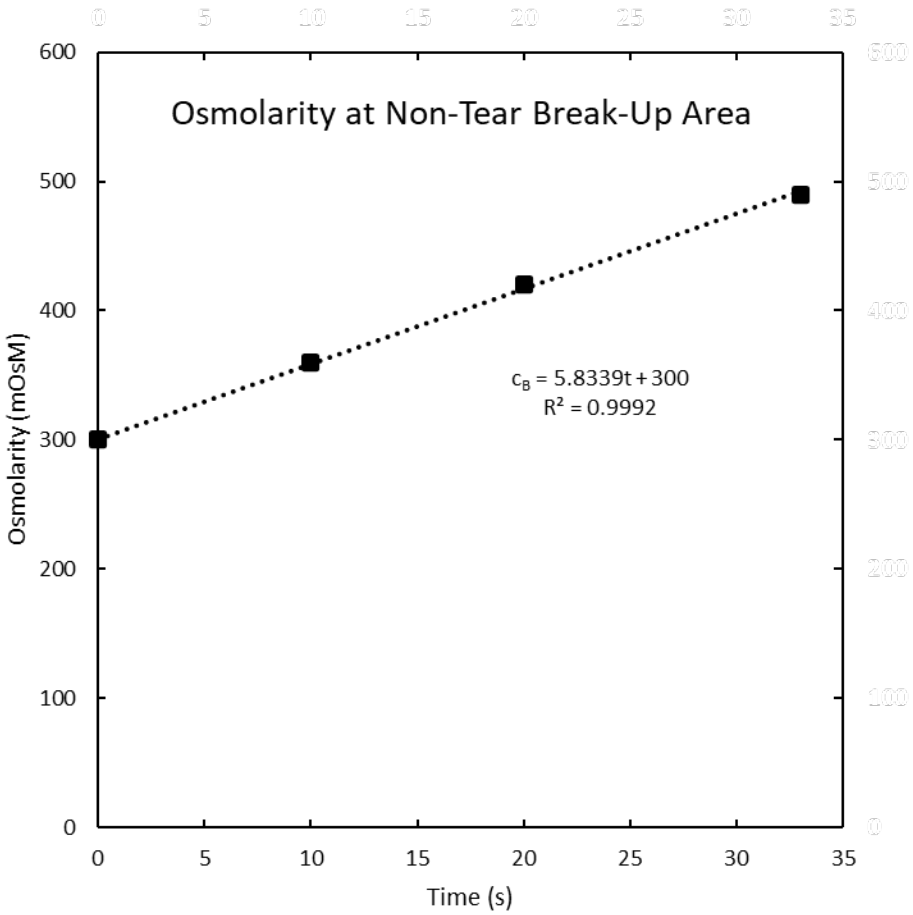

Figure 7.5. Fit of non-tear break-up area osmolarity, $c_B(t)$ in Equation 7.4 from Figure 7.3. Calculated osmolarities of non-tear break-up area of Peng et al.[34] are given as solid squares. The dashed line is a best fit of the data to the linear equation listed in the figure.

At the PoLTF/lens interface ($z = h_{PoLTF}$), local equilibrium salt partitioning

$$k_s c_{PoLTF} = c_{lens} \qquad z = h_{PoLTF} \tag{7.5}$$

and continuity of salt flux (i.e., $J_{lens} = J_{PoLTF}$) are imposed so that

$$-D_S \frac{\partial c_{lens}}{\partial z} = -D \frac{\partial c}{\partial z} \qquad z = h_{PoLTF} \tag{7.6}$$

where c_{PoLTF} and c_{lens} are the salt concentrations at the PoLTF side and lens side of the PoLTF/lens interface, respectively, and J_{PoLTF} and J_{lens} are the salt fluxes at the PoLTF side and lens side of the PoLTF/lens interface, respectively. To simplify the analysis, no-flux boundary conditions are demanded at the lens and PoLTF edges ($x = \pm 6$ mm) and at the PoLTF/cornea interface ($z = 0$). Thus, lateral salt exchange to the pre-conjunctival tear film/tear menisci or sagittal exchange to corneal epithelium, respectively, are not accounted for.[80] Therefore, salt originating from the PrLTF accumulates within the PoLTF during the interblink period.

The initial condition for the SCL is adapted from the periodic steady-state salt-concentration profile in the SCL at the beginning of an interblink (i.e., at t = 0) for normal and dry eyes and for low, medium, and high D_s.[80] Since this initial condition is involved, feasibility was assessed for using a spatially averaged lens-salt concentration as the initial profile. This approximation resulted in PoLTF/cornea interface osmolarities differing by less than 0.5 mOsM for every time point when compared to the results from using the actual periodic salt-concentration profile as the initial condition. Therefore, the average lens-salt concentration initial condition was implemented because it well reflects the actual initial lens-salt concentration profile and it simplifies numerical analysis.

Finally, the initial condition for the PoLTF salt-concentration profile also is uniform and set as the calculated time-averaged periodic steady state PoLTF concentration from Kim et al.[80] Depending on the D_s and normal/dry-eye condition being assessed, the initial conditions of the PoLTF and SCL are different. These changes, along with α of Equation 7.4, assess osmolarity profiles of the PoLTF at the corneal surface for various lens D_s and normal/dry eye combinations.

Numerical solution of Equations 7.1 and 7.2 is by finite-element analysis using Comsol Multiphysics 5.5 and requires amalgamation of Matlab R2019b (Mathworks, Natick, MA) to specify the PrLTF/SCL interface boundary conditions. Because the lens-anterior-surface concentration boundary condition in Figure 7.3 covers the time period of 33 seconds,[34] the analysis provided here extends out to 30 s.

In a small sample-size clinical study, Liu et al.[14] measured subject pain scores set between 0 to 10, with 0 reflecting no pain and 10 marking intolerable pain, upon direct instillation of hyperosmolar solutions onto the ocular surface. From those data, calculated peak lens-wear PoLTF osmolarities were converted into pain scores to reveal whether low-D_s SCL wear can meaningfully mitigate dryness discomfort.

7.4 Results

Figures 7.6a-c present the calculated transient osmolarity of the PoLTF at the corneal surface for low, medium, and high D_s, respectively, for normal eyes experiencing the localized osmolarity spike at the lens anterior surface. For Figures 7.6a-c, α in Equation 7.4 is set as 11, 9.5, and 9, respectively, to set the initial PrLTF osmolarity to be 311 mOsM, 309.5 mOsM, and 309 mOsM for low, medium, and high D_s, respectively. Figures 7.6b-c reveal that a salt spike at the lens anterior surface indeed penetrates through the lens to the corneal surface within an interblink. However, Figure 7.6a reveals that the low-D_s lens completely attenuates the PrLTF salt spike. Here, the osmolarity difference between any two chronological time points is ~0.1 mOsM; peaks are too small to visualize even after 30 s of interblink.

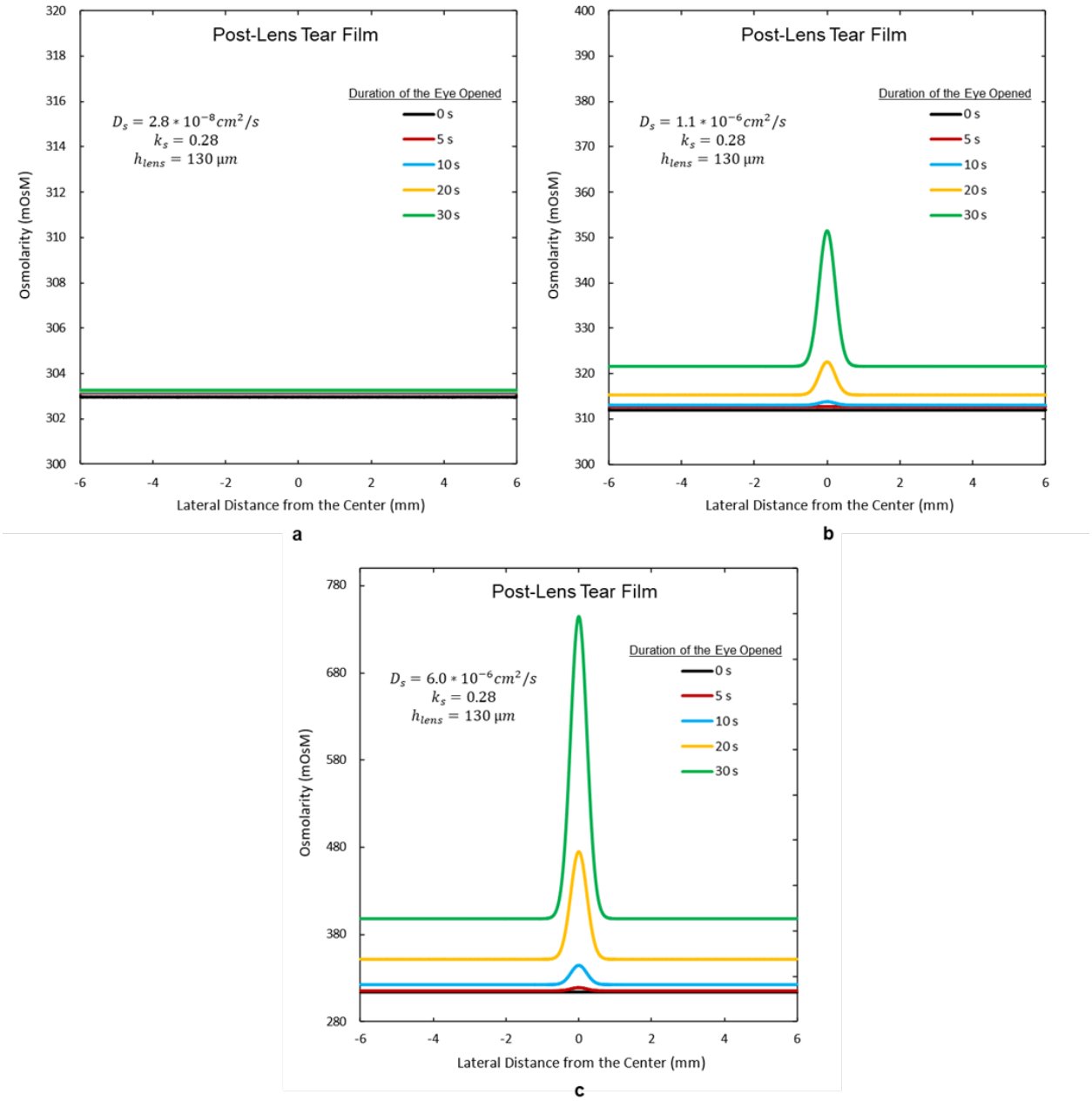

Figure 7.6. Salinity-spike growth kinetics due to local tear-film rupture at the lens anterior surface in Figure 7.3 for normal eyes. (a) transient PoLTF osmolarity profiles for low lens-salt diffusivity ($D_s = 2.8 \times 10^{-8}$ cm^2/s), (b) medium lens-salt diffusivity ($D_s = 1.1 \times 10^{-6}$ cm^2/s), and (c) high lens-salt diffusivity ($D_s = 6.0 \times 10^{-6}$ cm^2/s). Different ordinate scales are adopted in each graph. The PrLTF salinity spike penetrates through to the PoLTF/corneal interface for (b) and (c) but not (a).

Figures 7.7a-c provide PoLTF osmolarity profiles for low, medium, and high D_s values, respectively, for dry eyes. For Figures 7.7a-c, α in Equation 7.4 is set at 25, 20.5, and 20, respectively, to determine the initial PrLTF osmolarity as 325 mOsM, 320.5 mOsM, and 320 mOsM for low, medium, and high D_s, respectively.[80] Similar to the normal eye, a low-D_s lens eliminates the PrLTF salt spike at the corneal surface up to at least 30 s of interblink. Due to the

higher initial PrLTF and PoLTF osmolarities than those of normal eyes, PoLTF osmolarity at the corneal surface is significantly higher for dry eyes than for normal eyes at early time. However, the difference between normal and dry eyes diminishes at later time. Similar to the normal eye, low-D_s lens completely attenuates the PrLTF salt spike at the corneal surface up to at least 30 s of interblink.

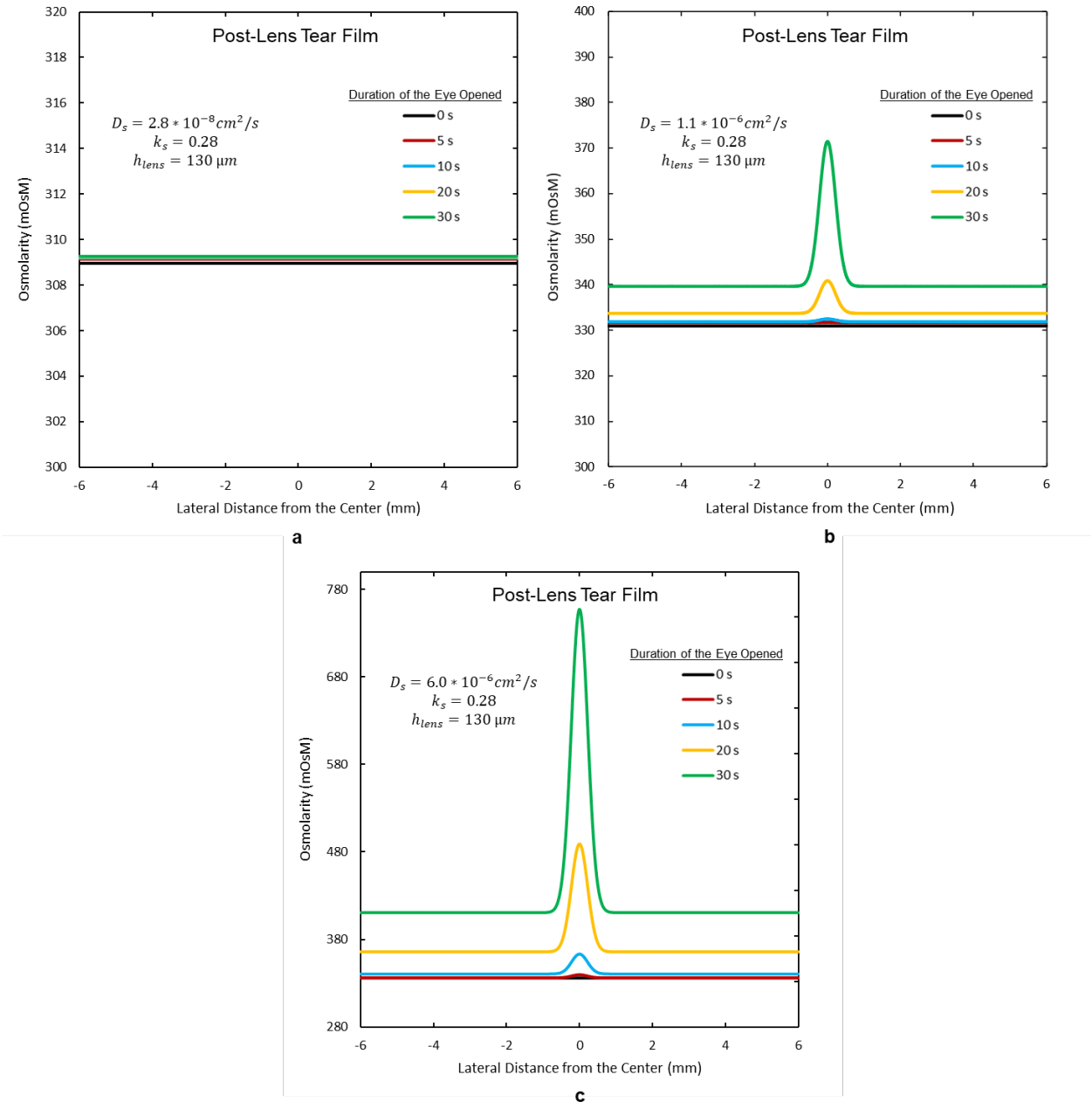

Figure 7.7. Salinity-spike growth kinetics due to local tear-film rupture at the lens anterior surface after Peng et al.[34] in Figure 7.3 for dry eyes. (a) transient PoLTF osmolarity profiles for low lens-salt diffusivity ($D_s = 2.8 \times 10^{-8}$ cm^2/s), (b) medium lens-salt diffusivity ($D_s = 1.1 \times 10^{-6}$ cm^2/s), and (c) high lens-salt diffusivity ($D_s = 6.0 \times 10^{-6}$ cm^2/s). Different ordinate scales are adopted in each graph. The PrLTF salinity spike penetrates through to the PoLTF/corneal interface for (b) and (c) but not for (a).

Figure 7.8a compares PoLTF osmolarities at the corneal surface as a function of interblink time for the three lens D_s values. 5 - 10 s is required for salt to diffuse through the lens and PoLTF to reach the corneal surface for D_s values above about 10^{-7} cm^2/s, albeit at much lower salt concentrations. Most importantly, Figure 7.8a demonstrates that for D_s values below about 10^{-7} cm^2/s, SCL wear well protects against corneal hyperosmotic exposure for both normal and dry eyes. Figure 7.8b converts the peak corneal salt concentrations in Figure 7.8a to clinical pain scores ranging between 0 and 10 based on the results of Liu et al.[14] Comparison with the no-lens pain scores shows that all three D_s values produce significantly less discomfort than that arising from no-lens wear.

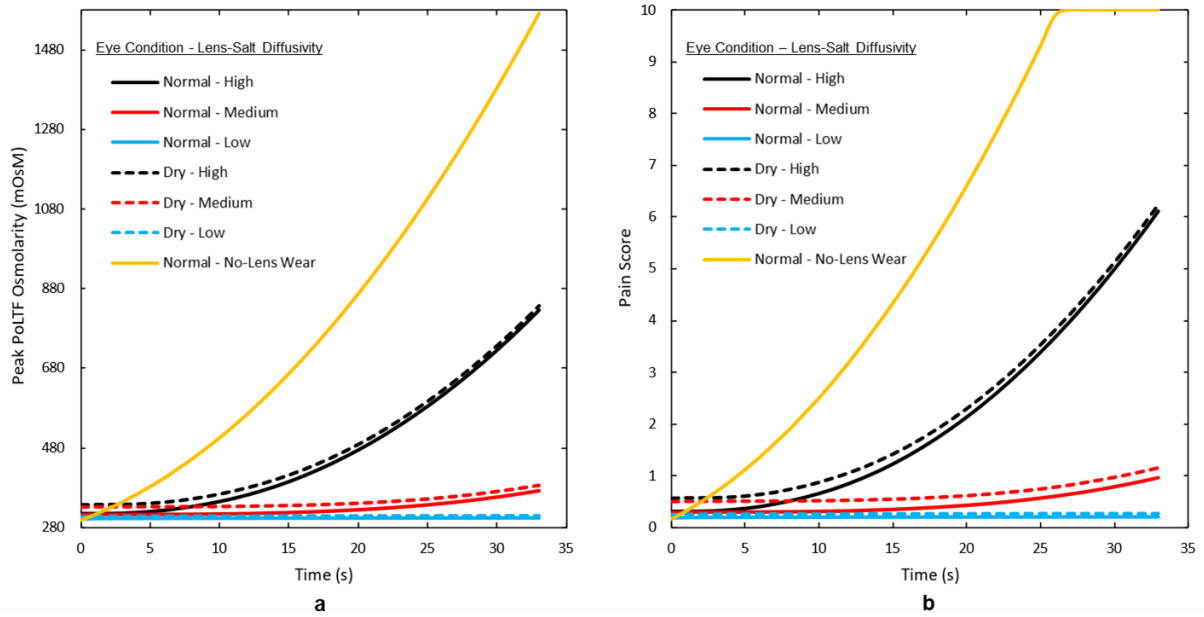

Figure 7.8. (a) Peak transient ocular-surface osmolarity with lens wear as a function of interblink time. (b) Clinical pain score as a function of interblink time. Clinical pain scores were determined from osmolarity values of (a) and the results of Liu et al.[14] Salt diffusivities are given as: low $D_s = 2.8 \times 10^{-8}$ cm^2/s (blue line), medium $D_s = 1.1 \times 10^{-6}$ cm^2/s (red line), and high $D_s = 6.0 \times 10^{-6}$ cm^2/s (black line). No-lens wear peak osmolarity from Figure 7.3 is shown as a yellow line.

Figure 7.9 assesses the effect of a nearby osmolarity spike arising from multiple tear ruptures on the anterior lens surface within one interblink for normal eyes. Figure 7.9a provides the PrLTF osmolarity profile when the spike apexes are 0.5 mm apart for a medium D_s lens. Corresponding PoLTF osmolarity at the corneal surface is provided in Figure 7.9b. All parameters are identical to the analysis done for determining Figure 7.6b. Due to the close proximity of the two peaks, the region between the peaks elevates in osmolarity for both PrLTF and PoLTF regions. Figure 7.9c depicts the PrLTF osmolarity profile when the spike apexes are 2.0 mm apart with other controllable parameters identical to those in Figures 7.6b and 7.9a. Corresponding PoLTF osmolarity at the corneal surface for Figure 7.9c is provided in Figure 7.9d. In this case, two peaks at the PrLTF act independently and do not influence each other. Although not explicitly shown here, results from Figures 7.9a and 7.9b imply that larger break-up area on the anterior lens surface results in larger high osmolarity regions in the PoLTF.

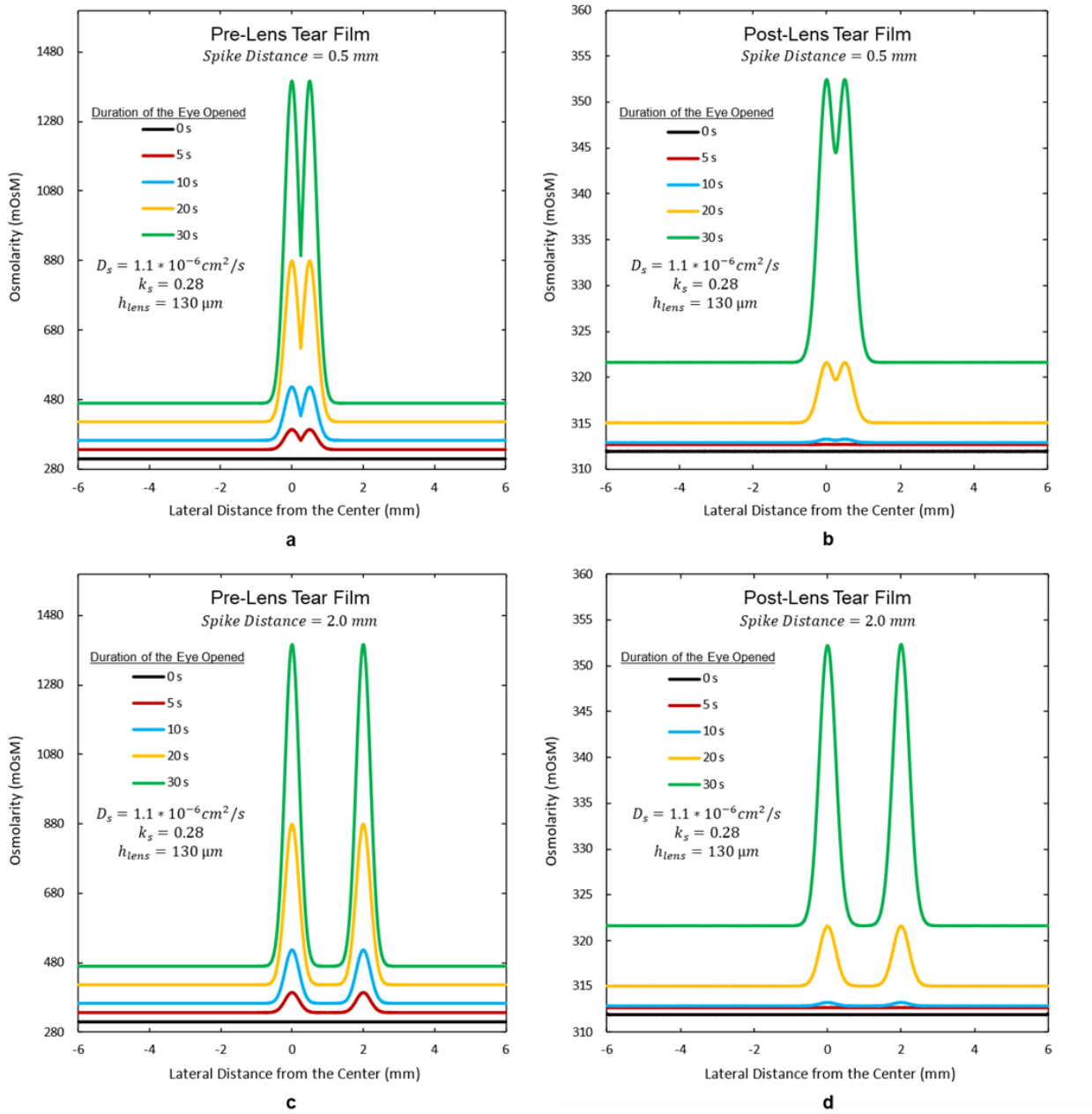

Figure 7.9. Salinity-spike growth kinetics due to local tear-film rupture at the lens anterior surface. (a) two spikes at the lens anterior surface with peaks separated by 0.5 mm; (b) corresponding PoLTF osmolarity at the corneal interface; (c) two spikes at the lens anterior surface with peaks separated by 2.0 mm; (d) corresponding PoLTF osmolarity at the corneal interface. (a) and (c) have different y-axis scales than do (b) and (d).

7.5 Discussion

Figures 7.6, 7.7, and 7.8a clearly demonstrate that low D_s SCLs can protect the cornea against localized hyperosmotic spikes formed in the PrLTF due to localized tear break-up and elevated evaporation. Even for medium and high-D_s SCLs, osmotic peaks are significantly smaller than those of the PrCTF summarized in Figure 7.8a. Localized peak salt concentrations when

translated into clinical pain scores in Figure 7.8b, strikingly confirm that SCL wear mitigates corneal hyperosmolarity. Even for dry eyes, correlated pain scores greater than unity are not achieved until after 10 s into an interblink, a time longer than most human interblinks. These results suggest why SCL wear allows longer maximum interblink intervals than without lens wear when subjects are asked to keep their eyes open for as long as possible.[272] Wear of a SCL protects the cornea from localized osmolarity spikes as long as lens wearers blink frequently. However, if lens wearers blink infrequently, which is typically the case when the lens wearers are reading, watching TV, or working on a computer, their corneas are more likely exposed to localized hyperosmotic spikes on the ocular surface. To ensure that the cornea is protected from localized osmolarity spikes, lens D_s can be lowered, as demonstrated in Figures 7.6a and 7.7a.

Interestingly, osmotic spikes at the ocular surface for normal and dry eyes during SCL wear are not significantly different for a given D_s; the difference further diminishes as eyes are open longer. The reason why the difference between normal and dry eyes diminishes at later times is the larger osmolarity difference between the PrLTF and the PoLTF resulting in a greater salt flux from the PrLTF to the PoLTF for dry eyes than for normal eyes. If the interblink period is set to even longer times (e.g., to min), normal and dry-eye osmolarities eventually merge. Because pain scores for normal and dry eyes in Figure 7.8b differ minimally for a given D_s, lens-wear discomfort due to localized hyperosmotic tear spikes is likely not influenced by lens wearers' baseline dry-eye symptomatology.

The single-spike analyses in Figures 7.6 and 7.7 show the behavior of one PrLTF osmotic spike on the ocular surface during lens wear. With actual lens wear, multiple spikes are expected to form across the lens surface and, therefore, across the ocular surface. Figure 7.9 shows that when tear break-up ruptures occur close to one another (e.g., peak-to-peak distance of 0.5 mm), there is a reinforcing influence (e.g., Figures 7.9a and 7.9b) on the osmolarity. These results are expected because two small nearby tear break-up areas can combine into a one large rupture area during a prolonged interblink period. Meanwhile, when tear ruptures are located far away from each other (e.g., peak-to-peak distance of 2.0 mm), osmolarity of the isolated break-up areas are independent of one another (e.g., Figures 7.9c and 7.9d).

Following the work of Peng et al.,[34] break-up areas in the PrLTF were initiated from depleted lipid layer and, therefore, have high localized evaporation rates. Such tear ruptures have the same localized evaporation and localized osmotic increase rates for both normal and dry eyes. This assumption is reasonable since inadequate lipid regions likely exhibit localized evaporation rates of water regardless of the subjects' dry-eye symptomatology. Thus, whole-eye tear evaporation rates during SCL wear[234] is due to the size and number of break-up spots on the lens and to the exposed ocular surface area. There is, however, a possibility that localized tear ruptures exhibit different evaporation rates for normal and dry eyes requiring further investigation.

This work assumes that the PrLTF-osmolarity increase due to localized tear break-up are the same as the pre-corneal tear-film osmolarity increase due to localized break-up areas during no-lens wear. In reality, non-invasive tear break-up times for SCL wear is faster than that for no-lens wear.[81] Both the results of Peng et al.[34] and here assume that localized break-up occurs immediately upon lid opening. Further, zero salt flux was imposed between the PoLTF and the cornea. Taking these effects together means that this work provides a worst possible scenario for localized hyperosmolarity in the PoLTF during SCL wear.

The mathematical analysis presented is equivalent to the maximum interblink period stress test conducted clinically.[272,285] Since osmotic initial conditions for PoLTF, PrLTF, and the SCL are those of Kim et al.,[80] calculated results demand that localized PrLTF spikes happen randomly

over the SCL surface. If, however, certain areas of the lens surface are more prone to tear rupture, then the localized hyperosmotic peaks may be even more saline than our calculations indicate. Further investigation is needed to elucidate PrLTF break-up patterns.

To convert determined localized hyperosmolarity results to pain scores, clinical results of Liu et al.[14] were utilized. A limit to this conversion is that the hyperosmolarity of localized break-up spots were analyzed in this work whereas Liu et al.[14] administered saline to the entire ocular surface. Because there are ~7,000 nociceptors per square millimeter[286] and approximately 70% of those are polymodal and sensitive to osmolarity,[287,288] it is likely that localized hyperosmotic spikes also trigger pain. Another limitation to utilizing the results of Liu et al.[14] is the small 5-subject size of their clinical study.

This work focuses on lens-wear irritation associated with hyperosmolarity. With SCL wear, however, there are multiple factors (e.g., lid-wiper epitheliopathy, blurry vision, lens edge, SCL surface dehydration, and lack of clear visual acuity) that can result in lens-wear discomfort. Nevertheless, SCL wear with all D_s values studied protects the corneal surface against random hyperosmotic spikes. Only the lowest D_s lens considered provides complete osmotic protection. Localized osmotic protection persists even when the interblink period is 30 s for both normal and dry eyes. Results of Kim et al.[80] and the calculations here confirm that SCL wear can protect the cornea both from spatial average hyperosmolarity and from localized hyperosmotic spikes.

Chapter 8

Conclusions and Suggested Future Directions

8.1 Conclusions

Transport of oxygen and salts across a contact lens during lens wear are critical for safe and comfortable wear. This dissertation mathematically models oxygen and salt transport across contact lenses accounting for relevant environmental factors, anatomical factors, and corneal metabolic kinetics to assess corneal edema and tear-compartment osmolarities. Results from the metabolic-edema models provide contact-lens designers with guidelines to minimize hypoxia-induced corneal edema for soft contact lenses (SCL), scleral lenses (SL), and multicomponent-embedded contact lenses. Meanwhile, results provided from the osmolarity models allow SCL designers to optimize salt diffusivity (D_s) to ensure that the cornea is not exposed to hyperosmotic tear, which correlates with dry-eye discomfort during no-lens wear.[15–24] Although this dissertation focuses on studying oxygen and salt transport across lens materials, various models in this dissertation can be modified to assess transport of different types of molecules across the contact lens. Detailed conclusions for each work are provided in each relevant chapter. This section summarizes important conclusions ascertained from this dissertation.

(1) Oxygen transmissibility and lens design are critical to reducing corneal edema with emerging novel contact lenses despite the high oxygen permeability of silicone-based lens materials. Chapter 2 shows that increased oxygen-transport resistance due to lens and post-lens tear-film (PoLTF) thicknesses results in hypoxia-induced central corneal edema. Although the amount of swelling induced by SL wear while awake is clinically safe, further improvement of lens materials for larger oxygen permeability (*Dk*) is necessary to wear these lenses during sleep. In Chapter 3, the metabolic-edema model presented in Chapter 2 is improved to assess central-to-peripheral corneal edema during SCL and SL wear. Results of Chapter 3 reveal that localized oxygen transmissibility (*Dk/L*) is significantly different locally and that maximum swelling with wear of SCL and SL do not typically occur at the central cornea. However, the difference in maximum edema and the central corneal edema is clinically insignificant for single-component contact lenses. For multicomponent-embedded contact lenses, however, Chapter 4 shows that central corneal edema can be significantly different from the edema at the noncentral cornea. Therefore, localized edema must be assessed with multicomponent-embedded contact lenses unlike single-component contact lenses. For modern silicone-based lens encasements, multicomponent-embedded contact lenses are expected to be safe for lens wear even if the embedment is oxygen impermeable as long as the embedment is placed far into the lens periphery. These novel lenses should also be designed with minimum embedment length and maximum embedment and encasement *Dk/L*s to minimize central-to-peripheral corneal edema.

(2) Limbal metabolic support to the cornea, particularly removal of lactate and introduction of bicarbonate, have significant impact on reducing noncentral corneal edema during hypoxia. Chapter 4 highlights that low-*Dk* embedments should be placed near the lens periphery to minimize corneal edema. This recommendation is because of limbal-metabolic support discussed in Chapter 3. Supply of bicarbonate ions and removal of lactate ions by the limbus changes the metabolic concentrations at the corneal endothelium to increase active water transport from the

stroma to the aqueous humor. Oxygen supply from the limbus to the cornea also lessens corneal edema by reducing anaerobic metabolism, which consumes bicarbonate and produces lactate ions. Interestingly, direct removal of lactate and supply of bicarbonate ions by the limbus is more effective in reducing corneal edema than is the oxygen supply from the limbus. The effect of limbal-metabolic support in reducing corneal edema is greatest at the corneal periphery and diminishes towards the central cornea.

(3) Minimizing salt diffusivity in soft contact lenses can protect the cornea from both local and spatially averaged hyperosmolarity. Diffusion-founded osmolarity models outlined in Chapters 6 and 7 show that SCL wear can protect the cornea from hyperosmolarity by lowering salt flux from the pre-lens tear film (PrLTF) to the PoLTF. Accurate osmolarity determination requires accurate measurement of tear evaporation (see Chapter 6) and production (see Chapter 5) rates. In Chapter 7, PoLTF localized osmolarity spike values are converted to clinical discomfort scores based on the results of Liu et al.[14]

These results reinforce that lens wear can protect the cornea from osmolarity-induced discomfort. Chapters 6 and 7 also show that D_s values required for good protection for both normal and dry eyes are possible with contact lenses that are already available in the market. Even though lower D_s is desired to avoid hyperosmotic PoLTF, too low of a D_s can result in lens adherence to the eye. Thus, lens D_s must be carefully chosen to ensure that both lens adhesion and hyperosmotic PoLTF are avoided.

8.2 Suggested Future Directions

This dissertation serves as a basis for numerous future works. Some potential future directions are listed below.

(1) Investigate the effect orthokeratology-lens wear has on corneal hypoxia. This dissertation focuses on contact lenses that change the way light refracts during wear to improve visual acuity. Orthokeratology lenses are worn overnight to shape the cornea into a desired shape to make light converge at the retina. Since morphing of the cornea is done while sleeping, the benefit of orthokeratology lenses is that these lenses do not have to be worn during the day. However, there is a concern to lens wear during sleep because the cornea is not exposed to the environment to receive oxygen from the environment. Unfortunately, hypoxia-induced edema cannot be measured clinically because orthokeratology lens morphs the shape of the cornea overnight and shadows corneal edema.[289] Our proposed metabolic-edema model can be used to assess corneal hypoxia due to orthokeratology-lens wear.

(2) Extend current metabolic-edema model to transient behavior. The current metabolic-edema model assesses lens-wear induced corneal edema at steady state. Although time to steady state is expected to occur in less than an hour,[290] the current metabolic-edema model cannot provide information regarding corneal edema upon lens insertion. By extending the current metabolic-edema model to include a time-dependent response, corneal hypoxia and edema can be investigated immediately after lens wear. This is potentially important for lenses that may be designed for drug delivery and that require short-term lens wear.

(3) Expand the osmolarity model to assess salt transport across multicomponent contact lenses. Embedded components discussed in Chapter 4 might be ion impermeable or have low D_s. To prevent lens adhesion to the ocular surface for lenses with these types of embedments, D_s of the

encasement might need to be increased significantly to allow enough ions to transport to the PoLTF. This can potentially lead to localized hyperosmotic spikes within the PoLTF at regions without the embedment to cause significant osmolarity-induced discomfort. The developed osmolarity model in Chapter 7 can be extended to study the effect of embedments in ion transport to optimize lens-wear comfort and lens adhesion.

(4) Clinical measurement of lens dryness discomfort while wearing soft contact lenses with known salt diffusivity. Chapters 6 and 7 results show that SCL wear can protect the cornea from hyperosmolarity. Although corneal hyperosmolarity and dry-eye discomfort correlate without lens wear,[15–24] there are no studies to date that investigate possible correlation between lens-wear dryness discomfort and salt diffusivity of SCLs. A clinical study measuring lens-wear dryness discomfort while wearing multiple SCLs with different D_s will test the predictions of Chapters 6 and 7. Such a study requires investigation of parameters beside D_s (e.g., lens geometry, lens coating) to be constant among all the SCLs used in the clinical study.

(5) Study transport of different molecules across the contact lens. This dissertation focuses on transport of oxygen and salt across the contact lens to understand how lens wear affects corneal hypoxia and PoLTF osmolarity. Some contact lenses are designed to release agents that ameliorate discomfort or release active drugs for treatment. By incorporating transport of other molecules in the osmolarity model described in Chapter 6, release rates of these agents can be determined. Extension of the osmolarity model to understand release kinetics of active agents will help develop therapeutic contact lenses.

Chapter 9

References

1. Fatt I, Weissman BA. *Physiology of the Eye. An Introduction to the Vegetative Functions*. 2nd ed. Butterworth-Heinemann; 1992.
2. Papas EB. The role of hypoxia in the limbal vascular response to soft contact lens wear. *Eye Contact Lens*. 2003;29(1):S72-S74.
3. Kim YH, Lin MC, Radke CJ. Limbal metabolic support reduces peripheral corneal edema with contact-lens wear. *Transl Vis Sci Technol*. 2020;9(7):44.
4. Sharif Z, Sharif W. Corneal neovascularization: Updates on pathophysiology, investigations & management. *Rom J Ophthalmol*. 2019;63(1):15-22.
5. Leung BK, Bonanno JA, Radke CJ. Oxygen-deficient metabolism and corneal edema. *Prog Retin Eye Res*. 2011;30(6):471-492.
6. Bonanno JA, Polse KA. Corneal acidosis during contact lens wear: Effects of hypoxia and CO2. *Invest Ophthalmol Vis Sci*. 1987;28:1514-1520.
7. Bonanno JA. Molecular mechanisms underlying the corneal endothelial pump. *Exp Eye Res*. 2012;95:2-7.
8. Maurice DM. The location of the fluid pump in the cornea. *J Physiol*. 1972;221(1):43-54.
9. Klyce SD. Stromal lactate accumulation can account for corneal oedema osmotically following epithelial hypoxia in the rabbit. *J Physiol*. 1981;321:49-64.
10. Klyce SD, Russell SR. Numerical solution of coupled transport equations applied to corneal hydration dynamics. *J Physiol*. 1979;292:107-134.
11. Li LY, Tighe B. Numerical simulation of corneal transport processes. *J R Soc Interface*. 2006;3(7):303-310.
12. Chhabra M, Prausnitz JM, Radke CJ. Modeling corneal metabolism and oxygen transport during contact lens wear. *Optom Vis Sci*. 2009;86(5):454-466.
13. Hirata H, Oshinsky M, Fried N. Short exposure to intense tear hyperosmolarity leads to functional alterations of the corneal nerves involved in tearing and/or ocular pain: Implications for dry eye disease. *Invest Ophthalmol Vis Sci*. 2013;54(15):2193.
14. Liu H, Begley C, Chen M, et al. A link between tear instability and hyperosmolarity in dry eye. *Invest Ophthalmol Vis Sci*. 2009;50(8):3671-3679.
15. Farris RL. Tear osmolarity variation in the dry eye. *Trans Am Ophthalmol Soc*. 1986;84:250-268.

16. Farris RL, Stuchell RN, Mandell D. Basal and reflex human tear analysis. I. Physical measurements: Osmolarity, basal volumes and reflex flow rate. *Ophthalmology*. 1981;88:852-857.

17. Gilbard JP, Farris RL, Santamaria JI. Osmolarity of tear microvolumes in keratoconjunctivitis sicca. *Arch Ophthalmol*. 1978;96(4):677-681.

18. Gilbard JP. Human tear film electrolyte concentrations in health and dry eye disease. *Int Ophthalmol Clin*. 1994;34:27-36.

19. Farris RL, Gilbard JP, Stuchell RN, Mandel ID. Diagnostic tests in keratoconjunctivitis sicca. *CLAO J*. 1983;9(1):23-28.

20. Lemp MA, Bron AJ, Baudouin C, et al. Tear osmolarity in the diagnosis and management of dry eye disease. *Am J Ophthalmol*. 2011;151(5):792-798.e1.

21. Mathers WD, Lane JA, Sutphin JE, Zimmerman MB. Model for ocular tear film function. *Cornea*. 1996;15:110-119.

22. Mishima S, Kubota Z, Farris RL. The tear flow dynamics in normal and in keratoconjunctivitis sicca cases. *Excepta Med*. 1971:1801-1805.

23. Tomlinson A, Khanal S, Ramaesh K, Diaper C, McFadyen A. Tear film osmolarity: Determination of a referent for dry eye diagnosis. *Invest Ophthalmol Vis Sci*. 2006;47(10):4309-4315.

24. Ogasawara K, Tsuru T, Mitsubayashi K, Karube I. Electrical conductivity of tear fluid in healthy persons and keratoconjunctivitis sicca patients measured by a flexible conductimetric sensor. *Graefes Arch Clin Exp Ophthalmol*. 1996;234:542-546.

25. van Tilborg MM, Murphy PJ, Evans KS. Impact of dry eye symptoms and daily activities in a modern office. *Optom Vis Sci*. 2017;94(6):688-693.

26. Tomlinson A, Khanal S. Assessment of tear film dynamics: Quantification approach. *Ocul Surf*. 2005;3:81-95.

27. Kulovesi P, Telenius J, Koivuniemi A, Brezesinski G, Vattulainen I, Holopainen JM. The impact of lipid composition on the stability of the tear fluid lipid layer. *Soft Matter*. 2012;8:5826-5834.

28. Mathers WD, Lane JA. Meibomian Gland Lipids, Evaporation, and Tear Film Stability. In: Sullivan DA, Dartt DA, Meneray MA, eds. *Lacrimal Gland, Tear Film, and Dry Eye Syndromes 2.* Springer; 1998:349-359.

29. Isreb MA, Greiner JV., Korb DR, et al. Correlation of lipid layer thickness measurements with fluorescein tear film break-up time and Schirmer's test. *Eye*. 2003;17:79-83.

30. Rosenfeld L, Cerretani CF, Leiske DL, Toney MF, Radke CJ, Fuller GG. Structural and rheological properties of meibomian lipid. *Invest Ophthalmol Vis Sci*. 2013;54:2720-2732.

31. Craig JP, Tomlinson A. Importance of the lipid layer in human tear film stability and evaporation. *Optom Vis Sci*. 1997;74(1):8-13.

32. Paugh JR, Tse J, Nguyen T, et al. Efficacy of the fluorescein tear breakup time test in dry eye. *Cornea*. 2020;39(1):92-98.

33. Braun RJ, King-Smith PE, Begley CG, Li L, Gewecke NR. Dynamics and function of the tear film in relation to the blink cycle. *Prog Retin Eye Res*. 2015;45:132-164.

34. Peng CC, Cerretani CF, Braun RJ, Radke CJ. Evaporation-driven instability of the precorneal tear film. *Adv Colloid Interfac*. 2014;206:250-264.

35. Cerretani CF, Radke CJ. Tear dynamics in healthy and dry eyes. *Curr Eye Res*. 2014;39(6):580-595.

36. Yeh TN, Graham AD, Lin MC. Relationships among tear film stability, osmolarity, and dryness symptoms. *Optom Vis Sci*. 2015;92(9):e264-e272.

37. Amparo F, Jin Y, Hamrah P, Schaumberg DA, Dana R. What is the value of incorporating tear osmolarity measurement in assessing patient response to therapy in dry eye disease? *Am J Ophthalmol*. 2014;157(1):69-77.e2.

38. Szalai E, Berta A, Szekanecz Z, Szûcs G, Módis L. Evaluation of tear osmolarity in non-Sjögren and Sjögren syndrome dry eye patients with the TearLab system. *Cornea*. 2012;31(8):867-871.

39. Cerretani C, Peng CC, Chauhan A, Radke CJ. Aqueous salt transport through soft contact lenses: An osmotic-withdrawal mechanism for prevention of adherence. *Cont Lens Anterior Eye*. 2012;35(6):260-265.

40. Nicolson P, Baron R, Charbrereck P, et al. Extended wear ophthalmic lens. US Patent 5, 965,631. 1999:1-37.

41. Harvitt DM, Bonanno JA. Re-evaluation of the oxygen diffusion model for predicting minimum contact lens Dk/t values needed to avoid corneal anoxia. *Optom Vis Sci*. 1999;76(10):712-719.

42. Takatori SC, Radke CJ. A quasi-2-dimensional model for respiration of the cornea with soft contact lens wear. *Cornea*. 2012;31(4):405-417.

43. Michaud L, van der Worp E, Brazeau D, Warde R, Giasson CJ. Predicting estimates of oxygen transmissibility for scleral lenses. *Cont Lens Anterior Eye*. 2012;35(6):266-271.

44. Compañ V, Oliveira C, Aguilella-Arzo M, Mollá S, Peixoto-de-Matos SC, González-Méijome JM. Oxygen diffusion and edema with modern scleral rigid gas permeable contact lenses. *Invest Ophthalmol Vis Sci*. 2014;55(10):6421-6429.

45. Holden BA, Mertz GW. Critical oxygen levels to avoid corneal edema for daily and extended wear contact lenses. *Invest Ophthalmol Vis Sci*. 1984;25(10):1161-1167.

46. Smelser GK, Chen DK. Physiological changes in cornea induced by contact lenses. *AMA Arch Ophthalmol*. 1955;53(5):676-679.

47. Wang J, Fonn D, Simpson TL. Topographical thickness of the epithelium and total cornea after hydrogel and PMMA contact lens wear with eye closure. *Invest Ophthalmol Vis Sci*. 2003;44(3):1070-1074.

48. Yang WH, Smolen VF, Peppas NA. Oxygen permeability coefficients of polymers for hard and soft contact lens applications. *J Membr Sci*. 1981;9(1-2):53-67.

49. Tyagi G, Collins MJ, Read SA, Davis BA. Corneal changes following short-term rigid contact lens wear. *Cont Lens Anterior Eye*. 2012;35(3):129-136.

50. Efron N. *Contact Lens Practice*. 3rd ed. Elsevier; 2018.

51. Tighe B. Silicone hydrogel materials - How do they work? In: Sweeney D, ed. *Silicone Hydrogels: The Rebirth of Continuous Wear Contact Lenses*. Butterworth-Heinemann; 2000:1-21.

52. Morgan PB, Efron N, Helland M, et al. Twenty first century trends in silicone hydrogel contact lens fitting: An international perspective. *Cont Lens Anterior Eye*. 2010;33(4):196-198.

53. Thompson TT. Tyler's quarterly soft contact lens parameter guide. *TQ*. 2018;35(3):1-68.

54. Sweeney DF. Have silicone hydrogel lenses eliminated hypoxia? *Eye Contact Lens*. 2013;39(1):53-60.

55. Ross AE, Bengani LC, Tulsan R, et al. Topical sustained drug delivery to the retina with a drug-eluting contact lens. *Biomaterials*. 2019;217:119285.

56. Yao H, Shum AJ, Cowan M, Lähdesmäki I, Parviz BA. A contact lens with embedded sensor for monitoring tear glucose level. *Biosens Bioelectron*. 2011;26(7):3290-3296.

57. Jiang H. An accommodative contact lens for presbyopic correction. In: *International Conference on Eye Disorders and Treatment*. J Clin Exp Ophthalmol. 2015;6(3):56.

58. Park J, Kim J, Kim SY, et al. Soft, smart contact lenses with integrations of wireless circuits, glucose censors, and displays. *Sci Adv*. 2018;4:eaap9841.

59. Yetisen AK, Jiang N, Castaneda Gonzalez CM, et al. Scleral lens sensor for ocular electrolyte analysis. *Adv Mater*. 2020;32:1906762.

60. Martin PS. Mojo Vision NanoLEDs for Invisible Computing. In: Strassburg M, Kim JK, Krames MR, eds. *Proc. SPIE 11302, Light-Emitting Devices, Materials, and Applications XXIV*. SPIE; 2020:1-8.

61. Vásquez Quintero A, Pérez-Merino P, de Smet H. Artificial iris performance for smart contact lens vision correction applications. *Sci Rep*. 2020;10(1):14641.

62. Farandos NM, Yetisen AK, Monteiro MJ, Lowe CR, Yun SH. Contact lens sensors in ocular diagnostics. *Adv Healthcare Mater*. 2015;4(6):792-810.

63. Syed IM, Kaur S, Milton HE, et al. Novel switching mode in a vertically aligned liquid crystal contact lens. *Opt Express*. 2015;23(8):9911-9916.

64. Senior M. Novartis signs up for Google smart lens. *Nat Biotechnol*. 2014;32(9):856.

65. de Smet J, de Backer P, Islamaj E, Joshi P, Cuypers D, de Smet H. A spherically shaped display for use as an artificial iris. *Euro Display*. 2013;44(S1):61-64.

66. Woltman SJ, Jay GD, Crawford GP. Liquid-crystal materials find a new order in biomedical applications. *Nat Mater*. 2007;6:929-938.

67. Mansouri K, Shaarawy T. Continuous intraocular pressure monitoring with a wireless ocular telemetry sensor: Initial clinical experience in patients with open angle glaucoma. *Br J Ophthalmol*. 2011;95(5):627-629.

68. Leonardi M, Pitchon EM, Bertsch A, Renaud P, Mermoud A. Wireless contact lens sensor for intraocular pressure monitoring: Assessment on enucleated pig eyes. *Acta Ophthalmol*. 2009;87:433-437.

69. Ho H, Saeedi E, Kim SS, Shen TT, Parviz BA. Contact lens with integrated inorganic semiconductor devices. In: *2008 IEEE 21st International Conference on Micro Electro Mechanical Systems*. IEEE; 2008:403-406.

70. Kim YH, Lin MC, Radke CJ. Central-to-peripheral corneal edema during wear of embedded-component contact lenses. *Cont Lens Anterior Eye*. 2022;45:101443.

71. Walker MK, Bergmanson JP, Miller WL, Marsack JD, Johnson LA. Complications and fitting challenges associated with scleral contact lenses: A review. *Cont Lens Anterior Eye*. 2016;39(2):88-96.

72. Swarbrick HA, Holden BA. Effects of lens parameter variation on rigid gas-permeable lens adherence. *Optom Vis Sci*. 1996;73(3):144-155.

73. Monticelli MV, Chauhan A, Radke CJ. The Effect of water hydraulic permeability on the settling of a soft contact lens on the eye. *Curr Eye Res*. 2005;30(5):329-336.

74. Chen SP, Massaro-Giordano G, Pistilli M, Schreiber CA, Bunya VY. Tear osmolarity and dry eye symptoms in women using oral contraception and contact lenses. *Cornea*. 2013;32(4):423-428.

75. Golebiowski B, Chao C, Stapleton F, Isabelle J. Corneal nerve morphology, sensitivity, and tear neuropeptides in contact lens wear. *Optom Vis Sci*. 2017;94(4):534-542.

76. Kojima T, Matsumoto Y, Ibrahim OMA, et al. Effect of controlled adverse chamber environment exposure on tear functions in silicon hydrogel and hydrogel soft contact lens wearers. *Invest Ophthalmol Vis Sci*. 2011;52(12):8811-8817.

77. Martin DK. Osmolality of the tear fluid in the contralateral eye during monocular contact lens wear. *Acta Ophthalmol*. 1987;65:551-555.

78. Sarac O, Gurdal C, Bostanci-Ceran B, Can I. Comparison of tear osmolarity and ocular comfort between daily disposable contact lenses: Hilafilcon B hydrogel versus narafilcon A silicone hydrogel. *Int Ophthalmol*. 2012;32:229-233.

79. Holden BA, McNally JJ, Egan P. Limited lateral spread of stromal edema in the human cornea fitted with a ('donut') contact lens with a large central aperture. *Curr Eye Res*. 1988;7(6):601-605.

80. Kim YH, Nguyen T, Lin MC, Peng CC, Radke CJ. Protection against corneal hyperosmolarity with soft-contact-lens wear. *Prog Retin Eye Res*. 2022;87:101012.

81. Graham AD, Lin MC. The relationship of pre-corneal to pre-contact lens non-invasive tear breakup time. *PLOS One*. 2021;16(6):e0247877.

82. Takahashi GH, Fatt I. The diffusion of oxygen in the cornea. *Exp Eye Res*. 1965;4:4-12.

83. Graham AD, Fusaro RE, Polse KA, Lin MC, Giasson CJ. Predicting extended wear complications from overnight corneal swelling. *Invest Ophthalmol Vis Sci*. 2001;42:3150-3157.

84. Sweeney DF. Clinical signs of hypoxia with high-Dk soft lens extended wear: Is the cornea convinced? *Eye Contact Lens*. 2003;29(1 Suppl):S22-25, S26-29, S192-194.

85. Arlt C. Clinical Effect of Tear Layer Thickness on Corneal Edema During Scleral Lens Wear. Aalen University. [Master's Thesis]; 2015.

86. Tan B, Zhou Y, Yuen TL, Lin K, Michaud L, Lin MC. Effects of scleral-lens tear clearance on corneal edema and post-lens tear dynamics: A pilot study. *Optom Vis Sci*. 2018;95(6):481-490.

87. Vincent SJ, Alonso-Caneiro D, Collins MJ, et al. Hypoxic corneal changes following eight hours of scleral contact lens wear. *Optom Vis Sci*. 2016;93(3):293-299.

88. Frisani M, Beltramo I, Grec M. Changes in corneal thickness by miniscleral contact lenses. *Cont Lens Anterior Eye*. 2015;38(2015):e38-e39.

89. Oculus. Oculus Pentacam, Pentacam HR interpretation guide 3rd edition. https://www.pentacam.com/fileadmin/user_upload/pentacam.de/downloads/interpretations-leitfaden/interpretation_guideline_3rd_edition_0915.pdf.

90. Tomey Inc. Operation Manual Handy Pachymeter SP-100. http://www.frankshospitalworkshop.com/equipment/documents/ophthalmology/user_manuals/Tomey SP-100 Pachymeter-Usermanual.pdf.

91. Tan B, Graham AD, Tsechpenakis G, Lin MC. A novel analytical method using OCT to describe the corneoscleral junction. *Optom Vis Sci*. 2014;91(6):650-657.

92. Chen S, Huang J, Wen D, Chen W, Huang D, Wang Q. Measurement of central corneal thickness by high-resolution Scheimpflug imaging, Fourier-domain optical coherence tomography and ultrasound pachymetry. *Acta Ophthalmol*. 2012;90:449-455.

93. Khaja WA, Grover S, Kelmenson AT, Ferguson LR, Sambhav K, Chalam KV. Comparison of central corneal thickness: Ultrasound pachymetry versus slit-lamp optical coherence tomography, specular microscopy, and Orbscan. *Clin Ophthalmol*. 2015;9:1065-1070.

94. Giasson CJ, Morency J, Melillo M, Michaud L. Oxygen tension beneath scleral lenses of different clearances. *Optom Vis Sci*. 2017;94(4):466-475.

95. Jaynes JM, Edrington TB, Weissman BA. Predicting scleral GP lens entrapped tear layer oxygen tensions. *Cont Lens Anterior Eye*. 2015;38(1):44-47.

96. Bryant MR, McDonnell PJ. A triphasic analysis of corneal swelling and hydration control. *J Biomech Eng*. 1998;120(3):370-381.

97. Hedbys BO, Dohlman CH. A new method for the determination of the swelling pressure of the corneal stroma in vitro. *Exp Eye Res*. 1963;2:122-129.

98. Hedbys BO, Mishima S. The thickness-hydration relationship of the cornea. *Exp Eye Res*. 1966;5(3):221-228.

99. Hodson S, Miller F. The bicarbonate ion pump in the endothelium which regulates the hydration of rabbit cornea. *J Physiol*. 1976;263:563-577.

100. Kedem O, Katchalsky A. Thermodynamic analysis of the permeability of biological membranes to non-electrolytes. *Biochimica Et Biophysica Acta*. 1958;27:229-246.

101. Langham ME. Glycolysis in the cornea of the rabbit. *J Physiol*. 1954;126:396-403.

102. Langham ME, Taylor IS. Factors affecting the hydration of the cornea in the excised eye and the living animal. *Brit J Ophthal*. 1956;40:312-340.

103. Newman J, Thomas-Alyea KE. *Electrochemical Systems*. 3rd ed. Wiley-Interscience; 2004.

104. Fatt I, Fink SE. The ratio of carbon dioxide to oxygen permeability of RGP contact lens materials. *Int Contact Lens Clin*. 1989;16(11-12):347-352.

105. Brennan NA. Beyond flux: Total corneal oxygen consumption as an index of corneal oxygenation during contact lens wear. *Optom Vis Sci*. 2005;82(6):467-472.

106. Rismondo V, Osgood TB, Leering P, Hattenhauer MG, Ubels JL, Edelhauser HF. Electrolyte composition of lacrimal gland fluid and tears of normal and vitamin A-deficient rabbits. *CLAO J*. 1989;15(3):222-228.

107. Giasson C, Bonanno JA. Corneal epithelial and aqueous humor acidification during in vivo contact lens wear in rabbits. *Invest Ophthalmol Vis Sci*. 1994;35(3):851-861.

108. Fischer FH, Wiederholt M. Human precorneal tear film pH measured by microelectrodes. *Graefes Arch Clin Exp Ophthalmol*. 1982;218(3):168-170.

109. Imre G. The role of lactic acid in neovascularization. *Arch Klin Exp Opthalmol*. 1977;201(3):263-266.

110. Fatt I, Goldstick TK. Dynamics of water transport in swelling membranes. *J Colloid Sci*. 1965;20(9):962-989.

111. Ooi EH, Ng EYK. Effects of natural convection within the anterior chamber on the ocular heat transfer. *Int J Numer Methods Biomed Eng*. 2010;27(3):408-423.

112. Nguyen TT, Bonanno JA. Lactate-H+ transport is a significant component of the in vivo corneal endothelial pump. *Invest Ophthalmol Vis Sci*. 2012;53(4):2020-2029.

113. Bird RB, Stewart WE, Lightfoot EN. *Transport Phenomena*. 2nd ed. John Wiley and Sons; 2002.

114. Dursch TJ, Li W, Taraz B, Lin MC, Radke CJ. Tear-film evaporation rate from simultaneous ocular-surface temperature and tear-breakup area. *Optom vis Sci*. 2018;95(1):5-12.

115. Bausch+Lomb. Package Insert: Boston XO2. http://www.bausch.com/Portals/77/-/m/BL/United States/Files/Package Inserts/Vision Care/bostonxo2packageinsert.pdf

116. Polse KA, Mandell RB. Critical oxygen tension at the corneal surface. *Arch Ophthalmol*. 1970;84:505-508.

117. Fatt I. Steady-state distribution of oxygen and carbon dioxide in the in vivo cornea. II. The open eye in nitrogen and the covered eye. *Exp Eye Res*. 1968;7:413-430.

118. Fatt I, Bieber MT. The steady-state distribution of oxygen and carbon dioxide in the in vivo cornea. I. The open eye in air and the closed eye. *Exp Eye Res*. 1968;7:103-112.

119. Fatt I, Freeman RD, Lin D. Oxygen tension distributions in the cornea: A re-examination. *Exp Eye Res*. 1974;18:357-365.

120. Fatt I, Lin D. Spatial distribution of oxygen in the cornea of a closed eye wearing a gas permeable contact lens. *Curr Eye Res*. 1985;4:723-724.

121. Kim YH, Tan B, Lin MC, Radke CJ. Central corneal edema with scleral-lens wear. *Curr Eye Res*. 2018;43(11):1305-1315.

122. Alvord LA, Hall WJ, Keyes LD, Morgan CF, Winterton LC. Corneal oxygen distribution with contact lens wear. *Cornea*. 2007;26(6):654-664.

123. Feizi S, Jafarinasab MR, Karimian F, Hasanpour H, Masudi A. Central and peripheral corneal thickness measurement in normal and keratoconic eyes using three corneal pachymeters. *J Ophthalmic Vis Res*. 2014;9(3):296-304.

124. Waltman ST. The cornea. In: Moses RA, ed. *Alder's Physiology of the Eye*. 7th ed. C.V. Mosby Co; 1981:38-48.

125. Martin R, de Juan V, Rodriguez G, Fonseca S, Martin S. Contact lens-induced corneal peripheral swelling: Orbscan repeatability. *Optom Vis Sci*. 2009;86(4):340-349.

126. Dunne MCM, Davies LN, Wolffsohn J. Accuracy of cornea and lens biometry using anterior segment optical coherence tomography. *J Biomed Opt*. 2007;12(6):064023.

127. Marsich MM, Bullimore MA. The repeatability of corneal thickness measures. *Cornea*. 2000;19(6):792-795.

128. Lam AK, Chen D. Pentacam pachometry: Comparison with non-contact specular microscopy on the central cornea and inter-session repeatability on the peripheral cornea. *Clin Exp Optom*. 2007;90:108-114.

129. Miranda MA, Radhakrishnan H, O'Donnell C. Repeatability of corneal thickness measured using an Oculus Pentacam. *Optom Vis Sci*. 2009;86(3):266-272.

130. Westphal V, Rollins AM, Radhakrishnan S, Izatt JA. Correction of geometric and refractive image distortions in optical coherence tomography applying Fermat's principle. *Opt Express*. 2002;10(9):397-404.

131. Herse P, Akakura N, Ooi C. Topographical cornea edema: An update. *Acta Ophthalmol*. 1993;71:539-543.

132. Bonanno JA, Polse KA. Central and peripheral corneal swelling accompanying soft lens extended wear. *Am J Optom & Physiol Opt*. 1985;62:74-81.

133. Holden BA, McNally JJ, Mertz GW. Topographical corneal oedema. *Acta Ophthalmol*. 1985;63:684-691.

134. Grytz R, Meschke G, Jonas JB. The collagen fibril architecture in the lamina cribrosa and peripapillary sclera predicted by a computational remodeling approach. *Biomech Model Mechanobiol*. 2011;10(3):371-382.

135. Sridhar MS. Anatomy of cornea and ocular surface. *Indian J Ophthalmol*. 2018;66(2):190-194.

136. Lira M, Pereira C, Real Oliveira MECD, Castanheira EMS. Importance of contact lens power and thickness in oxygen transmissibility. *Cont Lens Anterior Eye*. 2015;38(2):120-126.

137. Wang J, Fonn D, Simpson TL, Jones L. Precorneal and pre- and postlens tear film thickness measured indirectly with optical coherence tomography. *Invest Ophthalmol Vis Sci*. 2003;44:2524-2528.

138. Nichols JJ, King-Smith PE. Thickness of the pre- and post-contact lens tear film measured in vivo by interferometry. *Invest Ophthalmol Vis Sci*. 2003;44(1):68-77.

139. Kuang K, Xu M, Koniarek J, Fischbarg J. Effects of ambient bicarbonate, phosphate and carbonic anhydrase inhibitors on fluid transport across rabbit corneal endothelium. *Exp Eye Res*. 1990;50(5):487-493.

140. Goodwin ML, Harris JE, Hernandez A, Gladden LB. Blood lactate measurements and analysis during exercise: A guide for clinicians. *J Diabetes Sci Technol*. 2007;1(4):558-569.

141. FDA. Investigations Operations Manual 2019: Blood Serum Chemistry - Normal Values. Appendix C 6-7. https://www.fda.gov/media/75271/download

142. Tan B, Tse V, Kim YH, Lin K, Zhou Y, Lin MC. Effects of scleral-lens oxygen transmissibility on corneal thickness: A pilot study. *Cont Lens Anterior Eye*. 2019;42(4):366-372.

143. Hitzenberger CK, Baumgartner A, Drexler W, Fercher AF. Interferometric measurement of corneal thickness with micrometer precision. *Am J Ophthalmol*. 1994;118:468-476.

144. Chen W, Xu Z, Jiang H, Zhou J, Wang L, Wang J. Altered bulbar conjunctival microcirculation in response to contact lens wear. *Eye Contact Lens*. 2017;43(2):95-99.

145. Creech JL, Chauhan A, Radke CJ. Dispersive mixing in the posterior tear film under a soft contact lens. *Ind Eng Chem Res*. 2001;40:3015-3026.

146. Tse V, Tan B, Kim YH, Zhou Y, Lin MC. Tear dynamics under scleral lenses. *Cont Lens Anterior Eye*. 2019;42(1):43-48.

147. Efron N. Contact lens-induced corneal oedema. *Optician*. 1996;211(5540):1-8.

148. Fonn D, Holden BA, Gooley G, Kenefick J. Comparative physiologic performance of polymethyl methacrylate and gas-permeable contact lenses. *Arch Ophthalmol*. 1984;102:760-764.

149. Polse KA, Mandell RB. Etiology of corneal striae accompanying hydrogel lens wear. *Invest Ophthalmol Vis Sci*. 1976;15:553-556.

150. Maurice DM. The structure and transparency of the cornea. *J Physiol*. 1957;136:263-286.

151. McMahon TT, Polse KA, McNamara N, Viana MAG. Recovery from induced corneal edema and endothelial morphology after long-term PMMA contact lens wear. *Optom Vis Sci*. 1996;73(3):184-188.

152. Fisher D, Collins MJ, Vincent SJ. Conjunctival prolapse during open eye scleral lens wear. *Cont Lens Anterior Eyet*. 2021;44(1):115-119.

153. Hydrogel and silicone hydrogel lens general considerations. Contact Lens Spectrum. https://www.clspectrum.com/supplements/2010/july-2010/2010-contact-lenses-solutions-summary/soft-contact-lenses

154. Nefedov P. *Do Scleral Lenses Provide Adequate Oxygen Permeability for Overnight Lens Wear?* Pacific University [Master's Thesis]; 2016.

155. Smith GT, Mireskandari K, Pullum KW. Corneal swelling with overnight wear of scleral contact lenses. *Cornea*. 2004;23(1):29-34.

156. Giedd B. Understanding the nuances of contact lens materials. Contact Lens Spectrum. https://www.clspectrum.com/issues/1999/july-1999/understanding-the-nuances-of-contact-lens-material

157. Pajic B, Pajic-Eggspuchler B, Haefliger I. Continuous IOP fluctuation recording in normal tension glaucoma patients. *Curr Eye Res*. 2011;36(12):1129-1138.

158. Paugh JR, Chen E, Heinrich C, et al. Silicone hydrogel and rigid gas-permeable scleral lens tear exchange. *Eye Contact Lens*. 2018;44(2):97-101.

159. Fisher D, Collins MJ, Vincent SJ. Fluid reservoir thickness and corneal edema during open-eye scleral lens wear. *Optom Vis Sci*. 2020;97(9):683-689.

160. Niimi J, Tan B, Chang J, et al. Diurnal pattern of tear osmolarity and its relationship to corneal thickness and deswelling. *Cornea*. 2013;32:1305-1310.

161. Vincent SJ, Alonso-Caneiro D, Kricancic H, Collins MJ. Scleral contact lens thickness profiles: The relationship between average and centre lens thickness. *Cont Lens Anterior Eye*. 2019;42:55-62.

162. Casser L, Fingeret M, Woodcome T. *Atlas of Primary Eyecare Procedures*. 2nd ed. McGraw-Hill Education; 1997.

163. Nichols KK, Mitchell GL, Zadnik K. The repeatability of clinical measurements of dry eye. *Cornea*. 2004;23(3):272-285.

164. Telles R, Li W, Dursch TJ, Lin MC, Radke CJ. Human tear-production rate from closed-eye Schirmer-strip capillary dynamics. *Colloids Surf, A Physicochem Eng Asp*. 2017;521:61-68.

165. Li S, Kim YH, Li W, Lin MC, Radke CJ. Human lacrimal production rates from modified Schirmer-tear test. *Optom Vis Sci*. 2018;95(4):343-348.

166. Holly FJ, Lamberts DW, Esquivel ED, et al. Kinetics of capillary tear flow in the Schirmer strip. *Curr Eye Res*. 1982;2(1):57-70.

167. Holly FJ. Lacrimation kinetics as determined by a Schirmer-type technique. In: Sullivan DA, ed. *In Lacrimal Gland, Tear Film, and Dry Eye Syndromes*. Plenum Press; 1994:543-548.

168. Beebe WE, Esquivel ED, Holly FJ. Comparison of lacrimation kinetics in dry eye patients and normal. *Curr Eye Res*. 1988;7:419-425.

169. Holly FJ, Laukaitis SJ, Esquivel ED. Kinetics of lacrimal secretion in normal human subjects. *Curr Eye Res*. 1984;3:897-910.

170. Li N, Deng XG, He MF. Comparison of the Schirmer I test with and without topical anesthesia for diagnosing dry eye. *Int J Ophthalmol*. 2012;5:478-481.

171. Sakamoto R, Bennett ES, Henry VA, et al. The phenol red thread tear test: A cross-cultural study. *Invest Ophthalmol Vis Sci*. 1993;34(13):3510-3514.

172. Kuriki R, Hata T, Nakayama K, et al. Changes in tear volume and ocular symptoms of patients receiving oral anticancer drug S-1. *J Pharm Health Care Sci*. 2018;4(1):3.

173. Kojima T, Ibrahim OMA, Wakamatsu T, et al. The impact of contact lens wear and visual display terminal work on ocular surface and tear functions in office workers. *Am J Ophthalmol*. 2011;152(6):933-940.e2.

174. Srinivasan S, Chan C, Jones L. Apparent time-dependent differences in inferior tear meniscus height in human subjects with mild dry eye symptoms. *Clin Exp Optom*. 2007;90(5):345-350.

175. Yokoi N, Bron AJ, Tiffany JM, Maruyama K, Komuro A, Kinoshita S. Relationship between tear volume and tear meniscus curvature. *Arch Ophthalmol*. 2004;122(9):1265-1269.

176. Buckmaster F, Pearce EI. Effects of humidity on tests of tear production. *Clin Sci*. 2016;35(6):754-758.

177. Terry RL, Schnider CM, Holden BA, et al. CCLRU standards for success of daily and extended wear contact lenses. *Optom Vis Sci*. 1993;70:234-243.

178. Bland JM, Altman DG. Agreement between methods of measurement with multiple observations per individual. *J Biopharm Stat*. 2007;17:571-582.

179. Vaz S, Falkmer T, Passmore AE, Parsons R, Andreou P. The case for using the repeatability coefficient when calculating test-retest reliability. *PLOS One*. 2013;8(9):e73990.

180. Lira M, Oliveira ME, Franco S. Comparison of the tear film clinical parameters at two different times of the day. *Clin Exp Optom*. 2011;94(6):557-562.

181. Lee JH, Hyun PM. The Reproducibility of the Schirmer Test. *Kor J Ophthalmol*. 1988;2:5-8.

182. Atkinson AC, Donev AN. *Optimum Experimental Designs*. Oxford Science Publications; 1992.

183. Wong WK, Zhu W. Optimum treatment allocation rules under a variance heterogeneity model. *Stat Med*. 2008;27(22):1-20.

184. Mishima S, Gasset A, Klyce SD, Baum JL. Determination of tear volume and tear flow. *Invest Ophthalmol Vis Sci*. 1966;5(3):264-276.

185. Prabha JL. Tear secretion - A short review. *J Pharm Sci & Res*. 2014;6(3):155-157.

186. The definition and classification of dry eye disease: Report of the Definition and Classification Subcommittee of the International Dry Eye Workshop. *Ocul Surf*. 2007;5(2):75-92.

187. Feldman F, Wood MM. Evaluation of the Schirmer tear test. *Can J Ophthalmol*. 1979;14(4):257-259.

188. Baudouin C, Aragona P, Messmer EM, et al. Role of hyperosmolarity in the pathogenesis and management of dry eye disease: Proceedings of the OCEAN group meeting. *Clin Sci*. 2013;11(4):246-258.

189. Bron AJ, Tiffany JM, Yokoi N, Gouveia SM. Using osmolarity to diagnose dry eye: A compartmental hypothesis and review of our assumptions. *Adv Exp Med Biol*. 2002;506:1087-1095.

190. Gaffney EA, Tiffany JM, Yokoi N, Bron AJ. A mass and solute balance model for tear volume and osmolarity in the normal and the dry eye. *Prog Retin Eye Res*. 2010;29:59-78.

191. Gilbard JP, Carter JB, Sang DN, Refojo MF, Hanninen LA, Kenyon KR. Morphologic effect of hyperosmolarity on rabbit corneal epithelium. *Ophthalmology*. 1984;91:1205-1212.

192. Gilbard JP. Tear film osmolarity and keratoconjunctivitis sicca. *CLAO J*. 1985;11:243-250.

193. Gilbard JP, Rossi SR, Gray KL, Hanninen LA, Kenyon KR. Tear film osmolarity and ocular surface disease in two rabbit models for keratoconjunctivitis sicca. *Invest Ophthalmol Vis Sci*. 1988;29(3):374-378.

194. Luo L, Li DQ, Corrales RM, Pflugfelder SC. Hyperosmolar saline is a proinflammatory stress on the mouse ocular surface. *Eye Contact Lens*. 2005;31(5):186-193.

195. Li DQ, Luo L, Chen Z, Kim HS, Song XJ, Pflugfelder SC. JNK and ERK MAP kinases mediate induction of IL-1β, TNF-α and IL-8 following hyperosmolar stress in human limbal epithelial cells. *Exp Eye Res*. 2006;82(4):588-596.

196. Guzmán M, Miglio M, Keitelman I, et al. Transient tear hyperosmolarity disrupts the neuroimmune homeostasis of the ocular surface and facilitates dry eye onset. *Immunology*. 2020;161(2):148-161.

197. Hirata H, Rosenblatt MI. Hyperosmolar tears enhance cooling sensitivity of the corneal nerves in rats: Possible neural basis for cold-induced dry eye pain. *Invest Ophthalmol Vis Sci*. 2014;55(9):5821-5833.

198. Hirata H, Mizerska K, Marfurt CF, Rosenblatt MI. Hyperosmolar tears induce functional and structural alterations of corneal nerves: Electrophysiological and anatomical evidence toward neurotoxicity. *Invest Ophthalmol Vis Sci*. 2015;56(13):8125-8140.

199. Chauhan A, Radke CJ. Modeling the vertical motion of a soft contact lens. *Curr Eye Res*. 2001;22(2):102-108.

200. Kok JHC, Boets EPM, van Best JA, Kijlstra A. Fluorophotometric assessment of tear turnover under rigid contact lenses. *Cornea*. 1992;11:515-517.

201. Lin MC, Soliman GN, Song MJ, et al. Soft contact lens extended wear affects corneal epithelial permeability: Hypoxic or mechanical etiology? *Cont Lens Anterior Eye*. 2003;26(1):11-16.

202. Lin MC, Soliman GN, Lim VA, et al. Scalloped channels enhance tear mixing under hydrogel contact lenses. *Optom Vis Sci*. 2006;83(12):874-878.

203. McNamara NA, Polse KA, Brand RJ, Graham AD, Chan JS, McKenney CD. Tear mixing under a soft contact lens: Effects of lens diameter. *Am J Ophthalmol*. 1999;127:659-665.

204. İskeleli G, Karakoç Y, Aydn Ö, Yetik H, Uslu H, Kzlkaya M. Comparison of tear-film osmolarity in different types of contact lenses. *CLAO J*. 2002;28(4):174-176.

205. Stahl U, Willcox MDP, Naduvilath T, Stapleton F. Influence of tear film and contact lens osmolality on ocular comfort in contact lens wear. *Optom Vis Sci*. 2009;86(7):857-867.

206. Stapleton F, Marfurt C, Golebiowski B, et al. The TFOS international workshop on contact lens discomfort: Report of the subcommittee on neurobiology. *Invest Ophthalmol Vis Sci*. 2013;54(11):TFOS71-TFOS97.

207. McDonald JE, Brubaker S. Meniscus-induced thinning of tear films. *Am J Ophthalmol*. 1971;72:139-146.

208. Miller KL, Polse KA, Radke CJ. Black-line formation and the "perched" human tear film. *Curr Eye Res*. 2002;25(3):155-162.

209. Siddique JI, Braun RJ. Tear film dynamics with evaporation, osmolarity and surfactant transport. *Appl Math Model*. 2015;39(1):255-269.

210. Guan L, González Jiménez ME, Walowski C, Boushehri A, Prausnitz JM, Radke CJ. Permeability and partition coefficient of aqueous sodium chloride in soft contact lenses. *J Appl Polym Sci*. 2011;122:1457-1471.

211. Fraunfelder FT. Extraocular fluid dynamics - How best to apply topical ocular medication. *Trans Am Ophthalmol Soc*. 1976;74:457-487.

212. Tomlinson A, Doane MG, McFadyen A. Inputs and outputs of the lacrimal system: Review of production and evaporative loss. *Ocul Surf*. 2009;7:186-198.

213. van Best JA, Benitez del Castillo JM, Coulangeon LM. Measurement of basal tear turnover using a standardized protocol. *Graefes Arch Clin Exp Ophthalmol*. 1995;233:1-7.

214. Wong H, Fatt I, Radke CJ. Deposition and thinning of the human tear film. *J Colloid Interface Sci*. 1996;184:44-51.

215. Willcox MDP, Argüeso P, Georgiev GA, et al. TFOS DEWS II tear film report. *Ocul Surf*. 2017;15(3):366-403.

216. Craig JP, Willcox MDP, Argüeso P, et al. The TFOS international workshop on contact lens discomfort: Report of the contact lens interactions with the tear film subcommittee. *Invest Ophthalmol Vis Sci*. 2013;54(11):TFOS123-TFOS156.

217. Cedarstaff TH, Tomlinson A. A comparative study of tear evaporation rates and water content of soft contact lenses. *Am J Optom Physiol Opt*. 1983;60(3):167-174.

218. Dartt DA, Willcox MDP. Complexity of the tear film: Importance in homeostasis and dysfunction during disease. *Exp Eye Res*. 2013;117:1-3.

219. Bretherton FP. The motion of long bubbles in tubes. *J Fluid Mech*. 1961;10(2):166-168.

220. Nagyová B, Tiffany JM. Components responsible for the surface tensions of human tears. *Curr Eye Res*. 1999;19(1):4-11.

221. Tiffany JM, Winter N, Bliss G. Tear film stability and tear surface tension. *Curr Eye Res*. 1989;8:507-515.

222. Svitova TF, Lin MC. Tear lipids interfacial rheology: Effect of lysozyme and lens care solutions. *Optom Vis Sci*. 2010;87(1):10-20.

223. Ehlers N. The precorneal film: Biomicroscopical, histological and chemical investigations. *Acta Ophthalmol*. 1965;(Suppl. 81):1-134.

224. Tiffany JM. The viscosity of human tears. *Int Ophthalmol*. 1991;15:371-376.

225. King-Smith PE, Fink BA, Fogt N, Nichols KK, Hill RM, Wilson GS. The thickness of the human precorneal tear film: Evidence from reflection spectra. *Invest Ophthalmol Vis Sci*. 2000;41(11):3348-3359.

226. McMonnies CW. Aqueous deficiency is a contributor to evaporation-related dry eye disease. *Eye Vis*. 2020;7:6.

227. Nichols JJ, Mitchell GL, King-Smith PE. Thinning rate of the precorneal and prelens tear films. *Invest Ophthalmol Vis Sci*. 2005;46:2253-2361.

228. Stern ME, Gao J, Siemasko KF, Beuerman RW, Pflugfelder SC. The role of the lacrimal functional unit in the pathophysiology of dry eye. *Exp Eye Res*. 2004;78(3):409-416.

229. Sullivan DA. Tearful relationships? Sex, hormones, the lacrimal gland, and aqueous-deficient dry eye. *Ocul Surf*. 2004;2(2):92-123.

230. Glasson MJ, Stapleton F, Keay L, Willcox MDP. The effect of short term contact lens wear on the tear film and ocular surface characteristics of tolerant and intolerant wearers. *Cont Lens Anterior Eye*. 2006;29:41-47.

231. Khanal S, Tomlinson A, McFadyen A, Diaper C, Ramaesh K. Dry eye diagnosis. *Invest Ophthalmol Vis Sci*. 2008;49:1407-1414.

232. Khanal S, Tomlinson A, Diaper CJM. Tear physiology of aqueous deficiency and evaporative dry eye. *Optom Vis Sci*. 2009;86:1235-1240.

233. Kim YH, Graham AD, Li W, Radke CJ, Lin MC. Human lacrimal production rate and wetted length of modified Schirmer's tear test strips. *Transl Vis Sci Technol*. 2019;8(3):40.

234. Guillon M, Maissa C. Contact lens wear affects tear film evaporation. *Eye Contact Lens*. 2008;34(6):326-330.

235. Doane MG. Blinking and the mechanics of the lacrimal drainage system. *Ophthalmology*. 1981;88(8):844-851.

236. Zhu H, Chauhan A. A mathematical model for tear drainage through the canaliculi. *Curr Eye Res*. 2005;30:621-630.

237. Rolando M, Refojo MF. Tear evaporimeter for measuring water evaporation rate from the tear film under controlled conditions in humans. *Exp Eye Res*. 1983;36(1):25-33.

238. McCulley JP, Shine W. A compositional based model for the tear film lipid layer. *Trans Am Ophthalmol Soc*. 1997;95:79-93.

239. Korb DR, Greiner J v., Glonek T, et al. Human and rabbit lipid layer and interference pattern observations. In: Sullivan DA, Dartt DA, Meneray MA, eds. *Lacrimal Gland, Tear Film, and Dry Eye Syndromes 2*. Springer; 1998:305-308.

240. King-Smith PE, Hinel EA, Nichols JJ. Application of a novel interferometric method to investigate the relation between lipid layer thickness and tear film thinning. *Invest Ophthalmol Vis Sci*. 2010;51(5):2418-2423.

241. Kimball SK, King-Smith PE, Nichols JJ. Evidence for the major contribution of evaporation to tear film thinning between blinks. *Invest Ophthalmol Vis Sci*. 2010;51:6294-6297.

242. Peng CC, Cerretani CF, Li Y, et al. Flow evaporimeter to assess evaporative resistance of human tear-film lipid layer. *Ind Eng Chem Res*. 2014;53(47):18130-18139.

243. Boushehri A, Tang D, Shieh KJ, Prausnitz JM, Radke CJ. Water transport through soft contact lenses determined in a fan-evaporation cell. *J Membr Sci*. 2010;362:529-534.

244. Peng CC, Chauhan A. Ion transport in silicone hydrogel contact lenses. *J Membr Sci*. 2012;399-400:95-105.

245. Yasuda H, Lamaze CE, Ikenberry LD. Permeability of solutes through hydrated polymer membranes. Part 1. Diffusion of sodium chloride. *Makromol Chem*. 1968;118(1):19-35.

246. Berg JC. *An Introduction to Interfaces and Colloids: The Bridge to Nanoscience*. World Scientific Publishing Co. Pte. Ltd.; 2009.

247. Maki KL, Braun RJ, Ucciferro P, Henshaw WD, King-Smith PE. Tear film dynamics on an eye-shaped domain. Part 2. Flux boundary conditions. *J Fluid Mech*. 2010;647:361-390.

248. Finnemore VM, Korb DR, Greiner J v., Glonek T, Herman JP. Fluorescein dye concentration as a factor in tear film fluorescence. In: Sullivan DA, Dartt DA, Meneray MA, eds. *Lacrimal Gland, Tear Film, and Dry Eye Syndromes 2*. Springer; 1998:875-878.

249. Fatt I. Observations of tear film break up on model eyes. *CLAO J*. 1991;17:267-281.

250. Refojo MF, Miller D, Fiore A. A new fluorescent stain for soft hydrophilic lens fitting. *Arch Ophthalmol*. 1972;82(3):275-277.

251. Chen Q, Wang J, Shen M, et al. Tear menisci and ocular discomfort during daily contact lens wear in symptomatic wearers. *Invest Ophthalmol Vis Sci*. 2011;52(5):2175-2180.

252. del Águila-Carrasco AJ, Ferrer-Blasco T, García-Lázaro S, Esteve-Taboada JJ, Montés-Micó R. Assessment of corneal thickness and tear meniscus during contact-lens wear. *Cont Lens Anterior Eye*. 2015;38(3):185-193.

253. Tao A, Cai C, Shen M, et al. Tear menisci after overnight contact lens wear. *Optom Vis Sci*. 2011;88(12):1433-1438.

254. Wang J, Jiao S, Ruggeri M, Shousha MA, Chen Q. In situ visualization of tears on contact lens using ultra high resolution optical coherence tomography. *Eye Contact Lens*. 2009;35(2):44-49.

255. Hoch G, Chauhan A, Radke CJ. Permeability and diffusivity for water transport through hydrogel membranes. *J Membrane Sci*. 2003;214(2):199-209.

256. Mann A, Sáez-Martinez V, Lydon F, Tighe B. Investigating the permeation properties of contact lenses and its influence on tear electrolyte composition. *J Biomed Mater Res B*. 2019;107(6):1997-2005.

257. Dursch TJ, Taylor NO, Liu DE, Wu RY, Prausnitz JM, Radke CJ. Water-soluble drug partitioning and adsorption in HEMA/MAA Hydrogels. *Biomaterials*. 2014;35:620-629.

258. Brady JF. Hindered diffusion. In extended abstracts, AIChE Annual Meeting, San Francisco, CA. 1994:320.

259. Amsden B. Solute diffusion within hydrogels. Mechanisms and models. *Macromolecules*. 1998;31:8382-8395.

260. Brenner H, Edwards DA. *Macrotransport Processes*. Butterworth-Heinemann; 1993.

261. Liu DE, Kotsmar C, Nguyen F, et al. Macromolecule sorption and diffusion in HEMA/MAA hydrogels. *Ind Eng Chem Res*. 2013;52:18109-18129.

262. Refojo MF. Permeation of water through some hydrogels. *J Appl Polym Sci*. 1965;9:3417-3426.

263. Quinn TM, Grodzinsky AJ. Longitudinal modulus and hydrualic permeability of poly(methacrylic acid) gels: Effects of charge density and solvent content. *Macromolecules*. 1993;26:4332-4338.

264. Pratt KC, Wakeham WA. Self-diffusion in water and monohydric alcohols. *J Chem Soc, Faraday Trans II*. 1977:997-1002.

265. You J, Willcox MDP, Madigan MC, et al. Tear fluid protein biomarkers. *Adv Clin Chem*. 2013;62:151-196.

266. Dartt DA. Regulation of mucin and fluid secretion by conjunctival epithelial cells. *Prog Retin Eye Res*. 2002;21:555-576.

267. Leung T, Zhou Y, French HM, Lin MC. Increased corneal epithelial permeability after overnight sleep. *Invest Ophthalmol Vis Sci*. 2014;55:5718-5722.

268. Jones L, Hui A, Phan CM, et al. CLEAR - Contact lens technologies of the future. *Cont Lens Anterior Eye*. 2021;44(2):398-430.

269. Kim J, Kim M, Lee MS, et al. Wearable smart sensor systems integrated on soft contact lenses for wireless ocular diagnostics. *Nat Commun*. 2017;8(1):14997.

270. Chiou JC. The development of smart contact lens system: Taking dry eye syndrome diagnosis as an example. In: *Future Tech Expo*. 2019.

271. Badugu R, Jeng BH, Reece EA, Lakowicz JR. Contact lens to measure individual ion concentrations in tears and applications to dry eye disease. *Anal Biochem*. 2018;542:84-94.

272. Zhang J, Begley CG, Situ P, Simpson T, Liu H. A link between tear breakup and symptoms of ocular irritation. *Ocul Surf*. 2017;15(4):696-703.

273. Gad A, Vingrys AJ, Wong CY, Jackson DC, Downie LE. Tear film inflammatory cytokine upregulation in contact lens discomfort. *Ocul Surf*. 2019;17(1):89-97.

274. Belmonte C, Gallar J. Cold thermoreceptors, unexpected players in tear production and ocular dryness sensations. *Invest Ophthalmol Vis Sci*. 2011;52(6):3888-3892.

275. Malbouisson JM, Baccega A, Cruz A. The geometrical basis of the eyelid contour. *Ophthalmic Plast Recons*. 2000;16(6):427-431.

276. Fleiszig SMJ, McNamara NA, Evans DJ. The tear film and defense against infection. In: Sullivan DA, Stern ME, Dartt DA, Sullivan RM, Bromberg BB, eds. *Lacrimal Gland, Tear Film, and Dry Eye Syndromes 3*. Springer; 2002:523-530.

277. Argüeso P, Guzman-Aranguez A, Mantelli F, Cao Z, Ricciuto J, Panjwani N. Association of cell surface mucins with galectin-3 contributes to the ocular surface epithelial barrier. *J Biol Chem*. 2009;284(34):23037-23045.

278. Kim YH, Graham AD, Li W, et al. Tear-film evaporation flux for symptomatic and asymptomatic soft contact-lens wearers and relationship to tear properties. *Exp Eye Res*. 2022;In Review.

279. King-Smith PE, Reuter KS, Braun RJ, Nichols JJ, Nichols KK. Tear film breakup and structure studied by simultaneous video recording of fluorescence and tear film lipid layer images. *Invest Ophthalmol Vis Sci*. 2013;54(7):4900-4909.

280. Svitova TF, Lin MC. Evaporation retardation by model tear-lipid films: The roles of film aging, compositions and interfacial rheological properties. *Colloids Surf B*. 2021;197:111392.

281. Gilbard JP, Farris RL, Santa Maria JII. Osmolarity of tear micro volumes in keratoconjunctivitis sicca. *Arch Ophthalmol*. 1978;96:677-681.

282. Li W, Graham AD, Selvin S, Lin MC. Ocular surface cooling corresponds to tear film thinning and breakup. *Optom Vis Sci*. 2015;92(9):e248-e256.

283. Abelson MB, Ousler GW, Nally LA, Welch D, Krenzer K. Alternative Reference Values for Tear Film Break up Time in Normal and Dry Eye Populations. In: Sullivan DA, Stern ME, Tsubota K, Dartt DA, Sullivan RM, Bromberg BB, eds. *Lacrimal Gland, Tear Film, and Dry Eye Syndromes 3*. Springer; 2002.

284. Montani G, Martino M. Tear film characteristics during wear of daily disposable contact lenses. *Clin Ophthalmol*. 2020;14:1521-1531.

285. Ding JE, Kim YH, Yi SM, Graham AD, Li W, Lin MC. Ocular surface cooling rate associated with tear film characteristics and the maximum interblink period. *Sci Rep*. 2021;11:15030.

286. Müller LJ, Marfurt CF, Kruse F, Tervo TMT. Corneal nerves: Structure, contents and function. *Exp Eye Res*. 2003;76(5):521-542.

287. Maharaj RL. In vivo ocular surface osmolarity in a dry eye population. *Clin Refract Optom*. 2017;28(1):3-6.

288. Rosenthal P, Borsook D. The Corneal pain system. Part I: The missing piece of the dry eye puzzle. *Ocul Surf*. 2012;10(1):2-14.

289. Alharbi A, la Hood D, Swarbrick HA. Overnight orthokeratology lens wear can inhibit the central stromal edema response. *Invest Ophthalmol Vis Sci*. 2005;46(7):2334-2340.

290. Li LY, Tighe BJ, Ruberti JW. Mathematical modelling of corneal swelling. *Biomech Model Mechanobiol*. 2004;3(2):114-123.